Integrated Environmental Control Model

Technical Documentation

Prepared for the Federal Energy Technology Center
U. S. Department of Energy

By Michael B. Berkenpas
H. Christopher Frey
John J. Fry
Jayant Kalagnanam
Edward S. Rubin
Center for Energy and Environmental Studies
Carnegie Mellon University
Pittsburgh, PA 15213

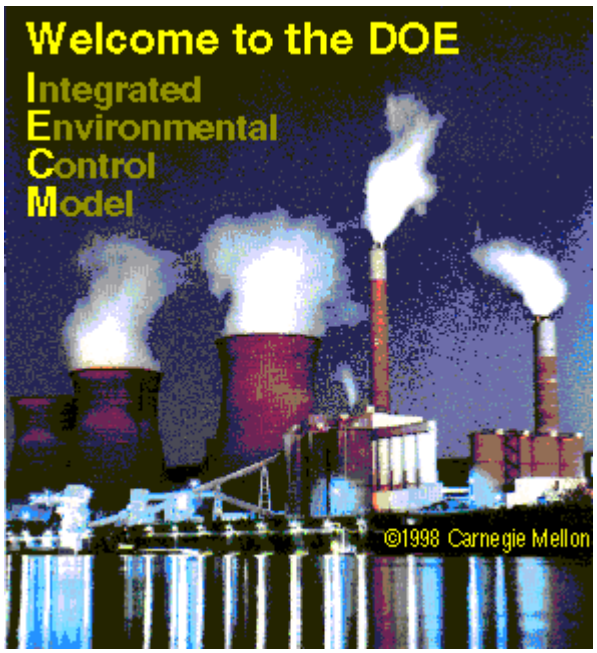

May 1999

Acknowledgements

This report is the result of research sponsored by the U.S. Department of Energy under Contract No. DE-AC22-92PC91346. The authors gratefully acknowledge the support and guidance of DOE throughout the course of this work. Many DOE contractors, research personnel, and process developers helped immeasurably during the course of this work, and we gratefully acknowledge their assistance and interest in this project. In particular, we wish to thank our project managers Lori Gould, Pat Rawls, Tom Feeley, and Gerst Gibbon for their help, guidance, and enthusiasm.

Contents

1. Introduction

The purpose of this contract is to develop and refine the Integrated Environmental Control Model (IECM) created and enhanced by Carnegie Mellon University (CMU) for the U.S. Department of Energy, Federal Energy Technology Center (USDOE FETC) under contract Numbers DE-FG22-83PC60271 and DE-AC22-87PC79864.

In its current configuration, the IECM provides a capability to model various conventional and advanced processes for controlling air pollutant emissions from coal-fired power plants before, during, or after combustion. The principal purpose of the model is to calculate the performance, emissions, and cost of power plant configurations employing alternative environmental control methods. The model consists of various control technology modules, which may be integrated into a complete utility plant in any desired combination. In contrast to conventional deterministic models, the IECM offers the unique capability to assign probabilistic values to all model input parameters, and to obtain probabilistic outputs in the form of cumulative distribution functions indicating the likelihood of different costs and performance results.

The previous version of the IECM, implemented on a Macintosh computer and containing a number of software and model enhancements, was delivered to USDOE FETC at the end of the previous contract in May 1991. The current contract continued the model development effort on the Macintosh to provide USDOE FETC with improved model capabilities, including new software developments to facilitate model use and new technical capabilities for analysis of environmental control technologies and integrated environmental control systems involving pre-combustion, combustion, and post-combustion control methods. This new enhanced Macintosh version was delivered in May 1995.

The most recent version of the IECM, implemented for a computer using the Windows operating system was delivered to USDOE FETC at the end of the recent contract in May 1999. Although the model capabilities remained the same, the Windows environment provides a better user interface, improved performance, and stability.

Future work will consider additional technical capabilities such as boiler NO_x controls, gasifiers, and mercury control technologies. Although the current IECM model is capable of configuring a wide variety of power plant configurations, it is only capable of simulating one session at a time. Improved model capabilities being considered would expand this limitation to include (1) optimization of user-specified model parameters to meet a user-defined objective and (2) synthesis of user-specified technologies into an optimized flow sheet based on user-specified objectives. These enhancements have been effective and powerful tools with related DOE projects.

2. Base Plant

2.1. Introduction

This chapter summarizes new economic models developed for pulverized coal -fired power plants with subcritical steam cycles. The cost models described here apply to the "base power plant" without any of the environmental control options that are separately modeled in the IECM. While the purpose of the IECM is to model the cost and performance of emission control systems, costs for the base plant are also needed to properly account for pre-combustion control options that increase the cost of fuel, and affect the characteristics or performance of the base plant. Base plant costs are also needed to calculate the internal cost of electricity, which determines pollution control energy costs. Originally, a simple exponential scaling model was used in the IECM to relate the base plant cost to plant size. The new models described here provide additional parameters for estimating base plant cost variations with key emission control design parameters based on more recent cost data.

The new cost models relate the capital costs to process parameters and the costs of labor and materials. These models reflect the most recent EPRI cost estimates. The capital cost models developed have been disaggregated by process area. The main factors that affect the capital cost of the base plant are the plant size, the coal rank, and the geographic location of the plant. The capital cost models are anchored to the base capital cost for a specific unit size and are adjusted to other sizes using scaling factors based on cost data provided by EPRI (1993) for base plants of different sizes using different coal types. The variable O&M costs are calculated from the variable costs for fuel, water consumption and bottom ash disposal (from the furnace). The fixed O&M costs are based on maintenance and labor costs.

This chapter is organized as follows: The first section provides the mathematical form of the capital cost models used for parameterizing cost sensitivity to size and coal type. The second section provides a description of the cost data used for this study in terms of the main factors that affect the capital costs. It also provides the costs models developed for the IECM. The third section provides the O&M cost models. The final section provides a numerical example to illustrate the use of these cost models.

2.2. Capital Cost Models

The three main factors that affect the capital cost of a base plant are its capacity, in MW, (also referred to as size), the coal type, and the location of the plant. The capacity of the plant determines the size of the (boiler) furnace and hence the capital

cost. For a given capacity, the heating value and the ash content of the coal influence the dimensions of the furnace and ash handling equipment, also affecting capital cost.

The mathematical model used to describe the sensitivity of the capital cost models to parameter variations is normalized against the cost for a reference base case. The effect of coal type is treated discretely using coal rank (bituminous, sub-bituminous, or lignite) as another cost-related parameter. The cost models for each coal rank are disaggregated by process area and are parameterized to scale with size for each coal type. Table 2-1 provides a description of the process areas for the base power plants.

Table 2-1. ***Process Areas for Base Plant***

Process Area	Description
10	Steam Generator
20	Turbine Island
30	Coal Handling
40	Ash Handling
50	Water Treatment
60	Auxiliaries

The general form of the capital cost model *for a given coal type* is shown below:

$$\frac{PC_i}{PC_i^{/}} = \left(\frac{MW}{MW^{/}} \right)^{f_i} \qquad (2\text{-}1)$$

where

i	process area
PC_i	process area capital (M$)
$PC_i^{/}$	reference base case process area capital (M$)
MW	plant size (MW)
$MW^{/}$	reference case plant size
f_i	scaling exponent, dependent on coal rank.

The cost models presented below provide the value for the scaling exponent, f_i, for each coal type.

2.3. Cost Data and Capital Cost Models

The cost data used for model development is based on a cost study conducted by EPRI (1993) that evaluated the capital costs of pulverized coal (PC) fired power plants using supercritical and subcritical steam cycles. Since most commercial U.S. plants employ subcritical steam cycles, this chapter has excluded the study of supercritical and other advanced steam cycle designs. The EPRI data have also been adjusted to remove the cost elements for systems or equipment that are modeled separately in the IECM, such as flue gas desulfurization systems.

The first subsection provides a brief discussion of the regional factors used for normalization when comparing costs of plants at different locations. The second subsection provides the derived cost models for the IECM showing the effect of varying unit size and coal type on the cost of PC plants with subcritical steam cycles.

2.3.1. Regional Cost Factors

The location of a plant influences a number of cost parameters such as the labor wage rates, labor productivity, bulk material costs, and uniform building codes which differ across states. Regional factors from the EPRI TAG manual (1993) have been used to provide aggregate factors for six different regions of the U.S. These are shown in Table 2-2.

Table 2-2 ***Regional Cost Factors***

EPRI Region (Reference Location)	Factor
Northeast (PA)	1.0
Southeast (GA)	0.87
E/W Central (WI)	0.97
West Central (MO)	1.03
South Central (TX)	0.84
West (UT)	0.92

Note:
The Northeast location (PA) is treated as the reference case.

In order to compare the effect of unit size or coal type on plant cost, cost estimates need to be normalized to a common reference. In the following sections, all cost numbers are presented normalized to the Northeast reference. To get costs for any other location, the cost estimates presented in this chapter should be multiplied by the appropriate regional factor.

2.3.2. Effect of Plant Size

Two coal types were considered for the EPRI base case studies to examine the effect of plant size — a bituminous Pittsburgh seam coal and a sub-bituminous Wyoming coal from the Powder River Basin. An overview of the base case studies is shown in Table 2-3. Note that all costs in this chapter are in 1993 dollars. The costs for the 600 MW case is based on two 300 MW units.

Table 2-3 Reference Cases for PC Base Plant Costs

Case Name	Size (MW, net)	State Location	Coal Name
B1	200	PA	Pittsburgh
B2	300	PA	Pittsburgh
B3	400	PA	Pittsburgh
B4	500	PA	Pittsburgh
B5	600	PA	Pittsburgh
B6	200	WI	Wyoming
B7	300	TX	Wyoming
B8	500	WI	Wyoming
B9	600	WI	Wyoming

The process capital cost estimates (EPRI 1993) for each coal type are presented separately. We first present the cost data and evaluate the scaling exponent for Pittsburgh coal and then for Wyoming coal. Cost studies for size sensitivity of lignite coals were not available, thus, the scaling components used for lignite are the values derived for sub-bituminous coals.

The cost estimates for Pittsburgh coal disaggregated by process area are shown in Table 2-4. Note that M$ denotes millions of 1993 dollars.

Table 2-4 ***Process Capital Costs for the Pittsburgh Coal (PA location) (M$ 1993)***

Case Name (MW)	Area 10	Area 20	Area 30	Area 40	Area 50	Area 60
B1 (200)	80.81	60.51	29.86	10.17	6.036	22.1
B2 (300)	112.6	82.97	39.81	12.04	7.646	30.31
B3 (400)	143.3	104.4	49.07	13.61	9.084	38.15
B4 (500)	172.9	124.9	57.73	14.97	10.38	45.61
B5 (600)	208.3	153.5	66.95	20.25	12.86	56.07

The 300 MW plant(case B2) is used as the reference base plant and the cost for other sizes is scaled against these process area base costs. The scaling exponents are derived by solving Equation (2-1) for f_i , for each of the cases shown in Table 2-4. The scaling exponents derived from the sensitivity studies are shown in Table 2-5.

Table 2-5 ***Scaling Exponent f_i for Pittsburgh Coal***

Size (MW)	Area 10	Area 20	Area 30	Area 40	Area 50	Area 60
200	0.8174	0.7785	0.709	0.4159	0.5831	0.7785
400	0.84	0.8	0.727	0.4265	0.5992	0.8
500	0.84	0.8	0.7277	0.4269	0.5993	0.8
Average (< 500)	0.82	0.79	0.72	0.42	0.59	0.79
> 600	0.8875	0.8875	0.75	0.75	0.75	0.8875

Notice that the average value for the scaling component is computed only over the 200-500 MW range. The 600 MW plant consists of two units of 300 MW each, so

the scaling component for sizes 600 and greater is treated separately. Since sensitivity studies for other bituminous coals are not available, *these scaling factors are used for all bituminous coals.* Note however, that the actual base cost (M$) for a 300 MW plant varies slightly for each bituminous coal type as shown in Table 2-6.

Table 2-6 ***Cost Estimates for 300 MW Plant by Coal Type (PA Location) (M$ 1993)***

	Pgh	Ill# 6	KY	Utah	WV
Area 10	112.6	115.1	105.3	113.6	111.7
Area 20	82.97	81.37	74.21	82.65	81.37
Area 30	39.81	45.91	39.28	43.79	39.58
Area 40	12.04	15.55	13.24	14.43	11.91
Area 50	7.646	7.58	7.239	7.482	7.579
Area 60	30.31	30.04	28.73	29.66	30.04

The cost data for Wyoming sub-bituminous coal is presented next with similar scaling exponents derived for the cost model. The cost data disaggregated by process area is presented in Table 2-7. Note that since the plants corresponding to these cases are in different regions of the U.S., the cost numbers have been normalized to an equivalent plant in PA (the reference location) using the regional location factors shown earlier in Table 2-2.

Table 2-7 ***Cost Estimates for Wyoming Coal (PA location) (M$ 1993)***

Size	Area 10	Area 20	Area 30	Area 40	Area 50	Area 60
200	87.28	59.34	43.74	11.07	5.957	21.91
300	114.5	74.73	56.35	12.66	7.326	29.04
500	186.7	122.4	84.56	16.29	10.25	45.21
600	224.9	150.5	98.06	22.03	12.69	55.58

Since the cost data for the 200, 500 and 600 MW size plants are for the same location (see Table 2-3) we use the 200 MW size plant (instead of the location-adjusted 300 MW plant) as the reference case. The scaling exponents for the Wyoming sub-bituminous coal are provided in Table 2-8.

Table 2-8 ***Scaling Exponents for Wyoming Coal***

Size	Area 10	Area 20	Area 30	Area 40	Area 50	Area 60
300	0.6686	0.5685	0.6249	0.3319	0.5104	0.6944
500	0.83	0.7905	0.7194	0.422	0.5923	0.7905
Average (< 500)	0.75	0.67	0.67	0.37	0.56	0.74
600	0.8616	0.8473	0.7349	0.6267	0.6885	0.8473

Once again the average value for the scaling component is computed only over the 200-500 MW range. The 600 MW plant consists of two units of 300 MW, so the scaling component for sizes 600 MW and greater is treated separately. *These scaling factors are used for all sub-bituminous coals.*

Cost estimates for different unit sizes for lignite coals were not provided in the EPRI study, therefore, it was not possible to calculate the scaling exponents for lignite coals. Instead, the scaling exponents derived for sub-bituminous coals were used for

lignite coals (lignite boilers are more similar to sub-bituminous than to bituminous units). Table 2-9 provides the capital cost estimates for a 300 MW base plant (i.e., assumed to be located in PA) using Texas lignite. The scaling factors for each process area, based on Table 2-8, are also provided.

Table 2-9 ***Cost Estimates for Lignite Coal (M$ 1993) and Scaling Exponents***

Size	Area 10	Area 20	Area 30	Area 40	Area 50	Area 60
300	131.1	74.73	73.22	23.53	7.32	29.04
Average (< 500)	0.75	0.67	0.67	0.37	0.56	0.74

The total capital requirement for a PC base plant is calculated as shown in Table 2-10. This includes the direct process capital costs and indirect costs associated with base power plants.

Table 2-10 ***Total Capital Requirement for Base Plant***

Component	Cost
Process Area Capital	
Steam Generator	PC_{10}
Turbine Island	PC_{20}
Coal Handling	PC_{30}
Ash Handling	PC_{40}
Water Treatment	PC_{50}
Auxiliaries	PC_{60}
Total Process Capital	$PC=PC_{10}+PC_{20}+PC_{30}+PC_{40}+PC_{50}+PC_{60}$
General Facilities *	0.10 PC
Eng. & Home Office Fees *	0.064 PC
Process Contingency *	0.003 PC
Project Contingency *	0.1167 PC
Total Plant Cost *	TPC=1.284 PC
Total Plant Investment (including AFUDC) *	TPI=1.103 TPC‡
Preproduction Cost *	0.02 TPI
Inventory Capital *	0.00034 TPI
Royalty *	0.00045 TPI
Total Capital Requirement *	TCR=1.00279 TPI
* These items show the model default values for indirect cost factors. The IECM allows these factors to be changed by the user. ‡ Based on a 4.1% cost escalation, 9.2% interest rate and 5 years construction.	

2.4. O&M Cost Models

The O&M costs for the base power plant consists of fixed costs and variable costs. The fixed operating cost consists of labor, maintenance labor, material, and administrative labor. A mathematical model for the fixed cost is provided by Equation (2-2).

$$
\begin{aligned}
FOM &= FOM_{labor} + FOM_{maint} + FOM_{admin} \\
FOM_{labor} &= labor \times N_{labor} \times 40 \text{ (hrs/week)} \times 52 \text{ (weeks/yr)} \\
FOM_{maint} &= 0.02\times C_{10} + 0.013\times C_{20} + 0.026\times C_{30} \\
&\quad + 0.046\times C_{40} + 0.013\times C_{50} + 0.013\times C_{60} \\
FOM_{admin} &= 0.07\times (FOM_{labor} + FOM_{maint})
\end{aligned}
\qquad (2\text{-}2)
$$

where,

FOM	=	fixed operating and maintenance cost, M$/yr
FOM_{labor}	=	operating labor, M$/yr
FOM_{maint}	=	maintenance material costs, M$/yr (coefficients based on EPRI TAG). 35% of these costs are allocated to maintenance labor and the rest to maintenance material.
FOM_{admin}	=	administrative costs (assumed to be 7% of total labor costs) M$/yr.
C_i	=	total plant cost for process area i based on default values in Table 2-10. This gives Ci = 1.284 PCi, i = (10,20,30,40, 50,60)
N	=	total number of laborers (at 40 hrs/week), (default 60)
labor	=	labor rate ($/hr), (default 23.4)

The variable costs include the fuel cost, water costs (used for the steam cycle), and bottom ash disposal cost. The fuel cost is based on the rate of coal use which, in turn, depends on the size of the plant. The ash disposal cost is proportional to the bottom ash generated. The variable operating and maintenance cost is given by:

$$
\begin{aligned}
VOM &= VOM_{coal} + VOM_{water} + VOM_{ash} \\
VOM_{coal} &= C_{coal} \times M_{coal} \times H_{yr} \\
VOM_{water} &= C_{water} \times M_{water} \times MW_{yr} \\
VOM_{ash} &= C_{ash} \times M_{ash} \times H_{yr}
\end{aligned}
\qquad (2\text{-}3)
$$

Where

H_{yr}	=	cf x 8760[1], operating hours per year
MW_{yr}	=	H_{yr} x MW, MW operating hours per year
cf	=	capacity factor, fraction
VOM	=	variable operating costs, M$/yr

[1] 8760 is the total number of hours in a year (24x365)

VOM_{coal} = fuel (coal) costs, M$/yr

VOM_{water} = water consumption costs, M$/yr

VOM_{ash} = ash disposal costs, M$/yr

M_{coal} = coal consumption, tons/hr

M_{water} = water consumption, gallons/MWh (default = 1000)

M_{ash} = bottom ash disposed, tons/hr

C_{coal} = as-delivered coal cost, $/ton

C_{ash} = bottom ash disposal cost, $/ton, (default 10.24)

C_{water} = water cost, $/gallon, (default = 0.7 per 1000 gallons)

2.5. A Numerical Example

The capital and O&M costs of a PC power plant of size 450 MW (net) operating at a 65% capacity factor using Illinois #6 bituminous coal have been estimated. The location of the plant is assumed to be in Kenosha, WI. The reference 300 MW base case cost for Illinois coal disaggregated by process area for the reference location of PA is provided in row 1 (from Table 2-3). The cost of locating in WI is shown in row 2 and is derived by multiplying the process area cost for the 300 MW base case by the scaling factor, 0.97, found in Table 2-2.

Table 2-11 ***Process Area costs for Example Reference Plant (M$ 1993)***

	Area 10	Area 20	Area 30	Area 40	Area 50	Area 60
300 (PA)	115.1	81.37	45.91	15.55	7.58	30.4
300 (WI)	111.7	78.93	44.54	15.08	7.35	29.14

2.5.1. Capital Costs

The scaleup in capital costs due to an increase in size from 300 MW to 450 MW would be calculated using the following template from Equation (2-1).

$$PC_i = PC_i^{/} \times \left(\frac{MW}{MW^{/}} \right)^{f_i}$$

For each process area, the base case process capital $PC_i^{/}$ for a 300 MW plant is shown in row 2 of Table 2-11 above. The scaling exponent for each process area is provided in Table 2-5 row 4 (bituminous coals). The process capital cost for each process area for a 450 MW plant would be calculates as shown:

$$PC_{10} = 111.7\,M \times \left(\frac{450}{300}\right)^{0.82} = 155.76\,M$$

$$PC_{20} = 78.93\,M \times \left(\frac{450}{300}\right)^{0.79} = 108.73\,M$$

$$PC_{30} = 44.54\,M \times \left(\frac{450}{300}\right)^{0.72} = 59.64\,M$$

$$PC_{40} = 15.08\,M \times \left(\frac{450}{300}\right)^{0.42} = 17.88\,M$$

$$PC_{50} = 7.35\,M \times \left(\frac{450}{300}\right)^{0.59} = 9.34\,M$$

$$PC_{60} = 29.14\,M \times \left(\frac{450}{300}\right)^{0.79} = 40.14\,M$$

$$\text{Total Process Capital (PC)} = \sum PC_i = 391.49\,M\$$$

$$\text{General Facilities (GFC)} = 0.10 \times 391.49 = 39.15\,M\$$$

$$\text{Eng. \& Home Office (EHO)} = 0.064 \times 391.49 = 25.06\,M\$$$

$$\text{Process Contingency } (C_{proc}) = 0.003 \times 391.49 = 1.17\,M\$$$

$$\text{Project Contingency } (C_{proj}) = 0.1167 \times 391.49 = 45.69\,M\$$$

$$\text{Total Plant Cost (TPC)} = \sum \left(PC + GFC + EHO + C_{proc} + C_{proj}\right) = 502.56\,M\$$$

$$\text{Total Plant Investment (TPI)} = 1.03 \times 502.56 = 554.32\,M\$$$

$$\text{Preproduction Costs} = 0.02 \times TPI = 11.09\,M\$$$

$$\text{Inventory Capital} = 0.00034 \times TPI = 0.19\,M\$$$

$$\text{Royalty} = 0.00045 \times TPI = 0.25\,M\$$$

$$\text{Total Capital Requirement} = 565.85\,M\$ = 1256\,\$/kW$$

2.5.2. Fixed O&M Costs:

The fixed O&M costs are calculated using Equation (2-2). The formulae from Equation (2-2) reproduced here with appropriate numeric values. Text is provided in brackets next to each number to explain the source of these numbers. Note that the total plant cost for each process area (denoted by C_i) is calculated as $C_i = 1.284\ PC_i$.

$$\begin{aligned}
FOM_{labor} &= \text{labor}\,(23.4\,\$/hr)\times N_{labor}\,(60\,\text{laborers}) \\
&\quad \times 40\,(\text{hrs/week})\times 52\,(\text{weeks/yr}) \\
&= 2.92\ \text{M\$/yr} \\
FOM_{maint} &= 0.02\times 199.9\,(C_{10}) + 0.013\times 139.6\,(C_{20}) \\
&\quad + 0.026\times 76.6\,(C_{30}) + 0.046\times 22.96\,(C_{40}) \\
&\quad + 0.013\times 11.99\,(C_{50}) + 0.013\times 51.5\,(C_{60}) \\
&= 9.69\ \text{M\$/yr} \\
FOM_{admin} &= 0.07\times(2.92\,(FOM_{labor}) + 9.689\,(FOM_{maint})) = 0.88\ \text{M\$/yr} \\
FOM &= 2.92\,(FOM_{labor}) + 9.69\,(FOM_{maint}) + 0.88\,(FOM_{admin}) \\
&= 13.49\ \text{M\$/yr}
\end{aligned}$$

2.5.3. Variable O&M Costs:

The variable O&M costs are calculated using Equation (2-3). The formulae from Equation (2-3) reproduced here with appropriate numeric values. Text is provided in brackets next to each number to explain the source of these numbers. Some of the variables such as coal consumption and bottom ash disposed are calculated using the IECM and provided as inputs to the model presented here. This is denoted by (IECM) in brackets.

$$\begin{aligned}
VOM_{coal} &= 35.75\{C_{coal}\ \$/\text{ton}\}\times 219.3\{M_{coal}\ \text{ton/hr}\} \\
&\quad \times 5694\{H_{yr}\ \text{IECM}\} \\
&= 44.68\ \text{M\$/yr} \\
VOM_{water} &= 7\times 10^{-4}\{C_{water}\ \$/\text{gallon}\}\times 10^{3}\{M_{water}\ \text{gallon/Mwh}\} \\
&\quad \times 450\times 5694\{MW_{yr}\ \text{IECM}\} \\
&= 1.79\ \text{M\$/yr} \\
VOM_{ash} &= 9.36\{C_{ash}\ \$/\text{ton}\}\times 8.83\{M_{ash}\ \text{tons/hr}\} \\
&\quad \times 5694\{H_{yr}\ \text{IECM}\} \\
&= 0.47\ \text{M\$/yr} \\
VOM &= 44.68\{VOM_{coal}\} + 1.79\{VOM_{water}\} + 0.47\{VOM_{ash}\}
\end{aligned}$$

2.5.4. Electricity Cost

The cost of electricity is calculated by levelizing the total capital requirement (TCR) and the total (fixed + variable) O&M costs on a per kWh basis. This done by using a fixed charge factor (fcf) for levelizing the TCR by assuming a 30 year life cycle of a power plant, and a O&M levelization factor (vclf). The algorithms for calculating these levelization factors are incorporated in IECM and the numbers used for the example here are based on the IECM. The calculation for cost of electricity is shown below:

$$E_{cost}\ (\text{mills/kWh}) = (\text{fcf} \times \text{TCR} + \text{vclf} \times \text{O\&M})/\text{MW}_{yr}$$

$$= (0.0877 \times 391.5 + 1.0 \times 60.4) \times 10^6 / (450 \times 0.65 \times 8760)$$

$$\approx 44\ \text{mills/kWh}$$

2.6. Sensitivity Analysis

The base plant cost models have been parametrized by cost and coal rank. Figure 2-1 below provides the total capital requirement (normalized in $/kW) for six U.S. coals (Table 2-12), and illustrates the economies of scale as a function of power plant size. Similarly, Figure 2-2 provides the total levelized electricity cost (in mills/kWh) for a base plant with no environmental controls. All costs are in constant 1993 dollars.

Figure 2-1 *Normalized base plant capital cost as a function of plant size for several coal types. All costs in constant 1993 dollars.*

Figure 2-2 *Levelized electricity cost (mills/kWh) as a function of plant size and coal type. All costs in constant 1993 dollars.*

Table 2-12 ***Characteristics of U.S. Coals Used for Sensitivity Analysis***

	App.MS	App.LS	Ill#6	WPCU	WPRB	NDL
HHV (Btu/lb)	13260	13080	10900	11240	8340	6020
Carbon (%)	73.81	73.87	61.22	64.20	48.18	35.04
Hydrogen (%)	4.88	4.75	4.20	4.60	3.31	2.68
Oxygen (%)	5.41	6.27	6.02	5.80	11.87	11.31
Chlorine (%)	0.07	0.06	0.17	0.01	0.01	0.09
Sulfur (%)	2.13	0.66	3.25	0.58	0.37	1.16
Nitrogen (%)	1.42	1.46	1.16	1.16	0.70	0.77
Ash (%)	7.23	10.08	11.00	11.00	5.32	15.92
Moisture (%)	5.05	5.79	13.00	7.54	30.24	33.03
Cost ($/ton)	32.07	36.94	29.49	27.18	12.46	12.22

2.7. References

Electric Power Research Institute (1993). Cost Studies for Pulverized Coal-Fired Power Plants. Data provided by Dr. C. McGowin.

Electric Power Research Institute (1993). TAG Technical Assessment Guide, Vol. 1: Electricity Supply - (Revision 7)

3. Selective Catalytic Reduction

3.1. Introduction to SCR Technology

Selective catalytic reduction (SCR) is a process for the post-combustion removal of NO_x from the flue gas of fossil-fuel-fired power plants. SCR is capable of NO_x reduction efficiencies of up to 80 or 90 percent. SCR technology has been applied for treatment of flue gases from a variety of emission sources, including natural gas- and oil-fired gas turbines, process steam boilers in refineries, and coal-fired power plants. SCR applications to coal-fired power plants have occurred in Japan and Germany. Full-scale SCR systems have not been applied to coal-fired power plants in the U.S., although there have been small-scale demonstration projects.

Increasingly strict NO_x control requirements are being imposed by various state and local regulatory agencies in the U. S. These requirements may lead to U.S. SCR applications, particularly for plants burning low sulfur coals (Robie et al., 1991). Furthermore, implicit in Title IV of the 1990 Clean Air Act Amendment is a national NO_x emission reduction of 2 million tons per year. Thus, there may be other incentives to adapt SCR technology more generally to U.S. coal-fired power plants with varying coal sulfur contents. However, concern remains over the applicability of SCR technology to U.S. plants burning high sulfur coals or coals with significantly different fly ash characteristics than those burned in Germany and Japan. There is also concern regarding the application of SCR to peaking units due to potential startup and shutdown problems (Lowe et al., 1991).

3.2. Process History and Development

SCR was invented and patented in the U.S. in 1959. It was used originally in industrial applications. In the 1970's, SCR was first applied in Japan for control of NO_x emissions from power plants. Japan was the first country to make widespread use of this technology in response to national emission standards for NO_x. In Japan, SCR has been applied to gas, oil, and coal-fired power plants. There were over 200 commercial SCR systems operating on all types of sources in Japan in 1985. The Japanese SCR systems tend to run at moderate NO_x removal efficiencies of 40 to 60 percent (Gouker and Brundrett, 1991). By 1990, a total of 40 systems had been installed on 10,852 MW of coal-fired power plants (Lowe et al., 1991).

Germany currently imposes more stringent NO_x emission standards than Japan. To meet the emission requirements, SCR has been adopted and applied to many coal-fired power plants. SCR will be required as a retrofit technology on a total of 37,500 MW of existing capacity. As of 1989, SCR had been applied in 70 pilot plants and

28 full scale retrofit installations, with the latter totaling 7,470 MW of hard coal-fired capacity (Schönbucher, 1989). By 1990, more than 23,000 MW of capacity were fitted with SCR systems (Gouker and Brundrett, 1991). These plants typically burn low sulfur coals (0.8 to 1.5 percent sulfur) with 0.1 to 0.3 percent chlorine. SCR has been retrofitted to power plants with both wet and dry bottom boilers, with variations on the location of the SCR system. As of 1989, 18 installations involve placement of the SCR system between the economizer and air preheater, while the remaining involve "low dust" or "tail-end" placement of the SCR downstream of the FGD system. Two of the high-dust retrofits involve wet bottom boilers (Schönbucher, 1989). In 1991, 129 systems were reported to have been installed on a total of 30,625 MW of coal-fired capacity (Lowe et al., 1991). The recent German progress in installing retrofit SCR systems is shown graphically in Figure 3-1.

The process environment for SCR in Germany is typically more demanding than that in Japan, with the requirement for higher NO_x removal with higher flue gas sulfur and ash loadings (Gouker and Brundrett, 1991). In both Japan and Germany, the SCR systems are not operated during startup or shutdown (Lowe et al., 1991).

SCR is being applied in the U.S. for NO_x control of natural gas and oil-fired gas turbine-based power generation systems. In 1990 SCR was installed at a total of 110 gas turbine units totaling 3,600 MW (May et al, 1991). While the operating environment for these systems is not as demanding as for coal-fired power plant applications, some of these applications do provide experience with systems firing sulfur-bearing fuels that encounter problems analogous to those anticipated in coal-based applications. In particular, ammonium salt formation and downstream effects have been studied (Johnson et al, 1990).

Recently, a number of U.S. projects for coal-fired applications of SCR technology have been initiated. These include, for example, a U.S. Department of Energy Clean Coal Program funded demonstration of SCR at Gulf Power Company's Plant Crist (DOE, 1992). SCR systems have also been permitted for two coal-fired cogeneration plants to be built in New Jersey (Fickett, 1993).

Since the 1970's, the cost of SCR has dropped substantially. For example, the levelized cost of SCR dropped by a factor of 3 in Japan within a 6 year period, while in recent years costs in Germany have dropped by an additional factor of 2. These improvements are due in part to the international competition among catalyst suppliers. SCR catalysts are available from manufacturers in Japan, Germany, and the U.S. U.S. manufacturers, such as Grace, expect improvements in catalysts to continue, resulting in potential further drops in capital and operating costs. For example, Grace is testing a new catalyst design that is expected to lead to a 50 percent increase in catalyst activity while also increasing catalyst life (Gouker and Brundrett, 1991).

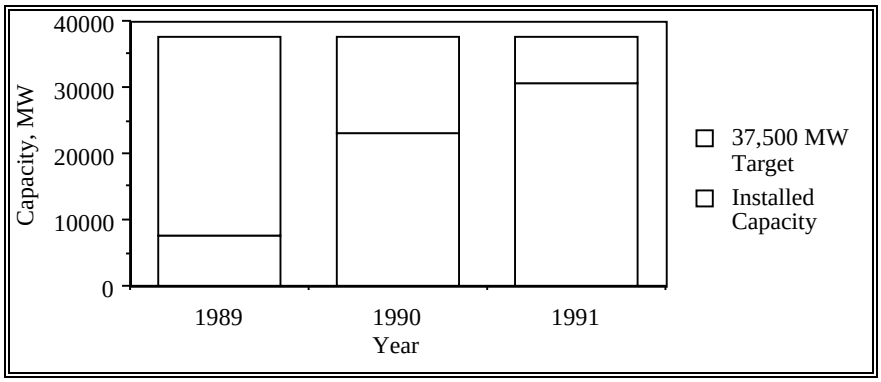

Figure 3-1 Targeted and Actual Installed Retrofit SCR Capacity in Germany

SCR has not yet been used commercially on coal-fired power plants in the U.S. The experience in Germany, which includes boiler types similar to those in the U.S., provides useful data for predicting SCR performance and cost in the U.S. However, U.S. coals, such as eastern bituminous coals, typically have a higher sulfur content than that of German coals. In addition, fly ash compositions may vary significantly. These differences lead to concerns about maintenance of catalyst activity and potential difficulties downstream of SCR reactors, such as deposition of ammonia salts.

The German experience is particularly useful for U.S. planners because German SCR systems are subject to a more relevant range of flue gas conditions than typical Japanese systems. For example, slagging wet bottom boilers produce different flue gas and flyash characteristics that can significantly affect catalyst performance (Offen et al, 1987).

3.3. Process Design

The general design considerations for the SCR NO_x control technology for coal-fired power plants are described here. These include the placement of the SCR system in a power plant, and a description of equipment associated with the SCR process area.

3.3.1. SCR Integration in the Power Plant

The SCR system can be located in several places in the coal-fired power plant flue gas stream (Schönbucher, 1989; Behrens et al, 1991). A key limitation of SCR systems is the operating temperature requirement. The operating temperature window for SCR systems is typically from approximately 550 to 750°F. Several possible locations are illustrated inFigure 3-2. These are:

1. "Hot-side" and "high-dust" SCR, with the reactor located between the economizer and the air preheater. In this configuration, shown in Figure 3-2a, the SCR is located upstream of a cold-side ESP and, hence, is subject to a high fly ash or "dust" loading. At full-load, the economizer outlet temperature is typically around 700°F. An economizer bypass is required to supply hot gas to the SCR during part-load operating conditions, in order to maintain the proper reaction temperatures (Lowe et al, 1991).
2. "Hot-side, low-dust" SCR, which features placement of the SCR system downstream of a hot-side ESP and upstream of the air preheater and FGD systems. This configuration has been employed in some Japanese coal-fired power plants, such as Takehara Power Station Unit 1 in Hiroshima (Behrens et al, 1991). This configuration has the advantage of minimizing the fly ash loading to the SCR catalyst, which leads to degradation in catalyst performance.
3. "Cold-side" or "Tail-end" placement of the SCR system downstream of the air preheater, particulate collector, and FGD system. This system minimizes the effects that flue gas contaminants have on SCR catalyst design and operation, but requires a gas-gas flue gas heat exchanger and duct burners to bring the flue gas up to reaction temperature (Lowe et al, 1991).

The most common configurations envisioned for U.S. power plants are the hot-side high-dust and post-FGD tail-end systems (Robie et al, 1991), with high-dust systems predominating. These are the two most common configurations employed in German coal-fired power plants retrofitted with SCR.

Recent German experience indicates increasing acceptance for tail-end systems. Prior to 1987, the number of high-dust installations was twice that of tail-end installation. But since 1987, the number of tail-end installations has been slightly greater. The tail-end systems have tended to be installed on smaller plants, however, and account for about one-third of total installed capacity. They have been preferred for wet bottom boiler applications (Lowe et al, 1991).

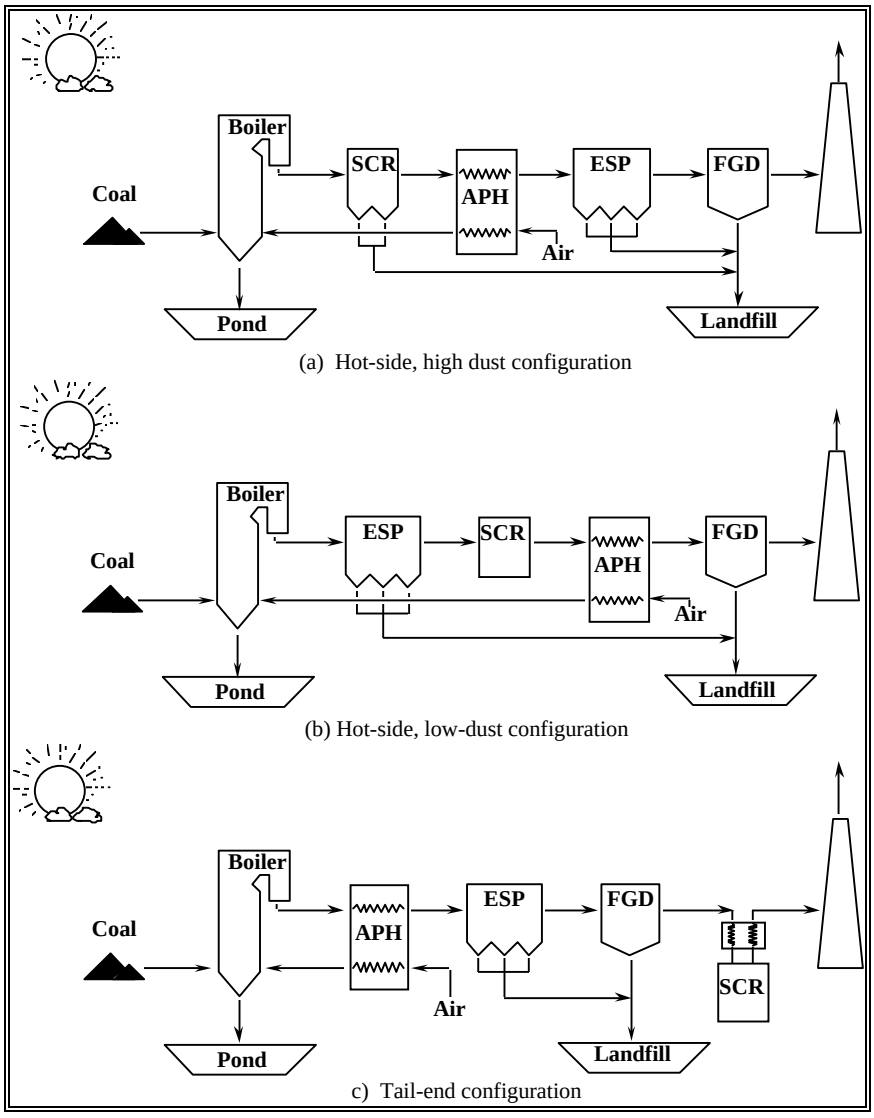

Figure 3-2 Alternative Placements of SCR systems in Coal-Fired Power Plants

In many evaluations, tail-end SCR systems have been charged with the full cost of flue gas reheat, even though a portion of the reheat would be necessary to maintain stack buoyancy for flue gas exiting the FGD system. Similarly, in comparing hot-side and tail-end systems, the significant efficiency penalty for the high-dust system when operating at part load, due to the need for economizer bypass, must be considered (Lowe et al, 1991).

3.3.2. The SCR Process Area

A schematic of the SCR system is given in Figure 3-3. The schematic assumes an SCR location in the hot-side, high-dust configuration. Ammonia is injected into the flue gas upstream of the SCR reactor vessel. The ammonia/flue gas mixture enters a reactor vessel, containing SCR catalyst. The catalyst promotes the reaction of ammonia and NO_x to form nitrogen and water vapor. Products of the SCR reactions may form ammonium sulfate or bisulfate, which can deposit on downstream equipment. Additional air preheater water washing is expected to be required to remove such deposits.

The SCR system consists primarily of a reactor housing containing catalyst material, an ammonia storage and handling system, an ammonia injection system, and a control system. In additional, air preheater wash water pretreatment may be required to remove ammonia from the wastewater.

A more detailed schematic of the SCR reactor housing is shown in Figure 3-4. SCR design philosophy has evolved over the last 20 years due to the accumulation of operating experience in Japan and Germany. Based on Japanese experiences, both vendors and users of SCR technology have identified the following key design considerations for hot-side SCR systems (Lowe et al, 1991):

- Vertical downward flue gas flow to prevent ash accumulation and to allow ash drop out.
- Linear gas velocities of 16-20 ft/sec at maximum continuous rating to prevent ash accumulation. Higher velocities would be expected to increase catalyst erosion.
- Use of grid shaped catalyst with channel spacing (pitch) of 7 to 7.5 mm to allow passage of dust and prevent ash accumulation and erosion.
- Elimination of catalyst seams along the gas flow direction to prevent ash accumulation and erosion.

Figure 3-3 Schematic Diagram of SCR System

Figure 3-4 Diagram of SCR Reactor Housing with Downward Flue Gas Flow

- Use of a "sacrificial" or dummy initial stage to prevent ash accumulation and erosion in downstream active catalyst layers.
- Removal of deposited ash using intermittent vacuuming or soot-blowing.
- Reliable ammonia feed control, including part load operation.
- Adequate ammonia feed distribution across the cross sectional flue gas flow area.
- Flue gas ducting and guide vane designs that ensure good mixing of the flue gas and ammonia feed.

Most of these features are illustrated in Figure 3-4.

A tail-end SCR system is illustrated in Figure 3-5 to show the configuration of the gas-gas heat exchanger and duct burner. The flue gas exiting the FGD system must be heated from approximately 130°F to a reaction temperature of approximately 625°F. The flue gas exiting the SCR can be cooled to a stack temperature near 225°F. Flue gas from the FGD system is preheating with flue gas exiting the SCR

system in a heat exchanger. The SCR inlet flue gas is then heated to reaction temperature using a duct burner.

3.3.2.1. Catalyst

SCR catalysts typically consist of a ceramic honeycomb substrate, a metal "carrier" and active components dispersed by the carrier on the honeycomb surfaces. A typical carrier is titanium dioxide (TiO_2). Vanadium pentoxide (V_2O_5) and tungsten trioxide (WO_3) are commonly used as active components for hot-side SCR applications (Schönbucher, 1989). WO_3 provides thermal and mechanical stability to the catalyst (Behrens et al, 1991). Catalysts based on titanium dioxide are best suited for operating temperatures of 280 to 400°C (536 to 752°F) (Schönbucher, 1989). At lower temperatures, catalyst activity drops substantially. At higher temperatures, catalyst material phase transition occurs, which causes irreversible activity loss (Bauer and Spendle, 1984). Catalysts using activated carbon may be employed for lower temperature applications near 100°C (212°F) (Schönbucher, 1989). The actual catalyst formulations which are offered commercially are closely held propriety information.

A key innovation from Japanese development of SCR technology has been the switch from noble metal oxides to base metal oxides for use as catalyst carrier materials, which has reduced many of the major problems associated with oil- and gas-fired flue gas applications. For coal applications, Japanese catalyst development also focused on improving catalyst geometry. To avoid plugging and erosion, parallel flow honeycomb and plate catalysts were developed. By the early 1980's, ceramic honeycomb and plate configurations have been developed that provide high surface areas while reducing the tendency for flyash plugging. In recent years, research has focused on understanding the deactivation mechanisms of SCR catalyst, particularly due to alkalis and trace metals such as arsenic (Gouker and Brundrett, 1991).

Figure 3-5 Schematic Diagram of Tail-End SCR System

V_2O_5 is the component which controls the reactivity of the catalyst. However, it also catalyzes the conversion of SO_2 to SO_3 (Behrens et al, 1991), which may lead to opacity, ammonium salt deposition, or acid condensation problems downstream. For high-sulfur coal applications, the amount of V_2O_5 is minimized by homogeneous distribution throughout the catalyst. To obtain NO_x reduction, properly mixed ammonia and NO_x must enter micropores in the catalyst, which are the active sites for the reactions which consume NO_x.

The catalyst is typically installed in a reactor housing in three layers, with provision for a dummy layer for flow straightening and distribution. In some designs, provision is also made for a fourth active catalyst layer. In these cases, the initial catalyst charge consists of three active layers. When catalyst activity drops to the design value, a fourth active layer is added. Then the four layers are changed out periodically to maintain overall catalyst activity. Catalyst modules may be loaded and unloaded from the reactor housing using a fork-lift track assembly and/or rollers (e.g., Behrens et al, 1991)

Ceramic, homogeneous, honeycombed catalyst elements approximately 6 inches square can be extruded to a length of about 39 inches (Behrens et al, 1991). SCR systems subject to high-dust loadings often include a dummy honeycomb or leading edge to control catalyst erosion (Lowe et al, 1991). Catalyst honeycomb design depends on the location of the SCR system in the power plant. For high-dust systems, catalysts with a large pitch (spacing within honeycomb cells) are employed, to allow passage of fly ash. For low dust systems, smaller pitch catalysts can be used (Schönbucher, 1989). These catalyst designs are illustrated in Figure 3-6.

3.3.2.2. Ammonia Handling

In Germany, strict safety standards have been applied to the shipment and handling of ammonia. Shipments by truck are not permitted if they are larger than 500 liters. Thus, anhydrous ammonia is shipped primarily by rail. A 15 to 30 day supply is typically stored at the plant in two double wall tanks. Double walled piping is also typically employed. The ammonia is diluted to an 8 percent mixture prior to introduction to the flue gas. The ammonia is vaporized in German facilities using warm water. In many U.S. gas turbine installations, electrical heating is used (Lowe et al, 1991).

3.4. Technical Overview

This section presents a detailed technical overview of SCR NO_x control technology for coal-fired power plants, with particular focus on the effects of flue gas components on catalyst performance and the effects of the SCR system on the power plant.

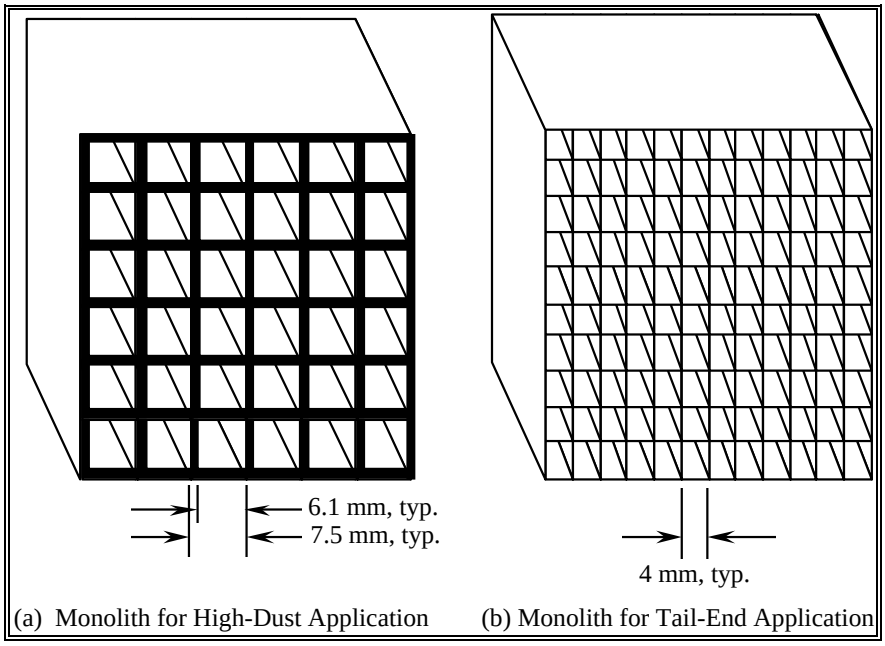

Figure 3-6 SCR Honeycomb Catalyst Monolith Designs

3.4.1. Process Chemistry

Nitrogen oxides in the flue gas are removed by reduction of NO_x by ammonia to nitrogen and water. The reduction occurs in the presence of a catalyst. Ammonia is injected in the flue gas upstream of the catalyst, as illustrated in Figure 3-3.

The principle reactions are:

$$4NH_3 + 6NO \rightarrow 5N_2 + 6H_2O$$

$$8NH_3 + 6NO_2 \rightarrow 7N_2 + 12H_2O$$

$$4NH_3 + 4NO + O_2 \rightarrow 4N_2 + 6H_2O \qquad (3\text{-}1)$$

$$4NH_3 + 2NO_2 + O_2 \rightarrow 3N_2 + 6H_2O$$

Of these reactions, Equation (3-1) is usually the most important. There is usually sufficient oxygen in the flue gas as a reactant. In addition, typically 90 to 95 percent of nitrogen oxides in the flue gas are in the form of NO.

Another overall reaction that may occur in the SCR unit is (Anderson and Billings, 1991):

$$2NH_3 + NO + NO_2 \rightarrow 2N_2 + 3H_2O \qquad (3\text{-}2)$$

The implication of the above reaction is that a molar ratio of ammonia to NO_x of 1:1 is sufficient to remove both NO and NO_2 when the NO/NO_2 mixture contains more than 50 percent NO.

Another important reaction occurring in the SCR reactor is the oxidation of sulfur dioxide:

$$2SO_2 + O_2 \rightarrow 2SO_3$$

Typically, 0.5 to 2 percent of the sulfur dioxide entering the SCR reactor is oxidized to sulfur trioxide (e.g., Bauer and Spendle, 1984). The resulting increased levels of sulfur trioxide at the SCR outlet increases the acid dewpoint of the flue gas, thus increasing the potential for sulfuric acid condensation on downstream components at temperatures of less than about 350°F. Sulfur trioxide may react with water vapor to form sulfuric acid (Johnson et al, 1990):

$$SO_{3(g)} + H_2O_{(g)} \leftrightarrow H_2SO_{4(g,l)}$$

where subscripts (g), (l), and (s) represent gas, liquid, and solid phases, respectively.

Unreacted ammonia exiting the SCR system ("ammonia slip") can react with sulfur trioxide to form compounds such as ammonium bisulfate and ammonium sulfate that deposit on downstream equipment. These compounds may result in plugging and corrosion. The key reactions for the formation of ammonium sulfate and bisulfate are (Johnson et al, 1990):

$$NH_{3(g)} + SO_{3(g)} + H_2O_{(g)} \leftrightarrow NH_4HSO_{4(l.,s)}$$

$$2NH_{3(g)} + SO_{3(g)} + H_2O_{(g)} \leftrightarrow (NH_4)_2SO_{4(l,s)} \qquad (3\text{-}3)$$

The formation of ammonium bisulfate (Equation (3-3)) is more sensitive to sulfur trioxide concentration than to ammonia concentration (Lowe et al, 1991).

As the flue gas cools in downstream equipment, the sulfuric acid may also react with ammonia to form condensate products (Johnson et al, 1990):

$$NH_{3(g)} + H_2SO_{4(g)} \leftrightarrow NH_4HSO_{4(l,s)}$$

$$2NH_{3(g)} + H_2SO_{4(g)} \leftrightarrow (NH_4)_2SO_{4(l,s)}$$

Reducing the ammonia slip and reducing the formation of sulfur trioxide can minimize the formation of ammonium bisulfate and other ammonia salts.

The key design considerations for SCR are the NO_x removal efficiency, the ammonia slip, and the SO_2 oxidation rate. While larger catalyst volumes allow higher NO_x removal efficiencies and/or lower ammonia slip, they tend to increase the oxidation

of SO_2. Furthermore, large catalyst volumes significantly increase the capital and annual costs of SCR.

3.4.2. Catalyst Sizing

A key performance issue associated with SCR systems is the required catalyst volume and the catalyst replacement schedule. One parameter often used to measure catalyst volume is the space velocity, which is given by:

$$SV = G_{FG} / V_c$$

An alternative parameter is the area velocity, which is given by:

$$AV = G_{FG} / V_c$$

The relationship between the space velocity and area velocity depends on the "geometric ratio" of the catalyst, which is the unit surface area per unit volume of the catalyst.

$$R_g = \frac{A_c}{V_c}$$

For honeycomb monolith catalysts, the important design parameter that determines the geometric ratio is the "pitch," or spacing between the hollow cells through which the flue gas passes. As described earlier, the catalyst pitch depends primarily on the dust loading in the flue gas. Larger pitches are needed to accommodate high-dust loadings, resulting in a lower geometric ratio. Current catalysts for high-dust application typically have a pitch of around 7.5 mm, with a wall thickness of 1.4 mm and a channel thickness of 6.1 mm. For tail-end applications, pitches of around 4 mm are typical. For gas-fired applications, pitches of 3 mm are reported using ceramic plate-type catalysts. Catalyst using thin metal substrates may have a pitch as low as 0.2 mm for clean flue gas applications (Gouker and Brundrett, 1991).

The space velocity is commonly used to describe the catalyst requirement. However, both the space velocity and area ratio, or the space and area velocities, are needed in order to specify both the catalyst volume and the catalyst area in contact with the flue gas. For example, a high-dust SCR system typically requires a smaller space velocity (more catalyst) than a low-dust system, due primarily to the lower area ratio of the high-dust catalyst designs.

The space velocity is a function of the desired NO_x removal efficiency and the required ammonia slip. For example, one EPRI paper suggests a maximum space velocity of 2,500/hr for a NO_x reduction efficiency of 80 percent and an ammonia slip of 5 ppm (Damon et al, 1987).

Based on German experience, typical space velocities for high-dust SCR systems with honeycomb catalysts of about 7 mm pitch are 2,000 to 3,000/hr, whereas for tail-end systems employing honeycomb catalysts with pitches of approximately 4 mm space velocities are 4,000 to 6,500/hr. Thus, 50 to 60 percent smaller catalyst volumes per unit flue gas flow can be installed on tail-end systems for equivalent NO_x removal performance. However, the flue gas volumetric flow rate may be higher for tail-end systems than for high-dust systems, partially offsetting this advantage (Lowe et al, 1991).

The actual required catalyst volume for a given application depends on a number of site-specific factors. The amount of plugging or catalyst poisoning will determine the effective catalyst activity. The activity will decrease with operating time. Therefore,

the initial catalyst volume must be large enough so that at the end of the design life there is sufficient active catalyst to maintain design performance levels.

Most SCR designs have a three layer catalyst. Although most U.S. SCR studies assume that all catalyst layers are changed out simultaneously, most Japanese and German designs are based on periodic replacement of only one catalyst layer at a time. Therefore, at any given time, there may be three layers with differing lengths of service and differing activity levels. In determining the initial catalyst charge, it is necessary to account for the loss of catalyst activity at the design point in the catalyst replacement scheme. For a three layer catalyst, the design point is the fourth catalyst change out.

To determine the catalyst activity at the design point, it is necessary to estimate the loss of catalyst activity as a function of time. Catalyst activity loss is a function of the catalyst formulation and geometry, the operating conditions associated with the flue gas, including temperature and composition, and the loading and composition of the fly ash. Recent papers, such as those presented at the 1991 Symposium on Stationary NO_x Control, provide examples of catalyst activity loss curves for specific power plant applications in Germany (e.g., Behrens et al, 1991; Gouker and Brundrett, 1991; Maier and Dahl, 1991).

3.4.3. Catalyst Fouling and Poisoning

Commercial operating experience in both Germany and Japan have provided insight into the mechanisms for catalyst fouling and poisoning. For coal-fired power plant applications, the primary cause of loss of catalyst activity was attributed to interactions between the catalyst and the flyash. As summarized by Gouker and Brundrett (1991), flyash has several effects on the catalyst, including:

- Fouling: Sub-micron ash particles may accumulate on the surfaces of the catalyst, and block the pores of the catalyst. This fouling or masking prevents NO_X and ammonia from reaching active catalyst sites, thereby reducing the effective catalyst surface area. This leads to a reduction in the performance of the catalyst.
- Plugging: Bulk plugging of the catalyst occurs when large accumulations of dust occur. Dust plugging may occur, for example, when large pieces of flyash on upstream equipment "flake" off. Wire screens located upstream of the catalyst help to break up these flakes. Soot blowing may also be required periodically to remove the flakes from the catalyst.
- Poisoning: Alkali metals from flyash are a source of catalyst poisoning. Water soluble alkali salts may be leached onto the catalyst due to moisture present on fly ash during startup or shutdown of the SCR unit. Alkali salts have been shown to form inactive complexes with vanadium and tungsten in laboratory studies.
- Erosion: Erosion problems may arise due to flue gas flow distribution problems. Flow straightening vanes and dummy "catalyst" layers have been employed in many installations to reduce this type of problem.

3.4.3.1. Japanese and German Experience

Due to improvements in catalyst technology, catalysts in Germany are not experiencing as much loss of activity as initially predicted based on Japanese high-dust, coal-fired applications (Gouker and Brundrett, 1991).

Behrens et al (1991) report that the typical levels of potential catalyst poisons in the flyash of Ruhr coal have "not appeared to significantly accelerate catalyst deterioration" of the hot-side high-dust SCR unit at the Reuter West power station. These contaminant levels include 4 to 5 percent K_2O, 6.3 percent of CaO, 1.5 percent of MgO, and 0.6 percent of P_2O_5. However, data reported by them does indicate that catalyst activity decreased to 65 percent of the level of the fresh catalyst after 30,000 hours.

At the Aichi 40 MW coal-fired boiler burning low sulfur coal, a hot-side high-dust SCR arrangement is employed. The catalyst has experienced low deterioration. After 30,000 hours of operating, the catalyst activity is 75 percent of the fresh catalyst. The primary cause of deactivation is reported to be the deposition of CaSi on the catalyst surface (Behrens et al, 1991).

While arsenic is commonly cited as the most significant catalyst poison, small sticky dust particles can cause more serious deactivation than arsenic. Furthermore, in some cases, SCR fires due to dust accumulations have occurred in Japan (Lowe et al, 1991).

German experience with SCR catalyst indicates that catalyst "lifetimes" of 3 to 4 years are possible and typical for high-dust systems. For tail-end systems, some operators report no measurable catalyst degradation, and expect to achieve up to 80,000 operating hours on a single catalyst charge. Japanese experience on clean flue gases has been similar (Lowe et al, 1991).

In many German wet bottom boilers, fly ash is recirculated to the boiler in order to slag the ash. Arsenic tends to concentrate preferentially in the fly ash during this process by 10 to 100 times compared to cases where no fly ash recirculation is used. A study of 14 wet bottom plants indicates that the actual arsenic concentration obtained in the flue gas is not monotonically proportional to the coal arsenic concentration, but may depend also on the calcium content of the flyash. Calcium oxide in the fly ash tends to produce arsenic, leading to higher arsenic concentrations in the fly ash and lower gaseous arsenic concentrations in the flue gas. This reduces the effect of arsenic as a catalyst poison. However, calcium can also "blind" the catalyst, if it does not react with arsenic (or perhaps other species). Hence, for flue gases where arsenic is not present, Japanese experience has been that fly ash calcium oxide contents of less than 1 percent permit long catalyst lives (e.g., 38,000 hours) while higher calcium contents of 5 to 8 percent result in shorter lives of less than 25,000 hours. For high sulfur coals that yield a gypsum ($CaSO_4 \cdot 2H_2O$) component in the fly ash, the deactivation of catalyst is less pronounced (Lowe et al, 1991).

3.4.3.2. Laboratory Studies of Poisons

A laboratory study by Chen et al (1990) examined the effect of several catalyst poisons on a laboratory-manufactured sample of 5 percent V_2O_2 catalyst on a TiO_2 carrier. Both catalyst pellets and a ceramic substrate honeycomb catalyst were evaluated. The specific catalyst poisons that were evaluated include five alkali oxides (Li_2O, Na_2O, K_2O, Rb_2O, and Cs_2O) and four additional compounds CaO, PbO, P_2O_5, and As_2O_3. In the experimental work, maximum catalyst activity was observed in the 200 to 300°C (392 to 572°F) temperature range. Commercial catalysts also include WO_3 as a component, which allows increased catalyst activity at higher temperatures of 300 to 400°C (572 to 752°F).

U. S. coals, and especially eastern bituminous coals, contain relatively high concentrations of alkali metals. Thus, the effects of alkali and alkaline earth metal oxides on catalyst are important in these applications. Catalyst activity was shown to decrease as the amount of alkali metal dopant was increased in the laboratory tests. The strength ordering of the alkali oxide poisons corresponds to their basicity, with Cs_2O having the most pronounced effect. The deactivation may occur due to acid-

base reactions forming alkali-vanadium compounds (e.g., $NaVO_3$). The poisoning due to CaO is weaker than that of the alkali metals. The basicity of CaO is also weaker than the weakest alkali oxide tested, Li_2O. Lead oxide, although a strong poison for automobile catalytic converters, is less important than the top three alkali metal oxides in deactivating the catalyst.

Although arsenic is often cited as the major catalyst poison concern, the experimental results of Chen et al (1990) indicate that As_2O_3 is a substantially weaker catalyst poison than the alkali metal oxides Na_2O, K_2O, Rb_2O, and Cs_2O. P_2O_5 was also found to be a relatively weak poison.

However, the poisoning effect of both As_2O_3 and P_2O_5 are temperature dependent, with increased catalyst deactivation at lower temperatures. P_2O_5 poisoning leads to the formation of phosphate on the catalyst surface, which changes the catalyst surface active properties, and the blockage of surface area and pores. In spite of its relatively low poisoning activity, As_2O_3 may be a more notable poison because it is often found in gaseous form, whereas many of the potentially stronger alkali metal oxides are contained in the molten coal ash.

SO_2 entering the SCR reactor is a precursor to the formation of SO_3, ammonium sulfates, and sulfuric acid. Under certain conditions, ammonium sulfate may deposit on the catalyst, leading to catalyst deactivation. However, SO_2 alone has shown a promoting effect on catalyst activity. Formation of surface sulfates on the catalyst may promote the acidity of the surface. The work of Chen indicates that poisoning is associated with increasing basicity of the catalyst due to other contaminants.

Chloride species may have either poisoning or promoting effects on the catalyst. The poisoning effects of chlorides are much weaker than those of the corresponding oxides of the same metals (e.g., NaCl and Na_2O). In fact, the chlorine atom has a promoting effect, while the alkali metal atom has a poisoning effect, with a net poisoning for NaCl and KCl. KCl is a stronger poison than NaCl, analogous to the metal oxide K_2O being stronger than Na_2O.

HCl appears to react with ammonia to form NH_4Cl, which consumes ammonia and reduces ammonia available for NO_x conversion. It also deposits on the catalyst at temperatures below 340°C (644°F). HCl also appears to react with lower vanadium oxides, which are formed by reduction with ammonia, to form VCl_4 and VCl_2, which are red-brown and green liquids, respectively. Some chlorides, such as Cu_2Cl, act as an SCR catalyst, which may be attributable to its acidity.

In a later study, Chen et al (1991) also added WO_3 to the catalyst formulation, yielding catalyst samples more representative of commercial offerings. They performed a set of tests with the same poisons as described above. WO_3 was found to improve catalyst activity and the resistance of catalyst to poisoning. However, similar qualitative results were obtained. Alkali compounds had the most pronounced effect in proportion to their basicity. Lead, arsenic, and phosphorous were also found to be weaker poisons than the strong alkali compounds tested. The addition of SO_2 decreased the activity of the WO_3 formulation catalyst, although when doped with alkali activity increased. Similar results were obtained for chloride related effects. In cases where vanadium chlorides form, catalyst activity will decrease.

The results of both studies (Chen et al, 1990; Chen et al, 1991) were not intended to identify the interactive simultaneous effects of multiple catalyst poisons in combination with masking or plugging, such as would occur in an actual flue gas. The purpose was to identify purely chemical mechanisms for catalyst poisoning to provide insight into actual deactivation mechanisms. Deactivation studies on actual flue gas slip streams will be conducted as part of a cooperative pilot plant program between EPRI and selected utilities (Flora et al, 1991).

3.4.4. Catalyst Life

Catalyst "life" is often reported as the number of operating hours between complete replacement of all catalyst in an SCR reactor. In many papers, catalyst life is described as if it is a property of the catalyst. However, it is actually a design variable. For example, there are trade-offs between catalyst life, space velocity, and catalyst replacement scheduling. In actual installations in Germany and Japan, the catalyst is installed in multiple layers and only one layer is replaced at a time according to a schedule.

In earlier EPRI-sponsored studies (e.g., Bauer and Spendle, 1984), the implicit assumption was that all catalyst would be replaced simultaneously at the end of a specified time interval. This leads to unnecessarily high operating costs. Japanese catalyst vendors and German SCR operators have both reported on the economic benefits of phased catalyst replacement schemes (e.g., Appendix B of Bauer and Spendle, 1984).

In a recent EPRI study, Robie et al (1991) assume that a catalyst life of four years will be realized for U.S. coal-fired high-dust applications. They also assume the same life for tail-end applications even though there are clear differences in operating environments for the two cases. This type of assumption may unnecessarily penalize the tail-end configuration when in fact the major benefit of this configuration is a decrease in catalyst activity loss over time.

3.4.5. Catalyst Disposal

In Japan and Germany, spent catalyst is returned to the manufacturer. In Japan, catalyst manufacturers have not found it economical to regenerate the catalyst, and the catalyst is often simply disposed of (Lowe et al, 1991). It is likely that spent catalyst would be classified as a hazardous waste in the U.S.

3.4.6. Impacts on Other Plant Components

SCR has effects on other components of the power plant, particularly for high-dust designs. According to Robie et al (1991), the main impacts are on the boiler, air heater, and induced draft fan. Other components affected are the FGD process, FGD reheat system, waste disposal system, and water treatment system. These impacts are summarized below.

- Air Preheater. Air preheater modifications are required due to the deposition of ammonium sulfates and bisulfates. Heat transfer surfaces must be replaced with heavier gauge metal and, in some cases, modified design surfaces. Additional water wash capability is required for air preheater cleaning. High pressure soot blowers are also required at both the hot and cold ends of the air preheater. Air preheater leakage may increase.
- Boiler. Loss of thermal efficiency results from air preheater modifications and, at part load operation, from an economizer bypass, which is required to maintain the reaction temperature in the SCR unit.
- Induced Draft Fan. In a new plant, a larger ID fan is required to overcome the pressure drop in the SCR reactor and any other incremental pressure drops associated with downstream effects. This pressure drop may be up to 11 inches of water.

- Forced Draft Fan. The forced draft fan for the combustion inlet air to the air preheater will have a higher mass flow rate due to increased air preheater air leakage.
- Stack. The increase in the SO_3 concentration of the flue gas could result in increased opacity of the flue gas plume if the SO_3 is not removed in the FGD system. Acid condensation would also be a potential source of concern.
- ESP. Because of the lower operating pressure of the ESP due to the pressure drop of the SCR system, higher flue gas temperature, and increased flue gas mass flow due to air preheater leakage and gases introduced for ammonia injection, the ESP will be required to handle a higher volumetric flow rate. In a new plant, therefore, a larger ESP will be required. The ESP may require additional reinforcement due to the lower, and negative, operating pressure. Although the SO_3 content of the flue gas will increase, the beneficial effect of this on ESP performance may be offset by the increase in flue gas temperature. Ammonium salt precipitation in the fly ash could improve agglomeration and reduce reentrainment.
- Ash Disposal/Reuse. Ammonia compounds contained in fly ash material decompose and release ammonia at elevated pH. Even at lower pH, ammonia fixation with alkaline species could result in an ammonia odor problem. Flyash containing ammonia compounds may not be suitable for use in cement manufacturing.
- Water Treatment. Water treatment in addition to typical plant waste water treatment is required to covert nitrogen species in the air preheater wash water to free nitrogen.
- FGD/Reheat. Because of the higher flue gas inlet temperature and mass flow rate, there will be an increase in the water evaporation rate for wet limestone systems. In addition, steam would be required for reheat. The FGD liquor recirculation rate may need to be increased to maintain the same SO_2 removal efficiency. Alternatively, reheat can be accomplished using flue gas duct burners.
- Auxiliary Power Consumption. The net plant output will be decreased by the electricity required to operate SCR process equipment. In addition, during times of soot blowing, the plant efficiency will be decreased slightly due to the use of process steam. Steam is also used for ammonia vaporization, and dilution air for ammonia injection is taken from the discharge of the primary air fans.

The effects of the tail-end SCR system are not as significant as for the high-dust configuration. The tail-end SCR will result in auxiliary power consumption, flue gas pressure drop, water washing of the reheat gas/gas heat exchanger and associated wash water treatment, increased requirement to eliminate mist carryover from the FGD system, and stack effects due to increased SO_3 concentration and higher stack temperatures. In addition, a duct burner may be required. Sootblowers and ash collection hoppers are not required for the SCR system in the tail-end configuration. In the tail-end configurations, separate dedicated dilution air fans are used for ammonia injection (Robie et al, 1991).

For tail-end systems, the leakage rate of the gas-gas heat exchanger used for reheat has been reported to be as high as 7 percent in German facilities. Such leakage allows untreated flue gas to leak into the treated gas prior to stack discharge, thereby effectively bypassing the SCR system.

3.4.7. SO_2 Oxidation

In the U.S., flue gases have typically higher SO_2 and SO_3 concentrations than experienced in Japan and Germany due to the predominance of high sulfur coals in many regions of the country. The oxidation of SO_2 leads to downstream effects such as ammonium sulfate and bisulfate formation and acid condensations as previously described. Sulfur trioxide and sulfuric acid formed downstream of the SCR can also lead to attack of duct liners. The formation of these condensates and deposits depends critically on the presence of ammonia and sulfur trioxide in the flue gas. However, to minimize this type of problem in U.S. applications may require optimization of catalysts for specific U.S. markets (Lowe et al, 1991).

According to data reported by Bauer and Spendle (1984), SO_2 oxidation is primarily a function of catalyst formulation, space velocity, and operating temperature.

3.4.8. Ammonia

A portion of the ammonia injected into the SCR system may pass through the reactor unchanged. Ammonia in the flue gas may react chemically or physically with other constituents of the flue gas, including fly ash. This may lead to maintenance and operational problems. Several key concerns are discussed further.

3.4.8.1. Ammonia Injection

In commercial SCR systems, a critical design issue is the injection of ammonia into the flue gas upstream of the SCR reactor. A key difficulty in ammonia injection is obtaining a uniform mixture of ammonia in the flue gas. Failure to achieve proper ammonia injection and mixing can lead to channeling of ammonia through the SCR system, resulting in high levels of ammonia slip through the SCR reactor and to downstream components in the flue gas path.

Obtaining a uniform distribution of the injected ammonia in the flue gas upstream of the SCR catalyst is often difficult. Flue gas flow modeling and flow straightening devices are often needed to understand and achieve proper flow distribution. Ammonia injection systems typically consist of 30 to 40 injection points per square meter. These injection nozzles are controlled either singly or in groups of several, and the flow of ammonia through them can be optimized to achieve a reasonably uniform ammonia distribution (±10-30 percent) in the flue gas. However, dust deposits on or around the nozzles can lead to plugging of some or alteration of the flue gas flow pattern. Thus, the flow patterns may change over time and require periodic checking and adjustment (Lowe et al, 1991).

3.4.8.2. Ammonia Retention in Catalyst

Some SCR catalysts may retain ammonia during operation. The ammonia is then released during transients or shut downs. This desorption process may take up to eight hours, based on currently known experience. The ammonia injection rate during low temperature operation should be adjusted to compensate for offgasing of ammonia from the catalyst to maintain ammonia slip within tolerable levels. Because of the absorption/desorption phenomena, changes in NO_x emissions may lag changes in the ammonia injection rate by 30 minutes (Lowe et al, 1991).

Control problems under load swing conditions, exacerbated by the time-lag phenomena, remain an issue, particularly for potential U.S. high sulfur coal applications (Lowe et al, 1991).

3.4.8.3. Effects on Air Preheater

The most common effect of ammonia slip that is discussed in the literature is the deposition of ammonium sulfates on downstream equipment. However, commercial operation has not always substantiated this concern. For example, in the Takehare Power Station Unit 1, featuring hot-side SCR downstream of a hot side ESP, no additional air preheater washings have been necessary during 34,000 hours of SCR operation. The SCR operates at 80 percent removal efficiency with a NO_x loading of 300 ppm. The lack of plugging of the air preheater by ammonium salts, even in spite of SCR inlet SO_2 concentrations of 1,000 to 1,500 ppm, is attributed to low NH_3 slip levels. These have been 0.2 ppm or less. SO_3 conversion was typically 0.08 to 0.21 percent (Behrens et al, 1991).

The high-dust hot-side SCR system in the Reuter West power station in Berlin, Germany has operated over 15,000 hours on coals with sulfur contents up to 1.2 percent. The typical NO_x removal efficiency is 85 percent with an ammonia slip of 1.5 ppmvd and an SO_2 conversion rate to SO_3 of about 0.5 percent (Behrens et al, 1991). No plugging of the air preheater is reported and no washing of the air preheater has been necessary since SCR startup. The SCR catalyst layers receive a weekly sootblowing.

In one German power plant, Neckar (1989) reports that approximately 5 percent of the ammonia leaving the SCR system is deposited as an ammonium salt in the air preheater, with typically about 50 percent of the ammonia absorbed onto fly ash. The ammonium salts are easily soluble in water, and can be washed. As water washing in the air preheater proceeds, the concentration of ammonia in the exiting water stream decreases. Wash water with a high ammonia concentration must be treated to remove the ammonia prior to entering the regular plant wastewater treatment system. Neckar suggests that the initial wash water with a high ammonia concentration can be pretreated separately from the larger volume of water with a low ammonia concentration, which may be suitable for direct feed to the existing waste water treatment plant.

In pilot plant testing of an SCR system, Shiomoto and Muzio (1986) report that ammonia entering the preheater tends to deposit on air preheater surfaces as solid ammonium compounds or to be absorbed onto fly ash. Furthermore, SO_3 in the flue gas is consumed in the formation of ammonium sulfate or bisulfate, and also was absorbed onto fly ash. The investigators report that essentially all of the gaseous SO_3 entering the air preheater during testing was removed from the flue gas.

The effects of deposits include fouling of heat transfer surfaces and increase of pressure drop in flue gas paths. These types of effects may be more pronounced during process upsets (Lowe et al, 1991).

3.4.8.4. Ammonia Absorption by Flyash

Another concern regarding ammonia slip has emerged in Germany. German experience has been that the typical Japanese criteria of 5 ppm maximum ammonia slip is often not stringent enough to permit commercial use of fly ash as a byproduct. Therefore, in many German installations ammonia slip must be limited to 3 or even 1 ppm (Lowe et al, 1991). Schönbucher (1989) reports that ammonia slip must be limited to 2 ppm to produce a byproduct fly ash acceptable to the cement industry.

Although ammonia does not alter the physical properties of concrete made from fly ash, ammonia captured in the fly ash is released during concrete mixing and may result in a noticeable odor. For ammonia concentrations of less than 60 mg per kg of fly ash, the odor is not noticeable. For the Altback/Deizisau power station Unit 5 in Germany, it appears that 20 to 80 percent of the ammonia slip is captured in the fly ash, with a mean value near 50 percent (Neckar, 1989).

Experimental studies by Shiomoto and Muzio (1986) indicate that most of the ammonia leaving the SCR system exits as a gas, with very little in the form of solid compounds or absorbed by fly ash. However, a portion of the gaseous ammonia is absorbed by flyash downstream of the SCR reactor, with higher ammonia partial pressures leading to increased absorption.

3.4.8.5. Ammonia Slip and Tail-End Systems

For tail-end systems, ammonia slip is not a significant concern because of the low concentration of sulfur in the flue gas. Therefore, the constraints on catalyst performance are less severe, allowing potentially greater degradation in catalyst activity (and associated increase in ammonia slip) before replacement is required. Ammonia slip constraints for tail-end systems are typically imposed by air emissions regulations, as opposed to downstream process requirements. Ammonia slip as large as 20 to 30 ppm is not expected to lead to operational problems in tail-end systems. Ammonia odor and plumes become noticeable when the ammonia concentration exceeds 50 ppm (Lowe et al, 1991). Ammonium salt deposition is expected to occur in the gas-gas heat exchanger used for flue gas reheat in tail-end SCR systems. Thus, heat exchanger water washing is also required in this case.

3.4.9. U.S. Outlook

Because the German and Japanese experiences cannot be directly applied to U.S. applications, EPRI and others are involved in pilot testing of SCR systems on selected slipstreams, analogous to the German testing of over 70 SCR pilot systems. These tests will provide additional data regarding cost and technical feasibility of SCR applied to plants firing domestic medium and high sulfur coals. EPRI will conduct as many as 14 separate tests (Lowe et al, 1991).

In the short term, low-dust tail-end SCR systems hold the most promise of reliable performance for high sulfur coal applications. This type of system would avoid the potentially excessive rate of air preheater fouling and catalyst deactivation that might otherwise be experienced in a high-dust configuration in high sulfur service (Lowe et al, 1991).

There are 105 operating cyclone units in the U.S. totaling over 26,000 MW. These are high NO_x emission technologies which are not easily amenable to combustion NO_x control. The typical NO_x emission rates for these units ranges from 0.8 to 1.8 lb/MMBtu, corresponding to flue gas concentrations of 500 to 1,100 ppm. Many of these units are also located in the Midwestern U.S., which is the major source of utility acid rain emissions. Thus, these boilers would appear to be a prime target for application of tail-end SCR systems (Lowe et al, 1991).

3.5. Performance Models

In this section, analytical performance models of SCR systems are presented. These include performance models for high-dust, hot-side and tail-end, low-dust SCR systems. For the hot-side system, downstream effects on the power plant air preheater are modeled. For the tail-end system, a gas-gas heat exchanger and duct burner used for flue gas reheat are modeled.

3.5.1. Catalyst Requirement

The catalyst requirement is a complex function of the physical and chemical properties of the catalyst, catalyst geometry, catalyst replacement philosophy,

reaction temperature, flue gas volumetric flow rate, flue gas characteristics such as NO_x concentration, ash concentration, ash composition, SO_2 concentration, gaseous poisonous species concentration (e.g., As_2O_3), the desired NO_x removal efficiency, allowable flue gas pressure drop, and the desired ammonia slip. The latter in turn affects downstream precipitation of solids, such as ammonium sulfate and bisulfate, and, hence, affects air preheater design in hot-side SCR systems.

Although a catalyst requirement model ideally would be sensitive to all of the above factors, insufficient data are available to support the development of such a model. For example, the interactive poisoning effects of multiple flyash constituents is not well-understood. Therefore, the approach taken here is to develop a model of intermediate detail that captures the key functional dependencies between catalyst requirement and process conditions. The model is based on empirical and design assumptions supplied by the user and power plant performance parameters calculated from the power plant performance model.

A number of theoretical models were reviewed as a possible basis for model development. In most cases, these models were not adopted directly here, but were used to identify key functional dependencies that could be modeled based on empirical data.

3.5.1.1. Factors Affecting Catalyst Requirement

In a report prepared by Shiomoto and Muzio (1986), there is an appendix containing comments by Kawasaki Heavy Industries, a Japanese manufacturer of SCR systems. KHI presents the development of a simplified equation for estimating catalyst space velocities based on NO_x removal efficiency, ammonia slip, linear velocity, reaction temperature, and catalyst activity. The functional form of this equation is a basis for the performance model developed here.

The simplest model of an SCR system for the purpose of determining catalyst requirement is based on a rate model for the chemical reaction of NO with NH_3, which is the predominate reaction occurring in the SCR reactor. Under the condition of an NH_3/NO_x molar ratio of 1.0, pilot plant testing in Japan has shown that a first order reaction occurs:

$$\frac{d[NO_x]}{dt} = -k[NO_x]$$

Integration of this equation yields the following relation between flue gas residence time in the catalyst and NO_x removal efficiency:

$$t = \frac{-\ln(1-\eta_{NO_x})}{k}$$

The catalyst space velocity is related to flue gas residence time in the catalyst by the following:

$$SV\ (1/hr) = \frac{3{,}600\ \text{sec}/hr}{t\ (\text{sec})}$$

Therefore, the catalyst space velocity is given by:

$$SV = \frac{3600\ \text{k}}{-\ln(1-\eta_{\text{NO}_x})} \qquad (3\text{-}4)$$

The rate constant, k, corresponds to the so-called catalyst "activity." The catalyst activity is a complex function of catalyst geometry, chemical formulation, and operating conditions.

In the typical case where the NH_3/NO_x molar ratio is less than 1.0, the apparent catalyst activity will be less than the actual catalyst activity. This is because the reaction between NH_3 and NO_x is 1:1, while for molar ratios of less than 1, the active sites populated with ammonia molecules are fewer than the active sites sought by NO_x molecules. This is not a limitation of the catalyst, but rather a limitation due to the scarcity of NH_3.

To adjust for this phenomena, KHI developed an empirical correction factor based on the "end-mole ratio," which is the NH_3/NO_x molar ratio at the SCR reactor exit. The end-mole ratio is the molar ratio of ammonia slip to unreacted NO_x. Thus, Equation (3-4) becomes:

$$SV = \frac{3600\,C\,(r_e)_a}{-\ln(1-\eta_{NO_x})} \qquad (3\text{-}5)$$

The value of the exponent "a" is obtained empirically from test data obtained for constant conditions except for changes in NO_x removal efficiency and end-mole ratio. Data plotted by KHI suggest that a typical value of "a" is 0.3.

Equation (3-5) was used as the basis for a regression model for space velocity based on design data provided by KHI in an earlier SCR design study published by EPRI (Bauer and Spendle, 1984). The purpose of the regression model was to determine the adequacy of the simplified model of Equation (3-5) for use in an SCR performance model. The results are shown graphically in Figure 3-7.

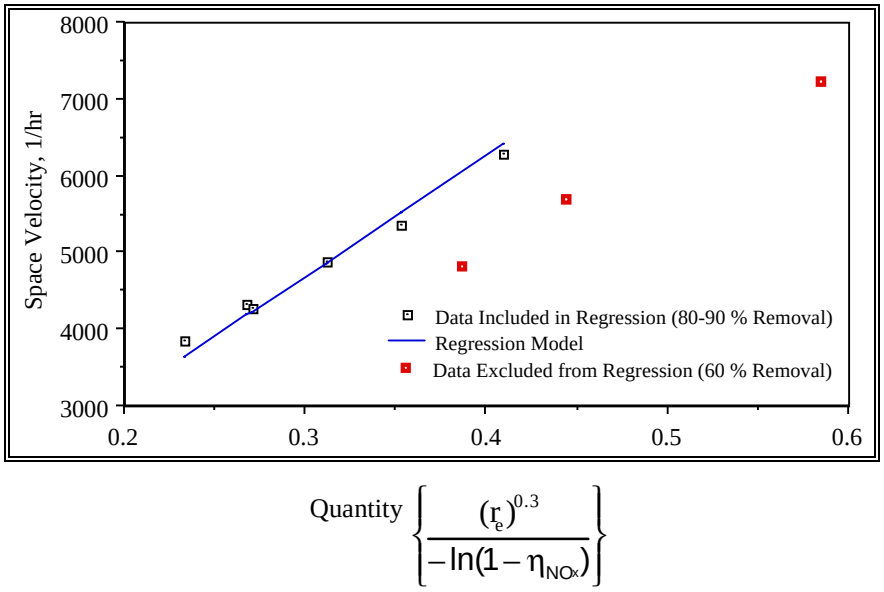

Figure 3-7 Regression Model of Space Velocity as a Function of NO_X Removal Efficiency and End-Mole Ratio

The regression analysis indicated that Equation (3-5) was valid for estimating space velocities for NO_x removal efficiencies of 80 and 90 percent, with varying end-mole ratios. However, the model could not also be applied simultaneously to the data for 60 percent NO_x removal. The results here suggest that the catalyst activities differ for the two sets of data. Bauer and Spendle (1984) do not report the design details, such

as linear velocity; therefore it is possible that design conditions were not the same for the two sets of data. Thus, it appears that the simple model of Equation (3-5) is a reasonable basis for correcting space velocity for differences in NO_x removal efficiency and end-mole ratio when all other factors are held constant.

To compare catalysts under different operating conditions, KHI suggests the following model:

$$\frac{\ln(1-\eta_2)}{\ln(1-\eta_1)} = C_r H_r \beta_r f_r W_r Q_r \left(\frac{m_2}{m_1}\right)^{0.3} \qquad (3\text{-}6)$$

From Equation (3-6), the performance of a specific catalyst may be estimated based on ratios of key performance parameters, assuming a reference catalyst. This formulation suggests that space velocity can be estimated based on a reference catalyst using multiplicative correction factors to adjust for differences in operating conditions.

Other models are possible, such as that reported by Chen et al (1991). The NO_x removal efficiency is estimated in this model based on detailed design information regarding the SCR catalyst, including catalyst geometry, film mass transfer coefficient, effective diffusivity, and reaction rate constant. However, data to support this detailed model are often not reported in published literature.

3.5.1.2. Model Form

The modeling approach adopted here is to assume a reference catalyst and to apply a series of multiplicative correction factors to adjust space velocity for different design conditions. The general formulation is:

$$SV = SV_{ref} \prod_{i=1}^{4} f_i$$

Each correction factor, f_i, is a ratio that reflects the difference in space velocity from the reference to design conditions due to differences in certain design parameters. If the reference and design conditions are the same, these correction factors have a value of unity. A total of four correction factors have been developed, based on: (1) NO_x removal efficiency; (2) end-mole ratio; (3) catalyst activity; and (4) reaction temperature.

Default reference conditions are included in the model. The reference parameters required include space velocity, NO_x removal efficiency, NO_x inlet concentration, ammonia slip concentration, a catalyst activity curve, a catalyst life, and an operating temperature.

NO_x Removal Efficiency

The correction factor for NO_x removal efficiency is based on the model formulation suggested by KHI. This correction factor is:

$$f_1 = f_{eff} = \frac{\ln(1-\eta_{ref})}{\ln(1-\eta)}$$

As the NO_x removal efficiency increases, the catalyst space velocity decreases, leading to a larger catalyst volume.

For tail-end SCR, a portion of the flue gas exiting the FGD system leaks across the gas-gas heat exchanger used for flue gas reheat. Therefore, a portion of the NO_x in the flue gas will also pass across the heat exchanger and into the stack gas. Because

of this, the NO_x removal efficiency in the SCR unit must be increased to compensate for the NO_x that bypasses the SCR system due to leakage. The required NO_x removal efficiency for the SCR system is calculated based on the overall NO_x removal efficiency required and the flue gas leakage rate across the gas-gas heat exchanger:

$$\eta = \frac{\eta_{overall}}{(1 - f_i)}$$

To satisfy this equation, the following constraint must be met:

$$\eta_{overall} + f_i \leq 1$$

This model assumes no additional NO_x formation in the duct burner.

End-Mole Ratio

The correction factor for end-mole ratio is based on the design ammonia slip, the design inlet NO_x concentration, and the design NO_x removal efficiency. The end-mole ratio is given by:

$$r_e = \frac{[NH_3]_{out}}{[NO_x]_{in}(1-\eta)}$$

The correction factor for end-mole ratio is given by:

$$f_2 = f_{r_e} = \left(\frac{r_e}{r_{e,ref}} \right)^{0.3}$$

Catalyst Activity

Experimental and commercial SCR operating data indicate that catalyst activity decreases with time, due to physical and chemical changes to the catalyst as previously discussed. The actual rate of catalyst activity deterioration depends on the operating conditions for the SCR reactor, and is usually not constant with time. Typically, there is an initial period of relative rapid catalyst deactivation, followed by a period of gradual activity change. A typical catalyst activity curve is shown schematically in Figure 3-8.

Schönbucher (1989) presents several curves for catalyst activity as a function of time for high-dust and tail-end SCR systems. For wet-bottom boilers with high-dust SCR, catalyst activity loss may range from 25 to 45 percent during the first 2,000 hours of operation, with less rapid changes during subsequent operation. For other applications, such as tail-end systems on wet or dry bottom boilers, catalyst activity loss is slight (e.g., 5 percent) over 10,000 hours of operation and appears to decrease at a relatively constant rate.

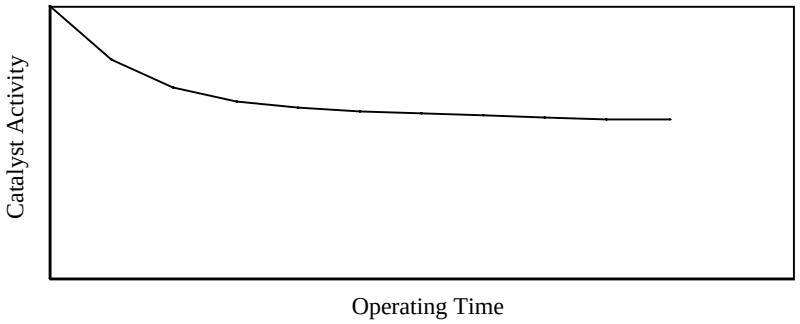

Figure 3-8 A typical Catalyst Activity Curve

To model catalyst activity loss, a simple function is employed to represent the catalyst activity curve. The purpose of this function is to provide a reasonable representation of the qualitative properties of catalyst activity loss for most cases. This function features two components: a minimum activity level and an exponential decay from the initial activity to the minimum activity levels. The initial activity is assumed to have a value of unity, while subsequent activity levels are relative to the initial activity.

$$A(t) = A_{\min} + A_{inc}\left\{\exp\left(-\frac{t}{\tau_a}\right)\right\} \qquad (3\text{-}7)$$

where:

$$A_{\min} + A_{inc} = 1$$

A model user specifies the minimum activity level, A_{min}, which determines the incremental initial catalyst activity, A_{inc}, that is subject to exponential decay. By also specifying one data point on the activity curve (an activity level $A(t_1)$ at time t_1), the activity decay time constant, t_a, can be estimated:

$$\tau_a = -\frac{t_1}{\ln\left(\frac{A(t_1) - A_{\min}}{A_{inc}}\right)}$$

For example, suppose we have a catalyst with a long term activity level of 75 percent of the initial value, and for which the measured activity after 8,000 hours was 85 percent of the initial activity. Then:

$$A_{\min} = 0.75$$

$$A_{inc} = 1 - A_{\min} = 0.25$$

$$\tau_a = -\frac{t_1}{\ln\left(\frac{A(t_1) - A_{\min}}{A_{inc}}\right)} = -\frac{8{,}000}{\ln\left(\frac{0.85 - 0.75}{0.25}\right)} = 8{,}730$$

and:

$$A(t) = 0.75 + 0.25\left\{\exp\left(-\frac{t}{8{,}730}\right)\right\}$$

This example is shown graphically in Figure 3-9. In addition, a case in which the minimum activity level is assumed to be zero is also shown, to illustrate the flexibility of Equation (3-7) for representing catalyst activity curves.

In typical SCR systems, multiple catalyst layers are employed. Furthermore, these catalyst layers are generally not replaced simultaneously. The overall catalyst relative activity in the case of multiple layers is the average of the individual catalyst layer relative activities (e.g., Nakabayashi and Abe, 1987). If we have N_c identical catalyst layers, and if each layer has been on-line for t_i hours at time t, then the average catalyst relative activity at any time t is given by:

$$A_{avg}(t) = \frac{1}{N_c}\sum_{i=1}^{N_c} A(t_i) \qquad (3\text{-}8)$$

However, we are usually interested in the activity at the design point of the catalyst, which corresponds to the activity level at the end of a catalyst layer replacement cycle. If we have N_c identical catalyst layers that are replaced one-at-a-time every t_r hours, the catalyst relative activity at the design point is:

$$A_{des} = \frac{1}{N_c}\sum_{i=1}^{N_c} A(i \cdot t_r) \qquad (3\text{-}9)$$

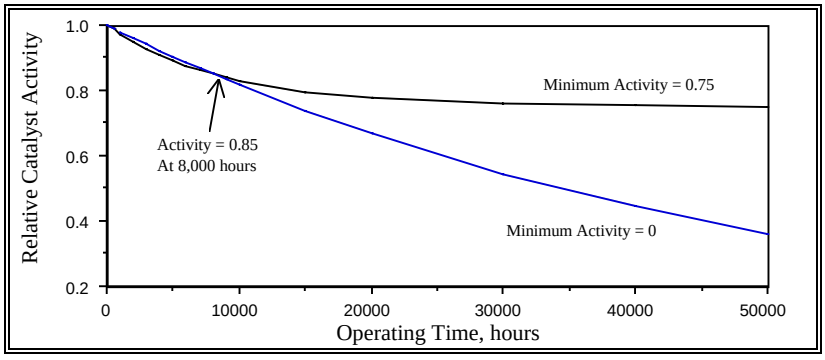

Figure 3-9 An example Catalyst Activity Curve

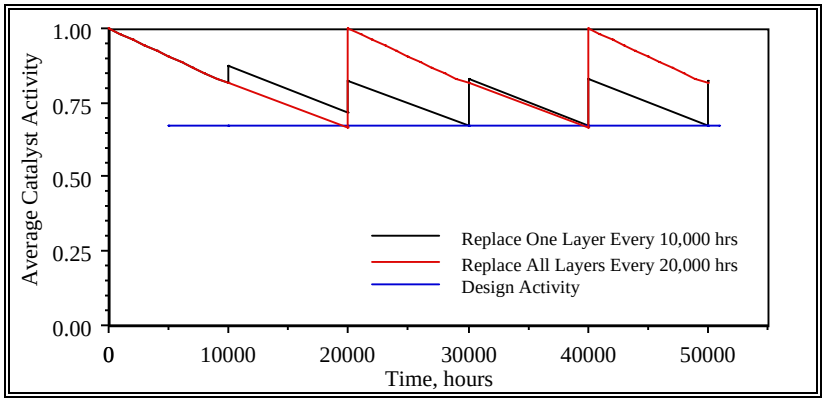

Figure 3-10 Illustrative Example of Average Catalyst Activity for a Three Layer Catalyst

The implications of Equations (3-8) and (3-9) are illustrated in Figure 3-10. In this figure, the instantaneous average catalyst activity of a three-layer catalyst is illustrated for two cases. The first case, shown in a solid line, assumes that one

catalyst layer is replaced every 10,000 hours, with a total time between complete catalyst replacements of 30,000 hours. The second case, shown as a dotted line, assumes that all catalyst layers are replaced simultaneously every 20,000 hours. For this particular illustrative case study, the design activity levels of both schemes are approximately the same. However, it is clear that by replacing individual layers sequentially, rather than simultaneously, the effective catalyst "life" is increased for a given volume of catalyst. In the illustrative example, catalyst life is 50 percent greater for the sequential replacement scheme compared to the simultaneous replacement scheme.

In the more general case, sequential replacement schemes may lead to larger initial catalyst volumes in order to achieve the same design activity as a simultaneous replacement scheme. For example, if we simultaneously replace all three catalyst layers in the illustrative problem every 10,000 hours, the design activity level would be approximately 80 percent. To achieve this design activity level with a sequential replacement scheme of one layer every 10,000 hours, the initial catalyst charge would need to be 20 percent larger, which increases capital costs. However, the annual costs associated with catalyst replacement would be reduced by 60 percent, because in the sequential scheme the same amount of catalyst is replaced in 24,000 hours as is required every 10,000 hours in the simultaneous replacement scheme. Thus, selection of a catalyst "life" design value involves trade-offs between capital and annual costs.

Another catalyst charging and replacement scheme involves using an initial charge less than the ultimate design catalyst quantity. For example, three catalyst layers might be used initially, with a fourth layer added at a later time. Then, the four catalyst layers are replaced sequentially similar to the previous case. This example is shown in Figure 3-11. The example has a design relative activity slightly less than that of the case in Figure 3-10, which implies that a larger overall catalyst volume is required to achieve the same actual design activity. However, the initial catalyst charge and the periodic catalyst replacement rate are nearly 20 percent less than that for the previous case. This system achieves a better utilization of catalyst. However, a disadvantage of this approach is an increased flue gas pressure drop across the reactor at the design point, due to the requirement for approximately 10 percent additional total catalyst charge compared to the previous case.

For the purpose of estimating a catalyst space velocity based on a reference data point, recall from Equation (3-4) that space velocity is directly proportional to catalyst activity. Therefore, the correction factor for space velocity due to differences in catalyst activity and catalyst replacement schedules is given by:

$$f_3 = f_A = \frac{A_{des}}{A(t_{ref})}$$

The design activity is calculated using Equation (3-9) based on the total number of layers to be included in the steady-state catalyst charge (i.e. including layers added to the initial charge at a later time). The reference activity level is estimated assuming that the entire catalyst charge is replace simultaneously at time t_{ref}.

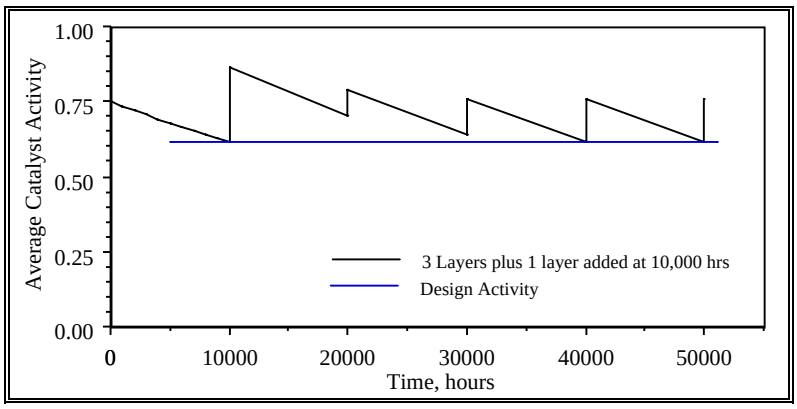

Figure 3-11 Illustrative Example of a Catalyst Addition and Replacement Scheme

Temperature

A temperature correction is assumed based on the Arrhenius relation for the reaction rate constant, which is given by:

$$k = k_o \exp\left(\frac{-E_a}{RT}\right)$$

A regression analysis using data from Bauer and Spendle (1984) was done to determine a value for the quantity E_a/R for use in the performance model. This was accomplished by rewriting Equation (3-5) as:

$$C = k_o \exp\left(\frac{-E_a}{RT}\right) = \frac{-\ln(1-\eta_{NO_x})(SV)}{3600(r_e)^a}$$

The quantity C was calculated using data presented in graphical form for NO_x removal efficiency as a function of temperature for a given ammonia slip, space velocity, and inlet NO_x concentration. From the regression analysis, the quantity E_a/R was estimated to be 7180, with an R^2 of 0.77 for 18 data points. Thus, the correction factor to adjust space velocity for differences in temperature is given by:

$$f_4 = f_T = \frac{\exp\left(\frac{-7180}{T}\right)}{\exp\left(\frac{-7180}{T_{ref}}\right)}$$

Initial and Annual Catalyst Volume Requirement

The SCR catalyst requirement is calculated based on the space velocity and flue gas volumetric flow rate. In cases where there are no later additions of catalyst layers, the catalyst volume is constant throughout the life of the plant. However, some designs assume that a new catalyst layer is added after some time period. In this case, the space velocity will decrease when the new layer is added. Thus, the total number of active catalyst layers may consist of catalyst layers existing at plant start-up and additional reserve layers added afterwards:

$$N_C = N_I + N_R$$

The initial catalyst volume is given by:

$$V_{c,i} = \frac{G_{FG}}{SV}\left(\frac{N_I}{N_C}\right)$$

The total catalyst volume is similarly given by:

$$V_c = \frac{G_{FG}}{SV}$$

The annual catalyst replacement rate depends in part on the catalyst design. In some studies, it is assumed that all catalyst layers are replaced simultaneously, while others assumed a phased approach to catalyst layer replacement. The number of catalyst layers replaced at the end of each replacement interval is given by:

$$N_{c,r} = 1 \text{ or } N_c$$

If only one layer is replaced at a time, then $N_{C,r}$ equals one. If all layers are replaced simultaneously, it equals the total number of layers in the catalyst. The number of layers replaced per year is:

$$N_{C,a} = \frac{N_{C,r}(8{,}760\ hr/yr)c_f}{t_r}$$

Thus, the catalyst volume replaced per year is:

$$V_{C,a} = V_C\left(\frac{N_{C,a}}{N_C}\right)$$

The catalyst "life" can be calculated based on the catalyst layer replacement interval and the number of layers replaced at the end of each interval:

$$L_C = \frac{(N_C/N_{C,r})t_r}{(8{,}760\ hr/yr)c_f}$$

In the case where all catalyst layers are replaced simultaneously, the catalyst life is the same as the catalyst replacement interval. Of course, the total volume of catalyst associated with each replacement scheme will differ.

3.5.2. Ammonia Requirement

The ammonia requirement is primarily a function of NO_x removal efficiency and the ammonia slip. The ammonia slip depends on the catalyst formulation and space velocity. However, it is treated here as a model input because insufficient data are currently available to develop a model of ammonia slip as a function of other variables. For each mole of NO and NO_2 that reacts in the SCR system, one mole of NH_3 is required (see Equations (3-1) and (3-2)). An excess amount of ammonia is required due to limitations related to diffusion of ammonia and NO_x to the catalyst's active sites. Typically, this excess ammonia leaves the SCR system unreacted. Thus, given a specified NO_x removal efficiency and ammonia slip, the molar ratio of ammonia to inlet NO_x is given by:

$$R_A = + \frac{[NH_3]_{out}}{[NO_x]_{in}}$$

The ammonia mass flow requirement is then given by:

$$M_{NH_3,in} = R_A \cdot M_{NO_x,in}$$

Ammonia is stored as a liquid. Many design studies assume that the ammonia is vaporized by mixing it with steam prior to injection into the flue gas. A typical minimum ratio of steam to ammonia is approximately 8, based on the use of medium pressure saturated steam. However, for safety reasons, ammonia dilution to 5 volume percent may be required, leading to a requirement for a steam-to-ammonia ratio of 19. The steam requirement for ammonia injection is given by:

$$M_{steam} = R_s \cdot M_{NH_3,in}$$

3.5.3. SO_3 Oxidation Rate

A portion of the SO_2 in the flue gas entering the SCR reactor is oxidized to SO_3. The percentage of SO_2 oxidized depends primarily on the reaction temperature, catalyst space velocity, and catalyst formulation. Regression analysis was used to develop two models representative of catalysts formulation for high sulfur and low sulfur operating environments. Data for both of these analyses were obtained from Bauer and Spendle (1984). For the high sulfur catalyst, which would be employed in high-dust hot-side applications, the fraction of SO_2 oxidized to SO_3, based on 31 data points, is given by:

$$f_{ox} = 2.38\times10^{-13} \cdot SV^{-1.06} \cdot (T-460)^{5.03}$$

For the low sulfur catalyst, which would be employed in tail-end applications, the following regression model based on 26 data points gives the fraction:

$$f_{ox} = 1.05\times10^{-13} \cdot SV^{-0.996} \cdot (T-460)^{5.05}$$

The coefficient of determination, R^2, for both of these regression models exceeds 0.99. SO_2 oxidation increases as space velocity decreases and as temperature increases.

3.5.4. Downstream Effects

Ammonia slip and SO_3 exiting the SCR system can combine to form ammonium sulfate and bisulfate, as previously discussed. Also, ammonia may be captured by fly ash prior to collection in the ESP. These downstream effects are of concern primarily for the hot-side SCR applications.

3.5.4.1. Air Preheater

The formation of ammonium salts is treated here empirically. Of primary concern is the amount of ammonia associated with ammonium salts deposited in the air preheater. The fraction of ammonia slip that is deposited as ammonium salts in the air preheater is treated as a parameter in the model, rather than as a calculated variable. The fraction of ammonia that is absorbed onto flyash is also a parameter in the model. The remaining portion of the ammonia slip is assumed to exit the plant with the flue gas leaving the stack. The ammonia partitioning coefficients must satisfy the following condition:

$$f_{NH_3,dep} + f_{NH_3,abs} + f_{NH_3,out} = 1$$

The molar flow rate of ammonia that is deposited as a solid in the air preheater is given by:

$$M_{NH3,dep} = f_{NH3,dep} \cdot \frac{[NH_3]_{out}}{[NO_x]_{in}} \cdot M_{NOx,in}$$

Similarly, the molar flows of ammonia absorbed by fly ash and emitted at the stack are given by:

$$M_{NH3,abs} = f_{NH3,abs} \cdot \frac{[NH_3]_{out}}{[NO_x]_{in}} \cdot M_{NOx,in}$$

$$M_{NH3,out} = f_{NH3,out} \cdot \frac{[NH_3]_{out}}{[NO_x]_{in}} \cdot M_{NOx,in}$$

The ammonia that deposits in the air preheater is removed periodically using water washing. As discussed by Neckar (1989), the concentration of ammonia in the wash water leaving the preheater is initially high, and then gradually decreases. The waste water from the washing may be separated into high and low ammonia concentration streams, with the high ammonia concentration stream requiring denitrification pretreatment before entering the regular plant waste water treatment system. The model includes provision for specifying the average ammonia concentration of the high concentration fraction of the spent waste water, as well as the portion of the deposited ammonia that is removed by this portion of the water. The model also includes a parameter for the ammonia concentration in the "low concentration" wastewater. These parameters are used to estimate the air preheater wash water requirement, with the concentrations specified in units of mg/l. The "high concentration" wash water requirement, in gallons/hour, is given by:

$$m_{wash,hc} = \frac{M_{NH3,dep} \cdot f_{hc}}{4.90141 \times 10^{-7} \cdot C_{NH3,hc}}$$

and the low concentration wash water requirement is given similarly by:

$$m_{wash,lc} = \frac{M_{NH3,dep} \cdot (1 - f_{hc})}{4.90141 \times 10^{-7} \cdot C_{NH3,lc}}$$

For tail-end SCR systems, the downstream effects are modeled similarly to those for hot-side systems. The partitioning of ammonia between ammonium salt deposition, ammonia absorbed onto fly ash, and ammonia retained in gaseous form will differ from the hot-side case. However, the gas-gas heat exchanger used for flue gas reheat will be subject to ammonia salt deposition and will require water washing. The spent wash water will require denitrification pretreatment prior to entering the plant waste water treatment system.

3.5.4.2. Catalyst Sootblowing

Catalyst sootblowing is required to remove ash that may mask or plug the catalyst. A sootblowing design by Bauer and Spendle (1984) is used as a basis to develop a model of the sootblowing steam requirement. The design basis includes steam sootblowing employing multiple sootblower sets. Bauer and Spendle report that the predicted steam requirement is 13,400 lb/hr for a total of approximately one hour per day, or an average of 31 lbmole/hr. There is no indication in the report that the steam requirement is a function of catalyst size, although such a relationship seems plausible. For example, Bauer and Spendle consider catalyst volumes ranging from 10,000 to 30,000 ft^3 but apparently assume the same sootblowing steam requirement for all cases. It is assumed here that the steam requirement reported by Bauer and

Spendle is typical of the base case catalyst design, which for the high-dust configuration had a catalyst volume of 16,146 ft^3. Furthermore, the steam requirement is assumed to scale with catalyst volume, used here as a measure of catalyst size:

$$M_{soot} = 31\left(\frac{SV}{16{,}146\,\text{ft}^3}\right)$$

This model does not account for any differences in catalyst masking or fouling rates associated with flue gas or fly ash characteristics.

3.5.5. Pressure Drop

The flue gas pressure drop associated with the SCR system includes pressure drops across: (1) ductwork and ammonia injection grid; (2) dummy catalyst layers for erosion control; (3) active catalyst layers; and (4) air preheater due to build up of deposits. Each of these sources of pressure drop are treated as input parameters in the model. The total pressure drop, in inches of water, across the SCR system is:

$$\Delta P_{scr} = n \cdot \Delta P_{cat} + n_d \cdot \Delta P_{dum} + \Delta P_{duct} + \Delta P_{aph,inc}$$

An additional consideration for hot-side SCR systems is the effect of the reduction in flue gas side pressure on the air leakage through the air preheater. For hot-side SCR systems, a nominal increase in the leakage rate of 10 percent is assumed. This is a model input parameter.

For tail-end systems, which are downstream of the air preheater, there is no incremental pressure drop associated with solids deposition in the air preheater. However, there is a pressure drop associated with flue gas reheating. Therefore, the pressure drop for the gas-gas heat exchanger used for reheat must be included. This pressure drop must be shared between the SCR system and the FGD system, for which reheat is often required also. Thus, a new parameter is introduced which represents the fraction of the gas-gas heat exchanger pressure drop that is solely attributable to the SCR system.

$$\Delta P_{scr} = n \cdot \Delta P_{cat} + n_d \cdot \Delta P_{dum} + \Delta P_{duct} + \Delta P_{GGH}\,(1 - f_{FGD})$$

The pressure drop term for ducting includes any pressure drop associated with the duct burner. These values must be specified as model inputs.

3.5.6. Energy Penalties

The energy penalties for the SCR system include electricity and steam consumption. The largest source of energy use is the incremental electricity required by the induced draft fan to overcome the flue gas pressure drops associated with the SCR system. In addition, electricity is required for the ammonia injection system, primary to compress vaporized ammonia for injection into the flue gas. Steam is consumed for ammonia vaporization and injection and for sootblowing in the SCR reactor. The steam consumption is converted to an equivalent electricity energy penalty based on the difference in enthalpy between the steam and water at standard conditions, the mass flow of steam used, and the steam cycle heat rate.

The energy penalty associated with operation of the induced draft fan to overcome the SCR flue gas pressure drop is given by:

$$E_{scr,fan} = \left(1.38\times10^{-6}\ \frac{MW}{cfm\cdot in\ H_2O}\right) G_{scr,in}\quad P_{scr}$$

The fan equation here assumes a fan efficiency of 85 percent. This equation also represents the energy penalty associated with a forced draft booster fan used in tail-end SCR systems.

The energy penalty associated with ammonia compression is calculated assuming a 100 psi differential compression with an 85 percent compression efficiency:

$$E_{scr,NH_3} = \left(3.47\times10^{-5}\ \frac{MW}{lb/hr}\right)\cdot\left(\frac{17.03lb}{lbmole}\right)\cdot M_{NH_3,in}$$

The energy penalty for steam use in the SCR system is calculated based on the steam mass flows, the enthalpy added to the steam by the steam cycle, and the steam cycle heat rate:

$$E_{scr,steam} = \frac{(M_{steam} + M_{soot})\left(\frac{18lb}{lbmole}\right)\left(\frac{1{,}000\ \text{BTU}}{\text{lb}}\right)\left(\frac{MW}{1{,}000\ \text{kW}}\right)}{HR_s}$$

The total energy penalty for the high-dust SCR system is:

$$E_{scr} = E_{scr,fan} + E_{scr,NH_3} + E_{scr,steam}$$

For the tail-end SCR system, natural gas used to fire the duct burner represents an additional energy loss. Natural gas is a fuel that could be used to generate electricity. Therefore, the energy penalty is calculated based upon the gross plant heat rate to estimate the equivalent electricity energy penalty associated with natural gas firing:

$$E_{scr,NG} = \frac{m_{NG} HHV_{NG}\left(\frac{MW}{1{,}000\ \text{kW}}\right)}{HR_g}$$

The total energy penalty for the tail-end SCR system is:

$$E_{scr} = E_{scr,fan} + E_{scr,NH_3} + E_{scr,steam} + E_{NG}$$

3.5.7. Flue Gas Reheat for Tail-End SCR

For the tail-end SCR system, the temperature of the flue gas exiting the FGD system must be raised to the reaction temperature required by the SCR system. Furthermore, the temperature of the gas exiting the SCR system can be reduce prior to entering the stack. Therefore, a gas-gas heat exchanger (GGHX) and a duct burner are employed for heating and cooling the flue gas, as shown in Figure 3-12.

Typically, a Ljungstrum type heat exchanger would be used for the flue gas reheat and cooling system. A portion of the higher pressure flue gas entering from the FGD system will leak into the flue gas stream exiting the heat exchanger to the stack. Therefore, an air leakage stream is modeled. For simplicity, it is assumed that the leakage flue gas is at the FGD system exit temperature. The flue gas leakage mass flow is estimated based on a leakage fraction as follows:

$$M_{leak} = f_l M_{FGD,o}$$

and the flue gas fraction entering the GGHX is given by:

$$M_{GGH,i} = (1 - f_l) M_{FGD,o}$$

In the GGHX, the untreated flue gas is heated from the FGD exit temperature to an intermediate temperature by cooling the treated flue gas exiting the SCR system. The heat transferred across the heat exchanger is given by:

$$Q_{GGH} = M_{GGH,i} (h_{fg}(T_{\text{int}}) - h_{fg}(T_{FGD}))$$

In the SCR computer model, the enthalpy of the flue gas is estimated using regression models for the enthalpy of each flue gas constituent at the given temperature.

The untreated flue gas must be heated an additional amount to reach the SCR reaction temperature. This additional heating is accomplished by use of a duct burner, which also introduces additional mass streams to the flue gas. The mass balance equation is:

$$m_{SCR,i} = m_{DB,i} + m_{NG} + m_{air}$$

Assuming that natural gas consists only of methane, the combustion reaction is:

$$CH_4 + 2(1 + r_{ea}) O_2 + 7.52(1 + r_{ea}) N_2 \rightarrow$$

$$CO_2 + 2H_2O + r_{ea} O_2 + 7.52(1 + r_{ea}) N_2$$

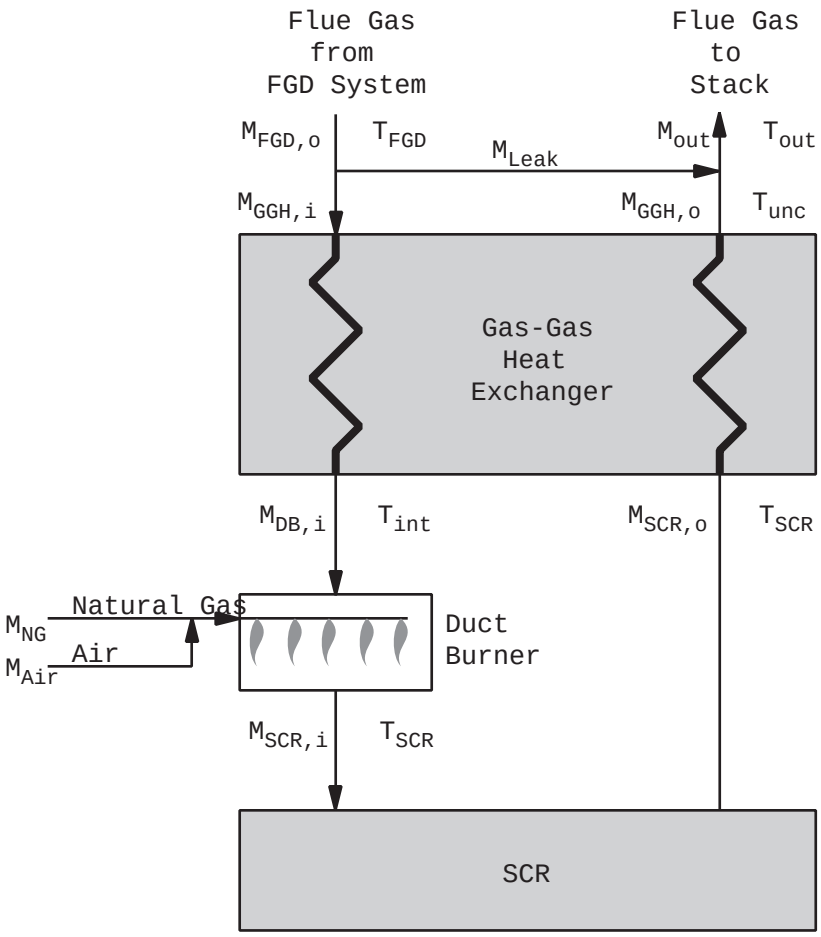

Figure 3-12 Schematic of Gas-Gas Heat Exchanger Performance Model

For each pound of methane consumed, 3.6 pounds of air are consumed at stoichiometric conditions. If excess air is also considered, the air mass flow is then given by:

$$m_{air} = 3.6(1 + r_{ea})m_{NG}$$

The energy balance equation for the duct burner may be written as:

$$m_{scr,i}h_{fg}(T_{SCR}) = m_{DB,i}H_{fg}(T_{\text{int}}) + m_{NG}h_{NG}(T_{NG}) + 3.6(1+r_{ea})m_{NG}h_{air}(T_{air}) + m_{NG}\Delta H_r$$

The heat of reaction for methane is 345,700 BTU/lbmole. In Equation (3-10), all variables are specified except for the natural gas mass flow rate. Therefore, this equation can be used to solve for the natural gas requirement:

$$m_{NG} = \frac{m_{SCR,i}h_{fg}(T_{SCR}) - m_{DB,i}h_{fg}(T_{\text{int}})}{h_{NG}(T_{NG}) + 3.6(1+r_{ea})h_{air}(T_{air})v + \Delta H_r} \qquad (3\text{-}10)$$

In the SCR system, ammonia and steam are added to the flue gas, and the flue gas composition changes due to chemical reactions occurring in the reactor vessel. The SCR exit temperature is assumed to be the same as the inlet temperature. The flue

gas exiting the SCR unit is cooled in the GGHX. The uncorrected temperature of the treated flue gas exiting the GGHX is estimated from the following relationship:

$$h_{fg}(T_{unc}) = h_{fg}(T_{SCR}) - \frac{Q_{GGH}}{m_{GGH,o}}$$

This equation is solved using an iterative technique to determine the flue gas temperature.

The treated flue gas from the SCR system is mixed with the flue gas leaking across the GGHX prior to entering the stack. The flue gas temperature entering the stack, corrected for the thermal mixing with the leakage air, is estimated using the following equation:

$$h_{fg}(T_{out}) = \frac{m_{GGH,o} h_{fg}(T_{unc}) + m_{leak} h_{fg}(T_{FGD})}{m_{out}}$$

where:

$$m_{out} = m_{GGH,o} + m_{leak}$$

3.6. SCR Capital Cost Model

The major equipment cost items for hot-side SCR systems include: (1) reactor housing; (2) catalyst; (3) ammonia storage and injection; (4) ductwork; (5) air preheater modifications; (6) induced draft fan modifications; (7) ash handling; and (8) water treatment. Additional costs may be incurred for flow modeling to properly design the ammonia injection system. For a tail-end system, there are no costs associated with air preheater modifications or ash handling. However, there are additional costs associated with the gas-gas heat exchanger and duct-burner used for flue gas reheat.

3.6.1. Reactor Housing

A reactor housing cost model was developed by Frey (1988). This model was later incorporated into the Integrated Air Pollution Control System (IAPCS) Version 4.0 computer program (Maibodi et al., 1990). The model was based on a statistical analysis of data from TVA (Maxwell and Humphries, 1985). The reactor housing costs include carbon steel reactor vessel with six inches of mineral wool insulation, vessel internals and supports, steam sootblowers, reactor crane and hoist, installation labor, foundations, structures, piping, and electrical equipment. The costs for the reactor housing exclude catalyst. The direct capital cost for the reactor housing is given by:

$$DC_R(1982) = 145{,}800 + 316.9\left(\frac{V_{TOT}}{N_{TOT}}\right)$$

This model was based on regression analysis of 12 data points and has a coefficient of determination (R^2) of 0.998. The catalyst volume per housing ranged from 5,000 to 17,000 ft^3.

A similar analysis was done for data reported by EPRI (Bauer and Spendle, 1984). A total of 18 cost estimates were reported with catalyst volumes ranging from roughly 4,000 to 14,000 ft^3. However, the nature of the model was substantially different from the TVA model. It appears that the TVA model is predicated on the assumption

of a simple linear relationship between reactor cost and catalyst volume. The EPRI data indicate a non-linear relationship, in which larger volumes yield a substantial economy of scale.

A more recent EPRI study is used here as a basis for developing a reactor cost model (Robie and Ireland, 1991). A total of 14 cost estimates are reported. However, two of these are for oil-fired power plants. All of the remaining 12 data points are for coal-fired power plants. The two oil-fired SCR applications appear to have substantially higher costs than for the coal-fired systems of similar catalyst volume; however, the basis for the difference is not reported. Of the dozen data points for coal-fired systems, one value is a duplicate. Therefore, 11 data points were used to develop a regression model of reactor housing cost versus total catalyst volume. The reactor housing includes flanged gas inlet and outlet, a single vertical downflow reactor, casing, ash hoppers, structural supports for catalyst modules, rectifying plate, baffles, turning vanes, walkways, stairs, monorails, hoists, and sootblowers. The catalyst volume includes both active and spare catalyst layers.

Robie and Ireland (1991) did not report the actual catalyst volumes for all 11 data points used in the regression model. Therefore, the catalyst volume was estimated based on the reported flue gas mass flow and flue gas molecular weight (which were used to calculated flue gas volumetric flow rate), active catalyst space velocity, and the ratio of the number of active plus spare catalyst layers to the number of active layers. Thus, the estimated total catalyst volume is given by:

$$V_{TOT} = \left(\frac{G^{o}_{fg}}{SV^{o}_{act}} \right) \left(\frac{N_{act} + N_{sp}}{N_{act}} \right)$$

where:

$$G^{o}_{fg} = \frac{\left(\frac{m_{fg}}{MW_{fg}} \right) \mathrm{R}\, \mathrm{T}^{o}_{fg}}{P^{o}_{fg}}$$

The space velocity is referenced to a standard temperature and pressure, which in this case is 32 °F and 1 atm. Therefore, the flue gas volumetric flow rate is calculated at standard temperature and pressure. The active catalyst space velocity is adjusted based on the ratio of total to active catalyst layers for the purpose of determining the total catalyst volume for the reactor housing. For the cases where the actual catalyst volumes were reported, these estimates were often in very close agreement and never diverged by more than five percent.

The cost data reported by Robie and Ireland (1991) are based on subcontract costs for the process area to which additional costs have been added. These additional costs are not documented or discussed in the EPRI report, but appear to have been applied consistently for every cost reactor cost estimate. They may reflect installation and integration costs not covered by the subcontract costs. The multiplier for these additional costs is a function of whether the SCR is for a new or retrofit application. The multipliers are substantially larger for retrofit applications, presumably reflecting site access difficulty and congestion impeding equipment installation. All reactor housing costs were normalized to a new plant basis for purposes of the regression analysis. This was done by estimating the multiplier between subcontractor cost and total direct cost for a new plant based on the two case studies for a new installation. The direct costs for the remaining cases were then estimated on a new installation basis by multiplying the subcontract costs with the new installation direct cost factor. The relationship between direct cost and the catalyst volume per reactor housing was evaluated using regression analysis.

The resulting regression model for the direct cost of the reactor housing is:

$$DC_R = 18.65\, N_{R,TOT} \left(\frac{V_{TOT}}{N_{R,TOT}} \right)^{0.489} \left(\frac{PCI}{357.3} \right)$$

This model has a coefficient of determination (R^2) of 0.94 and a standard error of $169,000. The regression model is shown graphically in Figure 3-13. The costs are reported in December 1989 dollars, but may be adjusted to other years using the *Chemical Engineering* Plant Cost Index.

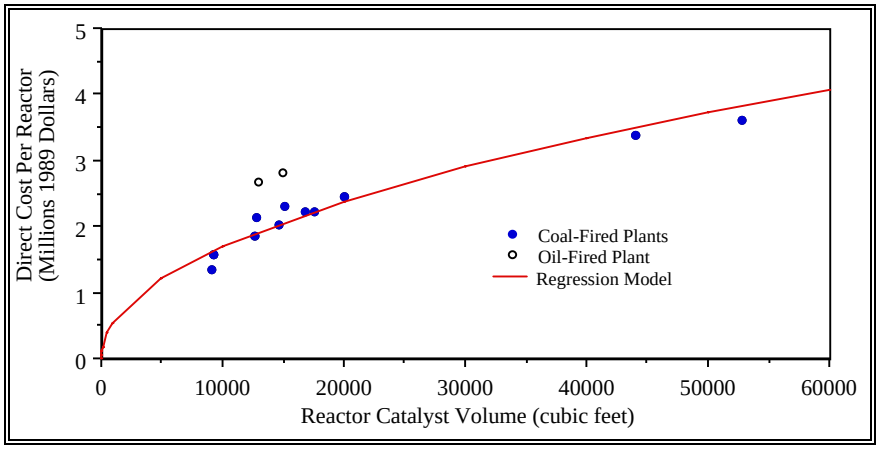

Figure 3-13 Direct Capital Cost Model for SCR Reactor Housing

From a statistical perspective, this regression model has significant limitations. The high coefficient of determination is influenced by the wide separation between two groups of data points. One set of data points are clustered for space velocities ranging from 10,000 to 20,000 cubic feet, whereas two other data points are close to 50,000 cubic feet. There is considerable scatter among the data points within the first cluster. However, because of the lack of reported detail regarding catalyst volumes and installation costs, it is not possible to reconcile these differences. Furthermore, there is no reported basis for the difference in values between the oil-fired and coal-fired data points. The oil-fired data points were excluded from the regression analysis, but are shown in Figure 3-13 for comparative purposes.

The regression model is satisfactory in representing the expected trend for SCR reactor housing cost. It is expected that there should be an economy of scale for increasing reactor housing size, and that the key measure of size is the total catalyst volume (including both active and spare catalyst layers).

3.6.2. Ammonia Handling and Injection

The direct cost for the ammonia injection process area was estimated based on analysis of eight data points taken from Robie and Ireland (1991). Six duplicate data points contained in their report were excluded from the statistical analysis. The ammonia unloading, storage, and supply system includes a horizontal bullet storage vessel with seven days supply capacity, an ammonia vaporizer, ammonia and dilution air mixer, ammonia injection grid, dilution air ductwork and dampers, and truck unloading station. The latter includes vapor recovery compressors, water deluge system, and transfer piping. The dilution air requirement is 20 parts air to one part ammonia. The regression model for ammonia process area direct costs is:

$$DC_{NH_3} = 50.8\,(m_{NH_{3,i}})^{0.482}\left(\frac{PCI}{357.3}\right)$$

This model has a coefficient of determination (R^2) of 0.87 and a standard error of $285,000. The regression model is shown graphically in Figure 3-14. Also shown in the figure is a regression model developed from data reported in an earlier EPRI report (Bauer and Spendle, 1984). The newer model yields costs that are lower than the previous model by a factor of approximately two. The reasons for the difference are not immediately clear. The earlier report used generally more conservative assumptions, reflecting higher levels of uncertainty perceived at that time for this technology.

Like the reactor housing direct cost model, the coefficient of determination for the ammonia injection system direct cost model benefits from the separation between clusters of data points. In this case, however, there is only one data point at the high end of the range of values for the predictive variable, ammonia flow rate. However, the model is satisfactory in reflecting economies of scale for larger sized systems.

3.6.3. Ductwork

Ductwork costs are considered both for hot-side and tail-end SCR applications.

3.6.3.1. Hot-Side SCR Applications

For a new hot-side SCR application, the ductwork associated with the SCR process includes economizer bypass ducts, economizer outlet duct, SCR inlet duct, SCR inlet control dampers, SCR outlet duct, SCR air preheater inlet plenum, various expansion joints in the ductwork, and dampers associated with the economizer bypass and air preheater cross-over ducting. Of the six major case studies reported by Robie and Ireland (1991), only two are for a new coal-fired power plant with hot-side SCR. Although these two case studies include five separate performance and cost estimates based on sensitivity analysis of key SCR performance characteristics, they are predicated on just two flue gas flow rates. Therefore, three of these estimates are duplicates. Because only two data points are available from this study to estimate duct costs as a function of flue gas flow, regression modeling was not employed to develop a direct cost model. Instead, a capacity-exponent model of direct cost versus flue gas volume flow rate was assumed as an appropriate function form. This formulation reflects the expected increase in cost that is associated with increases in flue gas volume flow rates. However, it implies that duct runs would be similar for differently sized systems. The parameters of this model, which include a multiplicative constant and an exponential coefficient, were estimated from the two data points. The resulting model is:

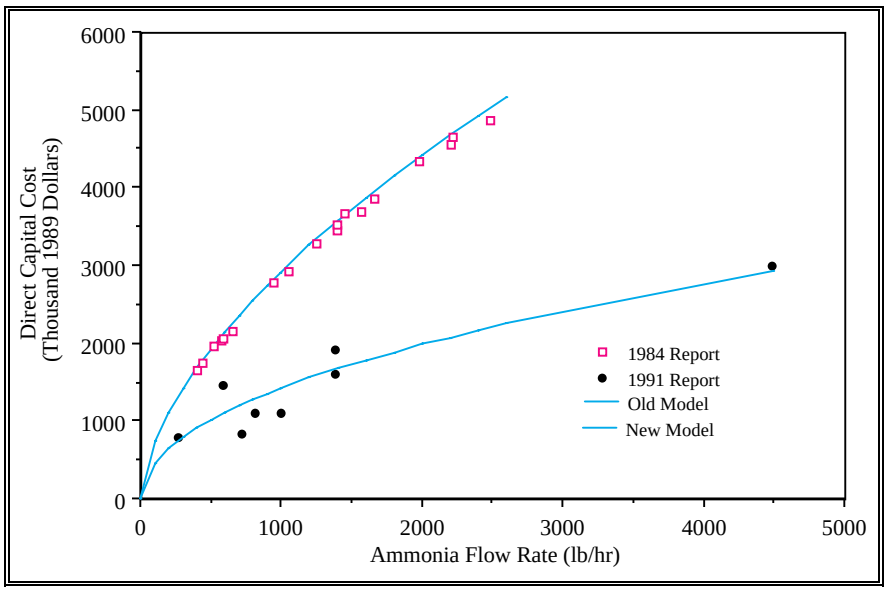

Figure 3-14 Direct Capital Cost Model for the Ammonia Handling and Injection System

$$DC_D = 14.2(G_{fg})^{0.7}\left(\frac{PCI}{357.3}\right)$$

The two data points used to estimate the parameters of this model are for flue gas flow rates of 3,026 and 2,713 macfm and direct costs of $4.44 and $4.10 million, respectively. This is a relative narrow range of values, but the resulting exponential scaling factor of 0.7 is consistent with scaling factors used in a variety of chemical engineering cost models.

3.6.3.2. Tail-End SCR Applications

For an SCR in the cold-side application, there are additional duct costs associated with the gas-gas heat exchanger. There are two data points available for estimating these costs. One is for a gas-gas heat exchanger system which has 5.6 percent gas leakage. The second is for a system with no leakage. In this latter case, there is a higher gas flow rate through the SCR system, thereby leading to increased duct costs. Because of the scarcity of data points, the costs for these two cases are estimated as a multiplier of the costs for ductwork for a hot-side SCR application. The general equation is:

$$DC_{D,CS} = f_{D,CS}\,14.2(G_{fg})^{0.7}\left(\frac{PCI}{357.3}\right)$$

where $f_{D,CS}$ is 1.90 for a GGH with 5.6 percent air leakage, and 2.15 for a GGH with no air leakage.

3.6.4. Air Preheater Modifications

For hot-side SCR systems, a potentially significant concern is the deposition of ammonia-based compounds on downstream components. Unreacted ammonia exiting the SCR system ("ammonia slip") can react with sulfur trioxide present in the flue gas to form compounds such as ammonium bisulfate and ammonium sulfate that deposit on downstream equipment. These compounds may result in plugging and

corrosion. The condensation of these compounds is most likely to occur on the cold and intermediate temperature heat transfer surfaces of the air preheater. In anticipation of deleterious effects, EPRI and others have recommended that air preheaters designed for use with SCR system be constructed with lower gauge (thicker) material, different geometries (e.g., combining intermediate and cold baskets of a conventional Ljungstrom air preheater into a single unit, to minimize seams where corrosion might occur), different materials, and larger motors, structure, and foundation to accommodate the larger weight of these modifications. Furthermore, more stringent provisions are made for soot blowing and water washing of the air preheater to remove the ammonia salts and any associated buildups at regular intervals. To enable an on-line water washing capability, crossover ducts and dampers are required. The changes in air preheater geometry and the effects of fouling can increase gas flow pressure drops. This in turn may increase gas leakage rates between the combustion air and flue gas sides of the heat exchanger.

Therefore, to accommodate the potential impacts of SCR systems on air preheater performance, a number of modifications are included in the design bases. Thicker material is used for the cold and intermediate heat transfer surfaces, in the region of the preheater where ammonia salt deposition is most likely. Furthermore, a corten steel alloy is used instead of carbon steel. A smoother heat transfer surface is used to aid in removing ammonia salts, but at the expense of reduced heat transfer and, hence, large heat transfer surface area. A larger motor is provided for the rotating Ljungstrom heat exchanger. Because of the additional weight of the heat exchanger, additional foundation and structural steel expense is incurred. High pressure steam sootblowers are installed in the cold-end of the heat exchanger. Water wash spray nozzles are also employed for on-line washing. Because of the increased heat transfer surface, there is a larger flue gas pressure drop which results, in turn, in a higher air leakage rate across the air preheater.

The costs of the major portions of the air preheater modifications, such as the increase in the heat transfer surface area and the associated increase in costs for special materials and increased structural support, are proportional to the size of the air preheater. Therefore, a cost model was developed for which the key parameter is a measure of the size of the air preheater.

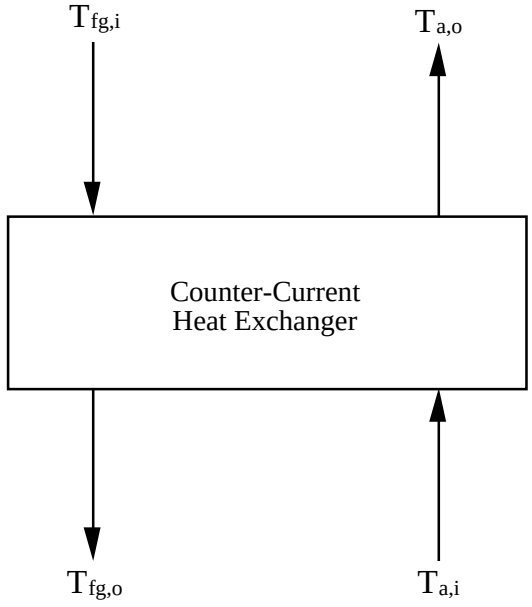

Figure 3-15 Simplified Schematic of a Counter-Current Flow Heat Exchanger

For a counter-current heat exchanger (see Figure 3-15), the heat transfer is given by:

$$q_{aph} = U_{aph} A_{aph} \Delta T_{LM,aph}$$

where

$$\Delta T_{LM,aph} = \frac{(T_{fg,i} - T_{a,o}) - (T_{fg,o} - T_{a,i})}{\ln\left(\frac{T_{fg,i} - T_{a,o}}{T_{fg,o} - T_{a,i}}\right)}$$

is the log-mean temperature difference (LMTD). The product of the universal heat transfer coefficient, U, and the heat exchanger surface area, A, is assumed here to be constant for an air preheater before and after modification for use with SCR. Prior to modification, the air preheater has a higher heat transfer coefficient and a lower surface area than after modification. However, the heat exchanger is designed in either case to accommodate the same inlet and outlet conditions and, hence, the same LMTD. The product UA is calculated based on the known flue gas and air inlet and outlet temperatures, the flue gas molar flow rate, and the average specific heat of flue gas. A typical value for the latter is 7.9 BTU/(lbmole-°R). Thus,

$$(UA)_{aph} = \frac{q_{aph}}{\Delta T_{LM,aph}} \qquad (3\text{-}11)$$

$$q_{aph} = M_{fg} c_{p,fg} (T_{fg,o} - T_{fg,i})$$

There are only two data points from the EPRI study which are directly relevant to estimating a reference basis for the product UA. These are the two cases involving installation of a new SCR system involving Ljungstrom air preheaters (Cases 1.0 and 2.0 in the EPRI report). Other cases reported are for modifications to shell and tube heat exchangers or for retrofit modification to Ljungstrom heat exchangers.

For the first case (Case 1.0), the inlet and outlet air temperatures are not given. The amount of heat transfer is estimated based on the flue gas cooling from 725°F to 270°F. Assuming an inlet air temperature of 80°F, and accounting for air leakage across the air preheater, the boiler air outlet temperature is estimated to be approximately 600°F. Using these values, the LMTD is estimated to be 155°F and the amount of heat transferred through the heat exchanger is 680 million BTU/hr. Therefore, the UA product in this case is 4.4 x 10^6 BTU/°F. Using a similar approach for Case 2.0 yields a UA product of 2.3 x 10^6. In this latter case, the reported primary air temperature (air preheater air-side outlet temperature) is inconsistent with the amount of heat transfer obtained from flue gas cooling, assuming an inlet air temperature of 80°F. Therefore, an independently calculated value of approximately 510°F was used.

The costs of air preheater modifications for the two cases are $1.37 million and $0.81 million, respectively (in December 1989 dollars). Assuming that the cost of the modification is proportional the UA product, then from these two cost estimates the following capacity-exponent cost model is obtained:

$$DC_{aph,\mathrm{mod}} = 1370\, \mathrm{N}_{T,aph} \left(\frac{UA_{T,aph}}{4.4x10^6 N_{T,aph}}\right)^{0.8} \left(\frac{PCI}{357.3}\right)$$

While this model is based on only two data points, it nonetheless appears to provide a qualitatively reasonable relationship between air preheater modification costs based

on the size of the air preheater. The model suggests a modest economy of scale for modifications to larger air preheaters.

3.6.5. Gas-Gas Heat Exchanger

The cost model for the gas-gas heat exchanger (GGH) used for cold-side SCR applications was developed in a manner similar to that for air preheater modifications. The GGH is a Ljungstrom heat exchanger, and typically there is one GGH per SCR reactor. Thus, in a typical 500 MW power plant, there would be two GGHs.

A simplified schematic of the GGH is shown in Figure 3-16. Gas exiting the flue gas desulfurization (FGD) system is heated by counter-current heat exchange with high temperature gas exiting the SCR reactor. The "untreated" gas entering the SCR system is heated by a duct burner.

There is only one case study in the EPRI report by Robie and Ireland which deals with a cold-side SCR. The UA product described in Equation (3-11) is assumed here as the key measure of heat exchanger size. Based on reported gas temperatures and flow rates, and correcting for gas leakage through the heat exchanger, the direct cost model is:

$$DC_{GGH} = 9100\, N_{T,GGH} \left(\frac{UA_{T,GGH}}{4.4x10^{6}\, N_{T,GGH}} \right)^{0.8} \left(\frac{PCI}{357.3} \right) \qquad (3\text{-}12)$$

This model is based on a GGH design with 5.6 percent gas leakage, on a mass basis. For a system with no leakage, multiply the cost given in Equation (3-12) by a factor of 2.4.

The cost of the duct burner is proportional to the amount of natural gas required to raise the flue gas temperature. The duct burners include combustion air fans, process controls, and a flame safeguard system. The capacity of the duct burners is expressed based on the heating value of the natural gas. The direct cost is given by:

$$DC_{DB} = 264\, N_{T,DB} \left(\frac{Q_{NG}}{90\ \mathrm{N_{T,DB}}} \right)^{0.6} \left(\frac{PCI}{357.3} \right)$$

where

$$Q_{NG} = \frac{m_{NG}\, HHV_{NG}}{10^{6}}$$

3.6.6. ID Fan and Booster Fan Costs

For a new SCR installation, the ID fans must be sized to deal with the increased flue gas pressure drop resulting from the additional ductwork and the SCR reactor. Typically, the increase in flue gas pressure drop is approximately 11 inches of water. The size of an ID fan and motor is proportional both to the flue gas flow rate and to the pressure drop. Therefore, the cost of the ID fan modifications is assumed here to be proportional to the difference in flue gas energy requirement necessary to overcome the flue gas pressure drop. This energy requirement is given by:

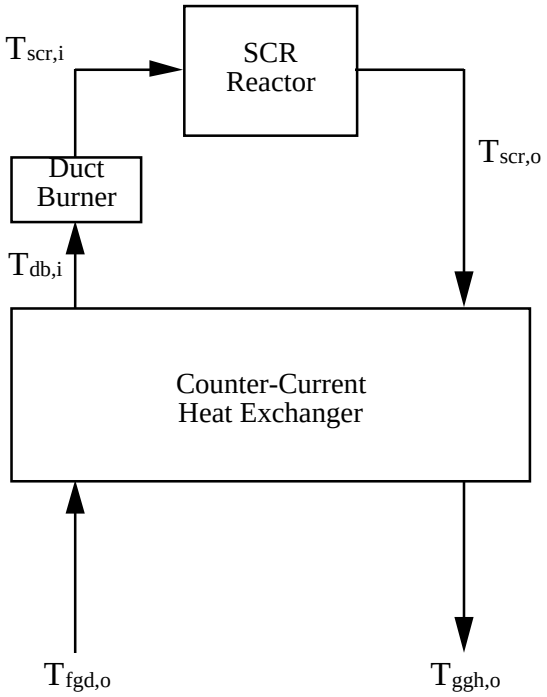

Figure 3-16 Simplified Schematic of the Gas-Gas Heat Exchanger Employed in Cold-Side SCR Systems

$$EC_{ID,dif} = \frac{\dot{Q}_{fg}\,\Delta P_{SCR}}{8{,}512\,\eta_{fan}} \qquad (3\text{-}13)$$

The fan efficiency is typically 85 percent. The cost of the ID fan differential is:

$$DC_{ID,dif} = 180\left(\frac{EC_{ID,dif}}{4{,}600}\right)^{0.6}\left(\frac{PCI}{357.3}\right)$$

In the case of a cold-side SCR system, a booster fan is required to overcome the flue gas pressure drop throughout the GGH and SCR components. Typically, the pressure drop across the cold-side system is approximately 14.5 inches of water. Thus, using Equation (3-13) to estimate the energy requirement as a function of the actual flue gas volumetric flow rate and the pressure drop, the cost of a cold-side SCR system booster fan is given by:

$$DC_{BF} = 810\,N_{T,BF}\left(\frac{EC_{BF}}{3{,}000\,\mathrm{N}_{T,BF}}\right)^{0.6}\left(\frac{PCI}{357.3}\right)$$

There is typically one booster fan per SCR reactor train.

3.6.7. Structural Support

The basis for the SCR cost estimates developed by Robie and Ireland (1991) include a separate cost for structural support. While the definition of this process area is lacking, it appears to be related primarily to the SCR reactor housing, ductwork, and air preheater. In the case of a cold-side SCR system, the structural cost is related to

the gas-gas heat exchanger, rather than the air preheater. As part of the data analysis, the structural cost was expressed as a percentage of the direct costs for the reactor housing, ductwork, and air preheater modifications for hot-side applications, and as a percentage of the direct costs for the reactor housing, ductwork, and gas-gas heat exchanger costs for cold-side applications. Of the 14 data points from the EPRI study, 12 of them yielded structural costs as a relatively narrow range of percentages of the appropriate direct costs. The mean value was 18.7 percent, with a range from 16.2 to 20.8 percent and a standard deviation of 1.4 percent. For one retrofit case with a high site congestion, the structural costs were 50 percent of the other selected direct costs. For a new SCR hot-side application, the structural costs are estimated as:

$$DC_s = f_s(DC_R + DC_D + DC_{APH})$$

and for a cold-side application the structural costs are estimated as:

$$DC_s = f_s(DC_R + DC_D + DC_{GGH})$$

where f_s has a mean value of 0.187. For a retrofit application, a value of f_s of as high as 0.5 may be appropriate.

3.6.8. Miscellaneous Other Direct Capital Costs

Other capital costs may be incurred for ash handling addition, water treatment addition, and flow modeling for a hot-side SCR system. For a cold-side system, costs are incurred for water treatment and flow modeling.

Flow modeling costs are similar for all systems and typically represent a flat fee for designing the ammonia injection system to assure proper mixing of ammonia and flue gas. The value used in the EPRI study was $100,000.

Ash handling addition is required for hot side systems to remove ash deposited in the bottom of the SCR reactor to existing ash piping or to an ash silo. This cost is small compared to the costs of reactors, ammonia injection, heat exchangers, and fans. Here, it is assumed to have a value of approximately $150,000 for a 550 MW power plant.

For hot-side applications, there is additional waste water burden associated with soot-blowing and water washing in the SCR system. In the cold-side system, additional equipment is required to collect GGH wastewater. For hot-side systems, the additional cost associated with water treatment are less than $150,000. For cold-side systems, they are approximately $500,000. These numbers are representative of a typical 550 MW power plant.

The direct cost for miscellaneous expenses of flow modeling, ash handling addition, and water treatment addition for a hot-side SCR system are:

$$DC_{misc} = \left\{100 + 300\left(\frac{MW_e}{550}\right)^{0.6}\right\}\left(\frac{PCI}{357.3}\right)$$

For a cold-side SCR system, the direct cost is:

$$DC_{misc,CS} = \left\{100 + 650\left(\frac{MW_e}{550}\right)^{0.6}\right\}\left(\frac{PCI}{357.3}\right)$$

3.6.9. Total Direct Cost

The total direct cost is the sum of all of the direct costs. The cost of the initial catalyst charge is also included here in the total direct cost, because it is such a large and integral part of the SCR system. One component of the direct cost not estimated in any of the above sections is the cost of general facilities associated with the SCR process area. Based on the estimates reported by Robie and Ireland, it appears that general facilities cost is approximately 4 percent of the sum of all other direct costs. The total direct cost for the hot-side SCR system is therefore:

$$TDC_{HS} = (1 + f_{GF})\left(V_{act}UC_{cat} + \sum_{i=1}^{7} DC_i\right)$$

where there are seven direct cost components (reactor housing, ammonia injection, ductwork, air preheater modifications, ID fan differential, structural, and miscellaneous).

For a cold-side system, the total direct cost is given by:

$$TDC_{CS} = (1 + f_{GF})\left(V_{act}UC_{cat} + \sum_{i=1}^{8} DC_i\right)$$

where there are eight direct cost components (reactor housing, ammonia injection system, ductwork, gas-gas heat exchanger, duct burner, booster fan, structural, and miscellaneous).

3.6.10. Other Capital Costs

Other capital costs include various indirect capital costs, as well as preproduction costs associated with startup and inventory costs associated with providing initial stocks of chemicals and fuels.

Engineering and home office fees are typically estimated as a percentage of the total direct cost. In this case, a value of 10 percent is assumed as the default.

$$C_{EHO} = f_{EHO}TDC$$

Project contingency costs are also approximately 10 percent, as assumed by Robie and Ireland. Usually, project contingency is assigned as a multiplier of the total direct cost (e.g., EPRI, 1986). For example:

$$C_{\mathrm{Pr}\,ojC} = f_{\mathrm{Pr}\,ojC}TDC$$

Process contingency costs are typically evaluated separately for each process area. The total process contingency is given by:

$$C_{\mathrm{Pr}\,ocC} = \sum_{i} f_{\mathrm{Pr}\,ojC}DC_i$$

Typical values of the process contingency are: five percent for reactor, catalyst, structural support, and fans; ten percent for ammonia storage, ductwork, air preheater modifications, and gas-gas heat exchanger; fifteen percent for water treatment addition, and twenty percent for ash handling addition.

The total plant cost, or overnight construction cost, is given by:

$$TPC = TDC + C_{EHO} + C_{\mathrm{Pr}ojC} + C_{\mathrm{Pr}ocC}$$

An allowance for funds during construction (AFDC) is calculated based on the TPC as a function of the amount of time it would take to construct an SCR system. An 18 month construction period for a new plant is assumed. Methods for computing the AFDC are documented elsewhere (e.g., EPRI, 1986) and are not repeated here. The total plant investment (TPI) represents the sum of the total plant cost and the AFDC.

The final measure of capital cost is the total capital requirement (TCR). The TCR includes the total plant investment plus costs for royalties, startup costs, and initial inventories of feedstocks. In this case, no costs are assumed for royalties. Preproduction costs typically include one month of both fixed and variable operating costs and two percent of total plant investment. In the case of an SCR system, by far the largest portion of the preproduction (startup) costs are represented by the two percent multiplier on TPI. Inventory capital is estimated as 0.5 percent of total process capital excluding catalyst. The costs for initial catalysts and chemicals is zero. The SCR catalyst is included in the process capital costs. Thus, for an SCR system, the total capital requirement is:

$$TCR = (1 + f_{PP})TPI + f_{IC}\sum_i DC_i$$

3.7. O&M Costs

The annual costs for SCR systems include fixed and variable operating costs. Fixed operating costs include operating labor, maintenance labor and materials, and overhead costs associated with administrative and support labor. Variable operating costs include consumables, such as ammonia and catalyst replacement. Costs for steam and electricity consumed from within the plant may also be estimated.

3.7.1. Fixed Operating Costs

The fixed operating costs are predicated on 4 hours of labor per day per SCR reactor train for operating labor, and 8 hours of labor per day per SCR train for maintenance labor. Maintenance materials are estimated as one percent of the total process capital cost, excluding catalyst. Administrative and support labor is estimated as 30 percent of operating and maintenance labor costs. Therefore, the total fixed operating cost is given by:

$$FOC = 1.3\,(4+8)\,365\,\mathrm{N}_{\mathrm{T,R}}UC_L + 0.01\sum_i DC_i$$

A typical labor rate would be $22/hour for a Midwest location.

3.7.2. Variable Operating Costs

The major component of the variable operating cost is for catalyst replacement. The analytical models for estimating catalyst replacement are reported by Frey (1993) and are not repeated here. Similarly, the ammonia mass flow requirement, the steam requirement for ammonia injection, and the electricity consumption for the SCR systems are also reported by Frey (1993).

Therefore, the total variable operating cost for the SCR system may be estimated as:

$$VOC = V_{C,a}UC_{cat} + 8{,}760c_f\left[\left(\frac{M_{NH_3,A,i}}{117.6}\right)UC_{NH_3} + \left(\frac{18M_{steam}}{1{,}000}\right)UC_{steam} + E_{scr}UC_{elec}\right]$$

The unit cost for catalyst is highly variable. Robie and Ireland (1991) used a value of $660/ft^3, but noted that at the time of their study, catalyst costs in Europe were as low as $330/ft^3. The unit cost of ammonia is typically $150/ton. The unit cost of steam is approximately $3.00/1,000 lb. The cost of power is often assumed to be 5 cents per kWh.

3.8. Nomenclature

3.8.1. Performance Models

3.8.1.1. English Letter Symbols

a	=	Constant
A_c	=	Catalyst area, ft^2
A_{min}	=	Minimum catalyst activity level
A_{inc}	=	Incremental catalyst activity subject to exponential decay (1-A_{min})
AV	=	Area velocity, ft/hr
c_f	=	Annual plant capacity factor, fraction of year
C	=	Constant representing catalyst activity for a given operating condition (e.g., temperature, inlet NO_x concentration) with NH_3/NO_x ratio equal to 1.0
$\vec{\mathbf{C}}_i$	=	Vector of concentrations of trace species in stream i, ppmw
$C_{NH3,hc}$	=	Concentration of ammonia in "high concentration" wash water, mg/l
$C_{NH3,k}$	=	Concentration of ammonia in "low concentration" wash water, mg/l
C_r	=	Ratio of catalyst activities for two catalysts.
E_a	=	Activation energy
E_i	=	Energy penalty for system i, MW
f_{FGD}	=	Fraction of gas-gas heat exchanger pressure drop that is normally associated with FGD flue gas reheat.
f_{hc}	=	Fraction of ammonia deposited on air preheater surfaces removed in high concentration wash water.
f_i	=	Generic correction factor
F_1	=	Fraction of flue gas exiting FGD system that leaks across gas-gas heat exchanger in tail-end SCR system
f_{NH_3}	=	Fraction of ammonia slip partitioned to fate i (e.g., "dep"=deposition on air preheater surfaces, "abs"=absorbed by flyash, "out"=emitted with flue gas)

f_{ox}	=	Fraction of SO_2 oxidized to SO_3 in the SCR reactor.
f_r	=	Ratio of correction factors for linear velocity and temperature
G_{FG}	=	Flue gas volumetric flow rate, ft^3/hr at standard conditions
G_{scr}	=	Flue gas volumetric flow rate in the scr system, ft^3/min
$H_i(T_j)$	=	Enthalpy of gas i at temperature j, BTU/lbmole
H_r	=	Ratio of catalyst layer heights
HR_g	=	Gross plant heat rate, BTU/kWh
HR_s	=	Steam cycle heat rate, BTU/kWh
k	=	Reaction rate constant. Also interpreted as catalyst "activity."
L_C	=	Catalyst life, years
m	=	End-mole ratio
m_i	=	Mass flow rate of species i, lb/hr
M_i	=	Molar flow rate of species i, lbmole/hr
N_C	=	Number of active catalyst layers
$N_{C,a}$	=	Number of active catalyst layers replaced each year, yr^1
$N_{C,r}$	=	Number of active catalyst layers replaced at each replacement interval
N_I	=	Number of active catalyst layers installed initially
N_R	=	Number of reserve catalyst layers installed at end of first catalyst replacement interval
n_d	=	Number of dummy catalyst layers
Q_r	=	Ratio of flue gas flow rates
p_i	=	Partition factor within a partition factor matrix for trace species i
$\mathbf{P}_{i \to j}$	=	Partition factor matrix for partitioning of trace species from stream i to stream j.
r_e	=	Exit molar ratio of NH_3 to NO_x at SCR reactor outlet.
r_{ea}	=	Ratio of air to stoichiometric requirement (excess air ratio).
R	=	Universal gas constant
R_A	=	Ratio of ammonia to nitrogen oxides, molar basis
R_g	=	Geometric ratio, ft^2/ft^3
R_S	=	Ratio of steam-to-ammonia, molar basis
S_r	=	Ratio of reactor cross-section areas
SV	=	Catalyst space velocity, 1/hr
SV_{ref}	=	Reference catalyst space velocity, 1/hr
t	=	Time, seconds
t_r	=	Catalyst replacement interval, hours
T	=	Temperature

V_c = Total catalyst volume, ft^3

$V_{c,i}$ = Initially installed catalyst volume, ft^3

$V_{c,a}$ = Volume of catalyst replaced each year, ft^3/yr

$V_{c,r}$ = Volume of catalyst replaced at each replacement interval, ft^3/interval

$[NH_3]_{out}$ = Ammonia slip, ppm

[x] = Concentration of species x, molar basis

3.8.1.2. Greek Letter Symbols

b_r = Ratio of fractions of reactor plugging

DH_r = Heat of reaction, BTU/lbmole reactant

DP_i = Pressure drop for component i

η_{NO_X} = NO_X removal efficiency, fraction

τ_a = Time constant for catalyst activity decay.

3.8.1.3. Subscripts

cat = Catalyst

DB = Duct burner

duct = Ducting

dum = Dummy catalyst

FG = Flue gas

FGD = Flue gas desulfurization

GGH = Gas-gas heat exchanger

i = in

NG = Natural gas

o = out

org = organics

scr = Selective catalytic reduction

stm = steam

tr = trace species

WW = Wash water

3.8.2. Cost Models

c_f = Plant capacity factor (fraction of the year at full load)

C_{ProcC} = Cost of project contingencies, $1,000

$DC_{aph,mod}$ = Direct capital cost of air preheater modifications, $1,000

DC_{BF} = Direct capital cost of the booster fan for cold-side SCR, $1,000.

DC_D = Direct capital cost of ductwork, $1,000

$DC_{D,CS}$ = Direct capital cost of ductwork for a cold-side SCR system, $1,000

DC_{DB} = Direct cost of duct burners for a cold-side SCR system, $1,000.

DC_{GGH} = Direct capital cost of the gas-gas heat exchanger for cold-side SCR, $1,000.

DC_{misc} = Direct capital cost of miscellaneous items, $1,000.

DC_{NH_3} = Direct capital cost of the ammonia injection systems, $1,000

DC_R = Direct capital cost of reactors, $1,000.

$EC_{ID,dif}$ = Electricity consumption associated with SCR flue gas pressure drop, kWh.

E_{scr} = Electricity requirement for SCR, kW

$f_{D,CS}$ = Factor for cold-side SCR duct costs

f_{IC} = Factor for inventory capital costs (0.005 of non-catalyst direct costs)

f_{PP} = Factor for preproduction costs (0.02 of TPI)

$f_{projC,i}$ = Project contingency factors for each process area.

$G°_{fg}$ = Flue gas volumetric flow rate, referenced to a standard temperature (32°F) and pressure (1 atm), ft^3/hr.

G_{fg} = Flue gas volumetric flow rate, at actual temperature and pressure, ft^3/hr.

HHV_{NG} = Higher heating value of natural gas, BTU/lb

m_{fg} = Mass flow rate of flue gas, lb/hr.

m_{NG} = Mass flow rate of natural gas, lb/hr

m_{NH_3i} = Mass flow rate of ammonia injected into the flue gas, lb/hr

$m_{NH_3A,i}$ = Molar flow rate of ammonia injected into the SCR system, lbmole/hr

M_{steam} = Molar flow rate of steam required for ammonia injection, lbmole/hr

MW_{fg} = Equivalent molecular weight of flue gas, lb/lbmole.

N_{act} = Number of active catalyst layers at plant startup.

N_{sp} = Number of spare catalyst layers at plant startup.

$N_{R,TOT}$ = Total number of reactor housings.

$N_{T,aph}$ = Total number of air preheaters

$N_{T,DB}$ = Total number of duct burners

$N_{T,GGH}$ = Total number of Gas-Gas Heat Exchangers.

$P°_{fg}$ = Reference pressure of the flue gas at standard conditions, 1 atm.

PCI = *Chemical Engineering* Plant Cost Index. For Dec. 1989, PCI = 357.3.

$\dot{Q}_{fg}$	=	Flue gas volumetric flow rate, actual ft^3/min.
Q_{NG}	=	Heating value of natural gas used in duct burners, BTU/hr.
R	=	Ideal Gas Constant, 0.730 (fte^3 atm)/(lbmole °R).
$SV°_{act}$	=	Active catalyst space velocity, referenced to a flue gas temperature of 32°F, 1/hr.
$T_{a,i}$	=	Temperature of air entering a heat exchanger, °R.
$T_{a,o}$	=	Temperature of air exiting a heat exchanger, °R.
$T°_{fg}$	=	Reference temperature of the flue gas at standard conditions, 32°F.
$T_{fg,i}$	=	Temperature of flue gas entering a heat exchanger, °R.
$T_{fg,o}$	=	Temperature of flue gas exiting a heat exchanger, °R.
UA	=	Product of universal heat transfer coefficient and heat exchanger surface area, BTU/°R
UC_{cat}	=	Unit cost of catalyst, $/$ft^3$.
UC_{elec}	=	Unit cost of electricity, $/kWh
UC_L	=	Unit cost of labor, $/hour
UC_{NH_3}	=	Unit cost of ammonia, $/ton
UC_{steam}	=	Unit cost of steam, $/1,000 lb
$V_{C,A}$	=	Volume of catalyst replaced annually, ft^3/yr.
V_{TOT}	=	Total volume of the catalyst, including active and spare layers, ft^3.

3.9. References

Anderson, C. M., and J. A. Billings. "Simple Calculation Measures NH_3 Slip for Cogeneration Units," *Power Engineering*, April 1991, pp. 42-44.

Balling, L., and D. Hein. "DeNO_x Catalytic Converters for Various Types of Furnaces and Fuels--Development, Testing, and Operation," in 1989 Symposium on Stationary Combustion Nitrogen Oxide Control, Volume 2. Electric Power Research Institute. Palo Alto, California. Report No. GS-6423. July 1989. pp. 7A-27 to 7A-40.

Bauer, T.K., and R.G. Spendle (1984), "Selective Catalytic Reduction for Coal-Fired Power Plants: Feasibility and Economics," CS-3603, Electric Power Research Institute, Palo Alto, CA, October.

Behrens, E. S., S. Ikeda, T. Yamashita, G. Mittelbach, and M. Yanai. "SCR Operating Experience on Coal-Fired Boilers and Recent Progress," presented at the 1991 Symposium on Stationary Combustion Nitrogen Oxide Control, Washington, DC, March 25-28, 1991.

Chen, J. P., M. A. Buzanowski, R.T. Yang, and J.E. Chicanowicz, "Deactivation of the Vanadia Catalyst in the Selective Catalytic Reduction Process," *JAWMA* 40(10):1403-1409 (December 1990).

Chen, J., R.T. Yang, and J.E. Chicanowicz. "Poisoning of SCR Catalysts," presented at the 1991 Symposium on Stationary Combustion Nitrogen Oxide Control, Washington, DC, March 25-28, 1991.

CMU (1993), "Development of the Integrated Environmental Control Model: Performance Models of Selective Catalytic Reduction (SCR) NOx Control Systems," Quarterly Progress Report prepared by Carnegie Mellon University for U.S. Department of Energy, June 1993.

EPA. Integrated Air Pollution Control System, Version 4.0, Volume 2: Technical Documentation Manual.

EPRI (1986). TAG - Technical Assessment Guide. Vol 1. P-4463-SR. Electric Power Research Institute. Palo Alto, CA. December.

Fickett, K.L., "Clean Coal-NOx for the 21st Century: Managing Permit Risk with Selective Catalytic Reduction (SCR) Technology," Paper 43a presented at the AIChE 1993 Summer National Meeting, Seattle, WA, August 14-18, 1993.

Flora, H., J. Barkely, G.Janik, B. Marker, and J.E. Chicanowicz, "Status of 1 MW SCR Pilot Plant Tests at Tennessee Valley Authority and New York State Electric and Gas," presented at the 1991 Symposium on Stationary Combustion Nitrogen Oxide Control, Washington, DC, March 25-28, 1991.

Frey, H. C. (1988), "Selective Catalytic Reduction Cost Algorithm for the Advanced Utility Simulation Model", Technical Memorandum to J. A. Martinez, Radian Corporation, July 8.

Gouker, T.R., and C.P. Brundrett. "SCR Catalyst Developments for the U.S. Market," presented at the 1991 Symposium on Stationary Combustion Nitrogen Oxide Control, Washington, DC, March 25-28, 1991.

Johnson, K.L., G.S. Shareef, and P.A. May. Evaluation of Oil-Fired Gas Turbine Selective Catalytic Reduction (SCR) NO_x Control. Prepared by Radian Corporation for the Gas Research Institute and Electric Power Research Institute. EPRI Report No. GS-7056. December 1990.

Koppius-Odink, J.M., et al. "The First DE-NO_x Installation in the Netherlands: A Demonstration Project at Epon-Nijmegen Power Station," in 1989 Symposium on Stationary Combustion Nitrogen Oxide Control, Volume 2. Electric Power Research Institute. Palo Alto, California. Report No. GS-6423. July 1989. pp. 6A-57 to 6A-83.

Kuroda, H., et al. "Recent Developments in the SCR System and Its Operational Experience," in 1989 Symposium on Stationary Combustion Nitrogen Oxide Control, Volume 2. Electric Power Research Institute. Palo Alto, California. Report No. GS-6423. July 1989. pp. 6A-39 to 6A-55.

Lowe, P.A., W. Ellison, and M. Perlsweig (1991), "Understanding the German and Japanese Coal-Fired SCR Experience," presented at the 1991 Symposium on Stationary Combustion Nitrogen Oxide Control, Washington, DC, March 25-28, 1991.

Maibodi, M., A. L. Blackard, and R. J. Page (1990), "Integrated Air Pollution Control System Version 4.0, Volume 2: Technical Documentation Manual," Prepared by Radian Corporation for U.S. Environmental Protection Agency, EPA-600/7-90-022b, December.

Maier, H., and P. Dahl, "Operating Experience With Tail-End and High-Dust Denox-Technics at the Power Plant of Heilbronn," presented at the 1991 Symposium on Stationary Combustion Nitrogen Oxide Control, Washington, DC, March 25-28, 1991.

Maxwell, J. D., and L.R. Humphries (1985), "Economics of Nitrogen Oxides, Sulfur Oxides, and Ash Control Systems for Coal-Fired Utility Power Plants," Prepared for U.S. Environmental Protection Agency, EPA-600/7-85-006, February.

May, P.A., L.M. Campbell, and K.L. Johnson. "Environmental and Economic Evaluation of Gas Turbine SCR NOx Control," presented at the 1991 Symposium on Stationary Combustion Nitrogen Oxide Control, Washington, DC, March 25-28, 1991.

Mori, T., and N. Shimizu. "Operating Experience of SCR Systems at EPDC's Coal-Fired Power Station," in 1989 Symposium on Stationary Combustion Nitrogen Oxide Control, Volume 2. Electric Power Research Institute. Palo Alto, California. Report No. GS-6423. July 1989. pp. 6A-85 to 6A-104.

Nakabayashi, Y., and R. Abe, "Current Status of SCR in Japan," in 1987 Symposium on Stationary Combustion Nitrogen Oxide Control, Volume 2. Electric Power Research Institute. Palo Alto, California. Report No. CS-5361. August 1987. pp. 25-1 to 25-29

Necker, I.P. "Experience Gained by Neckarwerke from Operation of SCR DeNO$_X$ Units," in 1989 Symposium on Stationary Combustion Nitrogen Oxide Control, Volume 2. Electric Power Research Institute. Palo Alto, California. Report No. GS-6423. July 1989. pp. 6A-19 to 6A-38.

Novak, M., and H.G. Rych. "Design and Operation of the SCR-Type NO$_X$ Reduction Plants at the Dürnrohr Power Station in Austria," in 1989 Symposium on Stationary Combustion Nitrogen Oxide Control, Volume 2. Electric Power Research Institute. Palo Alto, California. Report No. GS-6423. July 1989. pp. 7A-1 to 7A-26.

Offen, G.R., D.Eskanazi, M.W. McElroy, and J.S. Maulbetsch, "Stationary Combustion NO$_X$ Control," *JAPCA* 37(7):864-871.

Robie, C.P., and P.A. Ireland (1991), "Technical Feasibility and Cost of Selective Catalytic Reduction (SCR) NOx Control," GS-7266, Prepared by United Engineers and Constructors, Inc. for the Electric Power Research Institute, Palo Alto, CA, May.

Robie, C.P., P.A. Ireland, and J.E. Chicanowicz. "Technical Feasibility and Economics of SCR NO$_X$ Control in Utility Applications," in 1989 Symposium on Stationary Combustion Nitrogen Oxide Control, Volume 2. Electric Power Research Institute. Palo Alto, California. Report No. GS-6423. July 1989. pp. 6A-105 to 6A-124.

Robie, C.P., P.A. Ireland, and J.E. Chicanowicz. "Technical Feasibility and Cost of SCR for U.S. Utility Application," presented at the 1991 Symposium on Stationary Combustion Nitrogen Oxide Control, Washington, DC, March 25-28, 1991.

Rubin, E.S., J.S. Salmento, J.G. Barrett, C.N. Bloyd, and H.C. Frey, *Modeling and Assessment of Advanced Processes for Integrated Environmental Control of Coal-Fired Power Plants*, prepared by Carnegie-Mellon University for the U.S. Department of Energy, Pittsburgh, Pennsylvania, NTIS DE86014713, July 1986.

Rubin, E.S., J.S. Salmento, H.C. Frey, A. Abu-Baker, and M. Berkenpas, *Modeling of Integrated Environmental Control Systems for Coal-Fired Power Plants*, Final Report, Prepared by Carnegie-Mellon University for the U.S. Department of Energy, Pittsburgh, Pennsylvania, DOE Contract No. DE-AC22-87PC79864, April 1991, 214p.

Schönbucher, B. "Reduction of Nitrogen Oxides from Coal-Fired Power Plants by Using the SCR Process: Experiences in the Federal Republic of Germany with Pilot and Commercial Scale DeNOx Plants," in 1989 Symposium on Stationary

Combustion Nitrogen Oxide Control, Volume 2. Electric Power Research Institute. Palo Alto, California. Report No. GS-6423. July 1989. pp. 6A-1 to 6A-17.

Shiomoto, G.H., and L.J. Muzio, "Selective Catalytic Reduction for Coal-Fired Power Plants: Pilot Plant Results," Prepared by KVB, Inc. for the Electric Power Research Institute, Palo Alto, CA, Report No. CS-4386, April 1986.

U.S. Department of Energy, "Clean Coal Technology Demonstration Program: Program Update 1991", DOE/FE-0247P, February 1992.

4. Electrostatic Precipitator

4.1. Introduction

This chapter describes the development of analytical models for the performance and costs of high-performance particulate control technologies, focusing on electrostatic precipitators. Special attention is paid to developing models which can be used to estimate costs for systems whose performance is up to a factor of three below the present NSPS standards of 0.03 lb/MMBtu. Typically, the cost models relate the capital costs and the operating and maintenance (O&M) costs to process parameters and the costs of labor and materials. The capital cost models are anchored to a base capital cost for a specific size unit and adjusted according to the actual or design parameters. The performance models are constructed to estimate the process parameters for a desired level of emissions control. The primary motivation for these models is to estimate the costs of complying with environmental standards on a basis which reflects recent advances in control technology. Finally, we incorporate the uncertainties in various process parameters and inputs costs so as to allow a more rational and robust basis for comparing different technologies.

The development of the performance and cost models for electrostatic precipitators is discussed, followed by a numerical example which illustrates the use of these new models.

4.2. Background

ESPs have long been the work horse of particulate collection at coal-fired power plants. A large number of electrostatic precipitators were installed in power plants in the 1950's and 60's when 30-40% stack plume opacity was considered adequate. However, these ESP's were inadequate as the regulations in the 70's forced utilities to move to low sulfur coals with high resistivity ash. As a result it was not unusual for coal-fired power plants to suffer reductions in capacity due to excessive stack opacity. However, since the 80s due to a tremendous improvement in the technology, ESPs have demonstrated performance that is at least as good as modern day fabric filters. Older vintage ESPs (of 50s and 60s) performed at 0.1 lbs/MBtu for high sulfur coals. The ESPs in the 80s are almost twice the size[1] of the older ones (400-450 SCA today) and have demonstrated outlet emissions consistently well below 0.1 lbs/MBtu. In the utility industry (Kumar & Feldman, 1994), (Mastropietro, 1994a), the improved performance of ESPs has reduced the emissions of particulate matter from 0.1 lbs/MBtu to 0.01 lbs/MBtu over the last 15 years. In applications in the chemical industry (Kumar & Feldman, 1994), ESPs with SCA of 550-650 have been

used in pulp and paper industry (outlet emissions of 0.006 lbs/MBtu) and SCA of 800 has been used in refineries with outlet emissions as low as 0.003 lbs/MBtu. Therefore it is quite clear that properly sized ESPs are capable of achieving low particulate emissions that are below the 1979 NSPS standard of 0.03 lbs/MBtu.

In the next section, we describe updated performance models for sizing electrostatic precipitators. The process parameters for ESPs which affect the capital cost and O&M costs are explicated. Cost models parametrized by design parameters are then developed. Finally, we provide a numerical example to illustrate these cost models.

4.3. ESP Performance Models

ESPs consist of a series of parallel plates with rows of electrodes in between them and carry a high voltage of opposite polarity. As the particle laden flue gas enters the unit, the particles are charged by the electrodes and are attracted to the plates. At controlled intervals the plates are "rapped" which shakes the dust to a hopper below. However, some of the dust is reentrained, and is carried to the next zone or out of the stack. Most ESPs use rigid collecting plates with shielded air pockets ("baffles") through which ash falls into the hoppers after rapping. Collecting plate auxiliaries include inlet and outlet gas ducts, electrode frames, rappers, supporting framework, dust hoppers, and a protective outer shell. The discharge electrodes provide the corona. In most industrial applications a negative corona is used since its voltage-current characteristics are superior to those of a positive corona. The discharge electrodes are wires with diameters of typically 0.1-0.15 inches and are hung from a support frame with weights at the bottom. The dry dust is collected in hoppers which are usually of a pyramidal shape.

4.3.1. Ash Resistivity

The issue of proper sizing for electrostatic precipitation involves particle charging, particle collection, and removal of collected dust (Edgar, 1983; Oglesby & Nichols, 1978). In this section, we characterize the different parameters which affect electrostatic precipitation and sizing. The general equation used for describing the relationship between ESP size and collection efficiency is the so-called Deutsch-Andersen equation shown below:

$$\eta = 1 - \exp\left(-\frac{A}{V}w\right) \qquad (4\text{-}1)$$

where

η	=	collector removal efficiency
A	=	collector area, ft^2
V	=	volumetric flue gas flow rate, acfm
W	=	electrical migration velocity, ft/s
SCA	=	specific collection area, A/V

The specific collection area, SCA, is used as the sizing parameter for ESPs. The electrical migration velocity (also called precipitation rate parameter), *w*, is a critical parameter since it relates the removal efficiency to electrostatic precipitation. The most important factor which determines the electrical migration velocity is the *coal ash resistivity*. The resistivity in turn is a function of three main factors: (1) the flue gas composition, (2) ash composition, and (3) the temperature of the ash in ESP. The Bickelhaupt resistivity algorithms are commonly used to predict resistivity

(Bickelhaupt, 1986; Bickelhaupt & Altman, 1984). The algorithms are based on a resistivity-reciprocal absolute temperature curve which is derived from three separate effects discussed below.

1. Volume resistivity, ρ_V, can be described as the resistivity of flyash excluding the influence of flue gas composition. Ash composition, temperature, and physical characteristics of the particulate layer principally affect it.
2. Surface resistivity, ρ_S, results from the interaction of ash surface with adsorbed water vapor. Ash composition, gas temperature, gas moisture concentration and physical characteristics of ash affect it.
3. Acid resistivity, ρ_a, represents the conduction mechanism associated with adsorbed sulfuric acid vapor. It is affected by the sulfur content of coal.

The overall resistivity (ρ_{vsa}) is calculated by treating these individual resistances in parallel and is provided in the equation below:

$$p_{vsa} = \frac{p_a \times p_v \times p_s}{p_a \times p_v + p_v \times p_s + p_a \times p_s} \qquad (4\text{-}2)$$

We have implemented this algorithm for calculating coal ash resistivity in IECM and is shown in "Analytica Model Code for Ash Resistivity" on page 76. However, there is some discrepancy in the predictions of this model and values used in industrial practice especially for western coals (Mastropietro, 1994b; Sloat, 1994). As shown in Table 4-1, we introduce correction factors (Mastropietro, 1994b) for the Bickelhaupt models where appropriate. "Coal and Ash Analysis" on page 81 provides an ultimate analysis and the coal ash composition for each coal type (based on literature).

Table 4-1 ***Coal Resistivity***

Coal Type*	Industry Experience	Bickelhaupt algorithm	Correction factors
App.MS	E8-E10	1.3E9	1
WPCU	E9 - E10	7.6E10	1
Ill#6	E8 - E10	3E8	1
NDL	E8 - E10	3E8	1
WPRB (low) (high)	E9 - E11 E13	9E10 (low) 2E12(high)	1 (low) 10 (high)
App.LS	E12	1.2E12	1

* The coals used for comparison have the following attributes or properties:

App.MS = Appalachian Medium Sulfur (12.7 KBtu/lb. 2% S, 8% ash)

App.LS = Appalachian Low Sulfur (12.2 KBtu/lb, 0.5% S, 11.4% ash)

WPCU = Wasatch Plateau (Central Utah) (11.24 KBtu/lb, 0.6% S, 11% ash)

Ill#6 = East Central Illinois #6 (10.1 KBtu/lb, 4% S, 16% ash)

NDL = North Dakota Lignite (6.6 KBtu/lb, 0.7% S, 7.8 % ash)

WPRB = Wyoming Powder River Basin, (8.0 KBtu/lb, 0.5% S, 6.4% ash) the Na_2O content in ash varies 0.1-0.5%, 0.5% corresponds to low resistivity and 0.1% to high resistivity

4.3.2. Effective Migration Velocity

The next step in developing performance models involves correlating the total resistivity ρ_{sva} to the electrical migration velocity *w*. It is possible to develop a theoretical model which relates *w* to resistivity, which involves solving for the electric field and current density in the gas space between the collecting plates. This requires numerically solving for a set of partial differential equations which describe the electric field in between the plates (McLean, 1988; Oglesby & Nichols, 1978; White, 1977). Various computer-based theoretical models have been developed which represent in greater detail the electrical properties of ash and its particle size distribution (Lawless & Altman, 1989; Lawless & Plaks, 1989). However in practice, such idealized calculations often do not match experimental data well due to non-uniformities in gas flow distribution, gas sneakage, and rapping reentrainment. Moreover, it is desirable, especially in preliminary design, to have models that are relatively simple to use. In this report, we derive correlations between *w* and resistivity ρ_{sva} by deriving "effective" values for *w* corresponding to empirical data for *SCA* values for different coals and different emission limits. A modified version of the Deutsch equation, discussed below, is used to derive the effective values for *w*. These values are then correlated to the coal ash resistivity derived from the corrected Bickelhaupt algorithms.

The Deutsch-Anderson Equation (see (4-1)) is accurate only up to 95% removal efficiencies. Various empirical models have been developed to describe the "tailing off" of the efficiency curve at higher efficiencies ($\eta > 95\%$). One such empirically based performance model that has found widespread use and is able to effectively describe the efficiency curve for high *A/V* values was developed by White (White, 1977) and is provided in the following equation:

$$\eta = 1 - \exp\left(-\frac{A}{V} w_k \right)^k \qquad (4\text{-}3)$$

This equation is the so-called modified Deutsch equation. Typically, a value of $k \approx 0.6$ (Mastropietro, 1994b) is used in industrial practice today. In Table 4-2, typical *SCA* values for different removal efficiencies and coals are provided. The modified Deutsch equation (4-3) is used to derive the values for precipitation rate parameter w_k (column 5) corresponding to two sets of empirical SCA values. It is important to remember that when we use the modified-Deutsch equation (4-3), the rate parameter w_k ceases to have a physical interpretation (such as precipitation velocity for Equation (4-2)) and only provides a way to parameterize the effect of resistivity.

Table 4-2 ***Estimation of*** w_k

Coal	η %	SCA[1]	w_k[1]	SCA[2]	w_k[2]	w_k (aver)
	98	205	0.0474	175	0.0555	
App. MS	99.4	295	0.0515	270	0.0563	0.053
	99.8	415	0.0506	370	0.0568	
	98.7	255	0.0453	285	0.0406	
WPCU	99.6	385	0.0448	425	0.0406	0.043
	99.87	520	0.0452	575	0.0409	
	99.2	220	0.0627	230	0.06	
Ill #6	99.76	320	0.0625	335	0.0597	0.061
	99.92	425	0.0622	440	0.06	
	98.9	220	0.056	230	0.0535	
NDL	99.68	310	0.0556	335	0.0515	0.055
	99.89	420	0.0583	440	0.0556	
WPRB	98	280	0.0347			
(low resist)	99.5	405	0.0398			0.037
	99.8	550	0.0382			
WPRB	98			540	0.018	
(high resist)	99.5			835	0.0193	0.019
	99.8			1055	0.0199	
	98.65	320	0.0356	355	0.0321	
App.LS	99.6	490	0.0352	540	0.0319	0.034
	99.87	665	0.0353	735	0.032	

[1] SCA values are based on typical values suggested by vendors (Gaikwad & Sloat, 1992)

[2] SCA values used by Research-Cottrell (Mastropietro, 1994b)

The effective values calculated for w_k and the corresponding resistivities for each coal type (shown in Table 4-2) are summarized in Table 4-3.

Table 4-3 ***Summary of Resistivity and*** w_k

Coal	Resistivity (ohm-cm)	W_k
App.MS	1.3E9	0.053
WPCU	7.6E10	0.043
Ill #6	3E8	0.0612
NDL	3E8	0.055
WPRB (low)	9E10	0.037
WPRB (high)	2E13	0.019
App.LS	1.2E12	0.034

We now derive a regression model to develop a functional relation between resistivity and the parameter w_k. We find that a log-linear relationship (resistivity on

log-scale) provides an excellent fit for the data presented in Table 4-3. A regression analysis conducted in *Splus* presented in "Regression Analysis for w_k" on page 81 indicates that the log-linear relationship provides a R^2 =0.96. The functional relation between these two parameters is provided in Equation (4-4).

$$w_k = 0.1232972 - 0.003323934 \times \ln(\rho_{vsa}) \qquad (4\text{-}4)$$

This relationship can be used to estimate w_k for any given coal.

In summary, the new IECM performance models for cold-side ESPs are used as follows:

1. For a given coal, use the corrected-Bickelhaupt algorithm to calculate the resistivity, ρ_{vsa} of the flyash produced in the boiler. The resistivity depends on the coal ash composition, sulfur content, flue gas temperature, and moisture content.
2. Using Equation (4-4) and the resistivity, determine the parameter w_k.
3. Finally for a given emission limit (i.e. removal efficiency), determine the sizing parameter SCA using the modified-Deutsch equation (4-3).

Note that all the models developed in this section estimate the SCA values for a minimal spacing of 12 inches between plates.

4.3.3. Default Ash Composition

The new performance models implemented in IECM for cold-side ESPs requires as input coal ash composition, sulfur content, flue gas temperature, and moisture content. The coal ash composition needs to be specified with respect to the following ten constituents: SiO_2, Al_2O_3, Fe_2O_3, CaO, MgO, Na_2O, K_2O, TiO_2, P_2O_5, SO_3. In many cases, this information may not be readily available to the model user. We have developed a capability in IECM to pick default coal types for ash composition based on coal rank and sulfur content. Table 4-4 describes the rules used to pick default ash composition.

Table 4-4 ***Default Ash Composition***

Coal Rank	Classification	Default Ash Composition
Lignite	NDL	NDL
Sub-Bituminous	WPRB	WPRB
Bituminous	App.MS, App.LS, Ill#6, WPCU	If %S < 1.5% then App.LS else App.MS

For example, if the model user does not have readily available the ash composition of the coal, but knows the rank to be bituminous and sulfur content to be less than 1.5% then IECM uses this information to pick App.LS coal as a default for ash composition.

4.4. ESP Cost Models

The cost models for ESPs include both capital costs and operating and maintenance (O&M) costs. These models follow the economic premises for cost development and breakdown developed by EPRI (Gaikwad & Sloat, 1992). The cost areas used are shown below.

Table 4-5 ESP Process Areas

Process Area	Description
10	Collectors
20	Ductwork
30	Fly Ash Handling System
40	Differential Cost

The models developed in this report are based on data provided in two EPRI reports (Gaikwad & Sloat, 1992; Scheck, Mora, Belba, & Horney, 1985) and reflect price quotes from equipment vendors. In this section, we will first present the methodological basis used for model development.

4.4.1. Capital Cost Models

The major design parameters which can significantly impact the total system capital cost are *gas flow volume* (which depends on the generating unit size), *SCA*, the collecting plate area per transformer-rectifier (T-R) set and the spacing between collector plates. All calculations below are based on a default spacing of 12 inches. However, as the spacing between plates increases (as is the case with most modern ESPs), the SCA required also increases and this scaling is a simple ratio as shown in Equation (4-5).

$$\frac{SCA}{SCA^{/}} = \frac{D_{plates}}{D_{plates}^{/}} \qquad (4\text{-}5)$$

where

$SCA^{/}$ = SCA required for base case spacing, say 12 inches

$D^{/}_{plates}$ = default spacing between plates, i.e. 12 inches

The data used to choose different vectors of the design parameters are shown in Table 4-6. (Scheck, et al., 1985).

Table 4-6 ***Experimental Design***

Case	Size in MW	SCA ft^2/acfm	Area per T-R set (ft^2/T-R set)
Base	500	400	23750
1	250	400	23750
2	1000	400	23750
3	500	250	29700
4	500	800	23750
5	500	400	31700
6	500	400	19000
Range	250-1000	250-800	19000-31700

The costs for each vector of parameters in Table 4-6, broken down by process area is provided in Table 4-7, based on a 1985 EPRI study (Scheck, et al., 1985). Note that

this cost data is used to develop scaling models and actual numbers are not important.

Table 4-7 ***Capital Costs in $/kW, 1982 dollars***

Process Area	Case 1	Case 2	Case 3	Case 4	Case 5	Case 6	Base Case
10	34.60	29.71	20.68	55.98	29.65	33.99	32.06
20	0.88	0.85	1.00	1.01	1.01	1.01	1.01
30	8.82	4.99	5.17	8.40	5.71	6.79	6.25
40	0.74	0.74	0.74	0.75	0.74	0.74	0.74
Total	45.04	36.29	27.59	66.14	37.11	42.53	40.06

The mathematical model to describe the sensitivity of cost models to parameter variations is normalized against the cost for the base case. The general form of the cost model for each process area is as shown below:

$$\frac{PC_i}{PC_i^{/}} = \left(\frac{G}{G^{/}}\right)^f \times \left(\frac{SCA}{SCA^{/}}\right)^a \times \left(\frac{A_{T-R}{}^{/}}{A_{T-R}}\right)^b \times \left(\frac{SIL^{/}}{SIL}\right)^c \qquad (4\text{-}6)$$

where

PC_i = process area capital, $

$PC_i^{/}$ = process area capital, base case, $

G = inlet gas flow, acfm

$G^{/}$ = inlet gas flow, base case, acfm

$A_{T-R}{}^{/}$ = collecting area per set, base case AT-R

AT-R = collecting area per set, ft^2/set

SIL = ash rate to silo, tons/hr

$SIL^{/}$ = ash rate to silo, base case

Based on the cost data presented in Table 4-7, the exponents of the model in Equation (4-6) is estimated and presented in Table 4-8. Note that it is important to identify the cases which vary only one parameter from the base case since these allow direct estimation of the exponents. Note also that although the cost numbers in Table 4-7 are in $/kW, total $ need to be used in the model. Since the mathematical model is multiplicative, the exponents derived in Table 4-8 are independent of the base case used.[1]

Table 4-8 ***Exponents for Equation*** *(4-6)*

Area	*f*	*a*	*b*	*c*
10	0.89	0.81	0.266	0
20	0	0	0	0
30	0.59	0.34	0.34	0.1
40	0	0	0	0

In Table 4-8, some of the exponents have been chosen to be zero. This is because the variations for these process areas are not expected to influence cost. Also note that

these values for exponents have been averaged over several cases of available data. Due to the small size of the data set, no statistical analysis has been conducted. The exponents derived in Table 4-8 have been verified against some cost data collected more recently for unit sizes ranging from 125-500 MW (Gaikwad & Sloat, 1992), therefore the cost model can be used for the range 125-1000 MW.

The total capital requirement for ESPs is calculated as shown in Table 4-9. This includes the direct process capital costs and indirect costs associated with ESPs.

Table 4-9 ***Total Capital Requirement***

Particulate Collector	PC_{10}
Ductwork	PC_{20}
Flyash Handling	PC_{30}
ID fans	PC_{40}
Total Process Capital	$PC=PC_{10}+PC_{20}+PC_{30}+PC_{40}$
General facilities	0.01 PC
Eng. & Home Office Fees	0.05 PC
Process Contingency	0.05 PC
Project Contingency	0.2 PC
Total Plant Cost	TPC=1.31 PC
Total Plant Investment (including AFUDC)	TPI=1.063 TPC (3 years)
Preproduction Cost	0.002 TPI
Inventory Capital	0.005 TPC
Total Capital Requirement	TCR=1.002 TPI +0.005 TPC

4.4.2. O&M Cost Models

The O&M costs for ESPs consists of fixed costs and variable costs. The fixed operating cost consists of labor, maintenance labor, material, and administrative labor. A mathematical model for the fixed cost is provided by Equation (4-7).

$$
\begin{aligned}
FOM &= FOM_{labor} + FOM_{maint} + FOM_{admin} \\
FOM_{labor} &= labor \times N_{labor} \times 40\,(hrs/week) \times 52\,(weeks/yr) \\
FOM_{maint} &= 0.08 \times A_{esp} + 0.0134 \times C_{20} + 0.07 \times C_{30} + 0.025 \times C_{40} \\
FOM_{admin} &= 0.3 \times (FOM_{labor} + 0.4 \times FOM_{maint})
\end{aligned}
\qquad (4\text{-}7)
$$

where

FOM = fixed operating cost, M$/yr

FOM_{labor} = operating labor, M$/yr

$FOM_{maint.}$ = maintenance material costs, M$/yr, the coefficients based on EPRI TAG manuals

FOM_{admin} = administrative costs (assumed to be 30% of total labor costs) M$/yr, note that 40% of $FOM_{maint.}$ are assumed to be labor costs

A_{esp} = total collector area, ft^2

labor = labor rate, $/hour

N_{labor} = number of laborers at 40 hrs/week

C_i = capital for process area *i (20,30,40)*

Notice that the model has been developed analytically except that the dependence on unit size is based on process area costs.

Table 4-10 ***O&M costs in 1990 $/kW-yr***

O&M	125 MW	250 MW	500 MW
Ash	2.23	2.23	2.23
Power	1.41	1.31	1.23

Table 4-10 provides the variation in fixed and variable costs as a function of plant size (assuming a capacity factor of 65%). The variable cost includes the power cost and ash disposal cost. The ash disposal cost is proportional to the ash generated. The power costs are calculated based on the T-R set power and the other auxiliary power requirements. The variable operating cost is given by

$$\begin{aligned} \text{VOM} &= \text{VOM}_{\text{ash}} + \text{VOM}_{\text{power}} \\ \text{VOM}_{\text{ash}} &= cf \times C_{ash} \times 8760 \times T \\ \text{VOM}_{\text{power}} &= cf \times C_{power} \times 8760 \times \{TR' \times \left(\frac{G}{G'}\right) + AR' \times \left(\frac{G}{G'}\right)^{q}\} \end{aligned} \qquad (4\text{-}8)$$

where G, G' are as before and

VOM = variable operating costs, M$/yr

VOM_{ash} = ash disposal costs, M$/yr

VOM_{power} = power costs (includes T-R power and auxiliary power due to pressure drop etc), M$/yr

cf = capacity factor

T = ash disposal rate, tons/hr

C_{ash} = ash disposal cost, $/ton, (default 10.24)

C_{power} = power cost, cents/KWh, (5.54 c/kWh)

TR' = T-R set power as a function of efficiency, as shown in Equation (4-9)

AR' = Auxiliary power other than T-R set (includes energy penalty for pressure drop), 522 kW base case

q = 0.65, exponent derived from data in Table 4-9

Notice that Equation (4-8) is such that the base case cannot be changed arbitrarily. The T-R set power consumption is a function of removal efficiency and is given by Equation (4-9).

$$TR' = A \times \left(1 - \frac{\eta}{100}\right)^{r} \qquad (4\text{-}9)$$

where

A = constant in T-R set power

η = particle removal efficiency

r = exponent in Equation (4-9)

The values of constants A, r were determined based on quotes from various vendors (Gaikwad & Sloat, 1992), and are provided in Table 4-11.

Table 4-11 ***Parameters for Equation*** *(4-9)*

Coal	A	r
App.MS	78	-0.375
WPCU	81	-0.371
Ill.#6	95	-0.34
NDL	108	-0.353
WPRB (low)	102	-0.36
WPRB (high)	57	-0.39
App.LS	67	-0.40

4.4.3. A Numerical Example

We will use a base case of unit size 250 MW (0.95 Macfm), with a SCA of400 ft^2/acfm, 23750 ft^2/per T-R set, using Appalachian Medium Sulfur coal (ash content 8%, ash rate to silo =10.44 tons/hr). We estimate the cost of a unit with the following design parameters:

Size = 500 MW net(1.9 Macfm), SCA = 415 ft^2/acfm,

30000 ft^2/per T-R set, Capacity factor =65%,

Emission limit = 0.01 lb/MMBtu (99.86%), Ash disposal rate = 10.441 tons/hr

4.4.3.1. Capital Costs

$$PC_{10} = 8.53 \times \left(\frac{1.9}{0.95}\right)^{0.89} \times \left(\frac{415}{400}\right)^{0.81} \times \left(\frac{30000}{23750}\right)^{0.266} = 21.86M\$$$

$$PC_{20} = 0.835M\$$$

$$PC_{30} = 2.0825 \times \left(\frac{1.9}{0.95}\right)^{0.59} \times \left(\frac{415}{400}\right)^{0.34} \times \left(\frac{30000}{23750}\right)^{0.34} \times \left(\frac{10.44}{5.22}\right)^{0.1} = 3.68M\$$$

$$PC_{40} = 0.19M\$$$

Total Process Capital (PC) = 26.6 M$

General Facilities = 0.26 M$

Engg. & Home Office = 0.96 M$

Process Contingency = 1.33 M$

Project Contingency = 5.2 M$

Total Plant Cost (TPC) = 34.47 M$

TPI = 36.64 M$

Preproduction costs = 0.07 M$

Inventory Capital = 0.18 M$

Total Capital Requirement = 36.89 M$($ 73.78/kW)

4.4.3.2. Fixed Costs

$$FOM = FOM_{labor} + FOM_{maint} + FOM_{admin} = 0.53\,M\$/yr$$

$$FOM_{labor} = labor \times N_{labor} \times 40\,(hrs/week) \times 52\,(weeks/yr) = 0.12\,M\$/yr$$

$$FOM_{maint} = 0.08 \times C_{10} + 0.0134 \times C_{20} + 0.07 \times C_{30} + 0.025 \times C_{40} = 0.33\,M\$/yr$$

$$FOM_{admin} = 0.3 \times (FOM_{labor} + 0.4 \times 0.32) = 0.076\,M\$/yr$$

4.4.3.3. Variable Costs

$$VOM_{ash} = \frac{0.65}{1 \times 10^6} \times 10.24 \times 8760 \times 10.44 = 0.61\,M\$/yr$$

$$VOM_{power} = \frac{0.65}{1 \times 10^6} \times 0.0554 \times 8760 \times \{916.8 \times \left(\frac{1.9}{0.95}\right) + 522 \times \left(\frac{1.9}{0.95}\right)^{0.65}\} = 0.84\,M\$/yr$$

$$VOM = 1.45\ M\$/yr$$

4.5. Analytica Model Code for Ash Resistivity

We provide a listing of the Analytica model code for ash resistivity as implemented in the IECM.

```
Model resistivity

   Description: Model for ash resistivity based on
   Bickelhaupt's PB86-178126

   Author: jk3v

Model volume_r

   description: model for volume resistivity

   author: jk3v

variable lina

   units: atomic concentration in %

   description: the atomic conc. of lithium plus sodium,
   based on PB86-178126, appendix A, pg A-15

   definition:
   ashchar_atom[coalash_index='Na2O',coalindex=coals]

variable fe

   units: atomic concentration in %

   description: the atomic conc. of iron in ash, pg A-15

   definition:
   ashchar_atom[coalash_index='Fe2O3',coalindex=coals]

variable mgca

   units: atomic conc. in wt. %

   description: the atomic conc. of magnesium plus
   calcium, based on PB86-178126, appendix A, pg A-15
```

```
   definition:
   ashchar_atom[coalash_index='MgO',coalindex=coals]+ash
   char_atom[coalash_index='CaO',coalindex=coals]

function rv1(x,y,z:numeric)

   description: log(vol. resistivity) at 1000/T(K)=1.6,
   E=2 kV/cm, pg. 6-6, eq.2

   definition: 8.9434-1.8916*logten(x)-
   0.9696*logten(y)+1.237*(logten(z)-logten(2.5))

function rv2(x,y,z,E:numeric)

   description: log(vol. resistivity) at 1000/T(K)=1.6,
   E=12 kV/cm, pg. 6-6, eq.3

   definition:rv1(x,y,z)+(E-2)*(-0.03)

variable Iv

   units: log(ohm-cm)

   description: the line intercept of rv vs 1/T, pg. 6-
   6, eq. 4

   definition: rv2(lina,fe,mgca,12)-4334.5/625

function rv(temp:numeric)

   units: log(ohm-cm)

   description: vol. resistivity at any T, E=12 kV/cm

   definition: iv + 4334.5/temp

close volume_r

Model surface_r

   description: model for surface resistivity

   author: jk3v

function rs1(x:numeric)

   units: log(ohm-cm)

   description: surface resist. at 1000/T(K)=2.6,
   E=2kV/cm, water conc.(Cw)=9%

   definition: 10.7737 - 2.2334*logten(x)

function rs2(cw:numeric)

   units: log(ohm-cm)

   description: surface resist. at 1000/T(K)=2.6,
   E=2kV/cm,any Cw

   definition: rs1(lina)+(cw-9.0)*(-0.1280)

function rs3(cw,z:numeric)

   units: log(ohm-cm)
```

```
   description: surface resist. adjusted for mgca conc.,
   at 1000/T(K)=2.6, E=2kV/cm,any Cw

   definition: if mgca > 10 then rs2(cw)+0.56-0.056*z
   else rs2(cw)

function rs4(cw,z,E:numeric)

   units: log(ohm-cm)

   description: surface resist. adjusted for E

   definition: rs3(cw,z)+(E-2)*(-0.03)

function rs0(cw:numeric)

   units: log(ohm-cm)

   description: intercept for rs

   definition:
   rs4(cw,mgca,12)+logten(exp(1))*7.3895*10^(-
   4)*exp(2.3033*10^3/385)*cw

function rs(cw,temp:numeric)

   units: log(ohm-cm)

   description: surface resist. as function of design
   water conc.(cw) and temperature

   definition: rs0(cw)-logten(exp(1))*7.3895*10^(-
   4)*exp(2.3033*10^3/temp)*cw

close surface_r

function rvs1(cw,temp)

   units: ohm-cm

   description: surface and volume resistivities
   calculated as parallel resistances, E=12kv/cm

   definition:
   10^(rv(temp)+rs(cw,temp))/(10^rv(temp)+10^rs(cw,temp)
   )

model acid_r

   description: model for acid resistivity

   author: jk3v

variable rvs2

   units: ohm-cm

   description: vol/surface resistivity at
   1000/T(K)=2.4, E=12kV/cm

   definition: logten(rvs1(10,1000/2.4))+(-8)*(-0.03)

variable Ia1

   units: log(ohm-cm)
```

```
   description: intercept for ra1 based on mgca, fe
   conc.

   definition: if mgca < 5 and fe < 1 then 2.6354 else
   0.2915

variable ra1

   units: log(ohm-cm)

   description: acid resist. at 4ppm SO3, 10% H2O, 417K,
   4kV/cm

   definition: ia1 + 0.7669*rvs2

variable sa

   units:

   description: coefficient for ra2

   definition: if mgca < 5 and fe < 1 then -5.0 else -
   2.0502

variable ia2

   units

   description: intercept for ra2

   definition: ra1 - sa*logten(4)

function ra2(ca:numeric)

   units: log(ohm-cm)

   description: acid resist. at 4kV/cm,10%H2O, 417K, and
   any ca

   definition: ia2 + sa*logten(ca)

Index acid_i

   description: index for sa1 based on so3 conc.

   definition: ['1','2','3']

variable atom_i

   description: index for sa1 based on lina, mgca, and
   fe conc.

   definition: ['1','2','3']

variable acid_v

   description: value of sa1 index based on so3 conc.

   definition: if so3ppm(esp_gasin) < 2.75 then '1' else
   if so3ppm(esp_gasin) > 6.5 then '3' else '2'

variable atom_v

   description: value of sa1 based on mgca etc conc.

   definition: if lina > 1 and mgca > 5 then '1' else if
   fe < 1 and mgca < 3 then '2' else '3'
```

```
variable sa1
   description: slope of line denoting acid resisitivity
   vs 1/T
   definition: table(atom_i,acid_i)(-4.74, -4.85, -4.85,
   -28.39, -28.39, -28.39, -8.67, -9.71, -10.59)
function ia3(ca:numeric)
   description: line intercept for ra3
   definition: ra2(ca) -sa1[atom_i=atom_v,
   acid_i=acid_v]*2.4
function ra3(ca,temp)
   units: log(ohm-cm)
   description: acid resist. for any T, Ca and E=4kV/cm
   definition: ia3(ca) + sa1[atom_i=atom_v,
   acid_i=acid_v]*1000/temp
function ra(ca,temp)
   units: ohm-cm
   description: acid resist. for all ca, temp
   definition: 10^(1.95 + 0.76*ra3(ca,temp))
close acid_r
Close resistivity
```

4.6. Coal and Ash Analysis

Table 4-12 ***Ultimate Analysis for Coals***

	App.MS	WPCU	Ill#6	NDL	WPRB	App.LS
HHV	12.7K	11.24K	10.1K	6600	8020	12.2K
Carbon	0.697	0.642	0.575	0.397	0.48	0.67
Hydrogen	0.049	0.046	0.037	0.027	0.034	0.047
Oxygen	0.081	0.058	0.08	0.114	0.11	0.078
Chlorine	0	100u	1m	200u	300u	0
Sulfur	0.02	5.8m	0.04	6.8m	4.8m	5.5m
Nitrogen	0.013	0.0116	9m	6m	6.2m	0.013
Ash	0.08	0.11	0.16	0.078	0.064	0.114
Moisture	0.06	0.754	0.12	0.37	0.3	0.07

Table 4-13 ***Ash Analysis for Coals***

	App.MS	WPCU	Ill#6	NDL	WPRB	App.LS
SiO2	46.2	53.5	45	31.5	36.85	61
Al2O3	27.7	17.3	18	10.8	17.84	30
Fe2O3	17.2	4.5	20	13.4	5.36	2.9
CaO	3.4	10.7	7	25	26.59	0.91
MgO	0.8	2.4	1	7.1	5.48	0.76
Na2O	0.5	1.48	0.6	6.3	0.58	0.38
K2O	1.5	1.11	1.9	0.6	0.47	1.49
TiO2	1	0.7	1	0.2	1.28	0.09
P2O5	0.6	0.27	0.2	0.1	0.93	0.08
S03	1.1	7.04	3.5	4.6	3	0.2

4.7. Regression Analysis for w_k

The regression analysis for Equation (4-4) on page 70 was done using *Splus*. The analysis is presented here.

```
> data<-data.frame(wk,logr)
> data.fit<-lm(wk~logr,data)
> summary(data.fit)


Call: lm(formula = wk ~ logr, data = data)
Residuals:
 1 2 3 4 5 6 7
 -0.000486 0.003 0.002653 -0.003347 -0.00244 -0.002527
0.003147
```

```
Coefficients:
 Value Std. Error t value Pr(>|t|)
(Intercept) 0.1230 0.0073 16.7695 0.0000
 logr -0.0033 0.0003 -11.0365 0.0001

Residual standard error: 0.003153 on 5 degrees of freedom
Multiple R-Squared: 0.9606
F-statistic: 121.8 on 1 and 5 degrees of freedom, the p-
value is 0.0001063

> coefficients(data.fit)
 (Intercept) logr
 0.1230496 -0.003314819
```

4.8. References

Bickelhaupt, R. E. (1986). Fly Ash Resistivity Prediction Improvement with Emphasis on Sulfur Trioxide. No. EPA-600/7-86-010). EPA, Washington, DC.

Bickelhaupt, R. E., & Altman, R. F. (1984). A Method for Predicting the Effective Volume Resistivity of a Sodium Depleted Fly Ash Layer. JAPCA, 34, 832.

Edgar, T. F. (1983). Coal Processing and Pollution Control. Houston, TX: Gulf Publishing Co.

Gaikwad, R. P., & Sloat, D. G. (1992). Economic Evaluation of Particulate Control Technologies No. EPRI TR-100748). Electric Power Research Institute.

Kumar, K. S., & Feldman, P. L. (1994). Electrostatic Precipitators versus Fabric Filters: Fact versus Fiction. In Electrostatic Precipitators versus Fabric Filters: A symposium and Debate, . Crystal City, VA: ICAC.

Lawless, P. A., & Altman, R. F. (1989). An Integrated Electrostatic Precipitator Model for Microcomputers. In Proceedings: Eighth Particulate Control Symposium, Vol. 1: Electrostatic Precipitators, 1 (pp. 12-1:15). San Diego, CA: EPRI.

Lawless, P. A., & Plaks, N. (1989). An Advanced Microcomputer Model for Electrostatic Precipitators. In Proceedings: Eighth Particulate Control Symposium, Vol. 1: Electrostatic Precipitators, 1 (pp. 13-1:14). San Diego, CA: EPRI.

Mastropietro, R. A. (1994a). Achieving Low Particulate Emissions with Electrostatic Precipitators. In Electrostatic Precipitators versus Fabric Filters: Fact versus Fiction, Crystal City, VA: ICAC.

Mastropietro, R. A. (1994b). Performance models for low emission ESPs. In Research-Cottrell.

McLean, K. J. (1988). Electrostatic Precipitators. IEE Proceedings, 135, Pt. A(6), 341-61.

Oglesby, J. S., & Nichols, G. B. (1978). Electrostatic Precipitation. New York, NY: Marcel Dekker Inc.

Scheck, R. W., Mora, R. H., Belba, V. H., & Horney, F. A. (1985). Economics of Fabric Filters and Electrostatic Precipitators No. EPRI CS-4083). Electric Power Research Institute.

Sloat, D. G. (1994). Coal Ash Resistivity. In Sargent & Lundy.

White, H. J. (1977). Electrostatic Precipitation of Fly Ash. JAPCA, 27(3), 206.

5. Fabric Filter

5.1. Introduction

This chapter describes the development of analytical models for the performance and costs of high-performance particulate control technologies, focusing on fabric filters. Special attention is paid to developing models which can be used to estimate costs for systems whose performance is up to a factor of three below the present NSPS standards of 0.03 lb/MMBtu. Typically, the cost models relate the capital costs and the operating and maintenance (O&M) costs to process parameters and the costs of labor and materials. The capital cost models are anchored to a base capital cost for a specific size unit and adjusted according to the actual or design parameters. The performance models are constructed to estimate the process parameters for a desired level of emissions control. The primary motivation for these models is to estimate the costs of complying with environmental standards on a basis which reflects recent advances in control technology. Finally, we incorporate the uncertainties in various process parameters and inputs costs so as to allow a more rational and robust basis for comparing different technologies.

The initial development of the performance and cost models for fabric filters is discussed followed by a numerical example which illustrates the use of these new models. The next quarterly report will provide a similar update of the IECM electrostatic precipitator models, plus a brief discussion of the comparative advantages of different particulate control.

5.2. Fabric Filters for Electric Utilities

Fabric filters have been very effective in achieving the 1979 NSPS limits for coal-fired power plants. As a result, over 100 baghouses associated with 20,000 MW of generating capacity are in operation in the U.S. utility industry (Cushing, Bush, & Synder, 1990; Kumar & Feldman, 1994; Puille, 1985). These units routinely perform at efficiencies above 99.9% and produce clear stack plumes with less than 1% opacity. These fabric filters have been in operation with pulverized coal-fired boilers of various designs including some which are installed on fluidized bed combustion boilers. Operating experience in the U.S. has been predominantly with reverse gas cleaning (about 90%) with low air-to-cloth ratio baghouses. Bag failure rate has stabilized at about 1% per year through the 1980s and four-year bag life is now fairly common. In particular, there has been virtually no reduction in boiler availability due to baghouse malfunction since any target compartment can be brought off-line for baghouse replacement.

In this chapter, we will first discuss the important design parameters for fabric filters and their effects on capital and O&M costs. The design parameters are dependent on the bag cleaning method and this will be explicated. Cost models parameterized by design parameters are developed, along with a numerical example to illustrate the cost models.

5.3. Fabric Filter Design

Fabric filters are essentially huge vacuum cleaners consisting of a large number of long tubular filter bags arranged in parallel flow paths. As the ash-laden flue gas passes through these filters, almost all of the particulate matter is removed. Ash that accumulates on the bags is removed periodically by cleaning. For properly designed fabric filters, the size of the system is independent of the removal efficiency. Thus, efficiency can be improved without an associated increase in capital costs. The issue of a proper design is characterized by a number of parameters which we now discuss in some detail. We also provide the default operating values used in the industry today with an estimate of uncertainty to bound the variation observed in practice (Belba, Grubb, & Chang, 1992; Carr & Smith, 1984; Cushing, et al., 1990; Scheck, Mora, Belba, & Horney, 1985; Sloat, Gaikwad, & Chang, 1993).

There are various bag cleaning techniques that are used and this influences other process parameters in a non-trivial way. There are four available bag cleaning methods:

1. Reverse Gas Cleaning (RG): This is an off-line bag cleaning technique in which an auxiliary fan forces a relatively gentle flow of filtered flue gas backwards through the bags causing them to partially collapse and dislodge the dustcake. Over 90% of the U.S. utility baghouses use reverse-gas cleaning.
2. Reverse Gas/sonic cleaning (RG/S): A variation of RG in which low frequency pneumatic horns sound simultaneously with the flow of reverse gas to add energy to the dustcake removal process.
3. Shake/Deflate Cleaning (S/D): A method for offline cleaning. The bags are mechanically shaken immediately after or while a small quantity of filtered gas is forced back to relax the bags. The amount of filtered gas used is smaller than that used in RG cleaning.
4. Pulse-Jet Cleaning (PJ): A method for on-line cleaning in which pulses of compressed air are blown down inside and through the bags to remove dustcake while the bags are filtering flue gas. Wire support cages are used to prevent bag collapse during filtration and ash is collected outside of the bags.

The choice of the bag cleaning method is usually based on the type of coal being used (hence the filterability of the ash) and the historical experience with filtering the particular kind of ash. The choice of the bag cleaning method is a design decision and for the purposes of our models we assume that this is specified by the user. While reverse gas cleaning has been dominant in the past, studies have shown that it is not as effective as other methods in achieving low capital and O&M costs (Scheck, et al., 1985). RG/S and S/D impart more cleaning energy to the bags which results in thinner dustcakes and lower pressure drop. Such systems also can be at higher air-to-cloth (A/C) ratios, reducing costs. It appears that more recently, RG/S is emerging as a method of choice for full-scale, low A/C ratio utility baghouses on pulverized coal-fired boilers (Cushing, et al., 1990).

The most critical parameter in the operation of a baghouse is the relative system size which is characterized in terms of air-to-cloth ratio, defined as the volumetric flow rate of flue gas divided by the total bag cloth area. This ratio has the units of acfm/ft^2. The A/C ratio is determined based on the bag cleaning method, which controls the residual quantity of the material remaining on the bags. This in turn affects the resistance to gas flow and determines the pressure drop. Utility baghouses typically use A/C ratios of 1.5-4.0 acfm/ft^2 (net-net)[1] depending on the bag cleaning method. The cost of a baghouse is determined by the unit size which in turn depends on the gross A/C ratio and the volumetric flow rate. Given that the A/C ratio is the primary determinant of the unit size, and hence the capital and operating costs, it is desirable to operate at the highest A/C ratio that comfortably meets the performance specifications. Table 5-1 provides the typical values used for A/C ratio for various baghouse types based on industry experience (Belba, et al., 1992; Bustard, Cushing, & Chang, 1992; Cushing, et al., 1990; Puille, 1985; Sloat, et al., 1993).

Baghouse pressure drop is caused by pressure losses in gas flow as it moves through the bag fabric and dustcake. The pressure drop is usually measured in inches of water gauge or column (iwg or iwc) and is a measure of the energy required to move flue gas through the baghouse structure and bags. Flange-to-flange pressure drop is the pressure difference measured between the baghouse inlet and outlet flanges. It is the sum of ductwork and tubesheet pressure drops. Tubesheet pressure drop is measured across the tubesheet in a single compartment and consists largely of the pressure drop across the dustcake. Tubesheet pressure drop is the largest component of the flange-to-flange pressure drop and is useful since it can be controlled by the operator. However, it is the flange-to-flange pressure drop that is used in terms of a unit's energy consumption during operation and is used for sizing the ID fan. Baghouses are generally designed for a flange-to-flange pressure drop of about 6 -8 in. H_2O regardless of the cleaning method as a result of constraints from induced draft fans, ductwork stiffening, and other design details. Typical values for tubesheet pressure drop for given values of A/C ratios based on industry experience are also provided in Table 5-1.

Table 5-1 ***Typical Fabric Filter Design Parameters***

Baghouse Type	A/C Ratio net-net (acfm/ft^2)	Average tubesheet ΔP (in. H_2O)	Average Bag Life (years)
Reverse Gas	1.7 -2.0	3 x (A/C) +/- 20%	3-5
Reverse Gas Sonic	1.7 -2.0	2.5 x (A/C) +/- 20%	3-5
Shake-Deflate	2.5 - 3.0	2 x (A/C) +/- 15%	2-4
Pulse Jet	4.0 - 4.5	1.3 x (A/C) +/- 50%	2-4

U.S. utilities largely use woven fiberglass bag fabric because of high flue gas temperatures. Fiberglass can withstand temperatures up to 500 F and can be textured to control dustcake formation. But it is also susceptible to abrasion wear. The choice of the bag fabric affects the cost of the bag. Bags generally fall into two size categories: 30-36 ft in length and 1 ft in diameter, and 20 -22 ft in length and 8 in. in diameter. Bag life is generally not an issue (except for manufacturing defects and improper installation) and is usually between 3-5 years. All these parameters influence both the capital and operating costs. Once again, for the purposes of the models developed here these parameters are treated as design variables to be specified by the user. The effect of these choices on the cost of the baghouse has been modeled.

5.4. Cost Models for Fabric Filters

The cost models for the four types of fabric filters are developed for both capital costs and operation and maintenance (O&M) costs. These models follow the economic premises for cost development and breakdown developed by EPRI. The capital costs are developed on a process area by process area basis and the O&M are developed to reflect the fixed and the variable operating costs. The cost areas are shown in Table 5-2.

Table 5-2 ***Process Areas for Fabric Filter cost Models***

Process Area	Description
10	Collectors
20	Ductwork
30	Fly Ash Handling System
40	Differential Cost

The models developed in this report are based on price quotes from equipment vendors obtained for EPRI (Gaikwad & Sloat, 1992; Scheck, et al., 1985). The main difference in our treatment of these costs is that we have developed cost models parametrized by operating design parameters on a process area basis. In contrast, the EPRI models use aggregate costs (such as total capital requirement) for the development of parametrized models. In this subsection, we first present the methodological basis used for model development and then present the cost models.

In the development of cost models, we have treated the Reverse-Gas, Reverse Gas/Sonic and the Shake-Deflate baghouses as one class of systems and the Pulse-Jet fabric filter separately as another class. Engineering experience suggests that the difference in the economics between RG, RG/S, and SD baghouses can be treated parametrically through the operating design parameters A/C, ΔP, and bag life (Scheck, et al., 1985). This implies that the difference in costs between a RG baghouse and a RG/S baghouse is largely accounted by the difference in the design parameters and can be described by one set of cost models. The cost models for Pulse-Jet baghouses have been developed separately since it is a new technology and there is not sufficient experience to treat it parametrically in the context of the RG models.

The major design parameters which can significantly impact the total system cost of the fabric filter are *gas flow volume* (which depends on the generating unit size), *A/C ratio*, the *flange-to-flange pressure drop* in the baghouse, *bag life* and the *bag fabric* that is used for filtering. The costs of baghouses for different unit sizes and with variations in the above parameters are reflected in the models. The sensitivity of baghouse costs to variations in these parameters is analyzed to parameterize the cost models. We will now discuss in detail the experimental design and development the cost models for each system of baghouses separately.

5.4.1. Reverse Gas Systems

The experimental design used to choose different vectors of the design parameters for capital cost estimation (Scheck, et al., 1985) is shown in Table 5-3.

Table 5-3 ***Range of Model Design Parameters***

Case	Size in MW (acfm)	A/C Ratio (gross) cfm/ft^2	Bags per Compartment (No. of Compartments)
Base	500 MW (1.9 M)	2.0	360 (28)
1	250 MW (0.95 M)	2.0	360 (14)
2	1000 MW (3.8 M)	2.0	360 (56)
3	500 MW (1.9M)	1.6	396 (32)
4	500 MW (1.9M)	3.6	396 (14)
5	500 MW (1.9M)	2.0	648 (16)
6	500 MW (1.9M)	2.0	252 (40)
Range	250-1000 MW	1.6-3.6	252-648

The costs for each vector of parameters in Table 5-3, broken down by process area is provided in Table 5-4 based on a 1984 EPRI study (Scheck, et al. 1984). These costs are used only to obtain an exponential scaling factor for each process area. The actual cost-models are based on 1990 dollars.

Table 5-4 ***Process Area Capital Costs Used for Scaling Parameter Estimation (1982 $/kW)***

Process Area	Case 1	Case 2	Case 3	Case 4	Case 5	Case 6	Base Case
10	39.51	32.51	43.23	22.16	32.87	37.84	35.86
20	0.85	0.60	0.71	0.72	0.71	0.71	0.71
30	8.90	4.75	6.45	5.24	5.26	6.73	6.01
40	1.85	1.85	1.50	4.02	4.02	1.85	1.85
Total	51.11	39.71	51.89	32.14	40.69	47.13	44.43

The mathematical model to describe the sensitivity of cost models to parameter variations is normalized against the cost for the base case. The general form of the cost model for each process area is as shown below:

$$\frac{PC_i}{PC_i^{/}} = \left(\frac{G}{G^{/}}\right)^f \times \left(\frac{A/C^{/}}{A/C}\right)^a \times \left(\frac{B^{/}}{B}\right)^b \times \left(\frac{SIL}{SIL^{/}}\right)^c \qquad (5\text{-}1)$$

where

PC_i = process area capital, 1990 $

$PC_i^{/}$ = process area capital, base case, 1990 $

G = inlet gas flow, acfm

$G^{/}$ = inlet gas flow, base case, acfm

A/C = air-to-cloth ratio, acfm/ft2

$A/C^{/}$ = air-to-cloth ratio, base case, acfm/ft2

B = bags per compartment

$B^{/}$ = bags per compartment, base case

SIL = ash rate to silo, tons/hr

$SIL^{/}$ = ash rate to silo, base case, tons/hr

Based on the cost data presented in Table 5-4, the exponents of the model in Equation (5-1) are estimated and presented in Table 5-5. Note that it is important to identify the cases which vary only one parameter from the base case since these allow direct estimation of the exponents. Note also that although the cost numbers in Table 5-4 are in $/kW, total dollar needs to be used in the model. Since the mathematical model is multiplicative, the exponents derived in Table 5-5 are independent of the base case used.[1] The actual base costs used in the model are based on more recent EPRI studies for a 250 MW plant, although these costs are not significantly different from those reported in earlier studies.

Table 5-5 ***Model Scaling Factors***

Area	*f*	*A*	*b*	*c*
10	0.86	0.84	0.15	0
20	0.75	0	0	0
30	0.55	0.29	0.275	0.083
40	0	0	0	0

In Table 5-5, some of the exponents have been chosen to be zero. This is because the variations for these process areas are not expected to influence cost. Also note that these values for exponents have been averaged over several cases of available data. Due to the small size of the data set, no statistical analysis has been conducted. The exponents derived in Table 5-5 have been verified against cost data collected more recently for unit sizes ranging from 125-500 MW (Gaikwad & Sloat, 1992); therefore the cost model can be used for the range 125-1000 MW.

The total capital requirement for a reverse gas baghouse is calculated as shown in Table 5-6. This includes the direct process capital costs and indirect costs associated with reverse baghouses.

Table 5-6 ***Total Capital Requirement***

Component	Cost
Particulate Collector	PC_{10}
Ductwork	PC_{20}
Flyash Handling	PC_{30}
ID fans	PC_{40}
Total Process Capital	$PC=PC_{10}+PC_{20}+PC_{30}+PC_{40}$
General Facilities *	0.10 PC
Eng. & Home Office Fees *	0.05 PC
Process Contingency *	0.05 PC
Project Contingency *	0.2 PC
Total Plant Cost *	TPC=1.31 PC
Total Plant Investment (including AFUDC) *	TPI=1.063 TPC (3 years)
Preproduction Cost *	0.002 TPI
Inventory Capital *	0.005 TPC
Total Capital Requirement *	TCR=1.002 TPI +0.005 TPC

*These items are based on model default values for indirect cost factors. The IECM allows these factors to be changed by the user.

The O&M costs for the reverse-air baghouse consists of the fixed costs and the variable costs. The fixed operating cost consists of labor, maintenance labor, material, filter bags, and administrative labor. A mathematical model for the fixed cost is parametrized on unit size, the A/C ratio, bag cost and bag life and is provided by Equation (5-2).

$$\frac{FOM}{FOM'} = \left(\frac{G}{G'}\right)^{s} + \frac{N_{bags}}{10^{6}} \times \left(\frac{BC}{BF}\right) \times \left(\frac{G}{G'}\right) \times \left(\frac{A/C'}{A/C}\right) \qquad (5\text{-}2)$$

where G, G/, A/C, A/C/ are as defined in Equation (5-1), and

FOM = fixed operating cost, M$

FOM/ = fixed operating cost, base case (0.455 M$)

G = flue gas flow rate

G/ = flue gas flow rate, base case (0.95 Macfm)

A/C = air-to-cloth ratio, acfm/ft^2

A/C = air-to-cloth ratio, base case (2.0 acfm/ft^2)

BC = bag cost, $

BF = bag life, years

N_{bags} = numbers of bags in baghouse (360 x 14 default)

s = 0.48, exponent developed from data in Table 5-6.

Notice that the model has been developed largely analytically except that the dependence on unit size is based on data in Table 5-7 which is based on quotes from vendors (Gaikwad & Sloat, 1992). *Note that Equation* (5-2) *is such that the base case cannot be changed arbitrarily*.

Table 5-7 ***Data Used for Scaling Parameter Estimation of O&M Costs ($/kW-yr)***

O&M	125MW	250MW	500MW
Fixed	2.80	1.82	1.36
Ash Disposal	2.23	2.23	2.23
Power	1.82	1.69	1.61

The variable cost includes the power cost and ash disposal cost. The ash disposal cost is proportional to the ash generated. The power costs are calculated based on the ID fan power required to overcome the expected pressure drop across the baghouse and the other auxiliary power requirements. The variable operating cost is given by

$$VOM = cf \times [C_{ash} \times 8760 \times A + C_{power} \times 8760 \times (135 \times \Delta P \times \left(\frac{G}{G'}\right) + P_{aux} \times \left(\frac{G}{G'}\right)^{t})] \qquad (5\text{-}3)$$

where G, G' are as before and

VOM = variable operating costs, 1990 $

cf = capacity factor

A = ash disposal rate, tons/hr

C_{ash} = ash disposal cost, $/ton, (default = $10.24/ton)

C_{power} = power cost, cents/kWh

P_{aux} = auxiliary power requirement (323 kW)

ΔP = flange to flange pressure drop, inches of H_2O (7.5in)

t = 0.65, exponent derived from data in Table 5-6

Notice once again that Equation (5-3) *is such that the base case cannot be changed arbitrarily.*

5.4.1.1. A Numerical Example

We will use a base case of unit size 250 MW (0.95 Macfm), with a A/C ratio of 2 acfm/ft^2, with 360 bags/compartment, 14 compartments, using Appalachian Medium Sulfur coal (ash content 8%, ash rate to silo =10.44 tons/hr). We estimate the cost in 1990 dollars of a unit with the following design parameters:

Size = 500 MW (1.9 Macfm), A/C = 2 acfm/ft2,

396 bags/compartment, 32 compartments,

Bag life = 4 years, bag cost =$ 80/bag

Capacity factor =65%, flange-to-flange pressure drop = 7.5 in. H2O

Emission limit = 0.01 lb/MMBtu (99.86%), Ash disposal rate = 10.441 tons/hr

Capital Costs ($1990)

$$PC_{10} = 10.21 \times \left(\frac{1.9}{0.95}\right)^{0.86} \times \left(\frac{2}{1.6}\right)^{0.81} \times \left(\frac{360}{396}\right)^{0.15} = 21.89 M\$$$

$$PC_{20} = 0.3325 \times \left(\frac{1.9}{0.95}\right)^{0.75} = 0.56 M\$$$

$$PC_{30} = 2.06 \times \left(\frac{1.9}{0.95}\right)^{0.55} \times \left(\frac{2}{1.6}\right)^{0.29} \times \left(\frac{360}{396}\right)^{0.275} \times \left(\frac{10.44}{5.22}\right)^{0.083} = 3.32 M\$$$

$$PC_{40} = 0.19 M\$$$

$$PC = 21.89 + 0.56 + 3.32 + 0.19 = 25.96 M\$$$

General Facilities = 0.26 M$
Engg. & Home = 1.9 M$
Proc. Contingency = 1.9 M$
Proj. Contingency = 5.2 M$
TPC = 35.21 M$
TPI = 37.43 M$
Preproduction cost = 0.075 M$
Inventory capital = 0.176 M$
Total Capital Req = 37.68 M$ ($75.4/kW)

Fixed Costs

$$FOM = 0.455 \times \left(\frac{1.9}{0.95}\right)^{0.48} + \frac{396 \times 14}{1 \times 10^6} \times \left(\frac{80}{4}\right) \times \left(\frac{1.9}{0.95}\right) \times \left(\frac{2}{1.6}\right) = 0.91 M\$ / yr$$

Variable Costs

$$VOM = 0.65 \times \left(\frac{10.24 \times 8760 \times 10.441}{1 \times 10^6} + \frac{0.0554 \times 8760}{1 \times 10^6} \times \left[135 \times 7.5 \times \left(\frac{1.9}{0.95}\right) + 323 \times \left(\frac{1.9}{0.95}\right) \right] \right)$$

$$= 2.22 M\$ / yr$$

5.4.2. Pulse-Jet Systems

The experimental design used to choose different vectors of design parameters for capital costs are shown in Table 5-8. However, since Pulse-Jet fabric filters are evaluated with three different levels of pressure jets (low, intermediate, and high pressure) this design is used three times, once for each pressure level.

Table 5-8 ***Design Parameters for Pulse-Jet Systems***

Case	Size in MW (M acfm)	A/C Ratio (gross) acfm/ft^2	Bag length (feet)
Base	250 (0.9)	4	20
1	125 (0.475)	4	20
2	500 (1.9)	4	20
3	250 (0.9)	3	20
4	250 (0.9)	6	20
5	250 (0.9)	4	15
6	250 (0.9)	4	25
Range	125 - 500	3-6	15 -25

The costs for each vector of parameters in Table 5-8 broken down by process area is based on recent EPRI data for low, intermediate, and high pressure Pulse-Jet fabric filters (Gaikwad & Sloat, 1992).

The mathematical model to describe the sensitivity of the cost models to parameter variations again is normalized against the cost for the base case. The generalized form of the model for each process area is shown below:

$$\frac{PC_i}{PC_i^{/}} = \left(\frac{G}{G^{/}}\right)^j \times \left(\frac{A/C^{/}}{A/C}\right)^k \times \left(\frac{BL^{/}}{BL}\right)^l \times \left(\frac{BC}{BC^{/}}\right)^m \times \left(\frac{SIL}{SIL^{/}}\right)^i \qquad (5\text{-}4)$$

where

PC_i = process area capital, M$

$PC_i^{/}$ = process area capital, base case, M$

G = inlet gas flow, acfm

$G^{/}$ = inlet gas flow, base case, acfm

A/C = air-to-cloth ratio, acfm/ft^2

$A/C^{/}$ = air-to-cloth ratio, base case, acfm/ft^2

BL = bag length, feet

$BL^{/}$ = bag length, base case, feet

BC = bag cost $/bag

$BC^{/}$ = bag cost, base case, $/bag

SIL = ash rate to silo, tons/hr

$SIL^{/}$ = ash rate to silo, base case, tons/hr

i,j,k,l,m = exponents derived from data

The estimated exponents of the model in Equation (5-4) are presented in Table 5-9. The model is once again independent of the base case used.

Table 5-9 ***Exponents for Equation*** *(5-4)*

Area	*j*	*k*	*l*	*m*	*i*
10	0.85	0.72	0.44	0.15	0
20	0	0	0	0	0
30	0.56	0.12	0.10	0	0.13
40	0	0	0	0	0

InTable 5-9 some of the exponents are chosen to be zero since they do not influence the capital costs. All exponents for the process area 40 are chosen zero since the slight variation in cost is not consistent with the economics of scale. Moreover, the cost of process area 40 is less than 5% of the total process cost.

As with reverse gas baghouses, the O&M costs for pulse-jet baghouses consists of fixed and variable costs. The fixed operating costs consist of labor, maintenance labor, material, filter bags, and administrative labor. The mathematical model for the fixed costs is parametrized on unit size, A/C ratio, bag cost and bag life shown in Equation (5-5).

$$\frac{FOM}{FOM'} = \left(\frac{F}{F'}\right)^{u} + \frac{N_{bags}}{10^{6}} \times \left(\frac{BC}{BF}\right) \times \left(\frac{G}{G'}\right) \times \left(\frac{A/C'}{A/C}\right) \qquad (5\text{-}5)$$

where F, F', A/C, A/C' are as defined in Equation (5-1), and

FOM = fixed operating cost, M$

FOM' = fixed operating cost, base case,0.6325 M$

G = flue gas flow rate

G' = flue gas flow rate, base case, 0.95 Macfm

A/C = air-to-cloth ratio, acfm/ft2

A/C = air-to-cloth ratio, base case, 2 acfm/ft^2

BC = bag cost, $, (default $80)

BF = bag life, years, (default 3 years)

N_{bags} = numbers of bags in baghouse, (default 9050)

u = 0.63 exponent developed from data in Table 5-9.

This model has been developed largely analytically, however, the dependence on unit size is based on data in Table 5-10. (Gaikwad & Sloat, 1992).

Table 5-10 ***Relative O&M costs Used for Scaling Factor Estimation (in $/kW-yr)***

O&M	125 MW	250 MW	500 MW
Fixed	3.45	2.53	2.07
Ash	2.23	2.23	2.23
Power	2.06	1.96	1.88

The variable costs, as before, includes power cost and ash disposal costs. The variable operating cost is given by Equation (5-6):

$$VOM = cf \times \left(\begin{array}{l} C_{ash} \times 8760 \times A + C_{power} \times 8760 \\ \times \left[135 \times \Delta P \times \left(\frac{G}{G^{/}} \right) + P_{aux} \times \left(\frac{G}{G^{/}} \right)^{w} \right] \end{array} \right) \qquad (5\text{-}6)$$

where F, $F^{/}$ are as before and

VOM	=	variable operating costs, $
cf	=	capacity factor
A	=	ash disposal rate, tons/hr
C_{ash}	=	ash disposal cost, $/ton
C_{power}	=	power cost, cents/KWh (default 5.54)
P_{aux}	=	auxiliary power requirement, 742 kW
ΔP	=	flange to flange pressure drop, inches of H2O
w	=	0.85, exponent derived from data in Table 5-10

Notice once again that Equation (5-6) *is such that the base case cannot be changed arbitrarily*

5.4.2.1. A Numerical Example for Pulse-Jet Baghouses

We will estimate the capital and operating costs for a pulse-jet baghouse for the same design parameters as used in the example for reverse-gas baghouses. (Refer to Table 5-6 for indirect costs).

Capital Costs (1990 $)

$$PC_{10} = 5.925 \times \left(\frac{1.9}{0.95} \right)^{0.85} \times \left(\frac{4}{3} \right)^{0.72} \times \left(\frac{20}{15} \right)^{0.44} = 14.9M\$$$

$$PC_{20} = 0.375M\$$$

$$PC_{30} = 2.155 \times \left(\frac{1.9}{0.95} \right)^{0.56} \times \left(\frac{4}{3} \right)^{0.12} \times \left(\frac{20}{15} \right)^{0.1} \times \left(\frac{10.44}{5.22} \right)^{0.13} = 3.70M\$$$

$$PC_{40} = 0.19M\$$$

Total Process Capital (PC) = 19.165 M$

General Facilities = 0.19 M$

Engg. & Home Office = 0.96 M$

Process Contingency = 1.9 M$

Project Contingency = 3.8 M$

Total Plant Cost (TPC) = 26.0 M$

TPI = 27.65 M$

Preproduction costs = 0.055 M$

Inventory Capital = 0.13 M$

Total Capital Requirement = 27.835 M$ ($55.7/kW)

Fixed Costs

$$FOM = 0.6325 \times \left(\frac{1.9}{0.95}\right)^{0.63} + \frac{360 \times 14}{10^6} \times \left(\frac{80}{4}\right) \times \left(\frac{1.9}{0.95}\right) \times \left(\frac{4}{3}\right)$$

$$= 1.78 M\$ / yr$$

Variable Costs

$$VOM = \frac{0.65}{1 \times 10^6} \times \left(\begin{array}{l} 10.24 \times 8760 \times 10.44 \\ + 0.0554 \times 8760 \times \left[135 \times 6.7 \times \left(\frac{1.9}{0.95}\right) + 742 \times \left(\frac{1.9}{0.95}\right)^{0.8} \right. \end{array} \right.$$

$$= 1.6 M\$ / yr$$

5.5. References

Belba, V. H., Grubb, W. T., & Chang, R. (1992). The Potential of Pulse-Jet Baghouses for Utility Boilers. Part 1: A Worldwide Survey of Users. J. Air Waste Manage. Assoc., 42(2), 209.

Bustard, C. J., Cushing, K. M., & Chang, R. L. (1992). The Potential of Pulse-Jet Baghouses for Utility Boilers. Part 2: Performance of Pulse-Jet Fabric Filter Plants. J. Air Waste Manage. Assoc., 42(9), 1240.

Carr, R. C., & Smith, W. B. (1984). Fabric Filter Technology for Utility Coal-Fired Power Plants: A Series of Articles Reprinted from the "J. of Air Pollution Control Association" No. EPRI CS-3754-SR). Electric Power Research Institute.

Cushing, K. M., Bush, P. V., & Synder, T. R. (1990). Operating history and current status of fabric filters in the utility industry. J. Air Waste Manage. Assoc., 40, 1051.

Gaikwad, R. P., & Sloat, D. G. (1992). Economic Evaluation of Particulate Control Technologies No. EPRI TR-100748). Electric Power Research Institute.

Kumar, K. S., & Feldman, P. L. (1994). Electrostatic Precipitators versus Fabric Filters: Fact versus Fiction. In Electrostatic Precipitators versus Fabric Filters: A Symposium and Debate, . Crystal City, VA: ICAC.

Puille, W. (1985). 1985 Update, Operating History and Current Status in the Utility Industry. In Third Conference on Fabric Filter Technology for Coal Fired Power Plants, . Scottsdale, AZ:

Scheck, R. W., Mora, R. H., Belba, V. H., & Horney, F. A. (1985). Economics of Fabric Filters and Electrostatic Precipitators No. EPRI CS-4083). Electric Power Research Institute.

Sloat, D. G., Gaikwad, R. P., & Chang, R. L. (1993). The Potential of Pulse-Jet Baghouses for Utility Boilers. Part 3: Comparative Economics of Pulse-Jet Baghouse, Precipitators and Reverse-Gas Baghouses. J. Air Waste Manage. Assoc., 43, 120.

6. Flue Gas Desulfurization

6.1. Background to FGD Models

In this chapter we describe the use of systematic sensitivity analysis and multivariate regression for the development of analytical models for the performance and cost of high-performance wet lime/limestone FGD systems and dry lime sprayer systems. Special attention has been paid to FGD systems whose performance with respect to sulfur removal efficiency lies in the 90-98% range. The cost of using additives such as dibasic acid (DBA) as a design option for achieving high performance is also examined. The cost models developed relates the capital costs and the operating and maintenance costs to input variables describing performance parameters and the costs of labor and materials. Systematic sensitivity analysis is used to select and rank the set of input variables and multivariate regression is used for the development of functional relations between the input variables and costs (outputs). This systematic approach along with engineering judgment is used to develop aggregate models for costing high performance FGD systems. These aggregate models are appropriate in size and form for conducting uncertainty analysis using Monte Carlo methods in the IECM.

The chapter is organized as follows. Section 6.2 below describes the development of new FGD performance models. Based on a review of the literature, some approximate functional relations to describe FGD performance are presented. Section 6.3 on page 108 provides an overview of the methodological approach used to derive capital cost models. Four FGD systems are analyzed: (1) wet limestone with forced oxidation (LSFO), (2) dibasic acid enhanced wet limestone (LS/DBA), (3) a magnesium-enhanced wet lime system, and (4) a spray dryer with lime. The relations for direct process capital cost models are derived for each process area in Section 6.4 on page 116. The effects of different sparing philosophies on the capital cost are also examined. Cost models are then developed for the fixed operating and maintenance costs associated with operating a FGD system in Section 6.5 on page 124. Section 6.6 on page 125 develops models for the variable costs of reagent use, power use, waste disposal, energy consumption etc. Section 6.7 on page 129 provides a numerical example to illustrate the new models.

6.2. FGD Performance Models

In this section we describe the performance models used to provide key parameter inputs to the cost models described later. We begin with a brief survey of FGD

performance literature. Based on the literature, approximate functional relations between performance parameters are developed.

The analysis in this chapter is geared towards developing updated performance and cost models for four commercial FGD processes:

1. Limestone with Forced Oxidation (LSFO): A limestone slurry is used in an open spray tower with in-situ oxidation to remove SO_2 and form a gypsum sludge. The main advantages as compared to conventional systems is easier dewatering, more economical disposal of scrubber products, and decreased scaling on tower walls.
2. Limestone with Dibasic Acid Additive (LS/DBA): A modification to LSFO where dibasic acid (DBA) is added to act as a buffer/catalyst in the open spray tower. The main advantages are increased SO_2 removal and decreased liquid to gas ratio.
3. Magnesium Enhanced Lime System: A magnesium sulfite and lime slurry (maglime) is used to remove SO_2 and form a precipitate high in calcium sulfite. The high alkalinity of the maglime slurry allows very high SO_2 removal. However, the reagent cost is also higher and solid waste is not easily disposed.
4. Lime Spray Dryer: An atomized spray of a mixture of lime slurry and recycled solids is brought into contact with the hot flue gas. The water in the slurry evaporates leaving dry reaction products and flyash which drops out of the scrubber. A particulate control device such as a baghouse is also used to remove the rest of the dry products from the flue gas before releasing it. The SO_2 removal efficiency is the total of SO_2 removed in the scrubber and the baghouse.

6.2.1. Wet Limestone FGD Systems

Advanced wet limestone FGD systems are now designed to achieve SO_2 removal efficiencies in excess of 95%. The single loop countercurrent spray tower is the most commonly used device for the removal of SO_2. The design of spray towers for high efficiency without additives is achieved by using high liquid-to-gas (L/G) ratios and improving gas/liquid contact by spray nozzle design (Bhat, et al., 1993; Rader & Bakke, 1991) On the other hand, organic acids such as dibasic acid or adipic acid are added as buffers to improve performance (Blythe, et al., 1993; Moser & Owens, 1990; Smolenski, et al., 1993; Stevens, et al., 1993) In this section, brief descriptions and approximate relations for high performance LSFO and LS/DBA systems are provided. The approximate relations are gleaned from the literature to reflect US experience with high performance wet limestone FGD systems (Benson, 1993; Dene, et al., 1991; Johnson, 1993; Klingspor, 1993; Laslow, 1993; Moser & Owens, 1990; Noblett Jr., et al., 1990; Noblett Jr., 1993; Rader, 1993; Rader & Bakke, 1991; Smolenski, et al., 1993; Stevens, et al., 1993; Stevens, et al., 1991; Weilert, 1993; Weilert & Ratliff, 1990). The paragraph below provides some background (Corbett, et al., 1977; Noblett Jr., et al., 1990) for the scrubbing process, which is useful in understanding the bases for the relations, provided later.

The removal of SO_2 from flue gas in a lime/limestone scrubber depends on a gas-liquid-solid mass transfer process. The sulfur dioxide is transferred from the flue gas to the slurry liquid in the scrubber and subsequently precipitated as calcium salts. In this section we provide a very brief discussion of the key factors that affect the SO_2 removal efficiency from a theoretical standpoint. Against this backdrop we examine empirical data, which reflects the recent experience with high efficiency scrubbers, and develop an approximate response surface parameterized on the key variables.

The basis for the analysis of vapor-liquid mass transfer phenomena is the two-film theory in which the total resistance to mass transfer is expressed as the sum of individual resistances in the vapor and liquid phases near the interface. Based on expressions for molar flux in the gas and liquid films and assuming that the liquid-vapor interface is at equilibrium (Corbett, et al., 1977; Mehta & Rochelle, 1983; Rochelle, 1981; Rochelle, 1981), the overall mass transfer coefficient is written as:

$$K_g = \left(\frac{1}{k_g} + \frac{H}{e \times k_l} \right)^{-1} \qquad (6\text{-}1)$$

where k_g (mole/cm^2-sec-atm) and k_l (cm/sec) are individual gas and liquid phase mass transfer coefficients, H is a physical constant (atm/mol-liter) from Henry's Law and e is an enhancement factor to account for chemical reactions that permit SO_2 to diffuse through the liquid film as sulfite or bisulfite ions rather than as undissociated SO_2 (Chang and Rochelle 1980). The amount of SO_2 transferred from gas phase per unit time is the integral of the molar flux and the interfacial area for mass transfer. This leads to an expression for SO_2 removal efficiency as shown in Equation (6-2):

$$\eta_{SO_2} = 1 - \exp\left(- \frac{K_g \times a \times P \times V}{G} \right) \qquad (6\text{-}2)$$

where

a	=	interfacial mass transfer area per unit volume
V	=	scrubber volume
P	=	total pressure in scrubber
G	=	molar gas flow rate
K_g	=	mass transfer coefficient

The interfacial area is determined by the contractor design, gas distribution in the scrubber and the gas and liquid flow rates (or residence time in the scrubber). *V/G* is the residence time of flue gas in the scrubber and it depends on superficial velocity and size of the scrubber. The mass transfer coefficient, K_g is influenced by process variables. Any process variable which affects the physical or chemical properties of the two films may affect K_g. The individual mass transfer coefficients k_g and k_l describe the diffusion rates across two hypothetically stagnant films. In the following paragraphs we discuss the effect of various process parameters on the SO_2 removal efficiency and develop a response surface using the exponential form. All the relations developed in this section are based on a log-linear approximation, as suggested by Equation (6-1), and are developed as follows:

$$RTU = -\ln(1 - \eta_{SO2})$$

$$RTU = a + \sum_i b_i \times x_i \qquad (6\text{-}3)$$

where a and b_i parameters which represent the linear slope of the effect of process parameters x_i.

L/G is a key variable since it affects SO_2 removal by increasing the available liquid phase alkalinity and the interfacial mass transfer area. Increasing the L/G ratio brings more alkaline materials into the scrubber per mole of SO_2 scrubbed thus decreasing the liquid film mass transfer resistance and improving the SO_2 removal. This effect is magnified by an associated increase in the interfacial mass transfer area which

improves efficiency. Industry practice is based on a log-linear relation between η_{SO_2} and L/G ratio (Benson, 1993; Bhat, et al., 1993; Dene, et al., 1991; Klingspor, 1993; Rader, 1993). Typical values for η_{SO_2} and L/G are provided in the table below.

Table 6-1 Typical Values for SO_2 Removal and L/G.

η_{SO_2}	L/G(gpm/Kacfm)
90%	90
95%	130

Based on the values in the table above, an approximate relation[2] between sulfur removal efficiency and L/G is:

$$\eta_{SO_2} = 1 - \exp\{-(0.725 + 0.0175 \times L/G)\} \qquad (6\text{-}4)$$

where L/G is measured in gpm/1000 acfm. The effect of lime/limestone scrubbing chemistry on SO_2 removal can be understood by considering the mass transfer resistance from the gas and liquid film separately.

6.2.1.1. Liquid Film Limited Mass Transfer

Limestone systems are generally at least partially liquid film mass transfer limited. The liquid film mass transfer resistance is a strong function of liquid phase alkalinity. When SO_2 is absorbed by an aqueous scrubbing liquor, sulfurous acid is formed. Increasing the liquid phase or solid phase concentrations of alkaline materials (such as $CaCO_3$, $CaSO_3$, Mg^{++}) increases the liquid phase alkalinity which in turn improves SO_2 removal efficiency. Increasing the liquid phase alkalinity decreases the Henry's Law constant which in turn decreases the mass transfer resistance $H/(e\ k_l)$. The enhancement factor depends on the inlet SO_2 concentration and it decreases with increasing SO_2 concentrations thus increasing the mass transfer resistance. The k_l portion of the mass transfer resistance is a function of the hydraulics of the scrubber and depends on gas distribution and the geometry of scrubber.

Increasing the limestone stoichiometry (ϕ) improves liquid phase alkalinity and SO_2 removal. However the effect saturates and little improvement in SO_2 removal is observed over 1.1. Limestone utilization varies inversely with the pH and is a critical factor for the operating costs of SO_2 scrubbing. Most modern scrubbers are designed for high utilization of about 95% or higher. Therefore stoichiometry affects the performance in opposite ways. A detailed quantification of the effect of stoichiometry on pH is not straightforward and needs the development of process simulators (Agrawal & Rochelle, 1993; Noblett Jr., et al., 1990). It is possible to get an approximate idea of how SO_2 removal is affected by pH and in turn by ϕ based on empirical data (Klingspor, 1993; Noblett Jr., et al., 1990; Rader, 1993; Stevens, et al., 1991) as shown in Table 6-2 below:

[2] All relations developed in this section are based on a wet limestone/lime FGD tower with four spray headers per tower. The default process parameters are as follows: pH=5.3, ϕ=1.03, L/G=90, inlet SO2=1750 ppm (2.6% S coal), Cl =25,000 ppm (in the slurry) and superficial velocity in tower=10 fps.

Table 6-2 Stoichiometry and Alkalinity Approximations

η_{SO2}	pH	ϕ
90%	5.3	1.03
95%	6.0	1.1

Based on these numbers a linear approximation for the effect of stoichiometry can be represented by an additional term in Equation (6-4) as follows:

$$\eta_{SO2} = 1 - \exp\{-[0.725 + 0.0175 \times L/G + (10.0 \times \phi - 10.3)]\} \qquad (6\text{-}5)$$

Notice that the effect of stoichiometry is represented as an increase in SO_2 removal due to an increase in pH (caused by increasing ϕ) over the default value of 5.3.

An increase in the inlet SO_2 concentrations beyond 1000 ppm decreases the enhancement factor *e* which in turn increases the mass transfer resistance. The enhancement factor is a function of gas and solution composition (Chang & Rochelle, 1983) which affects the conversion of SO_2 to bisulfite. Typical values of SO_2 removal for different inlet SO_2 concentrations are provided below based on industry experience (Moser & Owens, 1990; Noblett Jr., et al., 1990; Stevens, et al., 1991).

Table 6-3 Inlet SO_2 Concentration

η_{SO_2}	SO_2 ppm
90%	2000 (2.8% S)
84%	4000 (4% S)

This can be represented by an additional term in Equation (6-5) which accounts for the loss of removal efficiency as the inlet SO_2 concentration increases over 2000 ppm.

$$\eta_{SO2} = 1 - \exp\left\{\begin{matrix} -[0.725 + 0.0175 \times L/G + (10.0 \times \phi - 10.3) \\ -2.5 \times 10^{-4}(SO_2 - 2000)] \end{matrix}\right\} \qquad (6\text{-}6)$$

Similarly calcium chloride accumulation in the slurry leads to a decrease in SO_2 removal. Chloride accumulation suppresses the desirable effects of alkali salts by permitting their accumulation as chloride salts rather than sulfate salts. The effect of accumulated Cl concentrations in the scrubber slurry on the SO_2 removal based on industry experience (Klingspor, 1993; Moser & Owens, 1990; Noblett Jr., et al., 1990; Rader, 1993; Stevens, et al., 1991) is provided below:

Table 6-4 Calcium Chloride Accumulation

η_{SO_2}	Cl ppm
86%	10000
80%	80000

This is represented by a term which represents the loss in removal efficiency as the chloride concentration in slurry increases above 25,000 ppm.

$$\eta_{SO2} = 1 - \exp\left\{\begin{array}{l} -[0.725 + 0.0175 \times L/G + (10.0 \times \phi - 10.3) \\ -2.5 \times 10^{-4}(SO_2 - 2000) + 5.14 \times 10^{-6}(Cl - 25000)] \end{array}\right\} \quad (6\text{-}7)$$

Addition of organic acids such as adipic, glutiric, and succinct acids to the scrubber slurry improves SO_2 removal efficiency. These acids are usually stronger than sulfurous acid and weaker than carbonic acid. This provides a buffering effect. First it assists limestone dissolution by lowering carbonate ion backpressure and hence more alkalinity in form of bicarbonate enters the scrubber in soluble form. Moreover, since sulfurous acid is a stronger acid, the organic acid ion acts as a base in SO_2 sorption. Dibasic acid (a mixture of) has been found to be the most effective organic acid for use as an additive in commercial scale scrubbers. This improves SO_2 removal and typically every 500 ppm addition of organic acids in the slurry improves SO_2 removal that is comparable to increasing the L/G by 30 gpm/Kacfm in a normal pH operating range of 5.3-5.8 (Blythe, et al., 1993; Rader & Bakke, 1991; Smolenski, et al., 1993; Stevens, et al., 1993). This simple approximation can be represented as follows:

$$\eta_{SO2} = 1 - \exp\left\{\begin{array}{l} -[0.725 + 0.0175 \times L/G + (10.0 \times \phi - 10.3) \\ -2.5 \times 10^{-4}(SO_2 - 2000) + 5.14 \times 10^{-6}(Cl - 25000) \\ +0.00042 \times DBA] \end{array}\right\} \quad (6\text{-}8)$$

where DBA represents the concentration (in ppm) of dibasic acid in the slurry. Figure 6-1 plots the sensitivity of SO_2 removal efficiency (η) to the reagent stoichiometry (ϕ) and the liquid to gas ratio (L/G) holding the SO_2, Cl and DBA concentration constant.

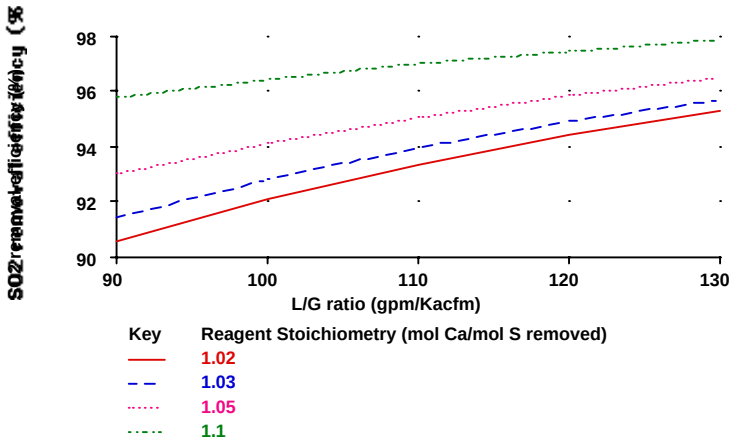

Figure 6-1 *IECM performance model for Wet Limestone FGD (with Forced oxidation). Constant parameter value for this case are [SO_2]=1260 ppm, [Cl]= 32360 ppm, and [DBA]=0 ppm.*

Figure 6-2 plots sensitivity of SO_2 removal efficiency (η) to the DBA concentration and the liquid to gas ratio (L/G) holding the SO_2, Cl and ϕ constant.

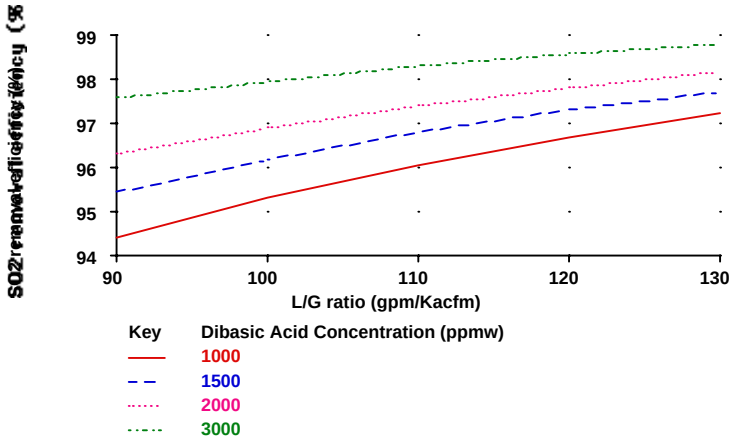

Figure 6-2 *IECM performance model for Wet Limestone FGD (with Forced oxidation). Constant parameter value for this case are [SO_2]=1260 ppm, [Cl]= 32360 ppm, and ϕ =1.03.*

6.2.1.2. Gas Film Limited

Systems with low inlet SO_2 concentrations are gas film limited, since the liquid phase alkalinity is sufficient to neutralize the dissolved SO_2. For gas film limited case the removal efficiency is largely determined by the contactor design and the L/G ratio; it is not affected by the liquid phase alkalinity. The SO_2 concentration at which the liquid film resistance becomes large enough to be comparable to the gas film resistance depends on the liquid phase alkalinity and L/G ratio. For typical limestone systems with L/G in the 90-130 gpm/Kacfm interval and with a pH between 5.3-5.8 the transition is in the 500-1000 ppm range. Therefore, for inlet SO_2 concentrations below 1000 ppm, the SO_2 removal can be treated as being gas film limited and the relation given in Equation (6-1) without the effects of liquid phase alkalinity can be used for determining SO_2 removal.

6.2.2. Wet Lime FGD System

Magnesium lime systems are also gas film limited. Maglime systems have abundant liquid phase alkalinity since lime has a higher solubility than limestone and magnesium species (usually about 2-4% by weight) provides additional liquid phase alkalinity. Hence the availability of liquid phase alkalinity does not impose any resistance in the absorption of SO_2 and the mass transfer coefficient K_g is based solely on the gas film resistance for inlet SO_2 concentrations from 500-5000 ppm. Typical values for η_{SO_2} and L/G for maglime systems are provided in the table below (Benson, 1993; Benson, et al., 1991; Johnson, 1993).

Table 6-5 *L/G for Mg-Lime*

η_{SO_2}	L/G(gpm/Kacfm)
95%	40
98%	56

Based on these values an approximate relation between sulfur removal efficiency and L/G is:

$$\eta_{SO_2} = 1 - \exp\{-(0.2 + 0.07 \times L/G)\}$$

where L/G is measured in gpm/1000 acfm. Figure 6-3 graphs the sensitivity of this model with the removal efficiency versus the L/G ratio for Mg-Lime systems.

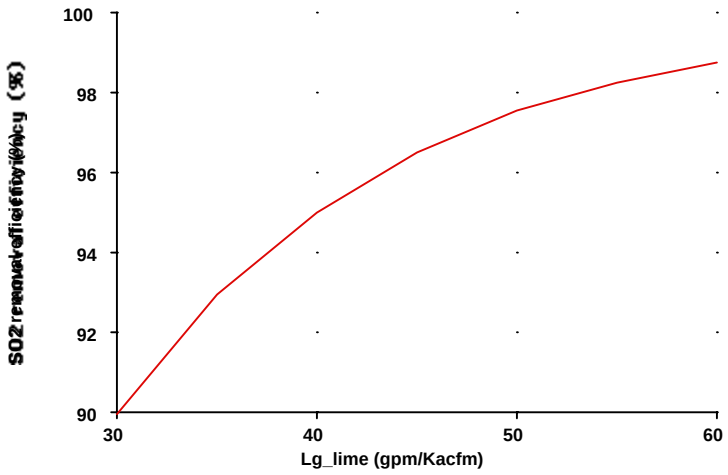

Figure 6-3 IECM performance model for Wet Mg-Lime FGD

6.2.3. Lime Spray Dryer System

Spray dryer scrubbers are sometimes used as an alternative to wet scrubbing since they provide simpler waste disposal and can be installed with lower capital costs. In a typical system, hot flue gas is contacted with finely atomized aqueous solution in the spray dryer. Dry products leave the spray dryer and are removed from the gas in a baghouse. The liquid phase consists of an aqueous slurry of slaked lime. The sulfur dioxide in the flue gas is absorbed into the droplets, which simultaneously evaporate on contact with the hot flue gas. Although some moisture still remains in the flue gas solids which later promotes further removal of SO_2 in the fabric filter. The total SO_2 removal is the sum of the removal in the dryer and the baghouse. In this subsection, we develop empirical relations to describe the total SO_2 removal (Blythe, et al., 1985; Blythe, et al., 1991; Brown & Felsvang, 1991).

The main process parameters that affect the SO2 removal efficiency are (Brown & Felsvang, 1991; Jozewicz & Rochelle, 1984):

1. Inlet SO_2 concentration,
2. Reagent ratio[3], (ϕ)
3. Calcium chloride concentrations in the liquid slurry (*Cl*),
4. Inlet flue gas temperature (T_{in}), and
5. Approach temperature to the adiabatic saturation temperature of the flue gas at outlet (ΔT).

Increase in the reagent ratio increases the alkalinity in the liquid phase, which improves the SO_2 removal. Effects of inlet SO_2 concentrations are similar to those in wet FGD systems. Low inlet SO_2 concentrations (< 1000 ppm) lead to gas film limited mass transfer and medium to high inlet SO_2 concentration leads to comparable contributions from both gas and liquid film resistance. As a result, we

[3] For spray dryers the reagent ratio is measured as moles of reagent supplied/mole of SO_2 *entering* the scrubber. Note that for wet FGD systems the reagent ratio is measured as moles of reagent/mole of SO_2 *removed*.

develop different response surfaces to describe the removal efficiency for low and high inlet SO_2 concentrations. Increasing the inlet temperature allows more water to be added to the spray dryer to achieve the same approach temperature. This in turn leads to a higher recycle ratio and increased mass transfer area thus improving the removal efficiency.

In order to understand the effect of the other parameters one has to consider the heat transfer characteristics of the spray dryer. The evaporation time, *t*, for a given droplet is also the time available for a droplet to absorb SO_2. As the approach to saturation temperature increases, the evaporation time decreases thereby decreasing removal efficiency. The addition of chlorides in the slurry improves the SO_2 removal efficiency of the spray dryer. This is due to the deliquescent properties of chlorides, which helps the droplet to retain water and hence increase the evaporation time. Hence chlorides are often used as additives to reduce the lime consumption. We now develop response surfaces to describe the overall SO_2 removal efficiency in spray dryers using data from pilot studies conducted by EPRI (1985, 1991) and Joy/Niro (Svend, et al. 1983). We use the log-linear form shown in Equation (6-3) to develop these response surfaces.

The reagent ratio is a key process variable and it affects the removal efficiency significantly. Typical value of SO_2 removal for different stochiometries are presented in Table 6-6 below:

Table 6-6 Reagent Stoichiometry

η_{SO_2}	ϕ
80%	0.9
90%	1.1

These values are representative of both low and high inlet SO_2 concentrations. Based on these numbers the log-linear approximation for the effect of reagent ratio is as follows:

$$\eta_{SO2} = 1 - \exp\{-(-1.495 + 3.45 \times \phi)\} \qquad (6\text{-}9)$$

This relation can be used for reagent ratios in the range of 0.9-1.8. Now we develop the response surface for low and high SO_2 concentrations separately.

6.2.3.1. Low Inlet SO_2 Concentrations ($\leq$ 1000 ppm)

The data presented in this section was collected against baseline conditions of 1000 ppm inlet SO_2, approach temperature of 20°F, and inlet temperature of 280°F. For low inlet SO_2 concentrations, the inlet temperatures in the range of 280-325°F has been observed to have no effect on the removal efficiency. However increasing the approach temperature to saturation from 20 to 40°F results in the requirement of higher stochiometries for the same removal efficiencies as shown in Table 6-7:

Table 6-7 Effect of 40°F Approach Temperature to Saturation

η_{SO_2}	ϕ
80%	1.1
85%	1.3

Averaging the effects of these values an additional term to describe this effect is added to Equation (6-6) as follows:

$$\eta_{SO2} = 1 - \exp\{-[-1.495 + 3.45 \times \phi - 0.05 \times (\Delta T - 20)]\}$$

As discussed earlier the deliquescent properties of calcium chloride improves the removal efficiency. A presence in the slurry resulting in 0.6% calcium chloride by weight in solids collected in the fabric filter results in higher removal efficiencies for the same stoichiometry as shown below:

Table 6-8 Effect of 0.6% Calcium Chloride

η_{SO_2}	ϕ
90%	1.0
95%	1.2

Averaging the effects based on these values can be accomplished with additional terms being added to Equation (6-7). Thus, the effect of the approach to saturation temperature and calcium chlorides can be described by Equation (6-10):

$$\eta_{SO2} = 1 - \exp\{-[-1.495 + 3.45 \times \phi - 0.05 \times (\Delta T - 20) + 0.58 \times Cl]\} \qquad (6\text{-}10)$$

This is the final form of the response surface for low SO_2 inlet concentrations.

6.2.3.2. Medium to High SO_2 Concentrations (> 1000 ppm)

The data presented in this section was collected against baseline conditions of the following values: 2000 ppm inlet SO_2, approach temperature of 20°F, and inlet temperature of 325°F. For inlet SO_2 concentrations greater than 1000 ppm, the removal efficiency increases with increases in inlet temperatures from 280-325°F. Decreasing the inlet temperature to 280°F decreases the removal efficiency to 80% for a given stoichiometry of 1.1. This effect is represented by an additional term to Equation (6-9) as follows:

$$\eta_{SO2} = 1 - \exp\{-[-1.495 + 3.45 \times \phi + 0.015 \times (T - 325)]\}$$

The presence of 0.4% by weight of calcium chloride in the fabric filter solids provides an improved efficiency of 90% for a reagent ratio of 1.0. This is described in by an additional term as follows:

$$\eta_{SO2} = 1 - \exp\{-[-1.495 + 3.45 \times \phi + 0.015 \times (T - 325) + 0.86 \times Cl]\}$$

Increasing the approach temperature to 30°F reduces the removal efficiency to 75% for a reagent ratio of 1.05. On the other hand increasing the inlet SO_2 concentration to 3000 ppm reduces removal efficiency to 80% at a reagent ratio of 1.1. These effects are included as shown below:

$$\eta_{SO2} = 1 - \exp\left\{\begin{matrix} -[-1.495 + 3.45 \times \phi + 0.015 \times (T - 325) + 0.86 \times Cl \\ -0.0007 \times (SO_2 - 2000) + 0.08475 \times (\Delta T - 20)] \end{matrix}\right\}$$

This is the final form of the response surface for high SO_2 inlet concentrations. Figure 6-4 plots the removal efficiency as a function of the inlet flue gas temperature for different stochiometries.

Figure 6-5 graphs the sensitivity of the removal efficiency as a function of the approach temperature for different stochiometries.

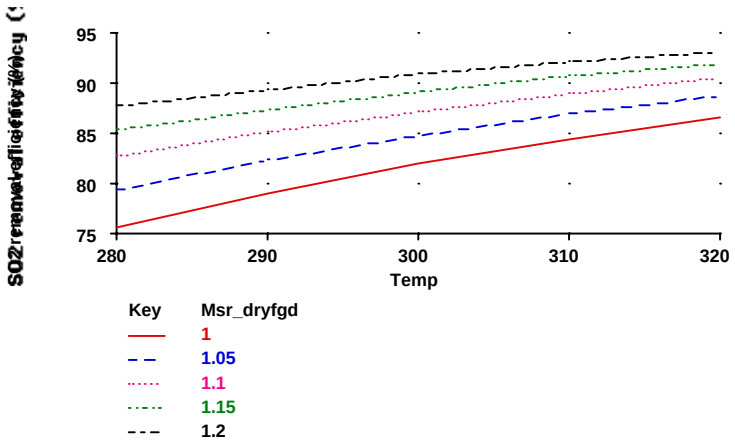

Figure 6-4 *IECM performance model for Lime Spray Dryer. Constant parameter value for this case are [Cl]=0.4% wt., [ΔT]=28 F, and [SO_2]= 1260 ppm*

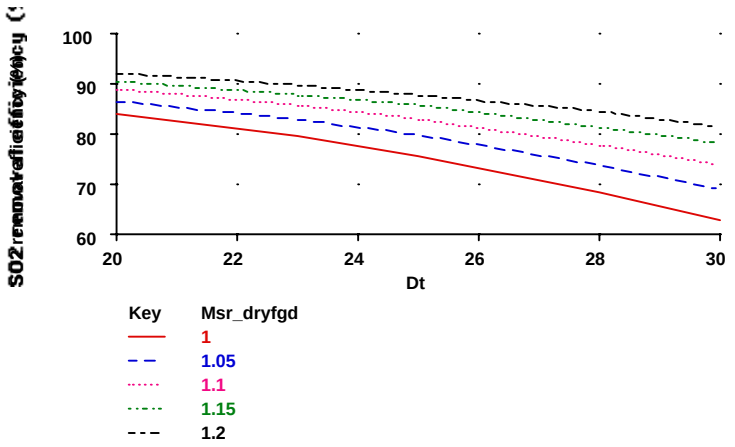

Figure 6-5 *IECM performance model for Lime Spray Dryer. Constant parameter value for this case are [Cl]=0.4% wt., [T]=300 F, and [SO_2]= 1260 ppm*

6.3. FGD Cost Models

The FGD cost models originally developed for the IECM were derived from a detailed FGD computer program developed in the late 1970's and early 1980's by the Tennessee Valley Authority (TVA). The TVA model was subjected to an extensive set of parametric runs, and the results were used to derive statistical "response surface" models which accurately represented the results of the TVA model in terms of a smaller number of key site-specific plant and design parameters. We follow a similar procedure in developing the new models reported here.

Changes in the design, performance and cost of FGD systems in the mid-to-late 1980's left the TVA model outdated as a basis for performance and cost estimation. The TVA modeling team also was disbanded during this period, and no further updates to the model were made. Instead, the most reliable and widely used estimates of FGD cost came from a new modeling effort sponsored by the Electric Power Research Institute (EPRI). This effort led to the development of a computer model called FGDCOST, which has become the new industry standard in the area. FGDCOST, however, does not contain any FGD performance models (all

performance parameters must be supplied by the user); hence, the development of the new performance models described earlier.

The new cost models that we developed were based on results from FGDCOST, a spreadsheet program model developed for EPRI which provides the most up-to-date cost models for fifteen FGD processes (Keeth, et al., 1991). The cost development and breakdown follow the EPRI economic premises. We have augmented FGDCOST to allow for systematic sensitivity analysis with large numbers of input variables. In order to allow the simultaneous variation of many input parameters, the values of the input parameters are read from a lookup table. The values for input variables are generated from sampling probability distributions. These values are imported into the tables. On each execution, the values of all the inputs are read from each row of the table, the corresponding performance parameters are calculated and finally the capital and O&M costs are written along the same row. The output columns can be now exported to other programs for sensitivity analysis and regression modeling. In the following paragraphs we provide a brief outline of the criteria used for designing costs estimates.

Cost is broken down in terms of capital and operating and maintenance costs. We describe in some detail the breakdown of the capital costs estimates. The process parameters that affect operating costs are also outlined.

6.3.1. Capital Costs

Models of capital cost focus first on the process capital requirements of each section of the FGD system. The process facilities costs are then used to determine the other capital costs. These are generally referred to as the indirect capital costs. The bases and items included for each component of the capital estimate is provided in Table 6-9. These standardized components are used throughout all the modules in the IECM and described more fully in the EPRI Technical Assessment Guide.

Table 6-9 ***Nomenclature for EPRI Cost Estimates***

Capital Investment	$/kW
Process Capital (incl. Sales tax)	A (from
General Facilities	B
Eng. & Home Office Fees	C
Project Contingency	D
Process Contingency	E
Total Plant Cost (TPC)	= A + B + C + D + E
Total Cast Expended (TCE)	TPC x Adjust factor*
AFDC (Allowance for Funds During Construction)	F
Total Plant Investment (TPI)	= TCE + F
Royalty Allowance	G
Preproduction Costs	H
Inventory Capital	I
Initial Catalyst and Chemicals	J
Land	K
Total Capital Required (TCR)	TPI + G + H + I + J + K

* Adjustment Factor for TCE per Table 3-4 of EPRI TAG (P6587-L)

6.3.1.1. Process Facilities Cost

The process capital estimate is broken down on an area-by-area basis for each process area. The costs areas along with the equipment used in each area are provided in Table 6-10. The equipment size is based on a mass balance for various flue gas species (such as SO_2, NO_x, HC_1, CO_2, N_2) performed by FGDCOST, which is similar to the mass balance calculations in the IECM. The sulfur content of the flue gas is the key variable in costing various aspects of the FGD process. Based on the mass balance, the required size of the various equipment in each process area is determined, which is then used to determine costs. The capital costs are also affected by the sparing philosophy for the absorber towers. The sum of the capital cost for all process areas provides the total process facilities cost.

Table 6-10 ***Cost Areas for Process Capital Breakdown (Source: EPRI)***

Area	Description
10	Reagent Feed System
20	SO_2 Removal System
30	Flue Gas System
40	Regeneration System
50	By-product System
60	Solids Handling System
70	General Support Area
80	Miscellaneous Equipment

10 Reagent Feed System – all equipment required for storage, handling and preparation of raw materials, reagents, and additives used in each process.

20 SO_2 Removal System – equipment required for SO_2 scrubbing, such as the absorption tower, recirculation pumps and other associated equipment.

30 Flue Gas System – duct work and fans required for flue gas distribution to the SO_2 scrubbing system, plus gas reheat as required.

40 Regeneration System – specific to regenerable reagent systems, equipment used to regenerate spent absorbent for return to the process, plus any preconditioning system for SO_2 or H_2S off-gas.

50 By-Product System – production equipment for salable process by-products and storage facilities for the final products.

60 Solids Handling System – equipment required for fixation, treatment, and transportation of all sludge/dry solids materials produced by each scrubbing process.

70 General Support Area – additional equipment required to support FGD system operation such as makeup water and instrument air.

80 Miscellaneous Equipment – This area will include plant modifications necessitated by the addition of the FGD system. Also included are costs for electrical equipment tie-ins and other associated systems.

6.3.1.2. Other Capital Costs:

Besides the process capital costs, a series of additional indirect costs are included in the IECM cost models. Following the EPRI format, these are represented as simple parameters whose values are user-specified. Their relationship to each other and to the direct facilities cost are shown in Table 6-9.

General Facilities: The general facilities costs include roads, office buildings, shops, laboratories etc. A cost factor (f_{gf}) of 5 - 20% of the process capital cost is used to evaluate this cost. A cost factor of f_{gf}=10% is used as default value in the FGDCOST models.

Engineering & Home Office Fees: An estimate of engineering, home office overhead and fees is included in capital costs estimates. A cost factor (f_{eho}) of about 10 -15% is used to estimate this expense. FGDCOST uses a value of f_{eho}=10% of the process facilities cost.

Project Contingency: Project contingency costs covers additional equipment and other costs that would arise from a more detailed design. Project contingency factors (f_{cproj}) range from 10 - 20% of process capital costs. An average value of about 15% is used in FGDCOST.

Process Contingency: A process contingency is applied to a new technology in an attempt to quantify the design uncertainty and the cost of a commercial scale system. The contingency factor (f_{cproc}) can range from 2-50% of the process capital costs. For FGD processes a contingency factor of 2% is used.

Total Plant Cost: The total plant cost (tpc) is the sum of process capital, general facilities, engineering and home office fees, and contingencies.

Total Cash Expended: The total cash expended is an estimate of the cash expected to be spend during the construction duration of the FGD system. This estimate accounts only for the escalation of costs up to the date of expenditure.

Allowance for Funds During Construction (AFUDC): The schedule for engineering procurement and construction is assumed to be two years for installation. For example, for an escalation of 5% a year, the total plant costs is multiplied by 0.0548 to calculate the allowance for interest expenses during a two year construction period. The IECM has general function which calculates the escalation costs given the escalation rate and the time for installation.

Total Plant Investment: The total plant investment is the sum of the total cash expended and the allowance for interest during construction.

Royalty Allowance: Royalties paid are 0.5% of the process capital.

Preproduction Costs: Preproduction costs are intended to cover operator training, equipment checkout, major changes in plant equipment, extra maintenance, and inefficient use of materials during plant startup. It is a sum of one-month fixed operating costs, one-month variable operating costs at full capacity and 2% of the total plant investment.

Inventory Capital: The inventory costs includes the expense of raw materials and other consumables based on a 100% capacity operation for 60 days.

Land: FGD system land requirements include the plant site area and disposal area. Land has not been included as a line item.

Total Capital Requirement: The total capital requirement is calculated as the total of all the costs enumerated above.

6.3.1.3. Operating & Maintenance Costs

Operating costs for FGD systems are separated into fixed and variable operating costs. Fixed costs include operating and maintenance labor, maintenance materials and administrative/support labor. Various factors based on EPRI premises are used to estimate these costs many of which are based on capital cost estimates. Variable operating costs include consumables such as fuel, water, power, chemicals, and solids disposal. **Error! Not a valid bookmark self-reference.** provides the operating cost criteria used. The fixed and variable O&M costs depend on the feed rate of reagent, sludge disposal costs, power for pumping, labor and other operations. Table 6-12 provides the default process design criteria used in our models.

Table 6-11 Criteria for Calculating Operating Costs

Fixed Operating Costs	Units	Rate
Operating Labor	Man-hrs	$20.00 (Jan. 1990)
Maintenance Labor – Slurry Handling	$/yr	3.2% of Process Capital
Maintenance Labor – Liquid Handling	$/yr	1.2% of Process Capital
Maintenance Material – Slurry Handling	$/yr	4.8% of Process Capital
Maintenance Material – Liquid Handling	$/yr	1.8% of Process Capital
Administrative & Support Labor	$/yr	30% of O&M Labor

Variable Operating Costs	Units	Jan 1990 $/Unit	Add'l Freight $/ton	30-Yr Level Factor	30-Yr Level $/Unit
Fuel Oil (#6)	gal	0.41	Incl	1.613	0.66
Raw Water	1000 gal	0.60	Incl	1.613	0.97
Cooling Water	1000 gal	0.16	Incl	1.613	0.26
Power	kWh	0.05	Incl	1.668	0.08
Methane	1000 ft^3	3.00	Incl	1.668	5.00
Lime	ton	55.00	Incl	1.613	88.72
Limestone	ton	15.00	Incl	1.613	24.20
Soda Ash	ton	93.00	43.00	1.613	219.37
Magnesia	ton	232.00	135.00	1.613	591.97
Ammonia	ton	145.00	5.50	1.613	242.76
Sulfur Emulsion	ton	220.00	Incl	1.613	354.86
Dibasic Acid	ton	360.00	Incl	1.613	580.68
Formic Acid	ton	800.00	20.00	1.613	1322.66
Allied Catalyst	ton	2500.00	45.00	1.613	4105.09
Claus Catalyst	ton	1000.00	Incl	1.613	1613.00
Disposal Charges					
Dry Solids (lined)	ton (dry)	9.29	Incl	1.613	14.98
Fly Ash (unlined)	ton (dry)	8.00	Incl	1.613	12.90
Sludge (truck to lined landfill))	ton (dry)	9.25	Incl	1.613	14.92
Sludge (truck to unlined l'fill)	ton (dry)	8.15	Incl	1.613	13.15
Sludge (ponded)	ton (dry)	6.00	Incl	1.613	9.68
Gypsum (pumped and stacked)	ton (dry)	4.75	Incl	1.613	7.66
Condensate	1000 lb	0.77	Incl	1.613	1.24
Steam					
0 – 70 psia	1000 lb	2.85	Incl	1.668	4.75
70 – 250 psia	1000 lb	3.50	Incl	1.668	5.84
250 – 400 psia	1000 lb	5.30	Incl	1.668	8.84
By-Product Credit					
Sulfur	Long ton	90.00	Incl	1.613	145.17
Sulfuric Acid	ton	50.00	Incl	1.613	80.65
Liquid Sulfur Dioxide	ton	230.00	Incl	1.613	371.00
Gypsum	ton	2.00	Incl	1.613	3.23

NOTE:
1000 gal = 3.785 m^3 , short ton = 0.9072 long ton, 1000 ft^3 = 28.32 m^3,
1000 lb = 453.6 kg

Table 6-12 ***Description of Default Criteria used in the Model***

Variable name	Units	Description	Default Value
gas	Kacfm	flue gas flow rate	971
MW	10^6 MW	Net plant capacity	300
L/G	gpm/Kacfm	liquid to gas ratio	90/55/30[a]
%S	%	% sulfur in coal by weight	2.6% 1750 ppm
stoichiometry (ϕ)		moles of Ca per mole of SO_2 removed	1.03/1.02/ 1.1[b]
labor	$/hr	FGD operating labor rate	20
reag	$/ton	reagent ($CaCO_3$/CaO) cost	15/55[d]
solid	$/ton	sludge disposal cost	8.15
stack	$/ton	sludge disposal - stacking cost	4.75
power	mills/kWh	power cost	50
steam	$/1000 lbs	steam cost	3.5
waterf	$/1000 gallons	fresh water cost	0.6
waterc	$/1000 gallons	cooling water cost	0.16
DBA_{ppm}*	ppm	scrubber slurry DBA concentration	1500
DBA_{feed}*	lbs DBA/ton SO_2 removed	DBA feed rate	20
DBA_{cost}[c]	$/ton	DBA additive cost	360
ΔP	inches of H_2O	total system pressure drop	10
ΔT	$^{\bullet}F$	temperature increase of scrubbed flue gas due to reheat	25

[a] the default values are: 90 gpm/Kacfm for LSFO and 55 gpm/Kacfm for LSDBA and 30 for Mg-lime System for a 90% removal efficiency.

B the stoichiometry for limestone systems is 1.03, for lime systems is 1.02, and for lime spray dryer is 1.1(note that for lime spray dryer the reported stoichiometry is moles of Ca per mole of inlet SO_2).

C these input variables for LS/DBA only

[d] limestone cost is 15 and lime cost is 55 $/ton

6.3.2. The Methodological Approach

Response surface construction is the central objective of the sensitivity analysis techniques presented in this section. Sensitivity analysis seeks to identify the set of input variables that have significant effect on the model output and to rank order them according to the magnitude of their effects. Once the relevant variables are identified regression methods can be used to develop adequate response surface replacements for the models. Subsequently probability distributions on the input variables can be used in conjunction with the response surface to derive the probability distributions of the model outputs. In this section, we briefly describe the use of Latin hypercube sampling (LHS) (Iman, et al., 1980) along with partial rank correlation coefficients (PRCC) to examine the influence of individual variables on the model output (Iman, et al., 1981a; Iman, et al., 1981b). Finally the use of regression analysis with log-linear transformations for developing response surfaces is described (Ang & Tang, 1975; Draper & Smith, 1966; Neter, et al., 1983).

6.3.2.1. Sampling and Ranking Methods

In order to perform sensitivity analysis it is necessary to obtain model output for various values of input variables. Latin hypercube sampling is used to select values for input variables. The LHS technique to select *n* different values from *k* different input variables operates in the following manner. For each variable, the range is divided into *n* non-overlapping intervals of equal probability. One value from each interval is selected at random with respect to the probability density in the interval. The *n* values for variable x_1 are paired at random with the *n* values of x_2 and these *n* pairs are paired at random with *n* values of x_3 and so on to generate *n* k-tuples. This is the Latin hypercube sample used as input to the model. The model is then exercised at each of these *n* input values to generate *n l*-tuples for *l* output variables of interest. This data set of *n k*-tuples of input values and *n l*-tuple of output values forms the basis for the rest of the analysis.

The importance of an input variable is derived by assessing its influence on the output variable. For linear relationships this can be assessed by the use of partial correlation coefficients (PCC) which measure the correlation between an input and output variable when the effects of all the other variables is removed. For nonlinear relations it becomes more difficult to assess the importance of individual variables. However, if the model output is a monotonic function of the input then it is possible to linearize the relationship by using rank transformations on the input and output values. A rank transformation involves replacing each value of a variable by its rank. Now the partial correlation coefficient on the rank transformed variables (PRCC) can be used to assess the importance of the input variables.

6.3.2.2. Regression Analysis

Once the important input variables are chosen, multivariate linear regression approaches can be used with the data set to construct response surfaces. If *k* input variables are chosen as relevant, a linear regression model is written as:

$$y_i = a + b_1 x_1 + b_2 x_2 + ... + b_k x_k + \varepsilon$$

where, ε is an error term which represents the variance in y_i unexplained by the model. The linear fit is obtained by selecting *a*, b_i so as to minimize the sum of squares between the model predictions and the data for y_i. Often the relationships between input and output variables are nonlinear. In this case it is often possible to use some data transformation to linearize the relationship. A commonly used transformation for exponential nonlinearities is the logarithm transform. Therefore an exponential relationship such as:

$$y_i = a \times x_1^{b_1} \times x_2^{b_2} ... \times x_k^{b_k}$$

is transformed to:

$$\ln(y_i) = \ln(a) + b_1 \ln(x_1) + ... + b_k \ln(x_k)$$

which has a linear relationship.

Common statistical tests are used to determine the adequacy of the regression model. The most common measure is the coefficient of multiple correlation (R^2) which is a ratio of the variation explained by the regression to the total variation in y_i. Values of R^2 near 1 represent good fits. R^2 however is not a sufficient measure of the goodness of fit of a model. The *t*-statistic is used to test if the partial regression coefficients *a*, b_i are significantly different from zero. Moreover an *F*-statistic can be used to check if any of the partial correlation coefficients are different from zero. This statistic provides an idea of the lack of fit of a regression model as a whole. However, for

large R^2 values this test is not informative. Standard error of a regression model provide an estimate of the variance in the residual errors for y_i. This can be used to compare across regression models (in terms of functional forms) and to conduct the Kolmogorov-Smirnov test to evaluate if the errors ε are normally distributed. The normality assumption underlies the most of the statistical tests used. Most statistical packages provide utilities for regression analysis and the statistical tests outlined in this section. The regression analysis for this work was done using *Splus* on the Andrew network (Becker, et al., 1988).

6.3.2.3. Analysis & Results

In the following sections we present the sensitivity analysis conducted with the FGDCOST model and provide response surface algorithms for capital costs and O&M costs based on results from FGD cost. A set of input variables is chosen and Latin hypercube sampling is used to generate a sample of 100 values for each variable using a uniform distribution for the given range. A Fortran77 package was used to generate the samples (Iman 81a). These samples are then imported into the sensitivity analysis module in FGDCOST and the model exercised to generate corresponding output values for capital and O&M costs. The data set consisting of the input samples and the corresponding output samples is used for response surface generation. PRCC, a Fortran77 package, is used to compute the partial rank correlation coefficients between the input and output variables. Note that linear relations are monotonic, hence a rank transformation does not affect the order of importance of the input variables. Using these coefficients the relevant variables for regression modeling are gleaned. *Splus* is used to generate regression models for capital and O&M costs.

6.4. FGD Capital Cost Models

In this section we present the response surface models for capital cost derived from applying the method outlined in the previous section to FGDCOST. The results are very robust and provide excellent reduced form models for capital costs parameterized on a few operating parameters (no more than four to five). The accuracy is within 5% of FGDCOST, which is well within the 20% uncertainty associated with FGDCOST. The standard error of the regression models are explicitly included in the IECM as an additional uncertainty in the costs (they are usually very small, about 1%).

In the following subsection we present the capital cost models by process areas for each of the four technologies outlined in the introduction. The format used for presenting the results is as follows. For each technology, the results of the PRCC analysis are presented in tabular form. Based on the results of this analysis, the most important variables for explaining the variation in the capital costs are identified. Usually the first four or five variables are chosen. Subsequently, regression models for each process area parameterized on these few important variables are presented.

Usually, the main variables which effect the process capital costs are flue gas flow rate (Kacfm), SO_2 the inlet SO_2 concentration in flue gas (ppm), L/G ratio (gpm/Kacfm), and stoichiometry. The capital costs are calculated in millions of dollars It is known from prior engineering experience that the relation between the capital costs and the input variables is exponential, hence we use logarithmic transformations on the variables and conduct a linear regression of the transformed variables. The general form of the regression model is the same for all process areas and is presented below.

$$\log(C_i) = a_i + b_i \times \log(gas) + c_i \times \log(SO_2) + d_i \times \log(L/G) + e_i \times \log(\phi) \quad (6\text{-}11)$$
$$i \in (10, 20, 30, 60, 70, 80)$$

where C_i is the process facilities cost of each area (denoted by the numbers 10,20,30,60,70,80) in millions of 1990 dollars. The coefficients and the significance of explanatory variables differ by process area. In the following sections we present the coefficients for each of the process areas based on a regression analysis using *Splus.*

6.4.1. Wet Limestone with Forced Oxidation

A PRCC analysis of the data set for LSFO was performed. Based on this analysis the input variables are ranked in order of importance in Table 6-13.

Table 6-13 ***PRCC Analysis for Limestone Forced Oxidation***

		Process Capital	
Variables	**Range**	**PRCC**	**Rank**
flue gas(Kacfm) (MW equivalent)	625-3350 (300-1000)	-0.992	1
L/G(gal/Kacfm)	90-130	0.336	4
SO_2(inlet SO_2 ppm)	0.5-5.0	0.806	3
stoichiometry	1.01-1.15	0.856	2
labor rate($/hr)	15-25	0.018	10
reagent cost($/ton)	10-20	-0.066	7
solid disposal	5-10	-0.161	5
power cost(mills/kwh)	40-60	-0.03	9
steam cost($/Klbs)	3-4	0.10	6
water ($/Klbs)	0.5-0.75	-0.059	8

Now we present the development of regression models using the variables identified from the PRCC analysis. The main variables that affect the process capital costs are flue gas flow rate (Kacfm), SO_2 the inlet SO_2 concentration in flue gas (ppm), L/G ratio (gpm/Kacfm), and stoichiometry (ϕ). The capital costs are expressed in millions of dollars (1990 M$) for all process areas. The coefficients for the regression model (Equation (6-11)) are provided in Table 6-14. Recall that the models estimates $\log(C_i)$. Figure 6-6 graphs the sensitivity of the cost models for different coals and sizes. The y-axis plot the normalized cost ($/kW) as a function of size (MW gross) for different coals.

Table 6-14 ***Regression Coefficients for LSFO***

Wet Limestone with Forced Oxidation						
Variables	**Area 10**	**Area 20**	**Area 30**	**Area 60**	**Area 70**	**Area 80**
intercept (a_i)	5.532139	5.199094	4.967549	3.728971	5.29923	5.118347
log(gas) - b_i	0.2047287	0.5526016	0.5968993	0.3751297	0.0963776	0.2987416
log(SO_2) - c_i	0.1998244	0.0171820	-	0.3600074	-	- 0.0070039
log(L/G) - d_i	0.064419	0.1531021	-	0.0984928	0.01744453	-
log(ϕ) - e_i	0.297487	-	-	0.2896275	0.0639004	- 0.4110633
R^2	0.96	0.998	0.997	0.96	0.97	0.999

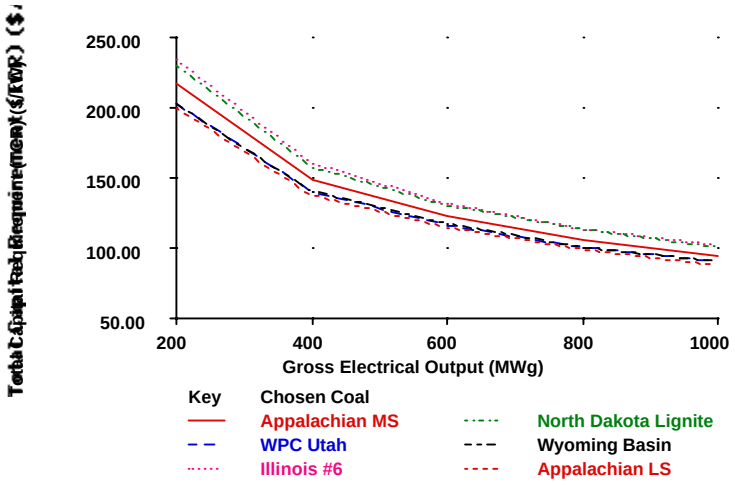

Figure 6-6 IECM cost model for LSFO with ϕ = 1.03

6.4.2. Wet Limestone with Additives

The PRCC analysis for the LS/DBA system was performed. Based on this analysis the input variables are rank ordered in terms of the magnitude of their influence on the costs in Table 6-15:

Table 6-15 ***PRCC analysis for Wet Limestone with Dibasic Acid***

		Capital Costs	
Variables	**Range**	**PRCC**	**Rank**
flue gas(Kacfm) size (MW)	625-3350 (300-1000)	-0.991	1
L/G(gpm/Kacfm)	50-90	0.293	4
%S(weight)	0.5-5.0	0.803	3
stoichiometry	1.01-1.15	0.852	2
labor rate($/hr)	15-25	0.071	9
reagent cost($/ton)	10-20	-0.031	11
solid disposal	5-10	-0.173	6
power cost(mills/kwh)	40-60	0.056	10
steam cost($/Klbs)	3-4	0.192	5
water fresh($/Klbs)	0.5-0.75	-0.073	8
DBA ppm	1-2K	0	12
DBA feed (lbs/ton of SO_2)	15-25	-0.147	7
DBA cost($/ton)	300-400	0	12

Now we present the development of regression models using the variables identified by the PRCC analysis. The regression analysis is parallel to the one presented for LSFO with a data set that is different, i.e. generated using a cost model for LS/DBA. The main variables which affect the process capital costs (expressed in 1990 M$) are flue gas flow rate (Kacfm), SO_2 in inlet flue gas, L/G ratio (gpm/Kacfm), and stoichiometry (ϕ). Note that the range of L/G for LS/DBA is between 60-90. Once again using logarithmic transformations, linear regressions (Equation (6-11)) are used for each process area. We provide highlights for each process area in Table 6-16. Figure 6-7 graphs the sensitivity of the normalized cost ($/kW) for different coals and sizes (MW gross).

Table 6-16 ***Regression Coefficients for Wet Limestone with DBA***

Wet Limestone with DBA						
Model Parameter	**Area 10**	**Area 20**	**Area 30**	**Area 60**	**Area 70**	**Area 80**
intercept (a_i)	5.656823	5.283843	4.967474	3.914778	5.33193	5.118347
log(gas) - b_i	0.2116698	0.5487767	0.5969214	0.3830471	0.0932564	0.2987416
log(SO_2) - c_i	0.1965567	0.0182601	-	0.3528121	0.0033284	-0.0070039
log(L/G) - d_i	-	0.1124185	-	-	-	-
log(ϕ) - e_i	0.3971839	-	-	0.6173974	0.0825347	-0.4110633
R^2	0.96	0.998	0.997	0.95	0.98	0.999

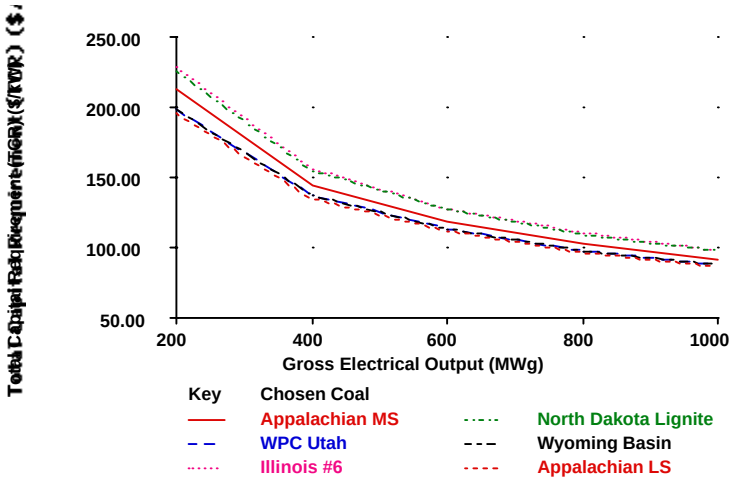

Figure 6-7 IECM cost model for Wet Limestone FGD with 1500 ppm of DBA as additive.

6.4.3. Magnesium-Enhanced Lime System

A PRCC analysis of the data set for Mg-Lime system was performed. Based on this analysis the input variables are ranked in order of importance in Table 6-17.

Table 6-17 ***PRCC Analysis for Mg-Lime***

		Process Capital	
Variables	**Range**	**PRCC**	**Rank**
flue gas(Kacfm) (MW equivalent)	625-3350 (300-1000)	-0.986	1
L/G(gal/Kacfm)	30-56	0.149	4
SO_2(inlet SO_2 ppm)	0.5-5.0	0.890	2
stoichiometry	1.01-1.15	0.801	3
labor rate($/hr)	15-25	0.13	6
reagent cost($/ton)	50-60	-0.069	8
solid disposal	5-10	-0.133	5
power cost(mills/kwh)	40-60	-0.051	10
steam cost($/Klbs)	3-4	0.064	9
water ($/Klbs)	0.5-0.75	-0.097	7

Now we present the development of regression models using the variables identified from the PRCC analysis. The main variables which affect the process capital costs are flue gas flow rate (Kacfm), SO_2 the inlet SO_2 concentration in flue gas (ppm), L/G ratio (gpm/Kacfm), and stoichiometry. The results are deduced from a regression analysis based on Equation (6-11) using *Splus*. The highlights are presented in Table 6-18. Figure 6-8 graphs the sensitivity of the normalized cost ($/kW) for different coals and sizes (MW gross).

Table 6-18 ***Regression Coefficients for Process Facilities Capital Cost***

Wet Limestone with Mg-Lime						
	Area 10	**Area 20**	**Area 30**	**Area 60**	**Area 70**	**Area 80**
intercept (a_i)	4.18205	5.343637	4.985706	3.805031	5.406733	5.118347
log(gas) - b_i	0.4287465	0.5571364	0.5965417	0.4408358	0.0859990	0.2987416
log(SO_2) - c_i	0.3973585	-0.0031376	-0.0057330	0.4067988	-0.0042571	-0.0070039
log(L/G) - d_i	-	0.0865696	-	-	-	-
log(ϕ) - e_i	-	-	-	-	0.0711735	-0.4110633
R^2	0.96	0.999	0.999	0.97	0.98	0.999

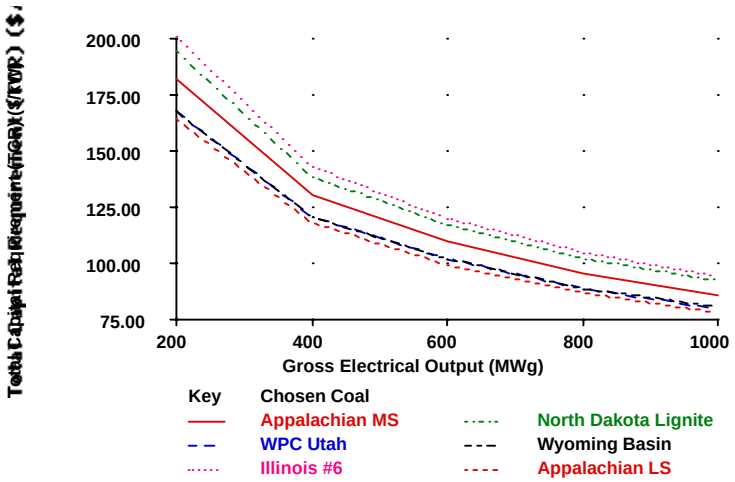

Figure 6-8 IECM cost model for Mg-enhanced Lime FGD with $\phi = 1.02$

6.4.4. Lime Spray Dryer

A PRCC analysis of the data set for the Lime Spray Dryer was performed. Based on this analysis the input variables are ranked in order of importance in the table below. Note however, that some of the key operating parameters are different for the Lime Spray Dryer. The water entering with the slurry spray vaporizes and the flue gas (along with the fly ash) carries the dried reaction products. These particles are then removed in the baghouse (downstream of the FGD) and a portion of the collected solids is recycled back to the absorber. The amount of recycle (lb of dry solids recycled/lb of lime added) is based on the sulfur content of the flue gas. The total slurry that is recycled to the absorber (gpm) depends on the recycle ratio (rr), stoichiometric ratio (ϕ) and the flue gas flow rate (gas). In order to determine the gpm we need to solve the process flowsheet of the LSD iteratively. In order to avoid this computational burden for the IECM we have developed a regression equation for the slurry flow rate as a function the recycle ratio, stoichiometry and the flue gas flow rate as shown below.

$$\log(gpm) = -0.9312959 + 0.9959784 \times \log(gas)$$
$$- 0.03043575 \times \log(rr) + 0.09146684 \times \log(\phi)$$

with R^2=0.994. The operating parameter gpm is used in the PRCC analysis (Table 6-19) and the regression analysis (instead of the equivalent L/G used for other technologies). The coefficients of the regression analysis are in Table 6-20.

Table 6-19 ***PRCC Analysis for Lime Spray Dryer***

		Process Capital	
Variables	**Range**	**PRCC**	**Rank**
flue gas(Kacfm) (MW equivalent)	625-3350 (300-1000)	-0.602	2
stoichiometry(ϕ	1.1-1.8	0.325	3
SO_2(inlet SO_2 ppm)	500-3500	0.827	1
gpm	70-400	0.151	5
labor rate($/hr)	15-25	0.061	9
reagent cost($/ton)	50-60	0.121	6
solid disposal	5-10	0.043	10
power cost(mills/kwh)	40-60	-0.165	4
steam cost($/Klbs)	3-4	0.084	8
water ($/Klbs)	0.5-0.75	0.106	7

Now we present the development of regression models using the variables identified from the PRCC analysis. The main variables which effect the process capital costs are flue gas flow rate (Kacfm), SO_2 the inlet SO_2 concentration in flue gas (ppm), L/G ratio (gpm/Kacfm), and stoichiometry. The results are derived from a regression analysis based on Equation (6-11) using *Splus*. The highlights are presented in Table 6-20. Figure 6-9 graphs the sensitivity of the normalized cost ($/kW) for the lime spray dryer for different sizes (MW gross) and coals.

Table 6-20 ***Regression Coefficients for Lime Spray Dryer***

Lime Spray Dryer						
Model Parameters	**Area 10**	**Area 20**	**Area 30**	**Area 60**	**Area 70**	**Area 80**
intercept (a_i)	-1.187585	-1.391273	-1.154033	-1.742325	-0.3249075	-0.9106584
log(gas) - b_i	-0.3133721	0.8549951	0.6044183	-	-	0.300299
log(SO_2) - c_i	0.386108	-	-	0.4840697	-0.0089210	-0.0052555
gpm - d_i	0.7677725	-0.0009575	-	0.00161753	0.00016397	-
log(ϕ) - e_i	0.3871053	-	-	-	-0.0177219	-
R^2	0.97	0.97	0.998	0.95	0.98	0.9999

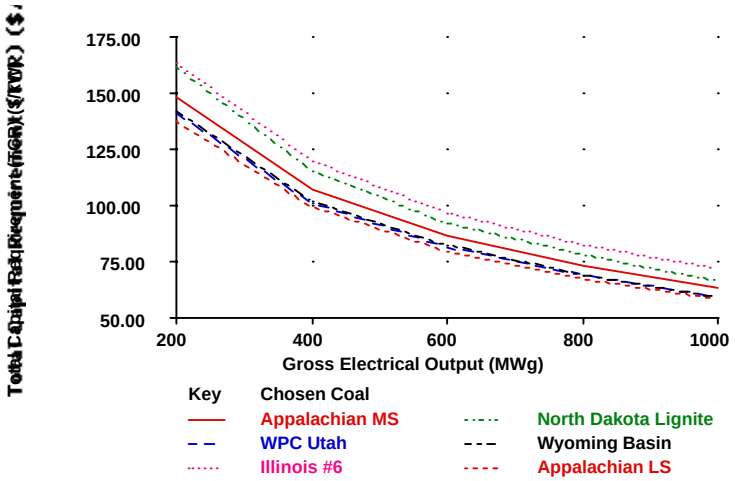

Figure 6-9 IECM cost model for Lime Spray Dryer for $\phi = 1.1$

6.4.5. Sparing Philosophy

The models developed in the previous subsections are based on the assumption of two operating absorber towers (each rated at 50% of the plant capacity, with a maximum of 650MW) and one spare absorber tower. With the recent development of advanced absorber towers of near 100% reliability it is possible to eliminate the spare tower and reduce capital costs significantly (no significant changes in variable costs). Another approach to reducing capital cost exploits the economy of scale by using single absorber towers of large capacity. In this subsection we develop scaling factors to estimate the reduction in capital costs for different FGD systems by changing the sparing philosophy. Note that in all the factors developed below, the scaling factors are derived by a regression of the capital cost of various sparing philosophies against the capital cost of the default system, i.e. an FGD with two operating towers and one spare absorber.

In order to estimate the reduction in capital costs from eliminating the spare tower, we set the number of spare towers in FGDCOST to zero and exercise the model for various values of input for the relevant variables such as flue gas flow rate (*gas*), SO_2 in flue gas, L/G, and stoichiometry (ϕ). The capital costs for system with no spares (C') is then regressed against the capital cost for the system with one spare tower (C) and correlation coefficient (s_i) of this regression provides us with the scaling factor we desire:

$$C_i^{/} = s_i \times C_i,\ i \in (20, 30)$$

where C_i is the process area (denoted by 20, 30) cost. The capital cost of the SO_2 removal system (includes absorber towers) and the flue gas system (includes piping to absorber towers) is affected by the sparing philosophy. We present results for those process areas whose capital cost is affected in Table 6-21. The columns under "Zero Sparing" characterize the reduction in capital cost by dropping the spare absorber. The columns under "One Absorber" characterize the reduction in capital cost by reducing the number of absorbers from two (rated @50% each) to one (rated @100% of capacity).

Table 6-21 ***Regression Coefficients for Different Sparing Philosophies***

System	Zero Sparing		One Absorber	
	Area 20	Area 30	Area 20	Area 30
LSFO	0.7306793	0.943658	0.5818281	0.9449641
LSFO with DBA	0.7213572	0.9436423	0.5692575	0.9316498
Mg-Lime	0.6926448	0.9437713	0.525391	0.9316498
Lime Spray Dryer	0.7114379	0.8002883	0.5126236	0.64543523

6.5. Fixed O&M Costs

The O&M costs for FGD consists of fixed costs and variable costs. The fixed operating cost consists of labor, maintenance labor, material, and administrative labor. A mathematical model for the fixed cost is provided below.

$$
\begin{aligned}
FOM &= FOM_{labor} + FOM_{maint} + FOM_{admin} \\
FOM_{labor} &= labor \times N_{labor} \times 40\,(hrs/week) \times 52\,(weeks/yr) \\
FOM_{maint} &= \sum_{i} \left(f_{maint}\right)_{i} \times TPC_i \text{ where i = process area} \\
FOM_{admin} &= f_{admin} \times (FOM_{labor} + f_{maintlab} \times FOM_{maint})
\end{aligned}
\qquad (6\text{-}12)
$$

where

FOM = fixed operating and maintenance cost, M$/yr

FOM_{labor} = operating labor, M$/yr

FOM_{maint} = maintenance material costs, M$/yr, (coefficients based on EPRI TAG, the fraction $f_{maintlab}$ of these costs are allocated to maintenance labor and rest to maintenance material).

FOM_{admin} = administrative costs, M$/yr (calculated as the fraction f_{2admin} of total labor costs)

TPC_i = total process capital for each process area, (10,20,30,40, 50,60)

N = total number of laborers (per week)

labor = labor rate ($/hr)

Figure 6-10 provides the levelized fixed costs (mills/kWh) as a function of size (MW gross) for different coals for wet limestone FGD systems. Similar sensitivity analysis can be conducted for other technologies.

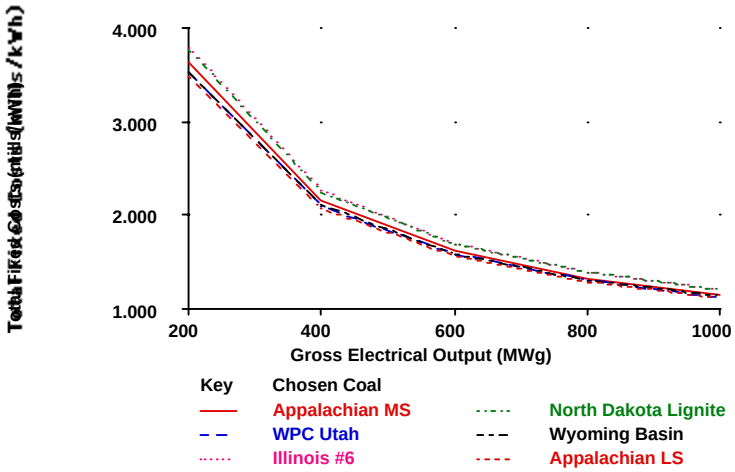

Figure 6-10 Fixed costs for all Wet Limestone FGD systems for 90% SO_2 removal, and default stoichiometry ϕ =1.03.

6.6. Variable O&M Costs

Variable operating costs include consumables such as reagents, additives, water, power, steam for reheat and the continuous costs related to solid disposal. The variable operating costs can be usually calculated directly based on engineering principles. In this section we outline the formulations based on basic engineering principles for the calculation of variables costs. We then characterize the parameters that are specific to the different FGD technologies. The total variable cost (in M$) is given as:

varcost = rcost + scost + dbacost + pcost + stcost + wcost

where,

rcost	=	reagent consumption, M$/yr
scost	=	solid disposal cost, M$/yr
dbacost	=	cost of dibasic acid feed, M$/yr
pcost	=	power consumption, M$/yr
stcost	=	steam consumption, M$/yr
wcost	=	makeup water cost, M$/yr

6.6.1. Reagent Cost

The total amount of reagent usage cost (rcost, M$/yr) depends on the total amount of reagent used and the cost of the reagent (reag, $/ton). The amount of reagent used (M_{reag} tons/yr) depends on the reactive species in flue gas (gas_i lbmole/yr), sulfur removal efficiency (η_{SO2}), the plant capacity factor, and the stochiometric ratio (ϕ). Therefore the model to calculate the total cost of reagent (rcost) used is:

$$rcost = reag \times M_{reag}$$

$$M_{reag} = \frac{1}{2000}\left(\sum_i (\eta_i \times \phi_i \times gas_i \times r_i) \times MW_{CaCO_3} \times cf \times 8766\right) / R_{purity} \quad (6\text{-}13)$$

where

$i \in (SO_2, SO_3, HCl)$

r_i = moles of reagent required per mole of species, I

$r_i \in (1, 1, ½)$

MW_{CaCO_3} = molecular weight of $CaCO_3$

R_{purity} = reagent purity (weight fraction of $CaCO_3$)

6.6.2. Solid Waste Disposal Costs

The solid waste disposal cost (scost, M$/yr) depends on the amount of solid waste and the unit cost of disposal (disposal, in $/ton). The amount of solid waste produced depends on the amount of reactive species scrubbed from the flue gas ($M_{disposal}$ tons/yr), the total amount of inerts in the slurry (M_{inerts}, tons/yr) and the amount of unused reagent in the slurry ($M_{unused\ reagent}$, tons/yr). Therefore the model to calculate the total cost of waste disposal (scost) is:

$$s_{cost} = disposal \times \left(M_{disposal} + M_{inerts} + M_{unused\ reag}\right)$$

$$M_{disposal} = \frac{1}{2000} \times \sum_i \left(\eta_i \times \phi_i \times gas_i \times r_i\right) \times MW_i \times cf \times 8766$$

$$M_{inerts} = \frac{M_{reag}}{2000} \times \left(1 - R_{purity}\right) \times cf \times 8766 \quad (6\text{-}14)$$

$$M_{unused\ reag} = \frac{1}{2000} \times \sum_{-} \frac{\left(\eta_i \times gas_i \times r_i \times (\phi_i - 1)\right) \times M_{CaCO_3}}{R_{purity}} \times cf \times 8766$$

where,

$i \in (SO_2, SO_3, HCl)$

r_i = moles of reagent required per mole of species

$r_i \in (1, 1, ½)$

$$MW_i = \begin{cases} \left(MW_{CaSO_4 \bullet 2H_2O}, MW_{CaSO_4 \bullet 2H_2O}, MW_{CaCl_2}\right) \text{Limestone System} \\ \left(MW_{CaSO_3 \bullet 5H_2O}, MW_{CaSO_3 \bullet 5H_2O}, MW_{CaCl_2}\right) \text{Lime System} \end{cases}$$

6.6.3. Power Costs

The power costs (pcost, M$/yr) depends on the unit cost of power (power, $/MWh), and power consumption in the reagent handling (P_{20}, MW) and flue gas handling systems (P_{30}, MW). Slurry is injected into the absorber towers at four levels to remove SO_2 and a pump serves each level. The power consumption for these pumps is proportional to the amount of slurry being pumped (Q, gallons/hr) and the total

dynamic head required. Similarly the power consumption for the I.D. fans to overcome the flow resistance (or equivalent pressure drop) of the absorber towers and ducts to the chimney is proportional to the total flue gas flow rate and the pressure drop. The total power consumption (P_{total}, MW) is given by:

$$\begin{aligned} p\cos t &= power \times P_{total} \times cf \times 8766 \\ P_{total} &= P_{20} + P_{30} \\ P_{20} &= \rho \times Q \times H / \eta_{pump} \\ P_{30} &= 0.12 \times 10^{-6} \times gas \times \Delta p / \eta_{fan} \end{aligned} \qquad (6\text{-}15)$$

where,

ρ	=	density of slurry (lb/gallon)
H	=	total dynamic head (ft)
gas	=	flue gas flow rate (acfm)
Δp	=	total pressure drop (inches of water)
Q	=	flow rate (gallons/hr = L/G x gas x 60 or gpm x 60)
η_{fans}	=	fan efficiency (fraction)
η_{fans}	=	pumping efficiency (fraction)

The power consumption due to I.D. fans (P_{30}) is easily calculated by assuming an efficiency for the centrifugal fans (usually 60-70%). The constant factor ($0.12x10^6$) is a conversion factor which provides power required in MW. The total dynamic head (H) and slurry density (ρ) are not easily available in the specification of FGD systems. In order to minimize the data requirements of the model we have developed a regression model which provides a proportionality constant for the slurry pumps by aggregating the head and density as a fraction of the slurry flow rate as follows:

$$P_{30} = k_t \times Q + c, \quad t \in (\text{LSFO, LS/DBA, Mg - Lime, LSD}) \qquad (6\text{-}16)$$

The units for k_t are in lb-ft/gallons and value reported in the table below includes the conversion factor for changing to MW. The constant c is in MW. The regression coefficients for the different technologies is provided in Table 6-22.

Table 6-22 ***Regression Coefficients for Power***

Technology	LSFO	LS/DBA	Mg-Lime	LSD
k_t	$3.6165x10^{-5}$	$3.8234x10^{-5}$	$3.2456x10^{-5}$	$9.99x10^{-5}$
c	-	-	0.21	-
R2	0.99	0.98	0.99	0.9

6.6.4. Steam Costs

The saturated gas exiting the absorbers at approximately 127°F is reheated to 152°F using steam heat. The steam cost (stcost, M$/yr) of reheating depends on the cost of electricity, heat rate, and the energy required (E_{reqd}, Btu/hr) to reheat the flue gas. The energy required is calculated as the change in enthalpy of the flue gas (ΔH_{127}^{152})

and the heat of vaporization for the water removed (ΔH_{vapor}). IECM calculates all the necessary thermodynamic relationships and properties.

$$E_{reqd} = \Delta H_{127}^{152} + \Delta H_{vapor} \qquad (6\text{-}17)$$

The cost of reheating is calculated by estimating the cost of the equivalent electricity that could have been generated if the steam had not been used for reheating:

$$stcost = E_{reqd}/hr \times power \times cf \times 8766 \qquad (6\text{-}18)$$

where *hr* is the steam cycle heat rate (Btu/kWh) and *power* is the cost of electricity ($/kWh).

6.6.5. DBA Costs

For systems that use organic acid additives (LS/DBA), the cost of replacing DBA which degrades on a yearly basis (dbacost, M$/yr) depends on the replacement cost of Dibasic Acid (C_{DBA}, $/ton), and the amount of DBA degradation (F_{DBA}, tons/yr), which depends on the amount of SO_2 removed (M_{SO2}, tons/yr) and the degradation of DBA per ton of SO_2 removed (D_{DBA}, lb of DBA/ton of SO_2 removed). This is characterized as follows:

$$dbacost = C_{DBA} \times F_{DBA}$$

$$M_{SO_2} = \frac{1}{2000} \times (\eta_{SO_2} \times gas_{SO_2} \times M_{SO_2}) \times cf \times 8766$$

$$F_{DBA} = \frac{1}{2000} \times D_{DBA} \times T_{SO_2} \times cf \times 8766$$

6.6.6. Water Costs

Water from the scrubbing slurry is lost due to evaporation in the scrubber. The water costs pertain to the supply needed to replenish this loss. The water cost (wcost, M$/yr) depends on the cost of fresh water (waterf, $/Kgallons), and the total amount of water used (Wtotal, Kgallons). The water costs are characterized as:

$$wcost = waterf/1000 \times W_{total}$$
$$W_{total} = W_{MW} \times 60 \times MW_{gross} \times hoursannual \qquad (6\text{-}19)$$

where W_{MW} is the water consumed (gallons/min) per MW gross. This consumption differs for different technologies. Nominal values used for model development are shown in Table 6-23.

Table 6-23 ***Water Consumption for FGD Systems***

Technology	LSFO	LS/DBA	Mg-Lime	LSD
W_{MW} (gpm/MW)	0.098	0.098	1.08	-

Figure 6-11 graphs the total levelized variable O&M costs (mills/kWh) as a function of size (MW gross) and coal type for Wet Limestone FGD. Similar analysis can be conducted for different technologies.

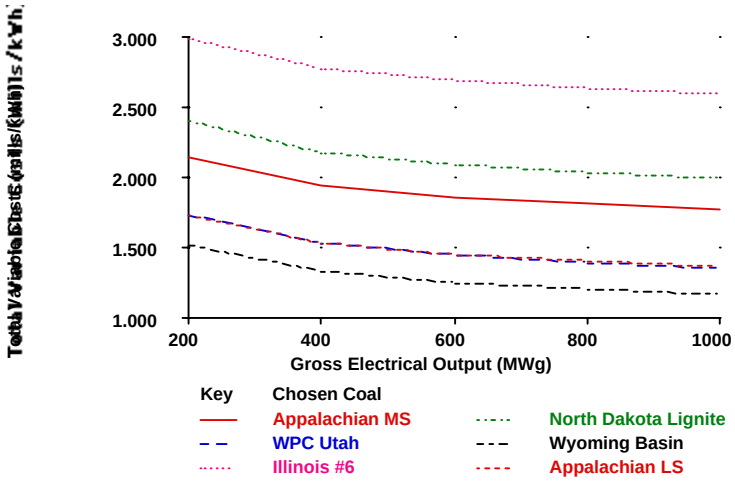

Figure 6-11 Variable costs for all Wet Limestone FGD systems for 90% SO_2 removal, and default stoichiometry ϕ = 1.03.

6.7. A Numerical Example

In this section we provide an illustrative example which uses the models developed above to calculate the capital and O&M costs for a given set of inputs. We compute costs for the limestone forced oxidation (LSFO) FGD system. A plant of gross capacity of 330 MW (300 net) which uses a medium sulfur Appalachian coal (2.13% sulfur and 0.07% chlorine) and operates at 65% capacity factor, yielding 5698 hours/yr of operation. We design the FGD system for a SO_2 removal efficiency of 95% with a stochiometric ratio of 1.03. The base case assumes 2 absorber towers and 1 spare tower. We use Equation (6-8) to evaluate the L/G ratio as shown.

$$0.95 = 1 - \exp\left\{\begin{array}{l} -(0.725 + 0.0175 \times \mathrm{L/G} + (10.0 \times 1.03 - 10.3) \\ -2.5 \times 10^{-4}(1260 - 2000) + 5.14 \times 10^{-6}(27900 - 25000)) \end{array}\right\}$$

$$\Rightarrow \mathrm{L/G} = 120 \text{ gpm/Kacfm}$$

The operating parameters of the power plant are calculated using IECM and are provided below

Table 6-24 IECM Operating Parameter Values

Operating parameters	Variable name	Value
flue gas flow rate, Kacfm	Gas	1064 Kacfm
SO_2 inlet concentration, SO_2, ppm	SO_2	1260 ppm
Chloride conc. in slurry stream, Cl, ppm	Cl	27900 ppm
L/G ratio, gpm/Kacfm	L/G	120 gpm/Kacfm

6.7.1. Capital Cost

The calculation of process facilities capital is based on Equation (6-11) and the regression coefficients in Table 6-19. The template for such calculations is provided in Table 6-25.

Table 6-25 ***Example Calculation of Process Capital Costs (1990 $)***

Wet Limestone with Forced Oxidation						
Variables	**Area 10**	**Area 20**	**Area 30**	**Area 60**	**Area 70**	**Area 80**
(a_i)	5.532139	5.199094	4.967549	3.728971	5.29923	5.11835
b_i x log(gas)	0.6197	1.673	1.807	1.136	0.2918	0.9043
c_i x log(SO_2)	0.6185	0.05318	-	1.114	-	-0.0217
d_i x log(L/G)	0.134	0.3184	-	0.2048	0.03627	-
e_i x log(ϕ)	3.819m	-	-	3.718m	820.3u	-5.277m
sum(variables)	6.908	7.243	6.774	6.187	5.628	5.996
C_i (M$)	8.094	17.52	5.949	1.54	0.425	0.99

The total process facilities cost is the sum over all process areas.

$$PFC = \sum_i C_i = 34.52\ M\$\ (1990)$$

$$= 34.86\ M\$\ (1993)$$

The IECM uses chemical engineering cost indices to provide the cost indexed by other years. The typical default year that is used in IECM is 1993, hence we scale the costs to this year and conduct all subsequent calculations in 1993 dollars. Note that a cost index of 1.01 has been used to provide all numbers in 1993 dollars. The indirect costs are calculated as fractions of the process capital based on Table 6-9 and Table 6-10. The calculations based on this are shown in Table 6-26.

Table 6-26 ***Capital Cost Summary (1993 $)***

Capital Investment	M$	$/kW
Process Facilities Capital $\sum_i C_i$	34.86	116.6
General Facilities (10%)	3.486	11.66
Eng. & Home Office Fees(10%)	3.486	11.66
Project Contingency (15%)	5.229	17.49
Process Contingency (2%)	0.6972	2.333
Total Plant Cost	47.76	159.8
Total Cash Expended (Adjust Factor=1)	47.76	159.8
AFDUC (Adjust Factor=0.0548)	1.156	3.867
Total Plant Investment (TPI)	48.91	163.7
Royalty Allowance (0.5%)	0.1743	0.5831
Preproduction costs	1.621	5.416
Inventory Capital	0.1647	0.5509
Total Capital Requirement	50.87	169.9

6.7.2. Fixed O&M Costs

The calculations for fixed operating costs are provided using the following default values for model parameters:

N = 32 (total number of laborers, per week)

labor = 21.87 $/hr (labor rate)

f_{maint} = (0.04,0.06,0.02,0.04,0.015,0.015)

f_{admin} = 30%

$f_{maintlab}$ = 40%

These calculations are based on Equation (6-12)

$$FOM_{labor} = 21.87 \times 32 \times 40 \text{ (hrs/week)} \times 52 \text{ (weeks/yr)}$$

$$= 1.44 \text{ M\$/yr}$$

$$FOM_{maint} = 0.04 \times TPC_{10} + 0.06 \times TPC_{20} + 0.02 \times TPC_{30} + 0.04 \times TPC_{60} + 0.015 \times TPC_{70} + 0.015 \times TPC_{80}$$

$$= 2.182 \text{ M\$/yr}$$

$$FOM_{admin} = 0.3 \times (FOM_{labor} + 0.4 \times FOM_{maint})$$

$$= 0.694 \text{ M\$/yr}$$

$$FOM = FOM_{labor} + FOM_{maint} + FOM_{admin}$$

$$= 4.32 \text{ M\$/yr } (14.42 \text{ \$/kW - yr})$$

6.7.3. Variable O&M Costs

The calculations for variable operating costs are providing using the following default values for model parameters:

η = 95% (SO_2 removal efficiency)

ϕ = 1.03 (reagent stoichiometry)

gas_{SO2} = 140.8 (lb moles/hr, IECM calculation)

gas_{SO3} = 1.63 (lb moles/hr, IECM calculation)

gas_{HCl} = 8.67 (lb moles/hr, IECM calculation)

ΔH_{127}^{152} = 19.7 MBtu/hr (IECM calculation)

ΔH_{vapor} = 1.24 MBtu/hr (IECM calculation)

reag = 15 $/ton (reagent cost)

cf = 65% (capacity factor)

R_{purity} = 94% (reagent purity, wt. fraction)

MW_{CaCO_3} = 100 (molecular weight)

$MW_{CaSO_4 \bullet 2H_2O}$ = 172 (molecular weight)

MW_{CaCl_2} = 112 (molecular weight)

6.7.3.1. Reagent Cost

This calculation is based on Equation (6-13)

$$T_{reag} = \frac{1}{2000}\left(\sum_i \begin{Bmatrix} (0.95\times 1.03\times 140.8\,(SO_2)\times 1) + \\ (0.95\times 1.0\times 1.63\,(SO_3)\times 1) + \\ (0.95\times 1.0\times 8.67\,(HCl)\times 0.5) \end{Bmatrix} \times 100\times 5698 \right) / 0.9$$

$$= 44.26K$$

$$rcost = 15.15\times T_{reag} = 0.671\,M\$$$

6.7.3.2. Solid Waste Disposal Costs

This calculation is based on Equation (6-14)

$$M_{disposal} = \frac{1}{2000} \times \left(\sum_i \begin{Bmatrix} (0.9 \times 1.03 \times 140.8\,(SO_2) \times 1 \times 172) + \\ (0.9 \times 1.0 \times 1.63\,(SO_3) \times 1 \times 172) + \\ (0.9 \times 1.0 \times 8.67\,(HCl) \times 0.5 \times 112) \end{Bmatrix} \times 5698 \right)$$

$$= 69.63K \text{ (tons/yr)}$$

$$M_{inerts} = 44.26K \times (1 - 0.94)/2000$$

$$= 3.365K \text{ (tons/yr)}$$

$$M_{unused\,reagent} = \frac{1}{2000} \times \left(\sum_i \begin{Bmatrix} (0.9 \times (1.03 - 1) \times 140.8\,(SO_2) \times 1) + \\ (0.9 \times (1.0 - 1.0) \times 1.63\,(SO_3) \times 1) + \\ (0.9 \times (1.0 - 1.0) 1.0 \times 8.67\,(HCl) \times 0.5) \end{Bmatrix} \times 100 \times 5698 \right) / 0.94$$

$$= 1.238\,K \text{ (tons/yr)}$$

$$scost = 8.15 \times \left(M_{disposal} + M_{inerts} + M_{unused\,reagent} \right)$$

$$= 0.605\,M\$$$

6.7.3.3. Power Costs

This calculation is based on Equations (6-15) and (6-16)

$$P_{20} = 3.62 \times 10^{-5} \times 120 \times 1064 + 0 = 3.34\,MW$$

$$P_{30} = 0.12 \times 10^{-6} \times 1064 \times 10/0.5 = 2.56\,MW$$

$$P_{total} = P_{20} + P_{30} = 5.73\,MW$$

$$pcost = 43.45 \times P_{total} \times 5698 = 1.78\,M\$$$

6.7.3.4. Steam Costs

This calculation is based on Equations (6-17) and (6-18)

$$E_{reqd} = 19.7\,(\Delta H_{127}^{152}, MBtu/hr) + 1.24\,(\Delta H_{vapor}, MBtu/hr)$$

$$= 20.94\,(MBtu/hr)$$

$$stcost = 20.94 \times 1K/7880 \times 43.45 \times 5698 = 0.665\,M\$$$

6.7.3.5. Water Costs

This calculation is based on Equation (6-19)

$$W_{total} = 0.098 \times 330 \times 60 \times 5698 = 11.06\,K gallons/year$$

$$wcost = 0.7\,(\$/K\,gallons) \times W_{total}$$

$$= 7721\$/yr\,(4.53 \times 10^{-3}\ mills/kWh)$$

6.7.3.6. Total Variable Operating Costs

The total variable costs (mills/kWh) are derived as the sum of the reagent, solid waste disposal, power and steam costs as follows:

fixcost = 4.32 M$

varcost = 0.671 + 0.605 + 1.78 + 0.665 + 0.0077 = 3.724 M$

totalcost = 8.04 M$ (4.735 mills/kWh)

6.7.4. Sparing Options

	Zero Sparing		One Absorber	
	Area 20	**Area 30**	**Area 20**	**Area 30**
LSFO	12.93 (17.69)	5.67 (6.01)	10.29 (17.69)	5.678 (6.01)

The numbers in (brackets) are capital costs for 2 towers and 1 spare (base case assumption) and are provided for comparison.

6.8. References

Agrawal, R. S., & Rochelle, G. T.,. (1993). Chemistry of Limestone Scrubbing. In SO_2 Control Symposium, Boston, MA.

Ang, A. H., & Tang, W. H. (1975). *Probability Concepts in Engineering Planning and Design*. New York: John Wiley & Sons.

Becker, R. A., Chambers, J. M., & Wilks, A. R. (1988). *The New S Language*. Pacific Grove, CA: Wadsworth & Brooks/Cole.

Benson, L. (1993). Wet Lime/Limestone Performance Modeling. In Radian Corp., Texas.

Benson, L., Hicks, R., & Johnson, H. (1991). Advanced Mg-Enhanced SO_2 and NO_x Control Pilot Plant. In SO_2 Control Symposium, Washington, DC.

Bhat, P. A., Johnson, D. W., & Jankura, B. J. (1993). Results of Babcock & Wilcox Limestone Wet FGD Pilot Program at EPRI's High Sulfur Test Center. In SO_2 Control Symposium, . Boston, MA.

Blythe, G. M., Burke, J. M., Lewis, D. L., & Thompson, C. (1985). *Field Evaluation of Utility Spray Dryer* No. CS-3954). EPRI.

Blythe, G. M., Lepovitz, L. R., & Thompson, C. M. (1991). *Evaluation of a 2.5MW Spray Dryer/Fabric Filter SO_2 Removal System* No. GS-7449). EPRI.

Blythe, G. M., Phillips, J. L., & Slater, T. (1993). Results of High Efficiency SO_2 Removal Testing at the Southwestern Electric Power Company's Henry W. Pirkey Station. In SO_2 Control Symposium, Boston, MA.

Brown, B., & Felsvang, K. (1991). High SO_2 Removal Dry FGD Systems. In SO_2 Control Symposium, Washington, DC.

Chang, C.-S., & Rochelle, G. T. (1983). Mass Transfer Enhanced by Equilibrium Reactions. *Ind. Eng. Chem. Fund.*, **21**, 379-385.

Corbett, W. E., Hargrove, O. W., & Merrill, R. S. (1977). *A Summary of Effects of Important Chemical Variables upon the Performance of Lime/Limestone Wet Scrubbing Systems.* No. FP-639). Radian Corporation.

Dene, C. E., Boward, W. L., Noblett, J. G., & Keeth, R. J. (1991). Development of Advanced Retrofit FGD Designs. In SO_2 Control Symposium, Washington, DC.

Draper, N. R., & Smith, H. (1966). *Applied Regression Analysis*. New York: John Wiley & Sons.

Iman, R. L., Davenport, J. M., & Zeigler, D. K. (1980). *Latin Hypercube Sampling (A Program User's Guide).* No. SAND79-1473). Sandia National Laboratories.

Iman, R. L., Helton, J. C., & Campbell, J. E. (1981a). An Approach to Sensitivity Analysis of Computer Models: Part I - Introduction, Input Variable Selection and Preliminary Variable Assessment. *Journal of Quality Technology*, **13**(3), 174-183.

Iman, R. L., Helton, J. C., & Campbell, J. E. (1981b). An Approach to Sensitivity Analysis of Computer Models: Part II - Ranking of Input Variables, Response Surface Validation, Distribution Effect and Technique Synopsis. *Journal of Quality Technology*, **13**(4), 232-40.

Johnson, H. (1993). Advanced Mg-Enhanced Wet FGDs. In

Jozewicz, W., & Rochelle, G. T. (1984). Modeling of SO_2 Removal by Spray Dryers. In Pittsburgh Coal Technology Conference, Pittsburgh, PA.

Keeth, R. J., Baker, D. L., Tracy, P. E., Ogden, G. E., & Ireland, P. A. (1991). *Economic Evaluation of Flue Gas Desulfurization Systems* No. GS-7193, Research Project 1610-6.). EPRI, Palo Alto, CA.

Klingspor, J. (1993). Wet Limestone Modeling. In ABB Environmental Systems.

Laslow, D. (1993). Wet Lime/Limestone Performance Modeling. In General Electric, Connecticut.

Mehta, R. R., & Rochelle, G. T. (1983). Modeling of SO_2 Removal and Limestone Utilization in Slurry Scrubbing with Forced Oxidation. In AIChE National Meeting, Houston, TX.

Moser, R. E., & Owens, D. R. (1990). Overview on the Use of Additives in Wet FGD Systems. In SO_2 Control Symposium, New Orleans, LA.

Neter, J., Wasserman, W., & Kutner, M. H. (1983). *Applied Linear Regression*. Homewood, ILL: R.D. Irwin.

Noblett Jr., G. E., DeKraker, D. P., & Moser, R. E. (1990). FGDPRISM, EPRI's FGD Process Model -- Recent Applications. In SO_2 Control Symposium, New Orleans, LA.

Noblett Jr., G. E., Hebets, M. J., & Moser, R. E. (1990). EPRI's FGD Process Model (FGDPRISM). In 1990 SO_2 Control Symposium, Washington, DC.

Noblett Jr., J. (1993). Wet Lime/Limestone Performance Modeling. In Radian Corp., Texas.

Rader, P. (1993). Wet Limestone Modeling. In ABB Environmental Systems.

Rader, P. C., & Bakke, E. (1991). Incorporating Full-Scale Experience into Advanced Limestone Wet FGD Designs. In 1991 SO_2 Control Symposium, Washington, DC.

Rochelle, G. T. (1981). Appendix A: Chemistry of Limestone Scrubbing. In R. H. Borgwardt (Eds.), *Limestone FGD Scrubbers: Users Handbook* EPA.

Rochelle, G. T. (1981). Appendix B: Operational Factors of Limestone Scrubbing. In R. H. Borgwardt (Eds.), *Limestone FGD Scrubbers: Users Handbook* EPA.

Smolenski, J., Phillips, J. L., Epsenscheid, A. P., & Shires, T. M. (1993). High Efficiency SO_2 Removal Tests at Tampa Electric Company's Big Bend Unit 4. In SO_2 Control Symposium, Boston, MA.

Stevens, G. E., Horton, W. M., Hargrove, O. W., & Owens, D. R. (1993). Evaluation of High SO_2 Removal Efficiency Upgrade Options: EPRI High Sulfur Test Center. In SO_2 Control Symposium, Boston, MA.

Stevens, G. E., Sitkiewitz, S. S., Phillips, J. L., & Owens, D. R. (1991). Results of High SO_2 Removal Efficiency Tests at EPRI's High Sulfur Test Center. In SO_2 Control Symposium, Washington, DC.

Weilert, C. (1993). Wet Lime/Limestone Performance Modeling. In Burns and McDonnell, Missouri.

Weilert, C. V., & Ratliff, J. (1990). Development and Use of Site-Specific FGD System Performance and Economic Models. In SO_2 Control Symposium, New Orleans, LA: EPRI/EPA.

7. Fluidized Bed Copper Oxide Process

7.1. Introduction

The fluidized bed copper oxide process is an advanced technology for controlling SO_2 and NO_x emissions from coal-fired power plants. The development of this process has been sponsored by the U.S. Department of Energy, Federal Energy Technology Center (USDOE FETC). Testing of the copper oxide process began at FETC in 1975 and has progressed through several stages in three different test units (Demski *et al*, 1982; Yeh *et al*, 1984; Plantz *et al*, 1986; Williamson *et al*, 1987). Key features of the copper oxide process are that it: (1) combines SO_2 and NO_x removal in a single reactor vessel; (2) is regenerative (i.e. the reagent is reused rather than disposed of); and (3) produces a saleable sulfur or sulfuric acid byproduct, in contrast to the sludge produced by conventional flue gas desulfurization systems (Drummond et al, 1985). Conceptual designs of commercial scale copper oxide systems were developed in the early 1980's (SMC, 1983a, b and c; 1984).

Based on mass and energy balances, FETC test results, and the conceptual design studies, a detailed performance and cost model of the copper oxide process was developed (Frey, 1987). The copper oxide process is in an early phase of development, with limited test data and no commercial operating experience. Uncertainties in system performance at the commercial scale lead to uncertainties in capital and operating costs. Furthermore, even if process performance were known with certainty, uncertainties regarding the costs of equipment and reagents would remain. To explicitly characterize these uncertainties, and to evaluate the overall uncertainty in process costs, a probabilistic engineering modeling framework has been developed.

Analytic models for a conventional pulverized coal (PC) power plant, coal cleaning processes, and selected conventional and advanced post-combustion pollution control systems are available in the Integrated Environmental Control Model (IECM), developed by Rubin et al. (1986, 1991, 1992). Details of the IECM's copper oxide process, power plant air preheater, sulfur recovery, and sulfuric acid recovery plant models are described elsewhere (Frey, 1987; Rubin et al., 1991; Frey and Rubin, 1991).

The models characterize mass and energy balances for key process equipment. The capital cost models are based on equipment cost estimates from the literature, adjusted for plant size using key process stream flow rates and exponential scaling

factors. Indirect capital costs, and variable and fixed operating costs, are also calculated using a standard approach (EPRI, 1986)

To characterize uncertainties in advanced emission control systems, the IECM is implemented in a probabilistic modeling environment (Henrion and Wishbow, 1987). Uncertainties in process parameters can therefore be characterized using a variety of user-specified probability distribution functions. The resulting uncertainty distributions for model outputs are calculated using median Latin hypercube sampling, a variant of Monte Carlo simulation.

Probabilistic modeling has several advantages over traditional sensitivity analysis. In probabilistic analysis, the values of any number of parameters may vary *simultaneously*, and the *likelihood* of obtaining particular results is explicitly estimated. Furthermore, statistical analysis on the model input and output data can be used to identify trends (e.g., key input uncertainties affecting output uncertainties) without need to re-run the analysis. This permits the identification of key input parameters when many other parameters are simultaneously uncertain.

The probabilistic performance and cost model of the copper oxide process has been applied in a number of case studies to evaluate uncertainty in process costs, payoffs from process design improvements, the dependence of system cost on process design conditions and the availability of byproduct markets, and the likelihood that the advanced process will yield cost savings relative to conventional technology (Frey *et al.*, 1989; Frey and Rubin, 1991; Frey and Rubin, 1992; Rubin *et al.*, 1988; Rubin *et al.*, 1989).

In this study, the performance model for the copper oxide process is updated to account for a recent study of the kinetics of sorbent regeneration (Harriott and Markussen, 1992). New models developed by Harriott (1992a,b,c) are employed to characterize the kinetics of both the sulfation and regeneration reactions. Furthermore, the mass and energy balances for the sorbent are modified to account for the formation of copper sulfite in the regenerator. Estimates of uncertainty in key process parameters form the basis for a probabilistic analysis of the fluidized bed copper oxide process.

7.2. Process Chemistry

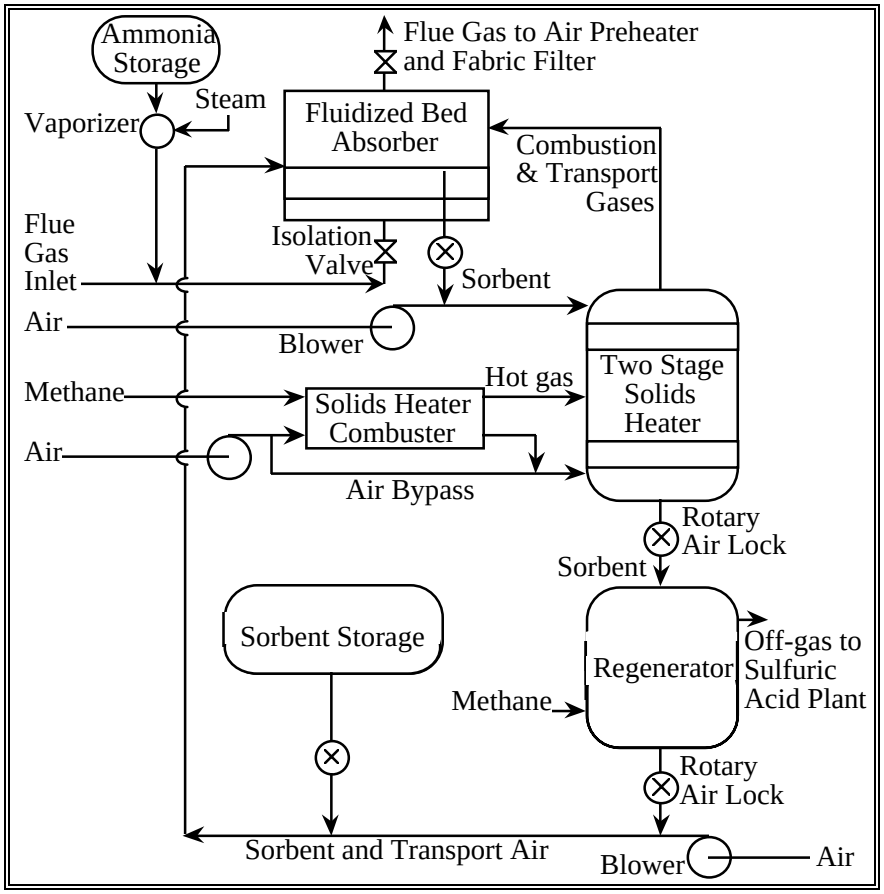

Figure 7-1 Schematic Diagram of the FETC Fluidized Bed Copper Oxide

The copper oxide sorbent circulates between an absorber and regenerator. A schematic of the process is shown in Figure 7-1. During the cycles, the sorbent composition undergoes changes due to chemical reactions occurring in both of these reactor vessels. In the absorber, copper oxide (CuO) reacts with sulfur oxides in the flue gas to form copper sulfate ($CuSO_4$). In a commercial-scale process, a bed of copper-impregnated sorbent, consisting of small diameter (e.g., 1/8 inch) alumina spheres, is fluidized by the power plant flue gas. In addition to sulfur dioxide removal, nitrogen oxides are also removed by reaction with ammonia injected into the inlet flue gas. The sulfated sorbent is transported to a solids heater, where the sorbent temperature is raised to achieve a reasonable regeneration residence time. The heated sorbent then flows by gravity to a regenerator reactor vessel. A portion of the copper sulfate is regenerated to copper oxide in the regenerator. The regenerated sorbent is then returned to the absorber.

The net chemical reactions occurring in the absorber are:

$$CuO_{(s)} + SO_{2(g)} + \tfrac{1}{2} O_{2(g)} \rightarrow CuSO_{4(s)} \qquad (7\text{-}1)$$

$$CuO_{(s)} + SO_{3(g)} \rightarrow CuSO_{4(s)}$$

$$4\,NO_{(g)} + 4\,NH_{3(g)} + O_{2(g)} \rightarrow 4\,N_{2(g)} + 6\,H_2O_{(g)}$$

$$2\,NO_{2(g)} + 4\,NH_{3(g)} + O_{2(g)} \rightarrow 3\,N_{2(g)} + 6\,H_2O_{(g)}$$

During sorbent regeneration, an offgas containing sulfur dioxide (SO_2) is evolved. In the regenerator, the sorbent flows downward in a moving bed, countercurrent to the regeneration off-gases. Copper oxide contained in the sorbent entering the regenerator may react rapidly with SO_2 in the exiting off-gas to form copper sulfite ($CuSO_3$) (Harriott and Markussen, 1992):

$$CuO_{(s)} + SO_{2(g)} \rightarrow CuSO_{3(s)} \qquad (7\text{-}2)$$

Thus, just inside the regenerator, the sorbent may consist of copper oxide, copper sulfite and copper sulfate. Some tests have also indicated the presence of compounds such as Cu_2O and Cu_2SO_3 within the regenerator (Harriott and Markussen, 1992). However, pending further studies to provide a design basis, these species are excluded from consideration in this model.

It is assumed that copper sulfite, copper sulfate, and copper oxide are regenerated to copper with efficiencies η_{r1}, η_{r2}, and η_{r3}, respectively. The regeneration reactions are:

$$CuSO_{4(s)} + \tfrac{1}{2}CH_{4(g)} \rightarrow Cu_{(s)} + SO_{2(g)} + \tfrac{1}{2}CO_{2(g)} + H_2O_{(g)} \qquad (7\text{-}3)$$

$$CuSO_{3(s)} + \tfrac{1}{4}CH_{4(g)} \rightarrow Cu_{(s)} + SO_{2(g)} + \tfrac{1}{4}CO_{2(g)} + \tfrac{1}{2}H_2O_{(g)} \qquad (7\text{-}4)$$

$$CuO_{(s)} + \tfrac{1}{4}CH_{4(g)} \rightarrow Cu_{(s)} + \tfrac{1}{4}CO_{2(g)} + \tfrac{1}{2}H_2O_{(g)} \qquad (7\text{-}5)$$

The regenerated copper is rapidly oxidized to copper oxide upon contact with oxygen in solids transport air or the flue gas:

$$Cu_{(s)} + \tfrac{1}{2}O_{2(g)} \rightarrow CuO_{(s)}$$

Similarly, any unregenerated copper sulfite is also assumed to completely oxidize to copper sulfate upon contact with oxygen:

$$CuSO_{3(s)} + \tfrac{1}{2}O_{2(g)} \rightarrow CuSO_{4(s)}$$

Thus, the sorbent entering the absorber is assumed to contain only copper oxide and copper sulfate.

The regeneration offgas is sent to a byproduct recovery plant. Here, it is assumed that elemental sulfur is recovered in a Claus plant. The Claus reaction is:

$$2\,H_2S_{(g)} + SO_{2(g)} \rightarrow 3\,S_{(l)} + 2\,H_2O_{(g)}$$

However, because the regeneration offgas contains no hydrogen sulfide, a portion of the SO_2 must be reduced with natural gas to produce the required quantity of hydrogen sulfide.

$$2\,CH_{4(g)} + 3\,SO_{2(g)} \rightarrow S_{(l)} + 2\,H_2S_{(g)} + 2\,CO_{2(g)} + 2\,H_2O_{(g)}$$

Thus, some elemental sulfur is obtained via the reducing reaction, while the remainder is obtained via the Claus reaction. The overall reaction is:

$$CH_{4(g)} + 2\,SO_{2(g)} \rightarrow 2\,S_{(l)} + 2\,H_2O_{(g)} + CO_{2(g)}$$

Thus, the overall required inlet molar flow rate of methane is one-half the molar flow rate of sulfur dioxide in the offgas. A portion of this requirement is met by unreacted methane contained in the regenerator offgas.

7.3. New Analytical Performance Models

New analytical models for the sorbent mass balance, the absorber sulfation reaction, regeneration, byproduct recovery, and energy penalties are derived and documented. These models supersede previous versions developed by Frey (1987).

7.3.1. Sorbent Mass Balance

To calculate the sorbent flow rate at the absorber inlet, a single equation that accounts for the key assumptions regarding process chemistry has been developed. This equation is based on a mass balance of copper, copper oxide, copper sulfite and copper sulfate. The basis for the sorbent mass balance per mole of SO_2 in the flue gas is given in Table 7-1. This approach can be extended to include other species (e.g., Cu_2O, Cu_2SO_4) if a design basis for the process chemistry can be characterized.

At the absorber inlet, the sorbent contains available copper (in the form of copper oxide) and an unknown molar amount of copper sulfate, which is residual unregenerated copper from the previous absorption/regeneration cycle. A portion of the copper oxide reacts with SO_2 in the flue gas to form additional copper sulfate. The available copper to sulfur molar ratio, R, is estimated using a kinetics model described in a later section.

As the sorbent enters the regenerator, a fraction of the copper oxide may react with SO_2, evolved in the lower regions of the regenerator, to form copper sulfite (based on Harriott and Markussen, 1992). The copper oxide, copper sulfite, and copper sulfate are regenerated to copper. Harriott and Markussen (1992) suggest that the regeneration efficiency for copper sulfite may be substantially lower than that for copper sulfate for a given regeneration residence time. Therefore, the regeneration efficiencies are parameterized for each species to permit investigation of the sensitivity of sorbent requirements to alternative assumptions regarding regenerator performance.

All of the species are assumed to be rapidly and completely oxidized after exiting the absorber and entering the solids transport system. Thus, all of the copper is assumed to be oxidized to copper oxide, and all of the copper sulfite is assumed to be oxidized to copper sulfate. The sorbent composition in the solids transport system is the same as that entering the absorber.

The mass balance is closed by solving for the unknown molar amount of copper sulfate entering the absorber per mole of SO_2. It can be shown that (see Table 7-1 on page 143 and Nomenclature on page 200):

$$R_{CuSO_4} = \frac{\eta_s(1-\eta_{r2}) + x_1(1-\eta_{r1})(R-\eta_s)}{\eta_{r2}}$$

This expression for R_{CuSO_4} also yields closure on the mass balance for CuO entering the absorber.

The molar flow rate of any copper species at any point in the process can be calculated by multiplying the absorber inlet molar flow of SO_2 by the appropriate coefficient in Table 7-1. For example, the molar flow rate of copper oxide at the absorber inlet is given by:

$$M_{CuO,A,i} = R \cdot M_{SO_x,A,i} \qquad (7\text{-}6)$$

where:

$$M_{SO_4,A,i} = M_{SO_2,A,i} + M_{SO_3,A,i}$$

The sorbent copper sulfate loading at the absorber entrance is given by:

$$M_{CuSO_4,A,i} = R_{CuSO_4} \cdot M_{SO_x,A,i} \qquad (7\text{-}7)$$

Note that the total molar amount of copper entering the absorber is greater than the available molar amount. The available copper to sulfur molar ratio is defined as R, and the total copper to sulfur molar ratio is given by:

$$R_{tot} = R + R_{CuSO_4}$$

A general formula is developed for calculating the sorbent mass flow as a function of the sorbent composition. Consider fresh sorbent, which contains copper only as copper oxide. The convention used in previous studies has been to define the sorbent composition based on the weight percent of copper, assuming that all of the copper is in the form of copper oxide. Therefore, the sorbent mass flow rate on an equivalent fresh sorbent basis is given by:

$$m_{s,\,fresh} = \left(\frac{MW_{Cu}}{W_{Cu}} \right) (M_{Cu} + M_{CuO} + M_{CuSO_3} + M_{CuSO_4})$$

However, in general, the sorbent may consist of other copper species as well. While the total molar amount of copper is not affected by the speciation, the mass flow is. Thus, factors must be included to account for the effect of different copper species on the sorbent mass flow rate. For example, for each mole of copper sulfate present in the sorbent, there is an incremental increase in sorbent mass flow rate due to the mass differential between a mole of copper oxide and a mole of copper sulfate. This difference must be calculated on a copper basis:

Table 7-1 ***Mass balance for sorbent in fluidized bed copper oxide process***

	Moles of Species Per mole of SO_2			
Location	Cu	CuO	$CuSO_3$	$CuSO_4$
Absorber Inlet	0	R	0	R_{CuSO4}
Absorber Outlet and Regenerator Inlet	0	$(R-\eta_s)$	0	$(R_{CuSO4}+\eta_s)$
Just Inside Regenerator	0	$(1-x_1)\ (R-\eta_s)$	$x_1\ (R-\eta_s)$	$(R_{CuSO4}+\eta_s)$
Regenerator Outlet	$\eta_{r3}\ (1-x_1)\ (R-\eta_s) + \eta_{r1}\ x_1\ (R-\eta_s) + \eta_{r2}\ (R_{CuSO4}+\eta_s)$	$(1-\eta_{r3})\ (1-x_1)$ • $(R-\eta_s)$	$(1-\eta_{r1})\ x_1\ (R-\eta_s)$	$(1-\eta_{r2})\ (R_{CuSO4}+\eta_s)$
Transport line and absorber inlet	0	$R = (1-x_1)\ (R-\eta_s) + \eta_{r1}\ x_1\ (R-\eta_s) + \eta_{r2}\ (R_{CuSO4}+\eta_s)$	0	$R_{CuSO4} = (1-\eta_{r1})\ x_1\ (R-\eta_s) + (1-\eta_{r2})$ • $(R_{CuSO4}+\eta_s)$

$$\Delta MW_{CuSO_4} = \frac{MW_{CuSO_4} - MW_{CuO}}{MW_{Cu}} = \frac{159.54 - 79.54}{63.54} = 1.26$$

The total effect of the weight difference is proportional to the weight fraction of copper as copper oxide in the sorbent. Thus, for a sorbent containing copper oxide and copper sulfate, the mass flow rate is given by:

$$m_s = \left(\frac{MW_{Cu}}{W_{Cu}}\right)\left\{M_{CuO} + (1 + 1.26W_{Cu})M_{CuSO_4}\right\}$$

This formulation is easily extended to account for other species, such as copper and copper sulfite. The general equation is therefore:

$$m_s = \left(\frac{MW_{Cu}}{W_{Cu}}\right)\left\{\begin{matrix}(1-0.252W_{Cu})M_{Cu} + M_{CuO} + (1+1.007W_{Cu})M_{CuSO_3} \\ + (1+1.26W_{Cu})M_{CuSO_4}\end{matrix}\right\} \qquad (7\text{-}8)$$

For example, the absorber inlet sorbent mass flow rate on a lb/hr basis can be calculated as:

$$m_{s,A,i} = \left(\frac{MW_{Cu}}{W_{Cu}}\right)\left\{R + (1+1.260W_{Cu})R_{CuSO_4}\right\} \cdot M_{SO_x,A,i}$$

The sorbent composition and mass flow at the absorber exit is given by:

$$M_{CuO,A,o} = (R - \eta_s) \cdot M_{SO_x,A,i} \qquad (7\text{-}9)$$

$$M_{CuSO_4,A,o} = (R_{CuSO_4} + \eta_s) \cdot M_{SO_x,A,i} \qquad (7\text{-}10)$$

$$m_{s,A,o} = \left(\frac{MW_{Cu}}{W_{Cu}}\right)\left\{(R-\eta_s) + (1+1.260W_{Cu})(R_{CuSO_4}+\eta_s)\right\}\cdot M_{SO_x,A,i} \quad (7\text{-}11)$$

The absorber exit sorbent composition is the same as that of the solids heater inlet and outlet and of the regenerator inlet. It is assumed that no chemical reactions occur in the solids heater.

Just inside the regenerator, a portion of the copper oxide may react with sulfur dioxide in the regenerator off-gas to form copper sulfite. Thus, at the regenerator outlet the sorbent may contain copper, copper oxide, copper sulfite, and copper sulfate. The molar flow rates of each of these four species are:

$$M_{Cu,R,o} = \left\{\begin{matrix}[\eta_{r3}(1-x_1)+\eta_{r1}x_1](R-\eta_s) \\ +\eta_{r2}(R_{CuSO_4}+\eta_s)\end{matrix}\right\}\cdot M_{SO_x,A,i} \quad (7\text{-}12)$$

$$M_{CuO,R,o} = [(1-x_1)(1-\eta_{r3})(R-\eta_s)]\cdot M_{SO_x,A,i} \quad (7\text{-}13)$$

$$M_{CuSO_3,R,o} = [x_1(1-\eta_{r1})(R-\eta_s)]\cdot M_{SO_x,A,i} \quad (7\text{-}14)$$

$$M_{CuSO_4,R,o} = \{(1=\eta_{r2})(R_{CuSO_4}+\eta_s)\}\cdot M_{SO_x,A,i} \quad (7\text{-}15)$$

The sorbent mass flow can be calculated by substituting Equation (7-12) for M_{Cu}, Equation (7-13) for M_{CuO}, Equation (7-14) for M_{CuSO_3}, and Equation (7-15) for M_{CuSO_4} into Equation (7-8). It is assumed that any copper and copper sulfite in the sorbent will react completely upon contact with oxygen in the sorbent transport system to form copper oxide and copper sulfate, respectively. Therefore, the sorbent composition entering the absorber is given by Equations (7-6) and (7-7).

The molar flow rate of the alumina oxide substrate is the same at all points in the absorption/regeneration cycle. As a convenience, this flow is calculated based on the absorber inlet sorbent mass flow:

$$M_{Al_2O_3} = \left(\frac{MW_{Cu}}{W_{Cu}} - MW_{CuO}\right)\left(\frac{1}{MW_{Al_2O_3}}\right)R_{tot}\cdot M_{SO_x,A,in}$$

Sulfation Reaction Model

Yeh et al. (1987) developed a kinetic model of the sulfation reaction, shown in Equation (7-1). Their model assumed plug flow of both the flue gas and the solids. This model had been employed in a previous version of the copper oxide process performance model (Frey and Rubin, 1991; Rubin *et al.*, 1991). Harriott (1992a) has developed a kinetic model for the sulfation reaction assuming that the solids in the fluidized bed are perfectly mixed. Harriott's model is:

$$\ln\left(\frac{y_o}{y_i}\right) = -\alpha\,\mathrm{R}\,y_i + \alpha\,(\mathrm{y_i} - y_o)$$

where:

$$\alpha = \frac{k_s\,P\,\rho_s\,\mathrm{Z\,A}}{\mathrm{F_s}}$$

The SO_2 removal efficiency is defined as:

$$\eta_s = \frac{y_i - y_o}{y_i}$$

Therefore, we may rewrite the sulfation model as:

$$R = \eta_s - \frac{\ln(1-\eta_s)}{\alpha\, y_i} \qquad (7\text{-}16)$$

The quantity (ρ_S Z A) in the kinetic parameter α is the sorbent bed inventory in the absorber. We note that the sorbent residence time is calculated based on the bed inventory and the feed rate:

$$t_{r,a} = \frac{\rho_s\, Z\, A}{F_s}$$

Thus, the term α is:

$$\alpha = k_s\, P\, t_{r,a}$$

The reaction rate constant, corrected for the sorbent copper loading, is given by (Yeh, 1992):

$$k_s = 1{,}573 \exp(-14.23\, W_{Cu}) \exp\left(-\frac{2{,}417.6}{T}\right) \qquad (7\text{-}17)$$

Test data reported by Yeh, Drummond, and Joubert (1987) were used with Harriott's sulfation model to estimate the available Cu/S ratio and to compare with experimental results. Table 7-2 shows the key process parameters measured during testing, including the available copper to sulfur molar ratio, R. The inlet SO_2 concentration is reported on a total gas flow basis, including moisture. These values were estimated from the dry SO_2 concentrations reported by Yeh et al and from the reported flue gas moisture content of approximately 7.5 percent. Estimates by Frey and Rubin (1991) of the molar ratio R based on test data using a reaction model developed by Yeh et al. (1987) are reported. Similarly, estimates of the Cu/S molar ratio based on the Harriott sulfation model are also reported.

As an example of the calculations, consider Test No. 1. The sorbent residence time is:

$$t_{r,a} = \frac{\rho_s\, Z\, A}{F_s} = \frac{I_b}{F_s} = \frac{614\,\text{kg}}{\left(372\,\frac{\text{kg}}{\text{hr}}\right)\left(\frac{hr}{60\,\text{min}}\right)} = 99.0\,\text{min}$$

The reaction rate constant is:

$$k_s = 1{,}573 \exp(-14.23\{0.051\}) \exp\left(-\frac{2{,}417.6}{723\,\text{K}}\right) = 26.87\,\frac{1}{atm\cdot\text{min}}$$

The kinetic parameter α is:

$$\alpha = k_s\, P\, t_{r,a} = \left(26.87\,\frac{1}{atm\cdot\text{min}}\right)(1\,\text{atm})(99.0\,\text{min}) = 2{,}661$$

The resulting copper-to-sulfur molar ratio is:

$$R = \eta_s - \frac{\ln(1-\eta_s)}{\alpha\, y_i} = 0.79 - \frac{\ln(1-0.79)}{2{,}661(2.109x10^{-3})} = 1.07$$

Figure 7-2 shows a comparison of the Cu/S ratio estimated using the FETC model versus experimental results. Figure 7-3 shows a similar comparison using the Harriott model.

The comparison of the Harriott and FETC sulfation models with experimental data indicates that Harriott's model provides generally better estimates of the Cu/S ratio than the FETC model. Although both models yield estimates typically within ± 10 percent of the experimentally measured values, the estimates from Harriott's model tend to be less scattered from the parity line. Harriott's model appears to be somewhat conservative in predicting Cu/S ratios slightly higher than the experimentally measured results. The model results diverge most noticeable for the high Cu/S ratios, which represents testing with low (18-inch) fluidized bed heights. Such bed heights are unlikely for commercial scale designs, and the experimental results themselves are considered less certain than the ones reported for higher bed heights. Therefore, Harriott's model is employed here.

Table 7-2 ***Comparison of Alternative Sulfation Models.***

1	0.79	2,109	450	5.1	372	614	0.99	0.95	1.07
2	0.71	2,109	460	5.1	290	614	0.78	0.78	0.87
3	0.90	2,177	400	5.1	669	636	1.57	1.74	1.78
4	0.91	2,479	400	5.1	854	641	1.80	1.75	1.94
5	0.70	2,479	465	5.1	351	638	0.80	0.78	0.85
6	0.81	2,479	400	5.1	423	638	0.96	1.10	1.16
7	0.91	2,868	405	5.1	1,053	696	1.71	1.89	1.89
8	0.90	1,943	420	5.1	762	585	1.86	1.75	2.01
9	0.67	2,174	480	5.1	154	523	0.65	0.67	0.75
10	0.91	2,118	425	5.1	453	469	2.00	1.15	1.68
11	0.70	2,729	425	5.1	479	491	0.89	0.95	1.00
12	0.82	2,729	415	5.1	668	491	1.27	1.44	1.45
13	0.91	2,313	400	5.1	1,352	505	2.76	2.47	3.13
14	0.88	2,220	350	5.1	1,111	472	2.70	2.65	3.26
15	0.89	2,081	390	5.1	1,127	448	2.93	2.37	3.13
16	0.90	2,174	390	5.1	1,177	446	3.27	2.08	3.25
17	0.95	1,989	415	7.0	311	376	1.99	1.92	2.15
18	0.93	1,758	425	7.0	375	399	2.03	2.24	2.23
19	0.90	1,943	440	7.0	412	422	1.60	1.91	1.89
20	0.70	2,165	465	5.1	488	195	1.11	2.40	1.51
21	0.78	2,035	455	5.1	839	241	1.96	2.06	2.35
22	0.84	1,989	455	5.1	859	208	2.30	3.13	3.15

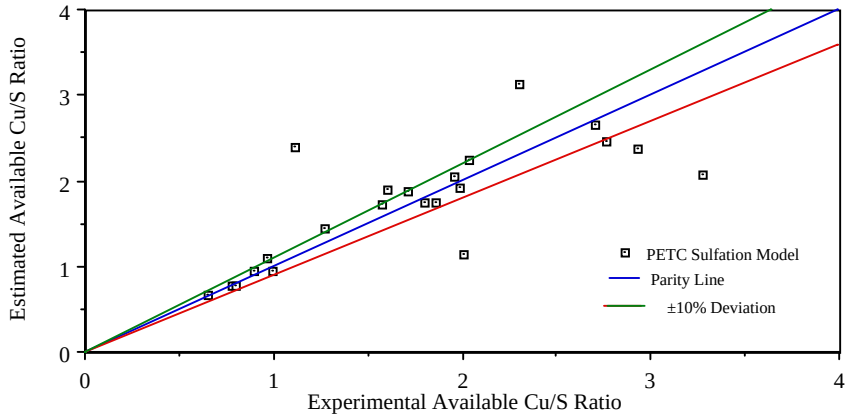

Figure 7-2 Comparison of copper-to-sulfur molar ratios from experimental results and from the FETC sulfation model.

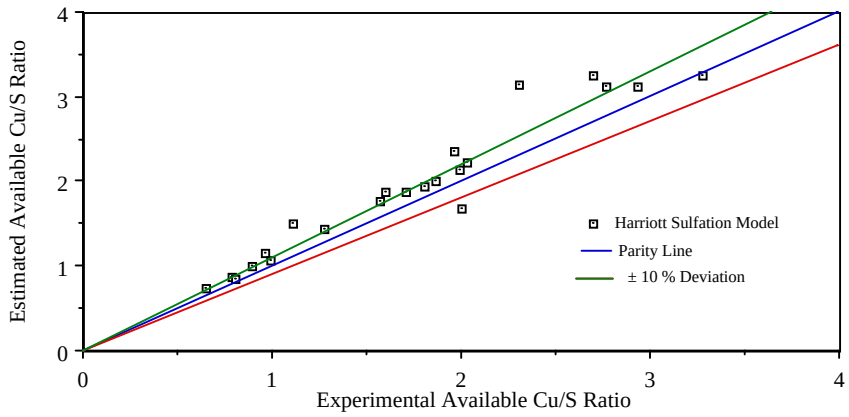

Figure 7-3 Comparison of copper-to-sulfur molar ratios from experimental results and from the Harriott sulfation model.

As a prerequisite to estimating the sorbent bed inventory, the absorber bed area is calculated based on the flue gas volumetric flow rate and the reactor bed gas superficial velocity:

$$A = \left(\frac{G_{FG}}{60\ V_s} \right)$$

The sorbent bed inventory and the sorbent feed rate should both be calculated on a consistent basis (e.g., fresh sorbent, or actual sorbent) to estimate the sorbent residence time. The simpler case is to base the calculations on equivalent fresh sorbent, in terms of mass flow and inventory. A calculation based on actual composition would yield the same ratio of bed inventory to feed rate, as both estimates would increase by the same proportion (assuming that the fluidized bed density increases proportionally for a given superficial velocity and bed height). Thus, the sorbent feed rate to be used in the sulfation model is:

$$F_s = \left(\frac{MW_{Cu}}{W_{Cu}} \right) \left\{ R + \left[\frac{\eta_s (1-\eta_{r2}) + x_1 (1-\eta_{r1})(R-\eta_s)}{\eta_{r2}} \right] \right\} \cdot \left(\frac{M_{SO_x,A,i}}{60\ \text{min/hr}} \right) \quad (7\text{-}18)$$

If this equation is used to estimate the sorbent feed rate, than the sorbent density used to estimate the sorbent bed inventory should be based on the expanded bed density for fresh sorbent. An expanded sorbent density (ρ_S) of 26.6 lb/ft^3 is used for this purpose. This density is valid for a four foot bed height with a superficial gas velocity of approximately 4.2 ft/sec.

Equation (7-18) is a function of the copper-to-sulfur molar ratio. In order to develop an explicit equation for R, it is necessary to rewrite Equation (7-18) as:

$$F_s = a + b \cdot R$$

where:

$$a = \left(\frac{MW_{Cu}}{W_{Cu}} \right) \left(\frac{M_{SO_x,A,i}}{60\ \frac{\text{min}}{hr}} \right) \left[\frac{\eta_s (1-\eta_{r2}) - x_1\ \eta_s (1-\eta_{r1})}{\eta_{r2}} \right] \quad (7\text{-}19)$$

$$b = \left(\frac{MW_{Cu}}{W_{Cu}} \right) \left(\frac{M_{SO_x,A,i}}{60 \frac{\text{min}}{hr}} \right) \left[\frac{\eta_{r2} + x_1(1-\eta_{r1})}{\eta_{r2}} \right] \qquad (7\text{-}20)$$

We also define the following quantities:

$$\hat{\alpha} = k_s \; \text{P} \; \rho_s \; \text{Z} \; \text{A} \qquad (7\text{-}21)$$

$$\beta = \frac{\ln(1-\eta_s)}{\hat{\alpha} \; \text{y}_\text{i}} \qquad (7\text{-}22)$$

The sulfation model in Equation (7-16) is then rewritten in terms of the quantities in Equations (7-19), (7-20), (7-21), and (7-22):

$$R = \frac{\eta_s - a \; \beta}{1 + \text{b} \; \beta} \qquad (7\text{-}23)$$

The sensitivity of the model to regeneration efficiency and fluidized bed height is illustrated in Figure 7-4, for the same conditions as given in the last example above. The figure indicates that for poor regeneration efficiencies, the required available Cu/S ratio can become excessive. For example, for a 48 inch bed height and a 50 percent regeneration efficiency, an available Cu/S ratio of 4.15 is required for 90 percent SO_2 capture. This available Cu/S ratio corresponds to a total Cu/S ratio of 8.3. However, for regeneration efficiencies greater than 80 percent, there is relatively little change in the required Cu/S ratio. For a 48 inch bed height, the Cu/S ratio decreases from 1.76 to 1.59 as the regeneration efficiency increases from 80 to 90 percent.

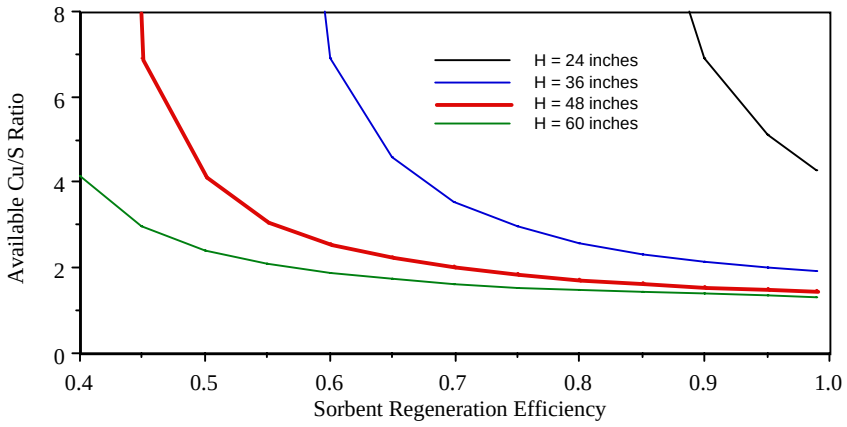

Figure 7-4 Sensitivity of Cu/S Ratio to regeneration efficiency and fluidized bed height.

7.3.2. Two-Stage Absorber Model

A promising alternative to the single-stage fluidized bed design described above is a design featuring two fluidized beds in series. A schematic of the two-stage fluidized bed absorber is shown in Figure 7-5. In the two-stage design, regenerated sorbent enters a first stage fluidized bed, where the sorbent reacts with flue gas which has already passed through a second stage sorbent bed. The partially sulfated sorbent from the first bed then goes to a second bed, where it contacts inlet flue gas. Each of the two beds can have different bed heights and sulfur capture efficiencies. The overall sulfur removal efficiency is given by:

$$\eta_s = \eta_{s2} + \eta_{s1}(1-\eta_{s2})$$

For each of the two beds, the general models given in Equation (7-16) and (7-23) apply. For the first stage, the sulfation model is:

$$R = \frac{\eta_{s1}(1-\eta_{s2}) - a\,\beta_1}{1 + b\,\beta_1} \qquad (7\text{-}24)$$

where

$$\beta_1 = \frac{\ln(1-\eta_{s1})}{k_s(T_1)\,\mathrm{P}\,\rho_s\,\mathrm{Z}_1\,\mathrm{A}\,\mathrm{y_i}}$$

and the subscripts for temperature, sulfur removal efficiency, and bed height refer to the first stage absorber bed. For the second stage, the sulfation model is:

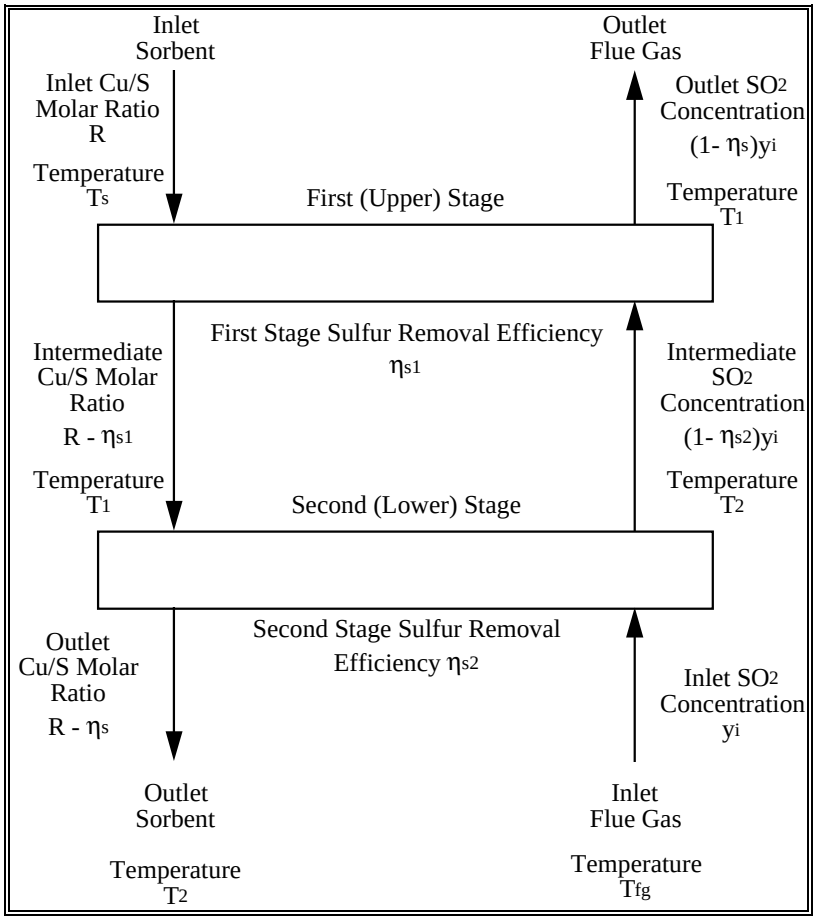

Figure 7-5 Simplified Schematic of a Two-Stage Fluidized Bed Absorber Model.

$$R = \frac{\eta_s - a\,\beta_2}{1 + \mathrm{b}\,\beta_2} \qquad (7\text{-}25)$$

where:

$$\beta_1 = \frac{1n(1-\eta_{s2})}{k_s(T_2)\,\mathrm{P}\,\rho_s\,\mathrm{Z}_2\,\mathrm{A}\,\mathrm{y_i}}$$

Typically, the desired overall sulfur removal efficiency is known. If the removal efficiency and bed height for one of the beds are specified, then the values for the other bed can be calculated.

Thus, the calculation procedure in the two-stage model is to specify an overall sulfur capture efficiency, a second stage fluidized bed height, and a second stage sulfur capture efficiency. The first stage capture efficiency is given by:

$$\eta_{s1} = \frac{\eta_s - \eta_{s2}}{1-\eta_{s2}}$$

The first stage bed height is given by:

$$Z_1 = \left(\frac{a + b\,\mathrm{R}}{\eta_{s1}(1-\eta_{s2}) - R}\right)\left\{\frac{\ln(1-\eta_{s1})}{k_s\,(T_1)\,P\,\rho_s\,\mathrm{A}\,\mathrm{y_i}}\right\}$$

In the limiting case in which the second stage capture efficiency is the same as the overall capture efficiency, the first stage capture efficiency and bed height go to zero. Thus, the two-stage model can reduce to the special case of a single stage model.

An additional consideration in the two-stage model is the need to estimate the bed temperatures for both stages. To estimate the bed temperature requires developing a mass balance for the sorbent and flue gas in each stage. The energy balance is a function of the sorbent mass flow rate, which depends on R. Therefore, it is necessary to iterate on solutions for R obtained from the kinetic-based models in Equations (7-24) and (7-25) and on solutions for the bed temperatures, which in turn affect the sulfation reaction rates. Such energy balance equations have been included in the computerized version of the two-stage absorber model.

The simplified energy balance for Stage 1 and Stage 2 of the absorber are given by:

$$m_s c_{p,s}(T_1 - T_s) + m_{fg} c_{p,fg}(T_1 - T_2) + \Delta H_{r,1} = 0 \qquad (7\text{-}26)$$

$$m_s c_{p,s}(T_2 - T_1) + m_{fg} c_{p,fg}(T_2 - T_{fg}) + \Delta H_{r,2} = 0 \qquad (7\text{-}27)$$

Assuming that the mass flow rates of flue gas and sorbent are approximately constant through the two stages of the absorber, and that the specific heats of both flue gas and sorbent are also approximately constant over the temperatures in the absorber inlet and outlet, Equations (7-26) and (7-27) can be solved for the first and second stage bed temperatures T_1 and T_2, respectively:

$$T_1 = T_2 + \frac{m_{fg} c_{p,fg}(T_2 - T_{fg}) + \Delta H_{r,2}}{m_s c_{p,s}} \qquad (7\text{-}28)$$

$$T_2 = \frac{(m_s c_{p,s} + m_{fg} c_{p,fg})(m_{fg} c_{p,fg} T_{fg} - \Delta H_{r,2}) + m_s c_{p,s}(m_s c_{p,s} T_s - \Delta H_{r,1})}{(m_s c_{p,s} + m_{fg} c_{p,fg})^2 - (m_s c_{p,s})(m_{fg} c_{p,fg})} \qquad (7\text{-}29)$$

The heats of reaction for each stage are based on the desulfurization and deNO_x reactions. For simplicity, it is assumed that all NO_x reduction reactions occur in the second (lower) stage. In the special case where there is only a single stage absorber, the energy balance of Equations (7-28) and (7-29) are not valid. The temperature

of the single fluidized bed may be estimated with the following model, assuming that the outlet sorbent and flue gas temperature is represented by T_2:

$$T_2 = \frac{m_s c_{p,s} T_s + m_{fg} c_{p,fg} T_{fg} - \Delta H_{r,total}}{m_s c_{p,s} + m_{fg} c_{p,fg}}$$

The two-stage absorber design offers an advantage over a single stage design in terms of reduced copper-to-sulfur ratio requirements for a given total sorbent inventory in the absorber vessel. An illustration of this is given in Figure 7-6. The available copper-to-sulfur molar ratio is shown with respect to the first stage sulfur removal efficiency. The total sulfur removal efficiency, and the total sorbent inventory in both stages of the absorber, are held constant at 90 percent and 829,500 lb, respectively. At a first stage removal efficiency of zero, only a single-stage absorber exists. The available Cu/S ratio for this base case is 1.59. As shown in Figure 7-7, all of the sorbent is allocated into a single absorber stage. When a second stage is added to the absorber design, the sulfur removal burden may be allocated between the two stages. As the sulfur removal efficiency in the first (upper) stage of the absorber increases, the sulfur removal efficiency in the second (lower) stage decreases. The portion of the total sorbent inventory allocated to the first stage increases non-linearly with first stage sulfur removal efficiency, as shown in Figure 7-7. The available Cu/S ratio reaches a minimum value of 1.23 at a first stage removal efficiency of approximately 83 percent, which corresponds to a second stage removal efficiency of approximately 40 percent. This represents a reduction in sorbent circulation rate of approximately 23 percent, while holding total sorbent bed inventory constant. These results clearly illustrate that a two stage design can yield substantial economic benefits compared to a single stage design.

If the total sorbent inventory in the absorber is allowed to increase, the sorbent circulation rate can be reduced further. For example, if we fix the second (lower) stage bed height at 48 inches, and the total sulfur removal efficiency at 90 percent, then the first stage bed height will vary as the removal efficiency of the second stage varies. An example of this analysis is shown in Figure 7-8. Again, the model reduces to the base case single stage absorber design when the sulfur removal efficiency of the second stage is set at 90 percent: the first stage bed height is zero and the available Cu/S ratio is 1.59. As the second stage removal efficiency is reduced, then sorbent must be added to the first stage bed to achieve the required overall sulfur removal efficiency. As more sorbent is added to the first stage, the total sorbent inventory increases, but the sorbent circulation decreases. For example, at a second stage removal efficiency of 29.4 percent, the required first stage bed height is 48 inches and the available Cu/S ratio is 0.98, a 38 percent reduction from the base case. However, the sorbent bed inventory is increased by 100 percent. (By contrast, if the same bed inventory were contained in a single 96 inch bed, the required available Cu/S ratio would be 1.16). The trade-offs between reduced sorbent circulation rate and increased bed inventory must be evaluated based on process economics.

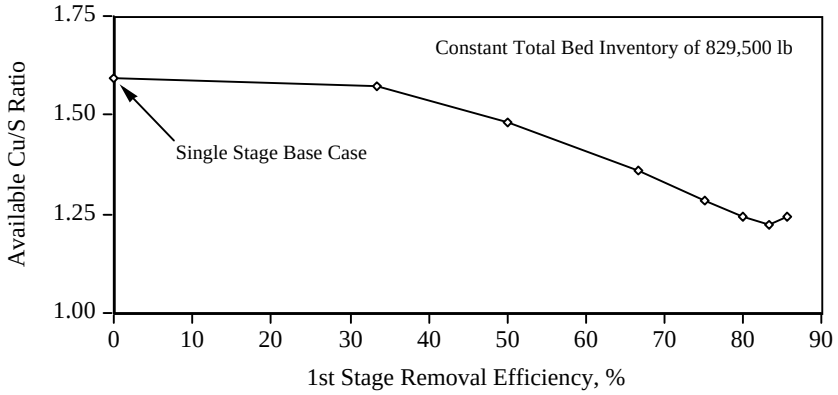

Figure 7-6 Sensitivity of the Cu/S Ratio to Distribution of Sorbent in Two Fluidized Beds

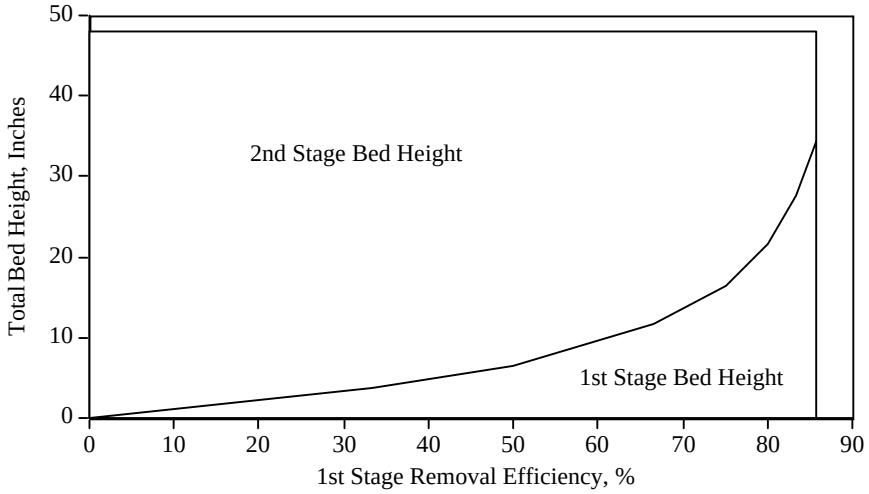

Figure 7-7 Distribution of Sorbent Between Two Absorber Stages with Constant Total Sorbent Inventory

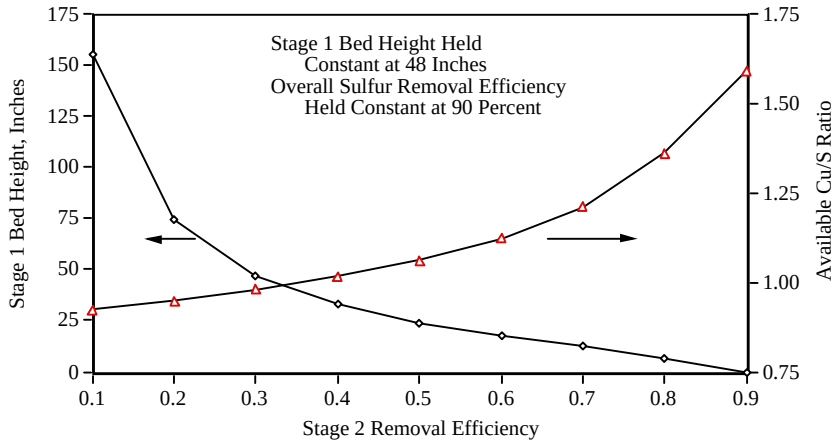

Figure 7-8 Sensitivity Analysis of the Two-Stage Absorber Model

7.3.3. Regeneration Performance Model

The key chemical equations governing the performance of the regenerator are given by Equations (7-2) to (7-5). The regenerator mass and energy balance for the copper oxide model developed by Frey (1987) is revised here based on the need to account for the potential formation of copper sulfite in the regenerator (Harriott, 1992c; Harriott and Markussen, 1992). Furthermore, a kinetic model developed by Harriott is used to estimate regenerator residence time associated with regeneration of copper sulfate.

7.3.3.1. Regenerator Mass Balance

The mass balance for sorbent in the regenerator is given by Equations (7-9) to (7-15). At the regenerator inlet, the molar fraction of total copper in the sorbent which is in the form of copper sulfate is given by:

$$x_{CuSO_4} = \frac{(R_{CuSO_4} + \eta_s)}{R_{tot}}$$

The mass balance for gaseous species in the regenerator includes methane at the regenerator inlet, and regeneration off-gas containing methane, sulfur dioxide, carbon dioxide, and water vapor.

The total amount of methane required for regeneration is estimated per Harriott (1992c) based on the minimum requirement for 100 percent regeneration and a multiplier for excess methane. For each mole of copper sulfate, one-half mole of methane is required, and for each mole of copper oxide or copper sulfite, one-quarter mole of methane is required, as indicated by equations (7-4) and (7-5). Thus, the total methane requirement is:

$$M_{CH_4,R,i} = R_{CH_4}[0.5x_{CuSO_4} + 0.25(1 - x_{CuSO_4})]R_{tot}\ M_{SO_x}$$

The amount of sulfur dioxide produced depends on the fraction of copper oxide converted to copper sulfite and the actual regeneration efficiencies for copper sulfite and copper sulfate. Sulfur dioxide is consumed by the conversion of copper oxide to copper sulfite, while it is produced by the regeneration of both copper sulfite and copper sulfate. The net production of sulfur dioxide is given by:

$$M_{SO_2,R,o} = [\eta_{r2} x_{CuSO_4} + (\eta_{r1} - 1)x_1(1 - x_{CuSO_4})]\,\mathrm{R_{tot}}\ \mathrm{M_{SO_x}} \qquad (7\text{-}30)$$

Water vapor is produced in all three of the assumed regeneration reactions. Thus, the total amount of water vapor produced is:

$$M_{H_2O,R,o} = \{\eta_{r2} \times_{\mathrm{CuSO_4}} + 0.5(1 - x_{CuSO_4}) \times [\eta_{r1} x_1 + \eta_{r3}(1 - x_1)]\} \times \mathrm{R_{tot}}\ \mathrm{M_{SO_x}} \qquad (7\text{-}31)$$

For each mole of water vapor produced, one-half mole of carbon dioxide is produced as shown in Equations (7-3), (7-4) and (7-5). Therefore, the total molar amount of carbon dioxide produced is:

$$M_{CO_2,R,o} = 0.5\,\mathrm{M}_{H_2O,R,o} \qquad (7\text{-}32)$$

The molar amount of methane consumed in the regenerator is the same as the molar amount of carbon dioxide produced. Therefore, the net amount of methane exiting the regenerator is given by:

$$M_{CH_4,R,o} = M_{CH_4,R,i} - M_{CO_2,R,o}$$

7.3.3.2. Regenerator Energy Balance

The regenerator energy balance is calculated based on the sorbent and gas mass balance given above, and the energy released or absorbed by the chemical reactions occurring in the regenerator. A total of four chemical reactions are assumed to occur within the regenerator and each has an associated heat of reaction.

For the reaction of copper oxide to form copper sulfite (Equation (7-2)), a heat of reaction cannot be calculated based on heats of formation because thermodynamic data for copper sulfite are not available in the standard reference literature (e.g., Barin and Knacke, 1973; Barin, I., O. Knacke, and O. Kubaschewski, 1977; Chase et al., 1985). Harriott (1992c) estimated a heat of reaction based on data for SO_2 oxidation and $CuSO_4$ formation. The estimated heat of reaction is ΔH_1 = -93,240 Btu/lbmole CuO.

Heats of reaction for the regeneration of copper sulfate and copper oxide (Equations (7-3) and (7-5), respectively) were estimated by Frey (1987) and are ΔH_2 = 30,700 Btu/lbmole $CuSO_4$ and ΔH_3 = -19,380 Btu/lbmole CuO, respectively. The heat of reaction for the regeneration of copper sulfite was estimated based on the heats of reaction for the regeneration of copper oxide and the conversion of copper oxide to copper sulfite:

$$CuO_{(s)} + SO_{2\,(g)} \rightarrow CuSO_{3\,(s)} \qquad \Delta H_1 = -93{,}240 \text{ Btu/lbmole CuO}$$

$$CuSO_{3\,(s)} + \frac{1}{4} CH_{4\,(g)} \rightarrow Cu_{(s)} + SO_{2\,(g)} + \frac{1}{4} CO_{2\,(g)} + \frac{1}{2} H_2O_{(g)} \qquad \Delta H_4 = ?$$

$$CuO_{(s)} + \frac{1}{4} CH_{4\,(g)} \rightarrow Cu_{(s)} + \frac{1}{4} CO_{2\,(g)} + \frac{1}{2} H_2O_{(g)} \qquad \Delta H_3 = \Delta H_1 + \Delta H_4$$

Thus:

$$\Delta H_4 = \Delta H_3 - \Delta H_1 = 73{,}680 \text{ Btu/lbmole } CuSO_4$$

The total heat of reaction for all chemical reactions in the regenerator is given by:

$$\Delta H_{r,tot} = x_1(1 - x_{CuSO_4})\Delta H_1 + \eta_{r2} x_{CuSO_4} \Delta H_2$$

$$+ \eta_3 (1 - x_1)(1 - x_{CuSO_4})\Delta H_3 + \eta_{r1}\, x_1 (1 - x_{CuSO_4})\Delta H_4$$

The total molar flow of solids entering the regenerator is:

$$M_{s,R,i} = M_{Cu,R,i} + M_{CuO,R,i} + M_{CuSO_3,R,i} + M_{CuSO_4,R,i} + M_{Al_2O_3,R,i}$$

The solids enter at a specified temperature $T_{R,i}$, which is the same as the solids heater outlet temperature. The enthalpy of the solids entering the regenerator is given by:

$$\hat{h}_s(T_{R,i}) = \frac{\sum_{j=Cu,CuO,CuSO_3,CuSO_4,Al_2O_3} M_{j,R,i} \quad \hat{h}_j(T_{R,i})}{\sum_{j=Cu,CuO,CuSO_3,CuSO_4,Al_2O_3} M_{j,R,i}}$$

The total molar flow and enthalpy of the solids at the regenerator outlet are similarly calculated.

Because thermodynamic data for copper sulfite are not available, the enthalpy of copper sulfite is estimated based on a multiplier and the enthalpy of copper sulfate:

$$\hat{h}_{CuSO_3}(T) = r_{\hat{h}}\,\hat{h}_{CuSO_4}(T)$$

The value of the multiplier is estimated to be between 0.7 and 0.9, based on comparison of the specific heats of copper oxide, copper sulfate, sulfur dioxide, and oxygen at a temperature of 500°C. The lower bound is based on comparing the specific heats of copper oxide and sulfur dioxide to the specific heat of copper sulfate, while the upper number is based on comparing the specific heat of copper sulfate minus oxygen to copper sulfate. A most likely value is assumed to be 0.8. This parameter can be treated as a probability distribution in the IECM pending development of thermodynamic data for copper sulfite.

The only inlet gas is methane, which enters at a temperature of $T_{CH_4,R,i}$. The total molar flow of the off-gases is:

$$M_{OG,R,o} = M_{SO_2,R,o} + M_{H_2O,R,o} + M_{CO_2,R,o} + M_{CH_4,R,o}$$

The off-gas is assumed to exit at the same temperature as the solids inlet. Therefore, the average enthalpy of the off-gas is given by:

$$h_{OG}(T_{R,i}) = \frac{\sum_{j=SO_2,H_2O,CO_2,CH_4} M_{j,R,o}\,\mathrm{h_j}(T_{R,i})}{\sum_{j=SO_2,H_2O,CO_2,CH_4} M_{j,R,o}}$$

The only unknown to be calculated in the energy balance is the temperature of the sorbent leaving the regenerator. The energy balance is given by:

$$M_{s,R,o}\,\hat{\mathrm{h}}_{\mathrm{s}}(T_{s,R,o}) + M_{OG,R,o}\,\hat{\mathrm{h}}_{\mathrm{OG}}(T_{R,i})$$

$$+ \Delta H_{r,tot} = M_{s,R,i}\,\hat{\mathrm{h}}_{\mathrm{s}}(T_{R,i}) + M_{CH_4,R,i}\,\hat{\mathrm{h}}_{\mathrm{CH_4}}(T_{CH_4,R,i})$$

To facilitate an explicit equation for the sorbent outlet temperature, the term for the outlet sorbent molar flow and enthalpy can be rewritten as:

$$M_{s,R,o}\,\hat{\mathrm{h}}_{\mathrm{s}}(T_{s,R,o}) = M_{s,R,o}\left[\hat{h}_{\mathrm{s}}(T_{R,i}) + c_{p,s}(T_{s,R,o} - T_{R,i})\right]$$

Thus, the temperature of the sorbent exiting the regenerator is given by:

$$T_{s,r,o} = T_{R,i} + \frac{\begin{bmatrix} M_{s,R,i}\,\hat{\mathrm{h}}_{\mathrm{s}}(T_{R,i}) + M_{CH_4,R,i}\,\hat{\mathrm{h}}_{\mathrm{CH_4}}(T_{CH_4,R,i}) \\ - M_{S,R,o}\,\hat{\mathrm{h}}_{\mathrm{s}}(\mathrm{T_{R,i}}) - M_{OG,R,o}\,\hat{\mathrm{h}}_{OG}(T_{R,i}) - \Delta H_{r,tot} \end{bmatrix}}{M_{s,R,o}\,\mathrm{c_{p,s}}}$$

Regenerator Residence Time

A kinetic model developed by Harriott and Markussen (1992) and Harriott (1992c) is used to estimate the residence time for the regeneration of copper sulfate. This model requires the development of a temperature profile within the regenerator. A schematic of this model is shown in Figure 7-9.

At a point "just inside" the regenerator, it is assumed that copper oxide has reacted to form copper sulfite. Thus, a mass and energy balance is developed for the uppermost

portion of the regenerator in which this reaction occurs. The molar sorbent composition after the formation of copper sulfite is given by:

$$M_{CuO_3,R,JI} = (1-x_1)(R-\eta_s)\cdot M_{SO_x,A,i}$$

$$M_{CuSO_3,R,JI} = x_1(R-\eta_s)\cdot M_{SO_x,A,i}$$

$$M_{CuSO_4,R,JI} = (R+\eta_s)\cdot M_{SO_x,A,i}$$

The molar gas composition just inside the regenerator is the same as that at the regenerator outlet, with the exception of the SO_2 component due to the absorption of SO_2 in the formation of copper sulfite. Therefore, the SO_2 molar flow rate just inside the regenerator is given by:

$$M_{SO_2,R,JI} = [\eta_{r2}\ \mathrm{x}_{CuSO_4} + \eta_{r1}\ \mathrm{x}_1\ (1-\mathrm{x}_{CuSO_4})]\ \mathrm{R}_{tot}\ \mathrm{M}_{SO_x,A,i}$$

with the molar flow rates of the other species the same as given by Equations (7-30), (7-31), and (7-32).

The temperatures of the sorbent and the regeneration gases are assumed to be the same just inside the regenerator. Therefore, the temperature just inside the regenerator is:

$$T_{R,JI} = T_{R,i} + \frac{\left[\begin{array}{l} M_{OG,R,o}\ \hat{\mathrm{h}}_{\mathrm{OG}}(T_{R,i}) - M_{s,R,i}\ \hat{\mathrm{h}}_{\mathrm{s}}(T_{R,i}) \\ + M_{s,R,JI}\ \hat{\mathrm{h}}_{\mathrm{s}}(T_{R,i}) - M_{OG,R,JI}\ \hat{\mathrm{h}}_{\mathrm{OG}}(T_{R,i}) + \Delta H_{r,JI} \end{array}\right]}{M_{OG,R,JI}\,c_{p,OG} - M_{s,R,JI}\,c_{p,s}}$$

where:

$$\Delta H_{r,JI} = x_1\ (1-\mathrm{x}_{CuSO_4})\ \Delta H_{r,1}\ \mathrm{R}_{tot}\ \mathrm{M}_{SO_x,A,i}$$

For small increments of conversion of copper sulfate to copper, a mass and energy balance is calculated to estimate the temperature profile in the reactor. This temperature profile is then used to estimate the average reaction rates for each increment, and the overall reaction residence time. If the number of increments in the kinetic model is n, then the incremental copper sulfate conversion is:

$$\Delta\eta_{r2} = \frac{\eta_{r2}}{n}$$

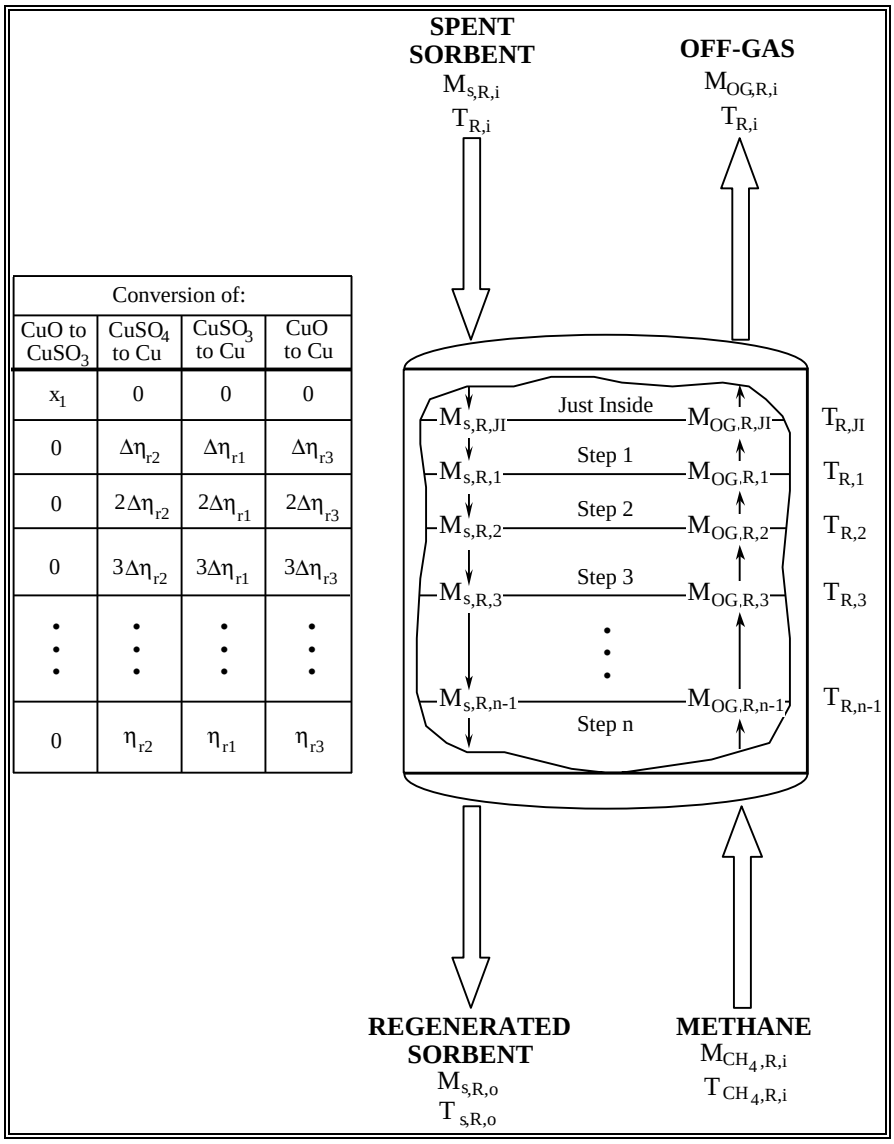

Conversion of:			
CuO to $CuSO_3$	$CuSO_4$ to Cu	$CuSO_3$ to Cu	CuO to Cu
x_1	0	0	0
0	$\Delta\eta_{r2}$	$\Delta\eta_{r1}$	$\Delta\eta_{r3}$
0	$2\Delta\eta_{r2}$	$2\Delta\eta_{r1}$	$2\Delta\eta_{r3}$
0	$3\Delta\eta_{r2}$	$3\Delta\eta_{r1}$	$3\Delta\eta_{r3}$
⋮	⋮	⋮	⋮
0	η_{r2}	η_{r1}	η_{r3}

Figure 7-9 Schematic of Regenerator Residence Time Model

Similarly, the conversion increments for regeneration of copper sulfite and copper oxide are assumed to be:

$$\Delta\eta_{r1} = \frac{\eta_{r1}}{n}$$

$$\Delta\eta_{r3} = \frac{\eta_{r3}}{n}$$

There are n regeneration increments. At the end of each regeneration increment, k (k=1,n), the sorbent composition is:

$$M_{Cu,R,k} = k\left\{\begin{matrix}[\Delta\eta_{r3}(1-x_1)+\Delta\eta_{r1}\,x_1](R-\eta_s) \\ +\Delta\eta_{r2}(R_{CuSO_4}+\eta_s)\end{matrix}\right\}\cdot M_{SO_x,A,i}$$

$$M_{CuO,R,k} = [(1-x_1)(1-k\Delta\eta_{r3})(R-\eta_s)] \cdot M_{SO_x,A,i}$$

$$M_{CuSO_3,R,k} = [x_1(12-k\Delta\eta_{r1})(r-\eta_s)] \cdot M_{SO_x,A,i}$$

$$M_{CuSO_4,R,k} = \{(1-k\Delta\eta_{r2})(R_{CuSO_4}+\eta_s)\} \cdot M_{SO_x,A,i}$$

The molar flow rate of the components of the regeneration gases at the bottom of each increment is given by:

$$M_{SO_2,R,k} = \begin{Bmatrix} (1-k)\Delta\eta_{r2}\ x_{CuSO_4} \\ +[(1-k)\Delta\eta_{r1}]x_1(1-x_{CuSO4}) \end{Bmatrix} R_{tot}\ M_{SO_x}$$

$$M_{H_2O,R,k} = (1-k)\begin{Bmatrix} \Delta\eta_{r2}x_{CuSO_4} \\ +0.5(1-x_{CuSO_4})[\Delta\eta_{r1}x_1+\Delta\eta_{r3}(1-x_1)] \end{Bmatrix} R_{tot}\ M_{SO_x}$$

$$M_{CO_2,R,k} = 0.5\, M_{H_2O,R,k}$$

$$M_{CH_4,R,k} = M_{CH_4,R,i} - M_{CO_2,R,k}$$

The heat of reaction for each conversion step in the regenerator is:

$$\Delta H_{r,k} = \Delta\eta_{r2}x_{CuSO_4}\Delta H_2 + \Delta\eta_{r3}(1-x_1)(1-x_{CuSO_4})\Delta H_3 + \Delta\eta_{r1}x_1(1-x_{CuSO_4})\Delta H_4$$

and the temperature is:

$$T_{R,k} = T_{R,k-1} + \left\{ \frac{\begin{matrix} M_{OG,R,k-1}\ \hat{h}_{OG}(T_{R,k-1}) - M_{s,R,k-1}\ \hat{h}_s(T_{R,k-1}) \\ +M_{s,R,k}\ \hat{h}_s(T_{R,k-1}) - M_{OG,R,k}\ \hat{h}_{OG}(T_{R,k-1}) + \ H_{r,k} \end{matrix}}{M_{OG,R,k}\ c_{p,OG} - M_{s,R,k}\ c_{p,s}} \right\}$$

The rate constant for the regeneration of copper sulfate is:

$$k_{s,r} = \begin{Bmatrix} 4.2\times10^7 \times F_w \times \exp\left(\frac{-21{,}700}{T}\right) \text{if T} \le 1{,}355°\text{R} \\ 11.2\times10^5 \times F_w \times \exp\left(\frac{-16{,}800}{T}\right) \text{if T} > 1{,}355°\text{R} \end{Bmatrix}$$

where the factor Fw is a correction based on the sorbent copper loading (Harriott, 1993):

$$F_w = 2.04\exp(-14.23\,W_{Cu})$$

and the reaction rate is:

$$r_k = \frac{k_{s,R,k}\ P_{CH_4,k}\ (\eta_{r2,eq,k} - k\Delta\eta_{r2})}{1 + K_1\ P_{CH_4,k} + K_2\ P_{SO_2,k} + K_3\ P_{CO_2,k}}$$

where:

$\eta_{r2,eq,k} = 1 - 0.9\, P_{CH4,k}$

The average reaction rate for each conversion interval is:

$$r_{k,ave} = \frac{r_{k-1} + r_k}{2}$$

and the total residence time required for regeneration of copper sulfate is:

$$t_{r,CuSO_4} = \sum_{k=1}^{n} \frac{\Delta\eta_{r2}}{r_{k,ave}}$$

Table 7-3 ***Regenerator Residence Time Model Input Assumptions***

Model Parameter	Deterministic	Probability (Nominal) Value	Distribution Values[a]
Methane Inlet Temperature	77 ^{o}F		
Sorbent Copper Loading	7 wt-%	Triangular	5,7,9 wt-%
Regenerator Inlet Temperature	900 ^{o}F	Triangular	850, 900, 910 ^{o}F
Absorber SO2 Removal Efficiency	90 %	Triangular	70, 90, 95 %
Copper Sulfate Regeneration Efficiency	80 %	Triangular	70, 80, 95 %
Copper Sulfite Regeneration Efficiency	40 %	Triangular	40, 40, 80 %
Copper Oxide Regeneration Efficiency	80 %	Triangular	70, 80, 95 %
Conversion of CuO to $CuSO_3$	100 %	Uniform	0-100 %
Available Cu/S Ratio	1.3	Triangular	1.5, 2.0, 3.0
Excess Methane Ratio	η_{r2}+.35	Uniform	η_{r2}+.10,η_{r2}+1

[a]For uniform distribution, actual ranges of values are shown. For triangular distribution, endpoints and mode are shown.

A simplified response surface model for residence time was developed based on statistical analysis of the residence time model. Eight of the residence time model input parameters were assigned probability distributions representing possible ranges of values that might be expected in future model applications. These assumptions are given in

$$t_{r,CuSO_4} = \sum_{k=1}^{n} \frac{\Delta\eta_{r2}}{r_{k,ave}}$$

Table 7-3. These distributions were sampled using Latin Hypercube sampling, a variant of Monte Carlo simulation, and the paired sets of sample values were used to calculate the corresponding residence times. A total of 100 sets of calculations were made. Linear regression analysis was used to correlated the resulting distribution of residence time values to each of the input distributions. The simplified model for regenerator residence time is:

$$t_{r,CuSO4} = 1.01 \cdot \exp\{8.31 + 0.10W_{Cu} - 0.009t_{s,R,i} + 0.90\eta_s + 3.76\eta_{r2} - 0.44x_1 - 0.39R - 1.03R_{CH4}\} \quad (7\text{-}33)$$

This regression model has a coefficient of determination (R^2) of 0.95. The standard error of the estimate of residence time is 1 minute. This model should not be extrapolated.

7.3.4. ByProduct Recovery

The regenerator off-gas is sent to a byproduct recovery plant for processing. As previously noted, elemental sulfur recovery using a Claus plant is the design basis for this study. A two-stage Allied Chemical design is assumed, based on previous studies (Ratafia-Brown, 1983; Rubin et al., 1991). The sulfur recovery efficiency for this design is estimated to be 95 percent, with the unconverted sulfur emitted as SO_2 in the Claus plant tailgas. Thus, the overall sulfur removal efficiency if the copper oxide process removes 90 percent of sulfur oxides from the flue gas would be only 85.5 percent. Such a design is likely to be unacceptable compared to conventional flue gas desulfurization systems, which are capable of 90 percent or greater sulfur capture.

Three approaches are possible to improve the overall system SO_x removal efficiency. These are: (1) increase the copper oxide removal efficiency to compensate for the Claus plant tailgas emissions; (2) recycle the tailgas emissions to the flue gas upstream of the fluidized bed absorber, and adjust the copper oxide removal efficiency; or (3) increase the sulfur capture efficiency of the Claus plant. The third option is not considered here, due to the need to obtain detailed design information that is not readily available. However, the first two options are considered in the copper oxide process performance model.

The first approach is easily modeled by adjusting the copper oxide sulfur oxides capture efficiency based on the sulfur recovery plant efficiency:

$$\eta_s = \frac{\eta_{s,overall}}{\eta_{Claus}}$$

For example, if an overall removal efficiency of 90 percent is required, and if the Claus plant recovers only 95 percent of the sulfur in the regenerator offgas, then the copper oxide process sulfur removal efficiency must be 94.7 percent. Such an increase in removal efficiency will substantially increase the sorbent requirement. Depending on the design assumptions, an increase sorbent circulation rate of over 40 percent may be required. Therefore, it is unlikely that this is the lowest cost approach.

The second approach is modeled by injecting into the flue gas just upstream of the fluidized bed absorber an amount of SO_2 equivalent to the sulfur molar flow in the Claus plant tailgas:

$$M_{SO2,recycle} = \left\{ \frac{(1-\eta_{Claus})\eta_s}{1-(1-\eta_{Claus})\eta_s} \right\} M_{SO2,FG}$$

The required absorber sulfur removal efficiency is given by:

$$\eta_s = \frac{\eta_{s,overall}}{\eta_{Claus} + (1-\eta_{Claus})\eta_{s,overall}}$$

In contrast to the example given above, the sulfur removal efficiency in the absorber is only 90.45 percent. Combined with the increased sulfur loading to the absorber, the tailgas recycle approach results in a modest increase in the sorbent circulation rate of typically less than 10 percent.

As part of process integration, the regeneration offgas must be dried and cooled prior to entering the sulfur recovery plant (Ratafia-Brown, 1983). A typical regenerator offgas is at a temperature of 875 to 910°F, with a moisture content of 40 to 45 percent. The design basis for gas inlet to the Claus plant calls for a temperature of 500°F with a moisture content of only 6 percent. The net effect of the gas treatment and cooling is to generate superheated steam, which may be used elsewhere in the power plant.

7.3.5. Energy Penalties and Credits

The copper oxide process consumes electrical energy to operate blowers and compressors associated with the pneumatic solids transport system and the combustor for the sorbent heater. Due to the flue gas pressure drop across the fluidized bed absorber, additional electrical energy is required to operate the power plant induced draft fan. The sulfur recovery system consumes a relatively small amount of power.

The electrical requirements of the various fans are estimated using the "fan equation" (McQuiston and Parker, 1982):

$$EC_{fan} = \frac{Q\Delta P}{8{,}512\eta_{fan}}$$

The fan efficiencies are assumed to be 85 percent. For the induced draft fan, the incremental pressure drop is estimated based on the fluidized bed height. For a 48 inch bed height, the pressure drop is approximately 28 inches of water (Frey, 1987). For the dense phase solids transport system between the regenerator and the absorber, the pressure drop is 22 psi (Roberts and Schaeffer, 1992). The pressure drop across the sorbent transport system between the absorber and the solids heater is estimated at 4.3 psi (Ratafia-Brown, 1983). The pressure drop across the solids heater combustor is estimated at 90 inches of water (Ratafia-Brown, 1983).

The copper oxide process and the sulfur recovery plant utilize methane for solids heating, sorbent regeneration, and regenerator offgas reduction. The methane represents an energy input into the power plant system.

Due to the exothermic reactions occurring in the fluidized bed absorber, as well as to the thermal energy added to the sorbent during solids heating, the temperature of the flue gas exiting the absorber is substantially higher than the inlet temperature. The temperature increase is typically on the order of 100°F. This additional energy may be recovered by the power plant air preheater, and used to increase the temperature of the combustion air entering the boiler. The calculation of this energy credit is described by Rubin et al. (1991, pp. 27, 44-46).

The copper oxide process uses steam for ammonia vaporization and injection. However, the offgas pretreatment section of the sulfur recovery plant produces steam, as previously described. Typically, the net effect is an energy credit. The thermal value of the steam is converted to an electricity equivalent basis using the

power plant gross steam cycle heat rate (excluding the boiler, see Rubin et al., 1991, p. 45 for details).

7.4. Cost Model

This section presents the economic model developed for the fluidized bed copper oxide process. The source of economic data for this model includes previous work by Frey (1987; 1991) as well as new data developed by A.E. Roberts and Associates (1994). The cost model is comprised of a capital cost model and an annual cost model.

7.4.1. Capital Cost Models

The capital cost of a complete fluidized bed copper oxide system includes the following major equipment items:

- Fluidized bed absorbers
- Ammonia Injection System
- Regenerator
- Solids Heater
- Sorbent Transport System
- Byproduct Recovery System

For each of these major systems, a direct capital cost model is developed.

7.4.1.1. Fluidized Bed Absorbers

The direct capital cost of the fluidized bed absorbers includes the absorber vessel, structural supports, dampers and isolation valves, refractory lining for the inside of the absorber, ductwork, instrumentation and control, and installation costs.

The absorber vessels are refractory-lined carbon steel of minimum one-half inch thickness. Each absorber vessel may be approximated as a cylinder. The internal diameter of the absorber vessel is determined based on the superficial gas velocity requirement. The materials cost of the absorber are proportional to the surface area of the absorber vessel.

The absorber vessel internal radius is given by:

$$r_a = \sqrt{\frac{G_{FG}}{60\,\pi\,V_s\;N_{a,O}}}$$

The diameter of the absorber vessel must be larger than this internal radius to accommodate the thickness of refractory lining. The design basis developed by A. E. Roberts and Associates (AERA) for the absorber includes a two-inch thick base or inner refractory covering the internal surface of the absorber vessel. A second "hot base" refractory layer approximately six inches thick is placed over the first layer. Thus, the vessel internal diameter is:

$$r_{v,a} = r_a + t_{ir} + t_{hr}$$

The surface area of the absorber vessel is approximated by the following equation for the surface area of a cylinder:

$$SA_a = 2\pi (r_{v,a})^2 + 2\pi r_{v,a} h_a$$

The design height of the absorber vessel is approximately 70 feet, based on the AERA design basis. The total height of the absorber assembly is larger when flue gas outlet ductwork is taken into consideration. The straight wall portion of the absorber vessel that is covered with refractory lining is approximately 35 feet.

The direct cost for the steel absorber vessel is estimated based on the ratio of surface areas referenced to a base case design. The AERA design is predicated on a flue gas volumetric flow rate of 500,000 scfm at 705°F and a superficial gas velocity of 4.5 ft/sec. Therefore, the required internal radius is 36.4 feet. Accounting for the 8 inch total thickness of the refractory, the steel vessel's internal diameter must be 37 feet. Therefore, the approximate surface area of the absorber vessel is 24,875 ft^2. The base cost estimate is $1,434,000 (in 1993 dollars) for a single absorber vessel of this size. Therefore, the direct cost model for the cost of the steel absorber vessel is given by:

$$DC_{a,v} = 1{,}434\ \mathrm{N_{a,T}} \left(\frac{SA}{24{,}875\ \mathrm{ft}^2} \right) \frac{\mathrm{PCI}}{1993\ \mathrm{PCI}}$$

Typically, there will be two 50% capacity absorber vessels with no spares. The cost of refractory is given by the refractory surface area, required to cover the sides of the absorber vessel, and a unit cost for refractory per square foot:

$$DC_{a,r} = 2\pi r_a h_{a,sw} N_{a,T} UC_r$$

In 1993, the unit cost of the total of 8 inches of refractory required for the absorber was approximately \$55/ft^2.

Each absorber requires structural supports. In the base case design, these are estimated at $100,000 per vessel. The structural support is assumed here to have some economy of scale with respect to size. As a default assumption, a six-tenths scaling rule is assumed:

$$DC_{a,s} = 100\ \mathrm{N_{a,T}} \left(\frac{SA_a}{24{,}875\ \mathrm{ft}^2} \right)^{0.6} \frac{\mathrm{PCI}}{1993\ \mathrm{PCI}}$$

The surface area of the absorber vessel is used as a surrogate variable for the size of the absorber system and, hence, the proportional size of the structural supports.

The costs for flue gas ductwork, flue gas isolation valves, and dampers are assumed to be proportional to the flue gas volumetric flow rate. Moreover, economies of scale are assumed. In the absence of more detailed information, the following direct cost model was developed:

$$DC_{a,d} = 300\ \mathrm{N_{a,T}} \left(\frac{G_{FG}}{1.1 \times 10^6\ ft^3/\mathrm{min}\ \mathrm{N_{a,O}}} \right)$$

In this model, the cost of ductwork, isolation valves, and dampers is estimated for a single absorber vessel, and is multiplied by the total number of absorber vessels.

The total direct cost for the absorber process area is given by:

$$DC_a = (1 + f_{ic,a})(DC_{a,v} + DC_{a,r} + DC_{a,s} + DC_{a,d})$$

where $f_{ic,a}$ is an installation cost factor for the absorber process area. A default value of 0.45 is suggested.

In addition to these direct costs, there is an incremental cost associated with increasing the pressure drop of the flue gas. The differential cost required to "modify" a new induced draft fan has been modeled by Frey (1994). The energy requirement required to overcome the absorber flue gas pressure drop is:

$$EC_{ID,dif} = \frac{G_{FG}\Delta P_{CuO}}{8{,}512\eta_{fan}\,\mathrm{N_{a,O}}}$$

The fan efficiency is typically 85 percent. The cost of the ID fan differential is:

$$DC_{ID,dif} = 180\,\mathrm{N_{a,T}}\left(\frac{EC_{ID,dif}}{4{,}600}\right)^{0.6}\left(\frac{PCI}{357.3}\right)$$

7.4.1.2. Ammonia Injection System

Ammonia is injected into the flue gas upstream of the absorber vessel. The ammonia injection system is comprised of the following equipment, based on the AERA design basis:

- One ammonia storage tank per absorber vessel, plus one common spare tank
- One air compressor per storage tank
- One vaporizer per absorber vessel
- Injection probes and nozzles for each absorber inlet
- Control panels

The cost of the ammonia injection system is most sensitive to the ammonia flow rate requirement for each absorber vessel. The ammonia flow rate requirement depends on the NO_x loading into the absorbers and the ammonia-to-NO_x molar ratio required to achieve a given level of NO_x control. The total ammonia mass flow rate is given by:

$$m_{NH3} = MW_{NH3}R_{NH3}M_{NOx}$$

Storage to provide 30 days supply of ammonia is required under the design basis. The total ammonia storage requirement is distributed among several tanks, depending on how many absorber vessels are used. Therefore, the storage capacity of each tank is given by:

$$C_{NH3} = \frac{m_{NH3}\,24\,\mathrm{D_{NH3}}}{(8.34\,\mathrm{lb/gallon})\,(\mathrm{N_{a,O}}+1)}$$

Based on Perry's *Chemical Engineer's Handbook* (6th Ed., p. 25-69), the exponential factor appropriate for horizontal tanks is 0.57. Based on a previous cost estimate developed by AERA, the cost of an 80,000 gallon ammonia storage tank is approximately $235,000. Therefore, the storage tank cost is given by:

$$DC_{ai,S} = (1+f_{ic,ai})\,235\,(\mathrm{N}_{a,O}+1)\left(\frac{\mathrm{C_{NH3}}}{80{,}000}\right)^{0.57}\frac{\mathrm{PCI}}{1993\,\mathrm{PCI}}$$

The detailed costs for other components of the ammonia injection system are not disaggregated in the AERA cost estimate. However, based on a previous AERA estimate, the total cost of the ammonia injection system was estimated as $2.3 million. This estimate was for an ammonia flow rate of 1,751 lb/hr, but involved

three 80,000 gallon storage tanks. Assuming an installation cost factor of 45 percent for the storage tanks, the net installed cost of the ammonia vaporization and injection system is $1.28 million. This cost should scale with the ammonia flow rate. Frey (1994) developed a direct cost model of an ammonia injection system for selective catalytic reduction (SCR) in which the scaling exponent was found to be 0.482. Therefore, the direct cost for the ammonia vaporization and injection components is estimated as:

$$DC_{ai,v} - 17.5(N_{a,T})(m_{NH_3})^{0.482}\ \frac{\text{PCI}}{1993\,\text{PCI}}$$

The direct cost of the ammonia injection system is therefore:

$$DC_{ai} = DC_{ai,S} + DC_{ai,v}$$

7.4.1.3. Regenerator

The regenerator is a carbon steel cylindrical vessel. The regenerator is sized to accommodate sorbent storage for a specified sorbent residence time. In the base case, AERA has designed a regenerator with a sorbent hold-up volume of 8,800 ft^3. The regenerator design features a 28 foot straight wall height. Here, it is assumed that the straight wall height is held fixed, and the radius is adjusted to accommodate various residence times.

The required regenerator radius is therefore given by:

$$r_R = \sqrt{\frac{m_{s,R,i}\,t_R}{60\,\rho_s\,\text{N}_{\text{R,O}}\pi\,h_{R,sw}}}$$

The total height of the regenerator is the straight wall height plus inlet and outlet clearances for gas flows. These clearances add approximately 17 feet to the straight wall height. The inside of the regenerator vessel walls are covered with two layers of refractory totaling 8 inches in thickness. Therefore, the steel vessel diameter is

$$r_{v,R} = r_R + t_{ir} + t_{hr}$$

The surface area of the regenerator vessel is approximated by the surface area of a cylinder:

$$SA_R = 2\pi(r_{v,R})^2 + 2\pi r_{v,R} h_R$$

In the base case, the regenerator has an equivalent overall height of 78 feet and a radius of 10 feet. The direct cost of the regenerator vessel is:

$$DC_{R,v} = 475\,\text{N}_{\text{a,R}}\left(\frac{SA_R}{5{,}530\,\text{ft}^2}\right)\frac{\text{PCI}}{1993\,\text{PCI}}$$

The direct cost of refractory is given by:

$$DC_{R,r} = 2\pi r_R h_R N_{R,T} UC_r$$

Each regenerator requires structural supports. In the base case design, these are estimated at $42,500 per vessel. The structural support is assumed here to have some economy of scale with respect to size. As a default assumption, a six-tenths scaling rule is assumed:

$$DC_{R,s} = 42.5\,\mathrm{N_{a,T}}\left(\frac{SA_a}{5{,}530\,\mathrm{ft}^2}\right)^{0.6}\frac{PCI}{1993\,\mathrm{PCI}}$$

The surface area of the absorber vessel is used as a surrogate variable for the size of the regenerator system and, hence, the proportional size of the structural supports.

The costs for ductwork, isolation valves, and dampers are assumed to be proportional to the regenerator offgas volume flow rate. Moreover, economies of scale are assumed. In the base case analysis, approximately 1,300 lbmole/hour of offgas is evolved from the regenerator. At 900 ^{o}F, the volumetric flow rate is 21,900 ft^3/min. Thus, in the absence of more detailed information, the following direct cost model was developed:

$$DC_{R,d} = 350\,\mathrm{N_{R,T}}\left(\frac{G_{OG}}{626\,\mathrm{lbmole/hr\ N_{R,O}}}\right)^{0.6}\frac{\mathrm{PCI}}{1993\,\mathrm{PCI}}$$

In this model, the cost of ductwork, isolation valves, and dampers is estimated for a single absorber vessel, multiplied by the total number of absorber vessels.

A methane feed system and a booster compressor and motor is required for the inlet methane to overcome the pressure drop through the regenerator. The booster compressor cost is assumed to be proportional to the methane flow rate. The cost equation is thus:

$$DC_{R,bf} = 350\,\mathrm{N_{R,T}}\left(\frac{M_{CH4,R,i}}{187\,\mathrm{lbmole/hr\ N_{R,O}}}\right)^{0.6}\frac{PCI}{1993\,\mathrm{PCI}}$$

The total direct cost for the absorber process area is given by:

$$DC_R = (1 + f_{ic,R})(DC_{R,v} + DC_{R,r} + DC_{R,s} + DC_{R,d} + DC_{R,bf})$$

where $f_{ic,R}$ is an installation cost factor for the absorber process area. A default value of 0.45 is suggested.

7.4.1.4. Solids Heater

The solids heater is a carbon steel cylindrical vessel. In the base case, AERA has designed a solids heater with an internal radius of 10 feet and a height of 50 feet. The side walls of the heater are lined with refractory material. The internal diameter of the solids heater is proportional to the mass flow of sorbent entering the vessel. The vessel contains two sorbent beds in which hot combustion gases from a methane combustor contact the sorbent in counter-current flow. Thus, for fixed bed heights in each stage, the solids heater internal radius varies with the sorbent mass flow rate as follows:

$$r_{SH} = 10\sqrt{\frac{m_{s,SH,i}}{400{,}000\,\mathrm{N_{SH,O}}}}$$

The inside of the solids heater vessel walls are covered with two layers of refractory totaling 8 inches in thickness. Therefore, the steel vessel diameter is

$$r_{v,SH} = r_{SH} + t_{ir} + t_{hr}$$

The surface area of the solids heater vessel is approximated by the surface area of a cylinder. Thus, for a single vessel, the surface area is:

$$SA_{SH} = 2\pi (r_{v,SH})^2 + 2\pi r_{v,SH} h_{SH}$$

In the base case, the solids heater has an equivalent overall height of 50 feet and an internal radius of 10 feet. The direct cost of the regenerator vessel is:

$$DC_{SH,v} = 360\ \mathrm{N_{SH,T}} \left(\frac{SA_{SH}}{4{,}060\ \mathrm{ft}^2} \right) \frac{\mathrm{PCI}}{1993\ \mathrm{PCI}}$$

The direct cost of refractory is given by:

$$DC_{SH,r} = 2\pi r_{SH} h_{SH} N_{SH,T} UC_r$$

Each solids heater requires structural supports. In the base case design, these are estimated at $72,500 per vessel. The structural support is assumed here to have some economy of scale with respect to size. As a default assumption, a six-tenths scaling rule is assumed:

$$DC_{SH,v} = 72.5\ \mathrm{N_{SH,T}} \left(\frac{SA_a}{4{,}060\ \mathrm{ft}^2} \right)^{0.6} \frac{\mathrm{PCI}}{1993\ \mathrm{PCI}}$$

The surface area of the solids heater vessel is used as a surrogate variable for the size of the solids heater system and, hence, the proportional size of the structural supports.

The costs for ductwork, isolation valves, dampers, and booster fans and motors are assumed to be proportional to the solids heater exit gas volumetric flow rate. Moreover, economies of scale are assumed. In the base case analysis, approximately 6,500 lbmole/hour of gas exits the solids heater at 830°F. Thus, in the absence of more detailed information, the following direct cost model was developed:

$$DC_{SH,d} = 608\ \mathrm{N_{SH,T}} \left(\frac{G_{SH,G,o}}{6467\ \mathrm{lbmole/hr\ N_{SH,O}}} \right)^{0.6} \frac{\mathrm{PCI}}{1993\ \mathrm{PCI}}$$

In this model, the cost of ductwork, isolation valves, dampers, booster fans, and booster fan motors is estimated for a single solids heater vessel, and multiplied by the total number of absorber vessels.

The total direct cost for the solids heater is:

$$DC_{sh} = (1 + f_{ic,SH})(DC_{SH,v} + DC_{SH,r} + DC_{SH,s} + DC_{SH,d})$$

where $f_{ic,R}$ is an installation cost factor for the absorber process area. A default value of 0.45 is suggested.

7.4.1.5. Sorbent Transport System

A dense phase pneumatic transport system is employed to transport sorbent from the regenerator outlet to the absorber inlet. The transport system includes valves, compressors, piping, filters, and surge bins. The total cost for this system reported by AERA is $6,580,000. The dense phase transport system was sized for a sorbent circulation rate of 1,000,000 lb/hr. The cost of the transport system is proportional to the sorbent circulation rate. Thus, the equipment cost for the dense phase transport system is:

$$DC_{ST,e} = 6{,}580\left(\frac{m_{s,A,i}}{1{,}000{,}000}\right)^{0.6}\frac{PCI}{1993\,\text{PCI}}$$

In addition, a sorbent storage silo is required. The cost of these silos is proportional to the sorbent circulation rate and the sorbent attrition rate, which determine the sorbent make-up rate. The nominal sorbent makeup rate is 500 lb/hr in the base case design. Therefore, the cost of the storage silos with air locks is:

$$DC_{ST,s} = 330\left(\frac{m_{s,makeup}}{500}\right)^{0.6}\frac{PCI}{1993\,\text{PCI}}$$

The total direct cost for the sorbent transport system is:

$$DC_{ST} = (1+ f_{ic,ST})(DC_{ST,e} + DC_{ST,s})$$

where $f_{ic,ST}$ is an installation cost factor for the solids transport process area. A default value of 0.45 is suggested.

7.4.1.6. Solids Heater Combustor

The cost of the combustor for the solids heater is proportional to the methane requirement:

$$DC_{SH,c} = 2{,}650(1+ f_{ic,SH,c})\left(\frac{m_{CH4,SH,i}}{225}\right)^{0.6}\frac{PCI}{1993\,\text{PCI}}$$

where $f_{ic,SH,C}$ is an installation cost factor for the solids heater combustor process area. A default value of 0.45 is suggested.

7.4.1.7. ByProduct Recovery

A performance and cost model of a byproduct recovery plant has been developed previously and is documented by Rubin et al (1991, pp. 143-147).

7.4.1.8. Air Preheater Modifications

The copper oxide process affects the power plant air preheater due to the highly exothermic sulfation reactions. The flue gas temperature in the fluidized bed absorber may increase by 100°F, depending on the flue gas sulfur content and the overall sorbent circulation rate. Thermal energy is added to the flue gas by exothermic sulfation and NO_x control reactions, as well as by transfer of sensible heat from the inlet sorbent to the flue gas. The energy added to the flue gas may be recovered to the power plant boiler by increasing the size of the air preheater, thereby increasing the temperature of the combustion air entering the furnace. This energy credit is discussed in detail by Frey (1987). A cost model for the air preheater modifications associated with capturing this energy credit is also given by Frey (1987).

7.4.1.9. Initial Sorbent Inventory

The initial sorbent requirement is governed primarily by the amount of sorbent hold up in the fluidized bed absorber, the regenerator, and the solids heater. It is assumed that the quantity of sorbent hold up in the transport system is small by comparison. The cost for initial sorbent fill is therefore:

$$C_{IS} = \left\{ \rho_s Z_A A_A + \left(\frac{m_s}{60} \right) t_R + 2\rho_s Z_{SH} A_{SH} \right\} UC_s$$

7.4.2. Total Capital Requirement

The total direct cost is the summation of the plant section direct costs. The cost of initial catalyst charge is also included here in the direct costs, because it is such a large and integral part of the copper oxide system. One cost area not included in the previous sections is that associated with general facilities and control systems. AERA estimates that the control system has a cost of approximately 10 percent of the other direct cost items. Therefore, the total direct cost is given by:

$$TDC = (1 + f_{GF})(DC_A + DC_{AI} + DC_R + DC_{SH} + DC_{ST} + DC_{SH,c} + DC_{BY} + DC_{APH}) + C_{IS}$$

Other capital costs include various indirect capital costs, as well as preproduction costs associated with startup and inventory costs associated with providing initial stocks of chemicals and fuels.

Engineering and home office fees are typically estimated as a percentage of the total direct cost:

$$C_{EHO} = f_{EHO} TDC$$

AERA has estimated that "process engineering" costs are approximately 20 percent of the equipment costs, or approximately 14 percent of the installed direct capital costs. The engineering and home office costs include the costs associated with: (1) engineering, design, and procurement labor; (2) office expenses; (3) licensing costs for basic process engineering; (4) office burdens, benefits, and overhead costs; (5) fees or profit to the architect/engineer. EPRI recommends that a value of 7 to 15 percent of the total direct cost, indirect construction cost, and sales tax be used. Therefore, a value of 15 percent is used here as a default.

Project contingency costs reflect the expected increase in the capital cost estimate that would result from a more detailed cost estimate for a specific site. Usually, project contingency is assigned as a multiplier of the total direct cost and selected indirect capital costs (e.g., EPRI, 1986). For example:

$$C_{\mathrm{Pr}\,ojC} = f_{\mathrm{Pr}\,ojC}(TDC)$$

A typical value for the project contingency for a preliminary level cost estimate, as defined by the EPRI Technical Assessment Guide, is 20 percent.

Table 7-4 ***Project Contingency Factors Recommended by EPRI***[a]

Type of Estimate	Design Information	Percentage of Direct Cost
Simplified	General site, process flow diagram	30 to 50
Preliminary	Major equipment, preliminary piping and instrumentation diagrams	15 to 30
Detailed	Complete process design, site-specific, engineering design in progress, construction contract and schedule.	10 to 20
Finalized	Complete engineering of process plant	5 to 10

[a] Expressed as a percentage of the total of total direct, total indirect, and process contingency.

Source: EPRI (1986)

A major cost item for advanced technology plants is the process contingency. The process contingency is used in deterministic cost estimates to quantify the expected increase in the capital cost of an advanced technology due to uncertainty in performance and cost for the specific design application. In the EPRI cost method, the process contingency is estimated based on separate consideration of contingencies for each process section. The contingency is expressed as a multiplier of the sum of the direct and indirect capital costs for each plant section. Recommended ranges of process contingency factors are shown in Table 7-4. The process contingency decreases as the commercial experience with a process area increases. For example, in a fully commercialized process, which has been used in similar applications, the process contingency may be zero. For a new concept early in the development stage, the process contingency may be over 40 percent of the process area cost. Experience has shown that cost estimates for innovative technologies early in the development phase tend to be low by a factor of two or more compared to the cost of the first commercial-size demonstration plant (EPRI, 1986; Merrow, Phillips, and Myers, 1981). However, the cost for subsequent plants tends to decrease, which is known as the "learning curve" effect. Process contingencies employed for innovative technologies are intended to represent the expected costs of a commercialized (e.g., fifth of a kind) plant (EPRI, 1986). The process contingency for each major plant section is estimated as follows:

$$C_{\mathrm{Pr}\,ocC} = \sum_i f_{\mathrm{Pr}\,ojC}\ DC_i$$

Typical values for the project contingency employed in previous studies are 0.25 for the absorber, solids heater, and regenerator, 0.5 for the sorbent transport system, and 0.1 for the sulfur recovery system. AERA employed 20 percent for all process areas.

The total plant cost, or overnight construction cost, is given by:

$$TPC = TDC + C_{EHO} + C_{\mathrm{Pr}\,ojC} + C_{\mathrm{Pr}\,ocC}$$

An allowance for funds during construction (AFDC) is calculated based on the TPC as a function of the amount of time it would take to construct a copper oxide system. A 36 month construction period for a new plant is assumed. Methods for computing the AFDC are documented elsewhere (e.g., EPRI, 1986) and are not repeated here. The total plant investment (TPI) represents the sum of the total plant cost and the AFDC.

The final measure of capital cost is the total capital requirement (TCR). The TCR includes the total plant investment plus costs for royalties, startup costs, and initial inventories of feed stocks. In this case, no costs are assumed for royalties. Preproduction costs typically include one month of both fixed and variable operating costs and two percent of total plant investment. Inventory capital is estimated as 0.5 percent of total process capital excluding catalyst. The costs for initial catalysts and chemicals is zero. The copper oxide initial sorbent requirement is included in the process capital costs. Thus, for a copper oxide system, the total capital requirement is:

$$TCR = \frac{VOC + FOC}{12} + (1 + f_{PP})TPI + f_{IC}\sum_i DC_i$$

7.4.3. Annual Costs

The annual costs for copper oxide systems include fixed and variable operating costs. Fixed operating costs include operating labor, maintenance labor and materials, and overhead costs associated with administrative and support labor. Variable operating costs include consumables, such as ammonia and sorbent replacement. Costs for steam and electricity consumed from within the plant may also be estimated.

7.4.3.1. Fixed Operating Costs

Fixed operating costs include operating labor, maintenance labor and materials, and overhead costs associated with administrative and support labor. The operating labor cost is based on an estimate of the number of personnel hours required to operate the plant multiplied by an average labor rate. It is common to assume that four shifts per day are required for plant operation, allowing two hours overlap for transition between shifts. Furthermore, an allowance for personnel on sick leave or vacation can be incorporated into the "shift factor." A shift factor of 4.75 is assumed as a default in this study, based on Bechtel (1988).

The number of operators required per shift for the copper oxide process is estimated by AERA to be five. The total operating labor cost is estimated by summing the number of plant operators per shift for all process areas, applying the shift factor, and applying the average labor rate as follows:

$$OC_L = ALR\frac{2{,}080\ hrs}{\text{yr}}SF(1 + 2\,\mathrm{N_{A,O}})$$

The cost for maintenance material and labor for new technologies is typically estimated as a percentage of the installed capital cost for each process section. The total maintenance cost for the plant is given by:

$$OC_M = f_M TPC$$

where a typical value of the maintenance cost multiplier, f_M, is 0.045 for a solids handling system. The total maintenance operating cost may be disaggregated into material and labor components using the following approach:

$$OC_{MM} = 0.60\,\mathrm{OC_M}$$

$$OC_{ML} = 0.40\,\mathrm{OC_M}$$

The administrative and support labor cost is assumed to be 30 percent of the operating and maintenance labor cost:

$$OC_{AS} = 0.30\,(OC_L + OC_{ML})$$

7.4.3.2. Variable Operating Costs

The variable operating costs include all consumable materials required for operation of the plant. These include the costs of sorbent for makeup of attrition losses, the cost of ammonia for injection into the fluidized bed absorber, and the cost of methane required for regeneration and solids heating. In addition, the electricity and steam consumption of the copper oxide process results in an energy penalty. However, the increased flue gas temperature in the fluidized bed absorber results in an energy credit.

The annual costs for sorbent makeup, ammonia, and methane consumption are given by:

$$VOC_s = 8{,}760\,c_f\,m_{s,makeup}UC_s$$

$$VOC_{NH_3} = 8{,}760\,c_f\,m_{NH_3,A,i}UC_{NH_3}$$

$$VOC_{CH_4} = 8{,}760\,c_f\,(m_{CH_4,SH} + m_{CH_4,R} + m_{CH_4,BY})UC_{CH_4}$$

Note that methane is required for solids heating, as a reducing gas for the regeneration reactions, and also as a reducing gas for off-gas pretreatment in the Claus plant.

The variable operating costs also include a byproduct credit for the sale of elemental sulfur produced by the Claus plant. The amount of this credit is given by:

$$VOC_{BY} = 8{,}760\,c_f\,\eta_{BY}\left(\frac{32\,M_{SO_2,R,o}}{2{,}000}\right)UC_S$$

A variable operating cost credit is also taken for a reduction in coal consumption associated with the increased combustion air inlet temperature, which in turn results from the higher flue gas temperature entering the air preheater. This credit is discussed by Frey (1987).

7.5. Sensitivity Analyses of the Fluidized Bed Copper Oxide Process

The copper oxide process performance and economic models are applied to several case studies to identify key process sensitivities and to identify potentially robust design configurations. These analysis are predicated on "deterministic" analyses, in which point-estimates are used for all model input parameters. In the following chapter, uncertainties in the copper oxide process will be quantified and evaluated.

7.5.1. Integration of copper oxide process and byproduct recovery system

The copper oxide process performance model is applied here to three case studies to compare alternative approaches for dealing with the Claus plant tailgas. The design basis is a 500 MW power plant. The coal composition and the calculated flow rate are given in Table 7-5, the calculated flue gas composition and flow upstream of the copper oxide process are given in Table 7-6, and the key design assumptions and

modeling results for the three cases are given in Table 7-7. These case studies are based on a single stage fluidized bed absorber. Case 1 represents a base case in which no measures are taken to correct for tailgas emissions. In Case 2, the SO_2 removal efficiency in the absorber is increased to compensate for the tailgas emissions. In Case 3, the tailgas emissions are recycled to the flue gas just upstream of the absorber, and the absorber sulfur removal efficiency is increased slightly to achieve an overall 90 percent removal efficiency. Cases 2 and 3 yield the same overall removal efficiency of 90 percent, while Case 1 achieves only 85.5 percent removal efficiency.

Table 7-5 ***Coal Composition and Model Results for Coal Input Flow Rate*** [a]

Component	Composition, (wt-% as fired)	Flow Rate (lb/hr)
Carbon	57.56	246,686
Hydrogen	4.14	17,743
Oxygen	7.00	30,000
Sulfur	3.12	13,371
Nitrogen	1.44	61,714
Ash	16.00	68,571
Moisture	10.74	46,029
TOTAL	100.00	428,571

[a] Gross plant capacity is 500 MW with a gross cycle heat rate of 9,000 BTU/kWh.

*Table 7-6****Model Results for Flue Gas Composition and Flow Rate*** [a]

Component	Composition (Volume %)	Flow Rate (lb/hr)	Flow Rate (lbmole/hr)
Nitrogen	73.229	3,091,870	110,371
Oxygen	3.217	155,175	4,849
Water Vapor	9.597	260,581	14,465
Carbon Dioxide	13.628	903,967	20,540
Sulfur Dioxide	0.260	25,129	393
Sulfur Trioxide	0.003	317	4
Nitrogen Oxide	0.062	2,810	10
Nitrogen Dioxide	0.003	227	5
TOTAL	100.000	4,440,070	150,720

[a] 95% of the coal sulfur is emitted, with 99% as SO_2. Ambient air is at 80°F and 65% relative humidity. Excess boiler air is 20%, and air preheater leakage is 19%.

While the design basis for Case 1 is likely to result in inadequate overall sulfur emissions control, Case 2 is likely to result in prohibitive costs. The sorbent circulation is increased by 28 percent to achieve the 94.74 percent absorber sulfur removal efficiency needed to compensate for the Claus plant tailgas emissions. Due to the higher sorbent circulation rate, the methane requirement for solids heating and regeneration is increased, contributing to a larger net energy penalty on the power

plant. In contrast, Case 3 achieves an overall sulfur removal efficiency of 90 percent with a modest increase in sorbent circulation rate of only six percent. Thus, Case 3 is clearly preferred over Case 2 for 90 percent overall sulfur control. The design basis for Case 3 is employed here for sensitivity analyses regarding absorber bed height, sorbent copper loading, and regeneration efficiency.

A detailed economic evaluation of the three Claus plant integration schemes is shown in Table 7-8. The total capital cost for the tailgas recycle approach is approximately 3 percent higher than an approach in which the tailgas is emitted with recycle or any type of compensation for SO_2 in the tailgas. The total capital cost increases by approximately 10 percent if the removal efficiency of the copper oxide process is substantially increased as a means to compensate for Claus plant tailgas emissions. The differences in total operating and maintenance (O&M) costs among the three schemes are even more pronounced. The recycle approach increases O&M costs by three percent, but the compensation approach leads to a 17 percent increase in O&M costs. Therefore, the tailgas recycle scheme appears to have relatively modest cost impacts while ensuring that overall sulfur control targets are achieved.

Table 7-7 ***Copper Oxide Process Design Assumptions and Model Results***

	Values		
Parameter	**Case 1**	**Case 2**	**Case 3**
Required SO_2 Removal Efficiency, %	90.0	90.0	90.0
Absorber SO_2 Removal Efficiency, %	90.0	94.7	90.5
Sulfur Plant Recovery Efficiency, %	95.0	95.0	95.0
Claus Tailgas Recycle to Flue Gas	No	No	Yes
Overall SO_2 Removal Efficiency, %	85.5	90.0	90.0
Net SO_2 Captured, lbmole/hr	339	357	357
NO_x Removal Efficiency, %	90.0	90.0	90.0
NO_x Captured, lbmole/hr	88.7	88.7	88.7
Flue Gas Inlet Temp., ^oF	705	705	705
Flue Gas Outlet Temp., ^oF	797	812	801
Number of Absorbers	2	2	2
Area per Absorber, ft^2	3,898	3,898	3,898
CuO Regeneration Efficiency, %	80	80	80
$CuSO_4$ Regeneration Efficiency, %	80	80	80
$CuSO_3$ Regeneration Efficiency, %	80	80	80
Conversion of CuO to $CuSO_3$, frac.	1	1	1
Absorber Sorbent Inventory, lb	829,496	829,496	829,599
Sorbent Circulation Rate (lb/hr, fresh)	714,811	913,387	757,940
Absorber Inlet Sorbent Flow (lb/hr)	727,411	929,487	771,300
Sorbent Circ. Rate (lb fresh/1,000 scf)	12.5	16.0	13.2
Sorbent Absorber Residence Time (min)	70	54	66
Sorbent Copper Loading (wt-%)	7	7	7
Available Cu/S Ratio	1.59	2.03	1.61
Total Cu/S Ratio	1.99	2.54	2.01
Copper Utilization (S rem./avail Cu)	0.57	0.47	0.56
NH_3/NO_x Molar Ratio	1.00	1.00	1.00
Ammonia (lb/hr)	1,763	1,763	1,763
Ammonia Injection Steam (lb/hr)	1,129	1,129	1,129
Superficial Flue Gas Velocity (ft/s)	4.5	4.5	4.5
Expanded Bed Height (inches)	48	48	48
Fluidized Bed Pressure Drop (in. H_2O)	27.7	27.7	27.7
Bed Attrition (% of bed inventory)	0.020	0.020	0.020
Circ. Attrition (% of circulation)	0.047	0.047	0.047
Overall Attrition (% of circulation)	0.070	0.065	0.069
Makeup Sorbent (lb/hr)	508	603	528
Methane (lb/hr)	10,455	12,107	10,983
Net Energy Impact (kW)	17,108	18,308	17,640

Table 7-8 ***Capital, Annual, and Levelized Costs for the Fluidized Bed Copper Oxide Process: A Comparison of Three Claus Plant Tailgas Integration Schemes[a]***

	Tailgas Integration Approach		
Description	**NoRecycle (Case 1)**	**Recycle (Case 3)**	**Compensate (Case 2)**
NH_3 Handling and Injection, M$	2.036	2.036	2.036
Fluidized Bed Absorber Capital, M$	6.381	6.381	6.381
ID Fan Differential, M$	0.401	0.401	0.401

Solids Heater, M$	3.472	3.565	3.888
Regenerator, M$	3.410	3.516	3.719
Sorbent Transport System, M$	8.375	8.669	9.728
Solids Heater Combustor, M$	3.741	3.828	4.134
Sulfur Recovery Plant, M$	13.316	13.831	14.664
Air Preheater Modifications, M$	5.339	5.623	6.585
Sorbent Inventory, M$	5.515	5.595	5.783
Total Direct Capital Cost, M$	56.633	58.230	62.474
Eng. & Home Office Fees, M$	8.495	8.735	9.371
Process Contingency, M$	13.026	13.393	14.369
Project Contingency, M$	7.389	7.585	8.142
Total Plant Cost ("overnight"), M$	85.542	87.943	94.357
Interest, M$ (current dollars)	8.088	8.315	8.922
Total Plant Investment, M$	93.630	96.258	103.279
Startup (Preproduction) Cost, M$	4.206	4.346	4.762
Working (Inventory) Capital, M$	0.232	0.239	0.258
Land Cost, M$	0.028	0.028	0.028
Total Capital Cost, M$	98.096	100.871	108.327
Total Capital, $/kW	207.5	213.1	227.9
Fixed Operating Cost, M$/yr	5.596	5.717	6.040
Sorbent Cost, M$/yr	14.485	15.075	17.307
Methane Cost, M$/yr	6.686	7.023	7.778
Ammonia Cost, M$/yr	0.795	0.795	0.795
Miscellaneous, M$/yr	0.441	0.441	0.441
Variable Operating Cost, M$/yr	22.407	23.334	26.321
Total O&M Cost, M$/yr	22.399	23.161	26.254
Revenue w/o Utilities, M$/yr	32.541	33.590	37.454
Utilities, M$/yr	2.943	2.966	3.052
Total Revenue, M$/yr	35.484	36.556	40.505
Total Rev, mills/kWh	13.173	13.552	14.955

[a] All costs are reported in 1993 dollars. Variable operating costs and levelized costs are calculated using a 65 percent plant capacity factor. The three Claus plant integration schemes are: (1) release tailgas to the atmosphere, with no adjustment for SO_2 emitted to the atmosphere in the tailgas; (2) recycle the tailgas to a point upstream of the fluidized bed absorber, to maintain an overall 90 percent sulfur removal efficiency; (3) increase the sulfur removal efficiency of the copper oxide process to compensate for tailgas SO_2 emissions.

7.5.2. Sorbent Bed Height: Single Stage Fluidized Bed Absorber

The sorbent bed height has a direct effect on the fluidized bed sorbent inventory. The bed inventory is in turn a determinant of sorbent residence time in the regenerator, which affects the Cu/S molar ratio required to achieve a given removal efficiency. As the bed height increases, the sorbent circulation rate decreases, as shown in Figure 7-10. However, as the bed height increases, the flue gas pressure drop and the induced draft fan electricity requirements increase. Figure 7-10 indicates that a minimum net energy penalty is achieved at a fluidized bed height of approximately 36 to 39 inches. However, the energy penalty is not the sole determinant of cost. Much of the equipment in the copper oxide process, including the solids heater and regenerator, is sized based on the sorbent circulation rate. Therefore, a reduction in sorbent circulation rate can yield significant capital cost savings. Furthermore, operating costs are reduced due primarily to lower sorbent replacement costs and lower methane requirements to heat and regenerate the sorbent.

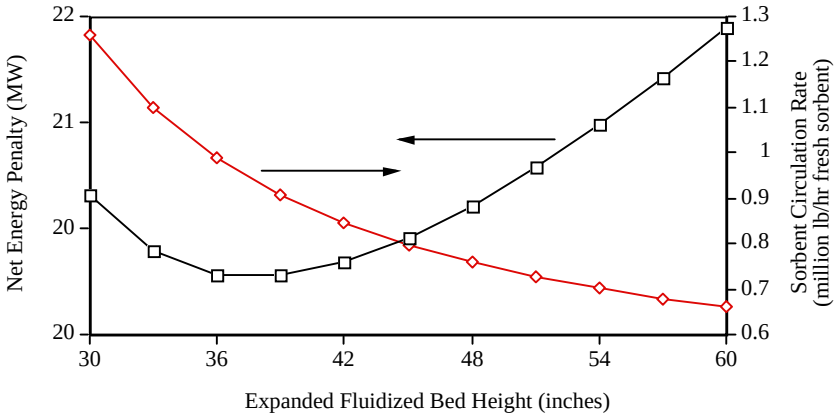

Figure 7-10 Sensitivity of Energy Penalty and Sorbent Circulation Rate to the Expanded Fluidized Bed Height for a Single-Stage Absorber-Based Copper Oxide System.

An economic analysis of the levelized cost for the copper oxide process versus expanded fluidized bed height is shown in Figure 7-11. The levelized cost for a single-stage absorber based system is shown to be highly sensitive to fluidized bed height, varying from 16.7 mills/kWh at a 30 inch bed height to approximately 13.4 mills/kWh at a 60 inch bed height. This analysis strongly suggests that the economics of the copper oxide process are favored by larger bed heights, larger sorbent residence time in the absorber, and reduced sorbent circulation rate, even though this is at the expense of increased flue gas pressure drop. The results also suggest that minimum costs are realized in the range of 57 to 60 inches. (The costs begin to increase for bed heights larger than 60 inches). However, these results do not take into account any changes in sorbent attrition that might be associated with larger bed heights, nor does it account for the incremental structural costs for the absorber vessel associated with substantially increasing the sorbent inventory. Thus, while these results are suggestive of the merits of higher bed heights, they are not conclusive.

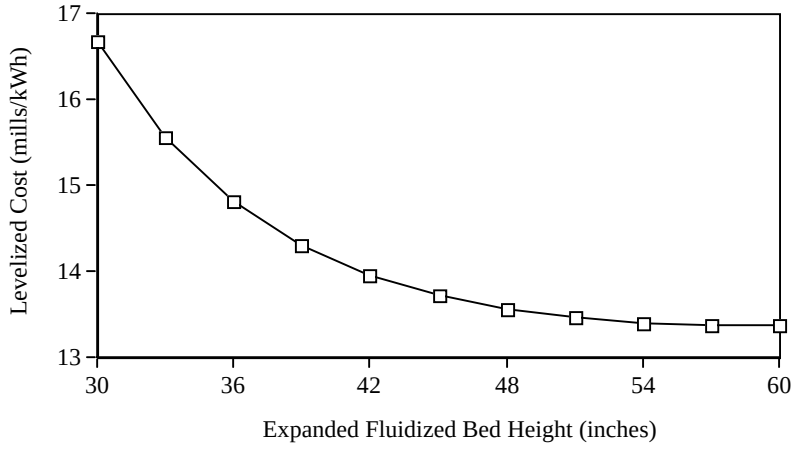

Figure 7-11 Sensitivity of Levelized Cost to the Expanded Fluidized Bed Height for a Single-Stage Absorber-Based Copper Oxide System.

While the costs of a single-stage absorber design are highly sensitive to bed height, the costs of optimally designed two-stage absorber systems are more nearly the same with variations in key design parameters. This is illustrated in Figure 7-12. For a two-stage design, there are two independent design parameters. These are the height

of the second stage, and the desired sulfur removal efficiency of the second stage. Specifying these two values determines the height and removal efficiency of the first stage of the absorber. A sensitivity analysis was performed in which the design height of the second stage absorber was varied from ten to forty inches, and in which four different values of sulfur removal efficiency were assumed for the second stage. The results in Figure 7-12 indicate that for any selected second stage bed height, there is an optimal (minimum total cost) second stage removal efficiency. While the levelized cost for any particular second stage bed height may be highly sensitive to the second stage removal efficiency (consider the different values of levelized cost obtained at a second stage bed height of 15 inches at removal efficiencies of 30, 40, 50, and 60 percent as shown in the figure), the levelized cost is not very sensitive to designs based on optimal selection of second-stage removal efficiency given a second-stage bed height. The least-cost solutions over the entire range from ten to forty inch second stage bed heights varies only between approximately 12 mills/kWh and 12.5 mills/kWh. Thus, the use of a two-stage design offers the opportunity to select relatively robust optimal designs. The minimum cost solution in Figure 7-12 is a second stage bed height of 16 inches with an associated removal efficiency of 30 percent. However, selection of a 22 inch bed height with a 40 percent removal efficiency yields nearly the same levelized cost value.

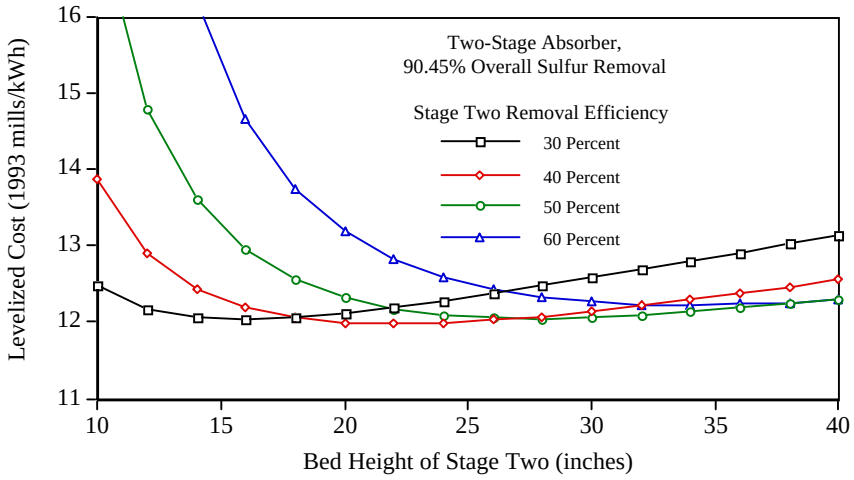

Figure 7-12 Sensitivity of Levelized Cost to the Design of a Two-Stage Absorber-Based Copper Oxide System.

A detailed economic comparison of the one and two stage absorber designs is given in Table 7-9. The two-stage design results in a substantial reduction in sorbent circulation rate compared to the one-stage design. Hence, the costs of equipment sized to accommodate the sorbent flow rate, such as the regenerator, solids heater, and sorbent transport system, are modestly reduced. There is an increase in sorbent inventory cost due to the large bed inventory in the two-stage system. The major impact of the two-stage design is seen in the annual costs, where the costs associated with makeup sorbent are reduced by over two million dollars. The overall effect is a reduction in levelized costs of 1.5 mills/kWh. Not taken into account in the cost model, however, are any additional costs for a two-stage absorber associated with the absorber vessel material or structural costs. The two-stage design is employed here in further sensitivity studies.

Table 7-9 ***Capital, Annual, and Levelized Costs for the Fluidized Bed Copper Oxide Process: A Comparison of Singe and Two-Stage Absorber Designs[a]***

	Absorber Design	
Description	**Single Stage**	**Two-Stage**
NH_3 Handling and Injection, M$	2.036	2.036
Fluidized Bed Absorber Capital, M$	6.381	6.381
ID Fan Differential, M$	0.401	0.413
Solids Heater, M$	3.565	3.101
Regenerator, M$	3.516	3.219
Sorbent Transport System, M$	8.669	7.255
Solids Heater Combustor, M$	3.828	3.357
Sulfur Recovery Plant, M$	13.831	12.784
Air Preheater Modifications, M$	5.623	4.437
Sorbent Inventory, M$	5.595	5.741
Total Direct Capital Cost, M$	58.230	53.022
Eng. & Home Office Fees, M$	8.735	7.953
Process Contingency, M$	13.393	12.195
Project Contingency, M$	7.585	6.833
Total Plant Cost ("overnight"), M$	87.943	80.003
Interest, M$ (current dollars)	8.315	7.565
Total Plant Investment, M$	96.258	87.568
Startup (Preproduction) Cost, M$	4.346	3.869
Working (Inventory) Capital, M$	0.239	0.215
Land Cost, M$	0.028	0.028
Total Capital Cost, M$	100.871	91.680
Total Capital, $/kW	213.1	194.922
Fixed Operating Cost, M$/yr	5.717	5.317
Sorbent Cost, M$/yr	15.075	12.828
Methane Cost, M$/yr	7.023	6.034
Ammonia Cost, M$/yr	0.795	0.795
Miscellaneous, M$/yr	0.441	0.441
Variable Operating Cost, M$/yr	23.334	20.098
Total O&M Cost, M$/yr	23.161	19.808
Revenue w/o Utilities, M$/yr	33.590	29.286
Utilities, M$/yr	2.966	2.975
Total Revenue, M$/yr	36.556	32.261
Total Rev, mills/kWh	13.552	12.038

[a] All costs are reported in 1993 dollars. Variable operating costs and levelized costs are calculated using a 65 percent plant capacity factor. The absorber capital cost for the two-stage design does not include any additional costs associated with a second stage distributor plate. The two-stage design is based on a lower stage with a 16-inch height operating at 30 % sulfur capture efficiency. The upper stage is approximately 37 inches in height and operates at approximately 86 percent sulfur capture efficiency.

7.5.3. Sorbent Copper Loading

Optimization of the sorbent copper content is a key design issue. The primary trade-off is between sorbent mass flow rate and sorbent attrition; however, the attrition characteristics of high copper sorbents are not well characterized. Data in Figure 7-13 for a two-stage absorber system point to the potential advantages of high copper loadings. Although the reaction rate constant (Equation (7-17)) decreases with increased copper loading, the net effect is a substantial reduction in the sorbent circulation rate. A change in sorbent copper loading of one percent from the base case value of seven weight-percent results in a change in sorbent circulation rate of approximately 100,000 lb/hr. However, there is little experience or data with highly loaded sorbents.

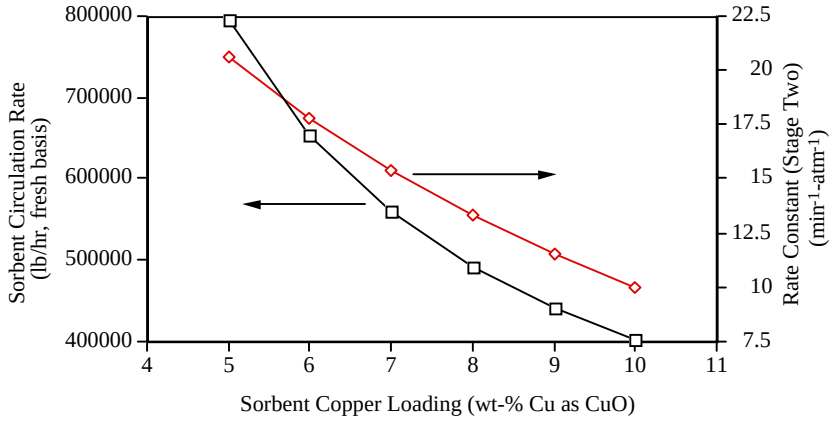

Figure 7-13 Sensitivity of Sorbent Circulation Rate and Second-Stage Kinetic Rate Constant to the Sorbent Copper Loading.

Neglecting possible changes in sorbent attrition rate, the economic implications of alternative sorbent copper loadings are show in Figure 7-14. Over the range from five to ten weight percent copper loading, capital cost varies by approximately $30/kW, while levelized costs vary by approximately 3 mills/kWh. The possible substantial reductions in cost associated with higher sorbent copper loadings suggest that there may be a considerable pay-off from research to improve sorbent copper loading or, alternatively, improve overall sorbent activity.

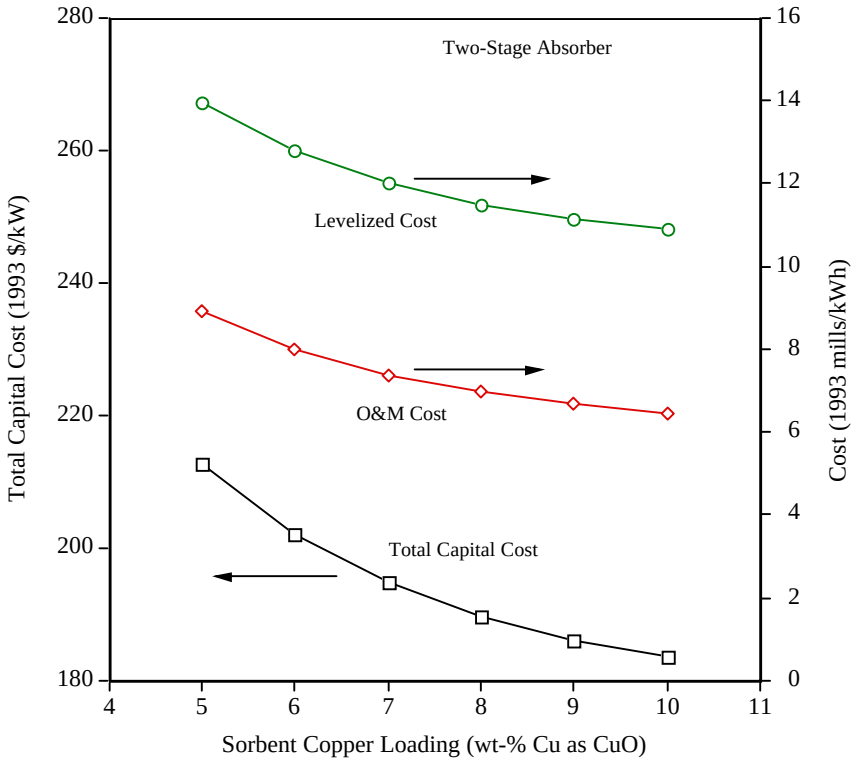

Figure 7-14 Sensitivity of Capital, O&M, and Levelized Costs to the Sorbent Copper Loading.

7.5.4. Regeneration Efficiency

A third area for process optimization is the sorbent regeneration efficiency. Three case studies are considered in Figure 7-15. The first is a case in which none of the copper oxide entering the regenerator is converted to copper sulfite. Thus, the only reactions occurring are Equations (7-3) and (7-5). In the second case, all of the copper oxide entering the regenerator is assumed to be converted to copper sulfite. The regeneration efficiencies for copper sulfate and copper sulfite are assumed to be the same. This case yields results that approach those of the first case as the regeneration efficiency approaches 100 percent. Finally, in the third case, the copper sulfite regeneration efficiency is assumed to be one-half that for copper sulfate. In this case, even at very high copper sulfate regeneration efficiencies, the unregenerated copper sulfite leads to a higher spent sorbent loading to the absorber and a correspondingly higher total Cu/S ratio than the other cases. These three cases illustrate that attention must be focused on understanding regeneration and its implications for process performance and economics.

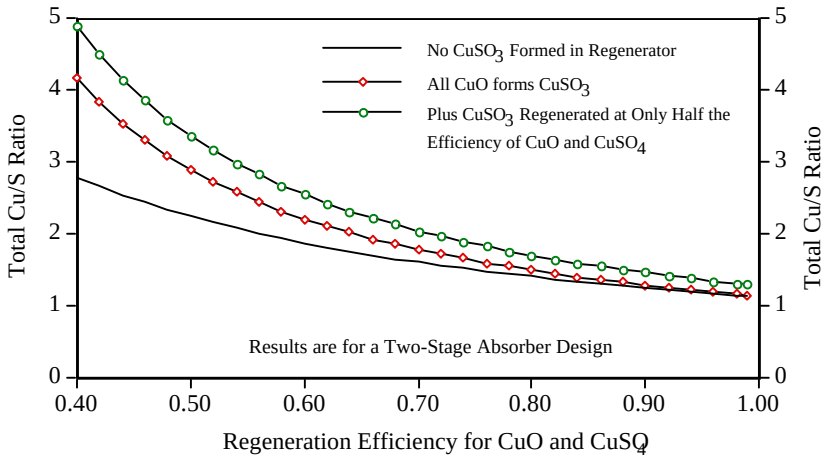

Figure 7-15 Sensitivity of the Total Cu/S Molar Ratio to Regeneration Efficiencies.

The economic implications of poor regeneration are shown in Figure 7-16. At low regeneration efficiencies, typical of those believed to have occurred in life cycle testing, the levelized costs may be as much as double or more the costs based on base case assumptions of 80 percent regeneration.

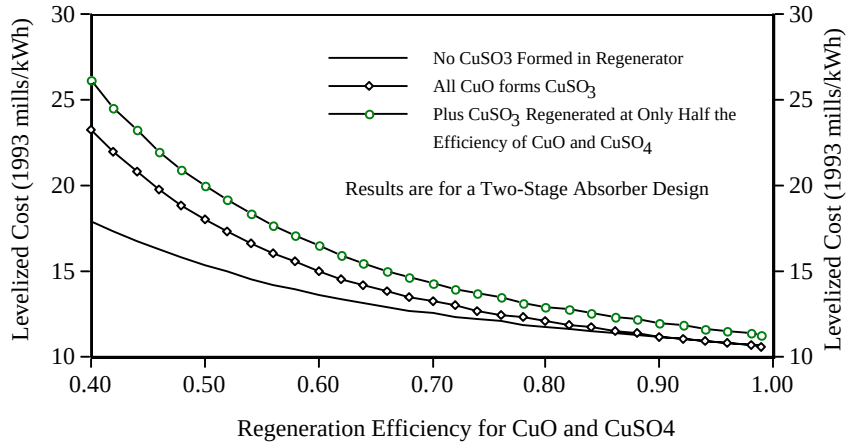

Figure 7-16 Sensitivity of Levelized Cost to Regeneration Efficiencies.

7.5.5. Regenerator Inlet Temperature

The regenerator sorbent residence required to achieve a given regeneration efficiency is a function of the temperature of the inlet sorbent. This sensitivity is shown in Figure 7-17, together with a sensitivity analysis for the total methane required for the copper oxide process. As the sorbent inlet temperature is reduced, the kinetics of the regeneration reactions slow, leading to a requirement for a longer sorbent residence time to achieve a given copper sulfate conversion efficiency to copper. As temperature is reduced, however, less methane is required in the solids heater combustor to provide hot gases for sorbent heating.

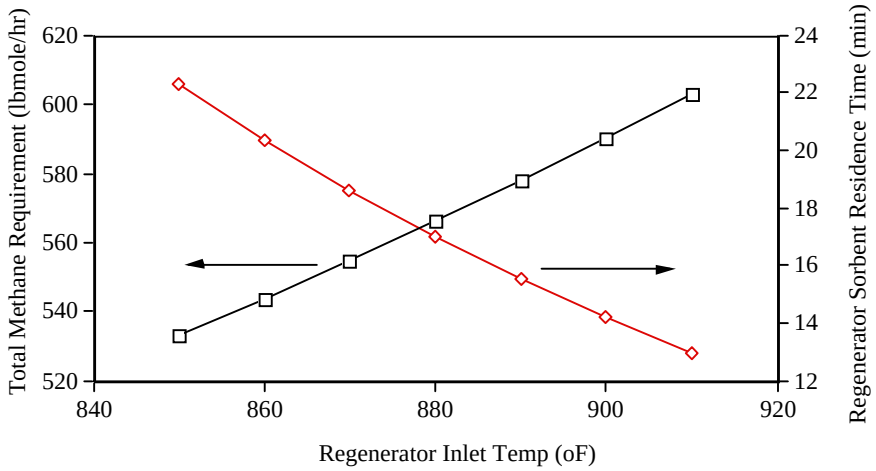

Figure 7-17 Sensitivity of Total Methane Requirement and Regenerator Residence Time to the Regenerator Inlet Temperature.

The net effect of varying the regenerator sorbent inlet temperature on the levelized cost of the copper oxide process is shown in Figure 7-18. As the inlet temperature is reduced, the levelized costs are also reduced. The previous base case assumption was an inlet temperature of 900°F, which results in a levelized cost of 12.04 mills/kWh. Reducing the inlet temperature to 850°F results in a levelized cost of 11.82 mills/kWh. While this is a modest savings on a percentage basis, for a 500 MW power plant operating at a 65 percent capacity factor this represents a savings of over $600,000/year. Further savings may be possible through additional reductions in the regenerator inlet temperature. However, such savings cannot be investigated with the current version of the residence time model. A simplified residence time model, Equation (7-33), is employed in the integrated performance and cost model of the copper oxide process. This model was developed based on the range of temperatures shown in Figure 7-18, and cannot be extrapolated. Development of a new response surface model sensitive to a wider range of temperatures is a need for future work.

A detailed comparison of a two-stage based absorber design with regenerator sorbent inlet temperatures of 900°F and 850°F is given in Table 7-10. The lower regenerator inlet temperature is used as the basis for further evaluation studies.

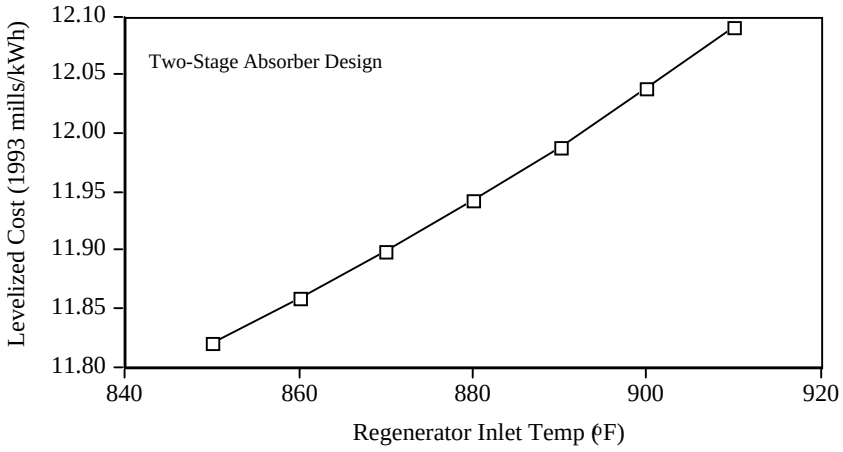

Figure 7-18 Sensitivity of Total Methane Requirement and Regenerator Residence Time to the Regenerator Inlet Temperature.

Table 7-10 ***Capital, Annual, and Levelized Costs for the Fluidized Bed Copper Oxide Process: Effect of Regeneration Temperature on Costs[a]***

	Regenerator Temperature	
Description	**900°F**	**850°F**
NH_3 Handling and Injection, M$	2.036	2.036
Fluidized Bed Absorber Capital, M$	6.381	6.381
ID Fan Differential, M$	0.413	0.414
Solids Heater, M$	3.101	2.756
Regenerator, M$	3.219	3.540
Sorbent Transport System, M$	7.255	7.258
Solids Heater Combustor, M$	3.357	2.668
Sulfur Recovery Plant, M$	12.784	12.785
Air Preheater Modifications, M$	4.437	3.784
Sorbent Inventory, M$	5.741	6.170
Total Direct Capital Cost, M$	53.022	51.956
Eng. & Home Office Fees, M$	7.953	7.793
Process Contingency, M$	12.195	11.950
Project Contingency, M$	6.833	6.626
Total Plant Cost ("overnight"), M$	80.003	78.326
Interest, M$ (current dollars)	7.565	7.406
Total Plant Investment, M$	87.568	85.732
Startup (Preproduction) Cost, M$	3.869	3.782
Working (Inventory) Capital, M$	0.215	0.208
Land Cost, M$	0.028	0.028
Total Capital Cost, M$	91.680	89.749
Total Capital, $/kW	194.922	191.428
Fixed Operating Cost, M$/yr	5.317	5.232
Sorbent Cost, M$/yr	12.828	12.884
Methane Cost, M$/yr	6.034	5.451
Ammonia Cost, M$/yr	0.795	0.795
Miscellaneous, M$/yr	0.441	0.441
Variable Operating Cost, M$/yr	20.098	19.571
Total O&M Cost, M$/yr	19.808	19.345
Revenue w/o Utilities, M$/yr	29.286	28.624
Utilities, M$/yr	2.975	2.954
Total Revenue, M$/yr	32.261	31.578
Total Rev, mills/kWh	12.038	11.821

[a] All costs are reported in 1993 dollars. Variable operating costs and levelized costs are calculated using a 65 percent plant capacity factor. The absorber capital cost for the two-stage design does not include any additional costs associated with a second stage distributor plate. The two-stage design is based on a lower stage with a 16-inch height operating at 30 % sulfur capture efficiency. The upper stage is approximately 37 inches in height and operates at approximately 86 percent sulfur capture efficiency. The first case is for a regenerator sorbent inlet temperature of 900°F. The second case is for a regenerator sorbent inlet temperature of 850°F.

7.6. Probabilistic Analysis

A probabilistic analysis was performed to evaluate uncertainties in the copper oxide process. This technology has been tested on only a small-scale, with no large-scale commercial experience that is required to verify expectations of performance and cost. Therefore, any estimate of performance or cost for this technology is subject to uncertainty.

A probabilistic analysis requires input assumptions or data regarding the uncertainties in key process and economic parameters. There are several types of uncertainty in trying to predict the commercial-scale performance and cost of a new process technology. These include statistical error, systematic error, variability, and lack of an empirical basis for concepts that have not been tested. Uncertainties may apply to different aspects of the process, including performance variables, equipment sizing parameters, process area capital costs, requirements for initial catalysts and chemicals, indirect capital costs, process area maintenance costs, requirements for consumables during plant operation, and the unit costs of consumables, byproducts, wastes, and fuel. Model parameters in any or all of these areas may be uncertain, depending on the state of development of the technology, the level of detail of the performance and cost estimates, and future market conditions for new chemicals, catalysts, byproducts, wastes, and other process components.

It may not always be possible to develop estimates of uncertainty based on classical statistical analysis, nor would such an approach be appropriate in many cases. Particularly for new process technologies, data may be lacking regarding some types of uncertainty. For example, the effect of scale-up on process performance may not be fully understood. Thus, analysis of bench-scale test data alone may be an insufficient basis for estimating the total uncertainty in a variable. When data are lacking, estimates of uncertainty must rely on the informed judgments of technical experts. Judgments regarding uncertainties can be encoded as probability distributions, using techniques discussed elsewhere (see Appendix A for an overview).

7.6.1. Input Uncertainty Assumptions

Uncertainties in specific performance and cost parameters were explicitly characterized using probability distributions. Identification of parameters that should be treated probabilistically, and the estimates of uncertainties for these parameters, were based on literature review, data analysis, and elicitation of expert judgments from USDOE FETC process engineers involved in technology development. This approach has also been applied by Frey et al. (1994) for evaluating an integrated gasification combined cycle (IGCC) system.

Table 7-11 ***Summary of Deterministic and Uncertainty Assumptions for the Fluidized Bed Copper Oxide Process.***[a]

		Distributions and their Parameters				
DESCRIPTION AND UNITS	**Det. Val.**	**Type**	**Min**		**Max**	**Mode**
Sorbent Attrition in Fluidized Bed, wt-% of total bed inventory	0.02	T	0.01	to	0.02	(0.011)
Sorbent Attrition in Transport, wt-% of sorbent flow rate	0.047	T	0.02	to	0.047	(0.047)
CuO Converted to $CuSO_3$ in Reg., fraction	1	T	0.45	to	1	(0.6)
Regeneration Efficiency for $CuSO_3$, frac.	0.8	U	0.4	to	0.8	
Standard Error of Estimate for Avail. Cu/S ratio, fraction of model estimate	1	N	0.9	to	1.1	(1)
Expanded Sorbent Density, lb/ft^3	26.6	T	24.5	to	28.7	(26.6)
Relative Enthalpy of $CuSO_3$ Compared to $CuSO_4$, fraction	0.8	T	0.7	to	0.9	(0.8)
Standard Error of Estimate of Regenerator Residence Time, min	0	N	-2	to	2	(0)
Ammonia Cost, $/ton	158	U	158	to	237	(158)
Natural Gas Cost, $/mscf	4.75	N	4.35	to	5.15	(4.75)
Sorbent Cost, $/lb	5.00	T	2.50	to	5.00	(5.00)
Sulfur Sales Price, $/ton	132	T	66	to	132	(132)
Indirect Cost Factor, fraction of direct cost	0.45	N	0.36	to	0.54	(0.45)
General Facilities Cost Factor, fraction	0.10	N	0.08	to	0.12	(0.10)
Eng. & Home Office Fees cost, fraction	0.15	N	0.12	to	0.18	(0.15)
Project Contingency, fraction	0.20	N	0.12	to	0.28	(0.20)
Absorber Direct Cost Contingency and Uncertainty, fraction	0.20	N	0.08	to	0.32	(0.20)
Ammonia Inj. DC Cont. and Unc., frac.	0.20	N	0.08	to	0.32	(0.20)
ID Fan Differ. DC Cont. and Unc., frac.	0.10	N	0.04	to	0.16	(0.10)
Regenerator DC Cont. and Unc., frac.	0.20	N	0.08	to	0.32	(0.20)
Solids Heater DC Cont. and Unc., frac.	0.20	N	0.08	to	0.32	(0.20)
Sorbent Trans. DC Cont. and Unc., frac.	0.20	N	0.08	to	0.32	(0.20)
Solids Htr Comb. DC Cont. & Unc., frac.	0.20	N	0.08	to	0.32	(0.20)
Sulfur Plant DC Cont. and Unc., frac.	0.10	N	0.04	to	0.16	(0.10)
Air Preheater Mod. DC Cont. & Unc., frac.	0.10	N	0.04	to	0.16	(0.10)
Total Direct Cost Uncertainty, factor	1	N	0.8	to	1.2	(1)
Pre-Production Cost Factor, frac.	0.02	N	0.016	to	0.024	(0.02)
Inventory Capital Cost Factor, frac	0.005	N	0.004	to	0.006	(0.005)
Maintenance Cost Factor, frac.	0.045	N	0.036	to	0.054	(0.045)

[a] DET. VAL. = deterministic (point-estimate) value. Five columns are shown to define probability distributions. The first indicates the type of distribution, where T = triangular, N = normal, and U = uniform. The remaining four columns provide the parameters of the distribution. For the uniform, the lower and upper bounds are given. For the triangular, the lower and upper bounds, and the mode (most likely) value are given. For the normal, the lower and upper bounds of the 95 percent confidence interval, and the mode, are given.

The characterization of performance uncertainties focused on sorbent attrition, sorbent regeneration, and parameters affecting sulfation in the absorber. Uncertainties in additional cost model parameters also were characterized, including direct and indirect capital costs, operating and maintenance costs, and the unit costs of consumables, byproducts, and wastes. These assumptions are given in Table 7-11.

Several of the input assumptions are shown graphically. The uncertainties for sorbent bed attrition and circulation attrition were assigned triangular distributions, as shown

in Figure 7-19 and Figure 7-20, respectively. In the case of bed attrition, experts at USDOE FETC believed that the performance of the copper oxide sorbent would be similar to that of the NOXSO sorbent, for which more test data and experience has been accumulated. While the default assumption is 0.02 weight-percent attrition as a percentage of the absorber bed inventory, it was felt that the attrition rate would improve with better sorbent formulations and improved absorber design. Thus, a "most likely" value representative of NOXSO experience was employed. For the circulation attrition rate, the default assumption is believed to be conservative. It was assumed that this value may actually be highly uncertain, and may be able to attain significantly lower values than the default. However, the distribution is weighted toward higher values.

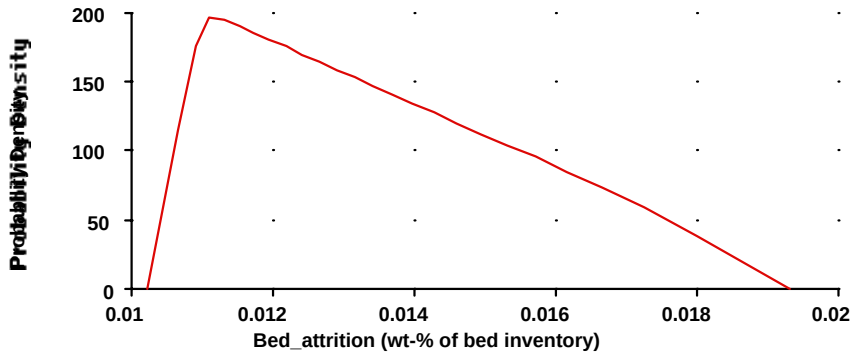

Figure 7-19Uncertainty Assumption for the Sorbent Bed Attrition Rate.

The uncertainty in the fractional conversion of CuO to $CuSO_3$ at the regenerator inlet is shown in Figure 7-21. This distribution is based on a judgment by USDOE FETC engineers for a regenerator sorbent inlet temperature of 850°F. The distribution is considerably broad due to the scarcity of data for characterizing this parameter. There is also considerable uncertainty as to whether $CuSO_3$ is formed, versus some other possible compounds containing copper and oxygen.

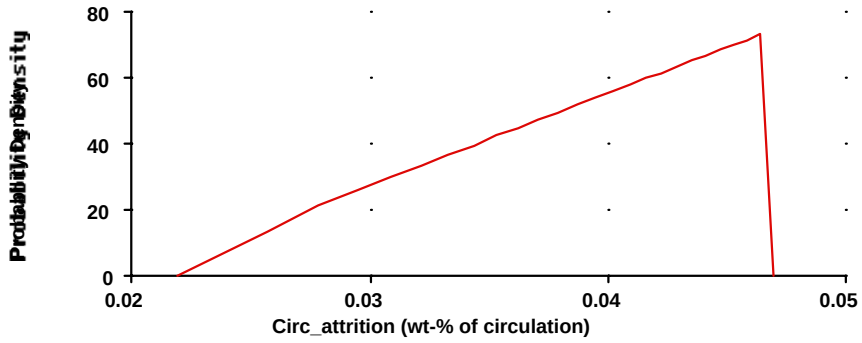

Figure 7-20 Uncertainty Assumption for the Sorbent Circulation Attrition Rate.

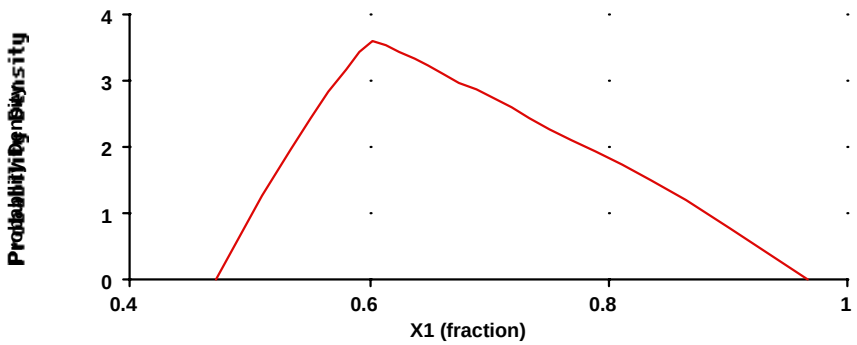

Figure 7-21 Uncertainty Assumption for the Fractional Conversion of CuO to $CuSO_3$ at the Regenerator Inlet.

The uncertainty in the regeneration efficiency for $CuSO_3$ is characterized as uniform distribution (see Figure 7-22), based on a judgment by USDOE FETC personnel. The lower end of the range represents a tentative observation in some preliminary experimental work on the kinetics of copper oxide sorbent regeneration. The upper end represents expectations for the regeneration of copper sulfate in a commercial scale regenerator.

The sorbent expanded density has exhibited considerable variability in previous experimental work. This variability is represented by the triangular distribution shown in Figure 7-23.

The uncertainty in sorbent unit cost is shown in Figure 7-24. USDOE FETC personnel believe that the sorbent cost will be reduced from its nominal value of $5/lb with commercialization of the technology and mass production of the sorbent.

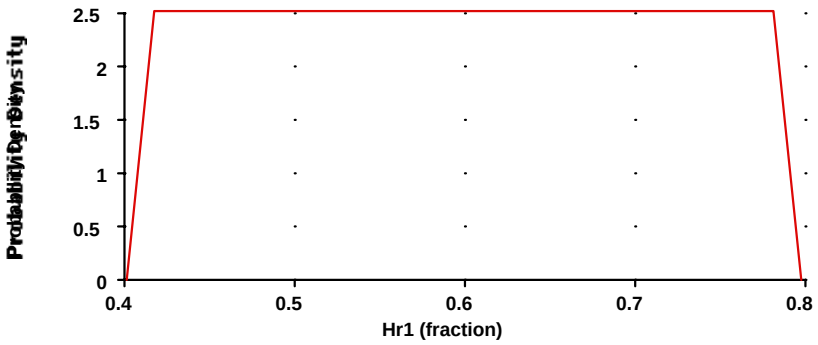

Figure 7-22 Uncertainty Assumption for the Regeneration Efficiency of $CuSO_3$.

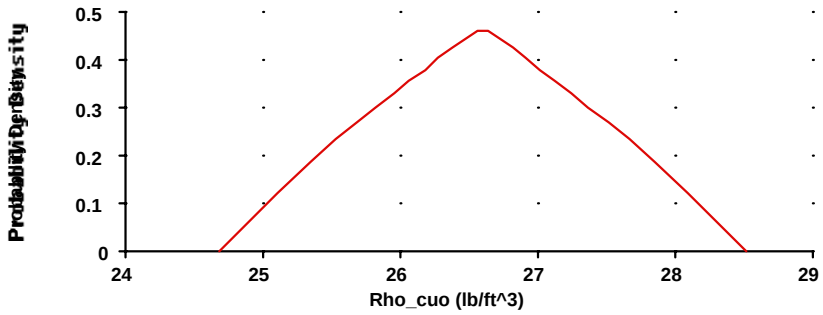

Figure 7-23 Uncertainty Assumption for the Sorbent Expanded Density.

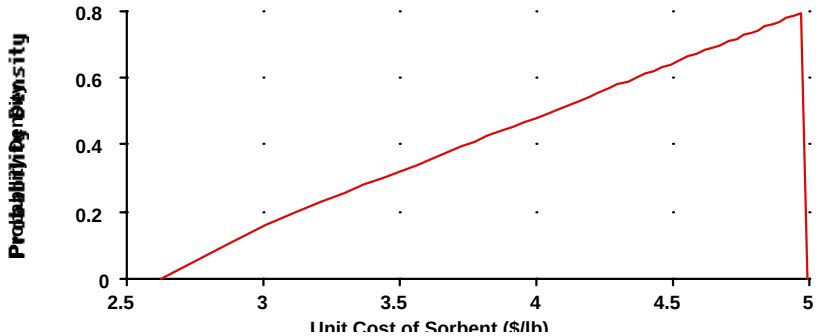

Figure 7-24 Uncertainty Assumption for the Sorbent Unit Cost.

Uncertainties in the cost parameters of the model are based on nominal assumptions and previous analyses of this and other power generation and environmental control technologies. For example, many of the multipliers used in capital cost models, such as engineering and home office fees, are estimated based on rules-of-thumb from recommended ranges of data. In such cases, the entire recommended range, rather than a single point estimate, is employed and represented as a distribution. In the case of contingency factors, uncertainty distributions were assigned to these to represent the lack of a detailed basis for selecting a single point value. These direct capital cost uncertainty distributions represent both the systematic error and uncertainty in predicted direct capital costs for each process area. See Frey and Rubin (1991, 1992) and Frey (1991) for more details on previous case studies.

7.6.2. Characterizing Uncertainty in Performance and Cost

The uncertainties in Table 7-11 were propagated through the performance and cost model of the copper oxide model using the probabilistic modeling features of the IECM. Selected examples of output results are shown in Figure 7-25 through Figure 7-34.

The first example is the regenerator residence time, which varies from approximately 22 minutes to 29 minutes as a result of uncertainties in factors such as the fractional conversion of copper oxide to copper sulfite at the regenerator inlet, and the standard error of the estimate for the residence time response surface model. Another example of a performance-related uncertainty is the copper-to-sulfur molar ratio. This varies from approximately 1.05 to 1.35, as shown in Figure 7-26. The copper-to-sulfur molar ratio is a key factor affecting the sorbent circulation rate, which is shown in Figure 7-27. The sorbent circulation rate varies from approximately 500,000 lb/hr to 700,000 lb/hr. This uncertainty in circulation rate results in uncertainty in the size and, hence, cost, of many equipment items in the copper oxide process.

An example of a capital cost uncertainty is shown in Figure 7-28 for the direct capital cost of the fluidized bed absorber. This varies from approximately six to seven million dollars, with 95 percent confidence. The uncertainty in regenerator residence time and sorbent circulation rate directly affect the sizing and cost of the regenerator vessel. The uncertainty in the cost of this vessel is shown in Figure 7-29. The 95 percent confidence interval for this vessel encloses a range of approximately $100,000. The uncertainty in the direct cost for all components of the regeneration process area is shown in Figure 7-30. The 95 percent confidence interval for the entire process area encloses a range of $500,000.

A performance uncertainty which affects the O&M cost is the make-up sorbent flow rate, shown in Figure 7-31. This flow rate is uncertain by a factor of approximately two.

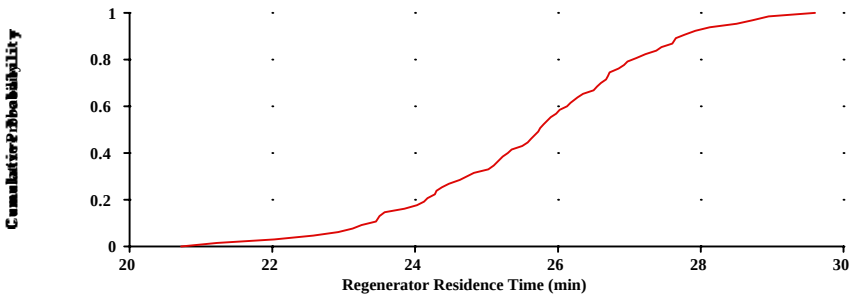

Figure 7-25 Uncertainty Result for Regenerator Residence Time.

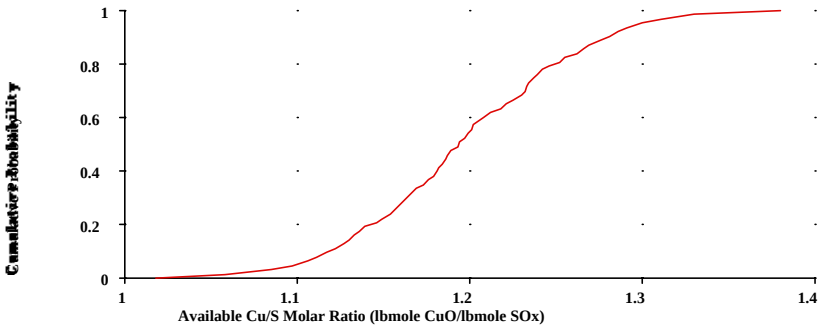

Figure 7-26 Uncertainty Result for Available Copper-to-Sulfur Molar Ratio.

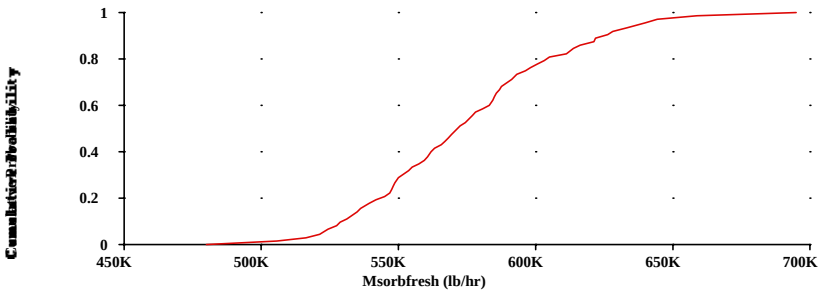

Figure 7-27 Uncertainty Result for Sorbent Circulation Rate (on a Fresh Basis).

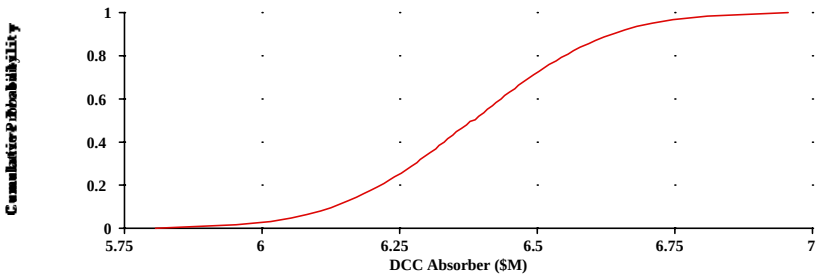

Figure 7-28 Uncertainty Result for the Direct Cost of the Absorber Process Area.

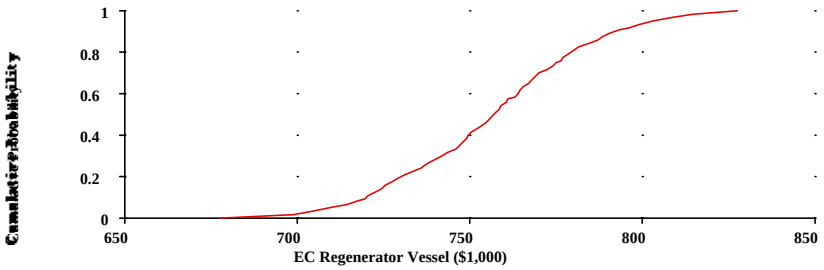

Figure 7-29 Uncertainty Result for the Equipment Cost of the Regenerator Vessel.

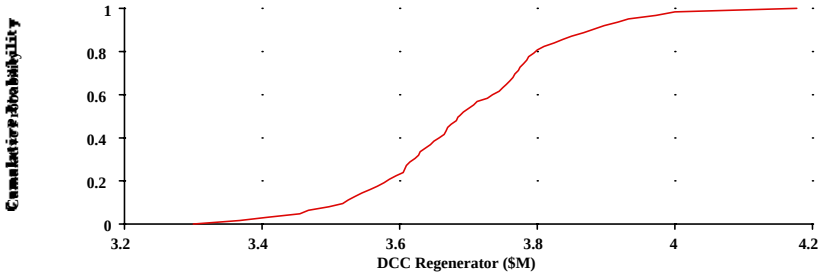

Figure 7-30 Uncertainty Result for the Direct Capital Cost of the Regenerator Process Area.

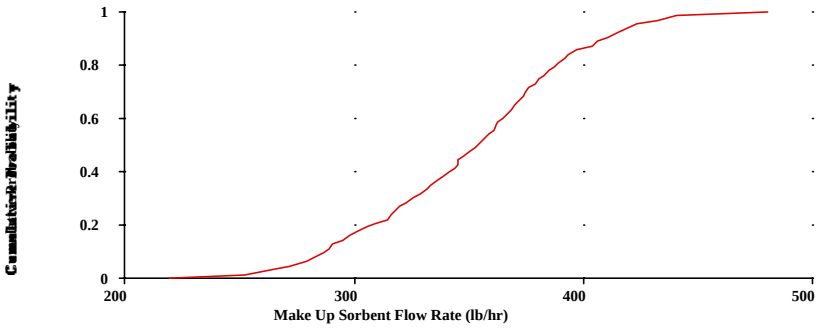

Figure 7-31 Uncertainty Result for the Make-Up Sorbent Flow Rate.

The ultimate measures of process viability are the total capital, annual, and levelized costs. The uncertainty in these parameters are shown in Figure 7-32, Figure 7-33, and Figure 7-34, respectively. Recall from Table 7-10 that the estimated deterministic capital cost was $191/kW, taking into account typical values of contingency factors employed in previous analyses. This corresponds closely to the mean value from the probabilistic simulation, which is $189/kW. The probabilistic analysis, however, indicates that there is a substantial probability that the capital cost could be higher than the nominal deterministic value, and may in fact by higher by $50/kW.

The deterministic estimate of 11.8 mills/kWh for the levelized cost of the copper oxide process is at the upper end of the distribution from the probabilistic simulation. Thus, it appears that potentially overly conservative assumptions may have been made in the deterministic estimate with regard to factors such as sorbent attrition and sorbent unit cost, which were assigned skewed distributions based on judgments by and discussions with process experts. The mean estimate for the levelized cost is 10.4 mills/kWh, or approximately 1.4 mills/kWh lower than the deterministic estimate.

In some ways, these results are contrary to general trends observed for cost estimates developed for technologies in early stages of development. Often, the cost of technologies are underestimated, and the performance is overestimated (e.g., Merrow et al., 1981). This trend has been observed in similar analyses of other process technologies (e.g., Frey and Rubin, 1992a). However, in this case, it appears at least somewhat plausible that the deterministic estimate may actually overestimate average costs, due to the importance of only a handful of parameters in influencing the uncertainty in levelized costs. The sensitivity of the results to specific uncertainty assumptions is considered in the next section.

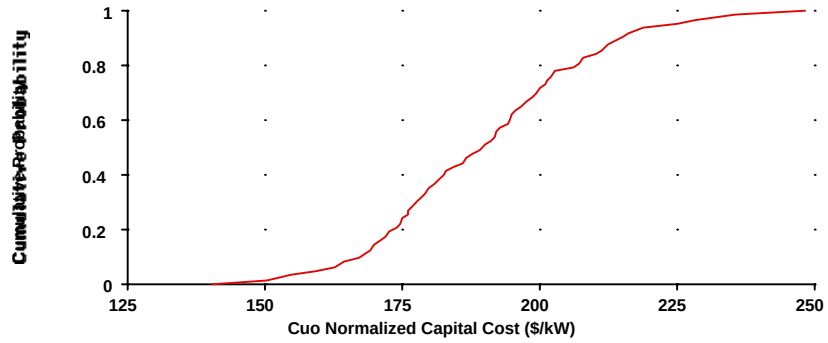

Figure 7-32 Uncertainty Result for the Copper Oxide Process Total Capital Cost.

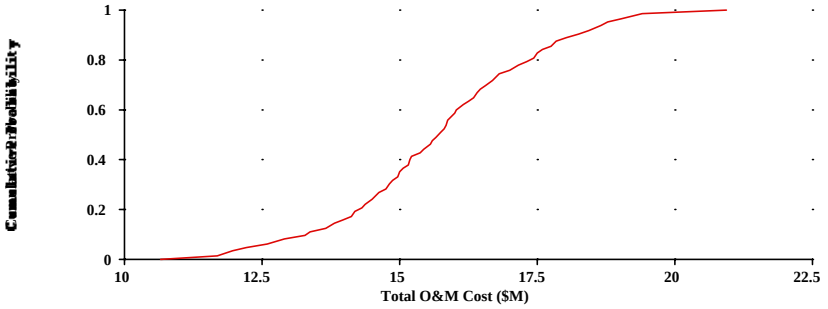

Figure 7-33 Uncertainty Result for the Copper Oxide Process Total Operating and Maintenance Cost.

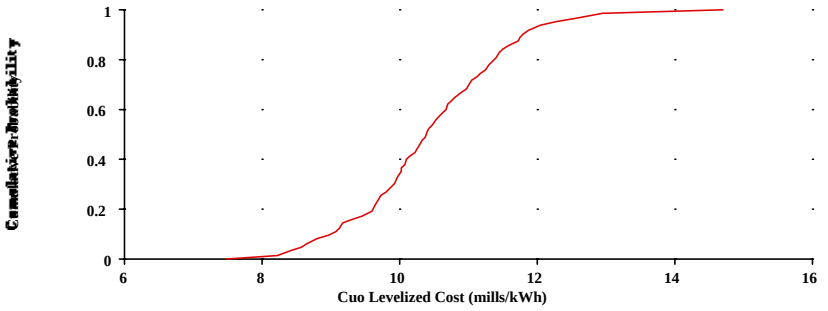

Figure 7-34 Uncertainty Result for the Copper Oxide Process Total Levelized Cost.

7.6.3. Identifying Key Sources of Uncertainty

One of the key advantages of probabilistic modeling is the capability to identify the key sources of uncertainty in model results when many model input variables are simultaneously uncertain. One technique for identifying key uncertainties is the use of rank correlation coefficients. The rank correlation coefficient provides a measure of the strength of the linear dependence between the rank ordering of sample values for model outputs (e.g., capital cost) to the rank ordering of sample values for model inputs (e.g., uncertainty in regeneration efficiency).

Five model output variables were selected for statistical analysis to identify key input sources of uncertainty. These are the available copper-to-sulfur molar ratio,

sorbent circulation rate, total capital cost, total O&M cost, and levelized cost. Approximately 30 inputs to the copper oxide process performance and economic models were specified as probability distributions. Therefore, the sensitivity of each of these five model output variables were evaluated with respect to each of the thirty input uncertainties, except in cases where no dependence exists. For example, the Cu/S ratio is not dependent on any of the economic uncertainty input assumptions.

A summary of the rank correlation results is given in Table 7-12. Strong correlations are highlighted with bold text. The uncertainty in the Cu/S ratio is most highly correlated with uncertainty in the standard error of the estimate of the Cu/S ratio, regeneration efficiency for copper sulfite, and the expanded sorbent density. The uncertainty in sorbent circulation rate is also most highly correlated with the standard error of the estimate of the Cu/S ratio. However, the input uncertainties which most influenced uncertainty in the Cu/S ratio and sorbent flow rate have little impact on the uncertainties in process costs. The capital cost uncertainty is most highly correlated with uncertainties in parameters of the capital cost model itself. Thus, uncertainty in capital cost is not driven, in this case, by uncertainties in performance parameters. This result is somewhat atypical of technologies which are not yet commercialized, for which many performance uncertainties must be resolved as a condition for developing more robust capital cost estimates. However, it is important to note that one effect of the adoption of a two-stage absorber design, versus the single-stage design employed in many previous evaluations, is a substantial reduction in overall sorbent circulation rates. This leads to a substantial reduction in the influence of sulfation-related uncertainties on uncertainties in process economics, and leads to a proportionally larger contribution from equipment cost uncertainties.

The O&M uncertainty is driven by both performance and cost parameter uncertainties. The sorbent attrition rate uncertainty, as represented by uncertainties in both bed and circulation attrition, results in substantial uncertainty in the sorbent make-up rate (a factor of two, as previously illustrated). Combined with the uncertainty in the future cost of commercially produced copper oxide sorbent, the O&M cost uncertainty is closely linked to sorbent replacement cost uncertainty. Uncertainties in sulfur byproduct markets also significantly influence O&M cost uncertainty.

The key factors driving uncertainty in levelized cost illustrate a key advantage of probabilistic analysis over conventional point-estimate approaches using contingency factors and other multipliers to account for uncertainty. The uncertainty in levelized cost is driven by a performance-related uncertainty (sorbent attrition), a capital cost related uncertainty (total direct cost), and an annual cost uncertainty (sorbent unit cost). These three sources of uncertainty interact to significantly affect uncertainty in levelized cost. This type of simultaneous interaction among performance and cost uncertainties is not addressed in traditional cost estimating approaches.

An alternative approach to identifying key uncertainties is to use a technique that might be described as "probabilistic sensitivity analysis". This approach is illustrated in Figure 7-35. The contributions of various groups of uncertain parameters to the uncertainty in levelized cost is evaluated by running the copper oxide process models with probabilistic values for selected groups of variables, while holding all other variables at their nominal (deterministic) values. The results of this sensitivity analysis indicate that the range of values for levelized costs is determined mostly by the range of values from the economic-related uncertainties, but that the performance and economic uncertainties interact to shift the total costs of the process downward. This effect results from the negative skewness of many of the distributions and to differences between the deterministic assumptions, which may be overly conservative in some cases, and the most likely values in the probabilistic assumptions.

Table 7-12 ***Absolute Values of Rank Correlations Between Key Model Outputs and Input Uncertainties.***

	Selected Model Outputs				
DESCRIPTION AND UNITS	**Cu/S**	**m_S**	**TCC**	**O&M**	**COE**
Sorbent Attrition in Fluidized Bed, wt-% of total bed inventory			0.04	**0.28**	0.14
Sorbent Attrition in Transport, wt-% of sorbent flow rate			0.12	**0.53**	**0.38**
CuO Converted to $CuSO_3$ in Reg., fraction	0.04	**0.19**	0.03	0.03	0.02
Regeneration Efficiency for $CuSO_3$, frac.	**0.21**	**0.47**	**0.19**	0.18	0.16
Standard Error of Estimate for Avail. Cu/S ratio, fraction of model estimate	**0.96**	**0.86**	0.16	0.14	0.15
Expanded Sorbent Density, lb/ft^3	**0.19**	0.18	0.09	0.04	0.00
Relative Enthalpy of $CuSO_3$ Compared to $CuSO_4$, fraction	0.09	0.12	0.06	0.10	0.11
Standard Error of Estimate of Regenerator Residence Time, min			0.04	0.07	0.09
Ammonia Cost, $/ton			0.05	0.06	0.02
Natural Gas Cost, $/mscf			0.08	0.12	0.03
Sorbent Cost, $/lb			0.09	**0.60**	**0.39**
Sulfur Sales Price, $/ton			0.05	**0.28**	0.15
Indirect Cost Factor, fraction of direct cost			0.16	0.01	0.01
General Facilities Cost Factor, fraction			0.04	0.04	0.04
Eng. & Home Office Fees cost, fraction			0.07	0.03	0.00
Project Contingency, fraction			**0.30**	0.06	0.08
Absorber Direct Cost Contingency and Uncertainty, fraction			0.03	0.08	0.02
Ammonia Inj. DC Cont. and Unc., frac.			0.01	0.12	0.07
ID Fan Differ. DC Cont. and Unc., frac.			0.04	0.02	0.02
Regenerator DC Cont. and Unc., frac.			0.02	0.09	0.05
Solids Heater DC Cont. and Unc., frac.			0.02	0.03	0.01
Sorbent Trans. DC Cont. and Unc., frac.			0.06	0.01	0.01
Solids Htr Comb. DC Cont. & Unc., frac.			0.05	0.08	0.06
Sulfur Plant DC Cont. and Unc., frac.			0.06	0.02	0.03
Air Preheater Mod. DC Cont. & Unc., frac.			0.01	0.05	0.05
Total Direct Cost Uncertainty, factor			**0.89**	0.19	**0.38**
Pre-Production Cost Factor, frac.			0.18	0.04	0.00
Inventory Capital Cost Factor, frac			0.05	0.13	0.04
Maintenance Cost Factor, frac.			0.06	0.12	0.05

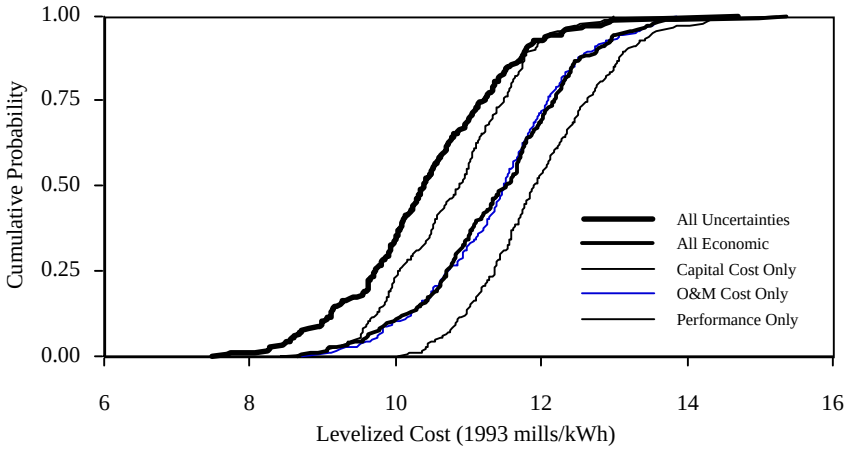

Figure 7-35 Uncertainty Result for the Copper Oxide Process Total Levelized Cost.

7.6.4. Evaluating Design Trade-Offs Probabilistically

The significant levels of uncertainty identified in key measures of process performance suggest that comparisons of design alternatives should be evaluated taking into account uncertainties. For example, a key result from the deterministic sensitivity analyses in the previous chapter was that the cost of a two-stage absorber-based system would offer substantial cost savings compared to a single-stage absorber based system. A nominal cost savings of 1.4 mills/kWh was estimated. This result is revisited using probabilistic assumptions.

The results of a comparison based on the difference in levelized cost for a one-stage absorber system versus a two-stage absorber system is shown in Figure 7-36. The difference is carefully calculated by pairing samples values from two probabilistic simulations, one for each design option. Because the input uncertainties are correlated between the two systems, this pairing is required. The sample values from the two-stage simulation were subtracted from the corresponding paired sample values for the one-stage system.

The results show considerable uncertainty in the total savings, ranging by a factor of approximately four from 0.7 to 2.8 mills/kWh. However, these results do illustrate that there is certain to be a cost savings, and that the cost savings may be substantially higher than the deterministic estimate.

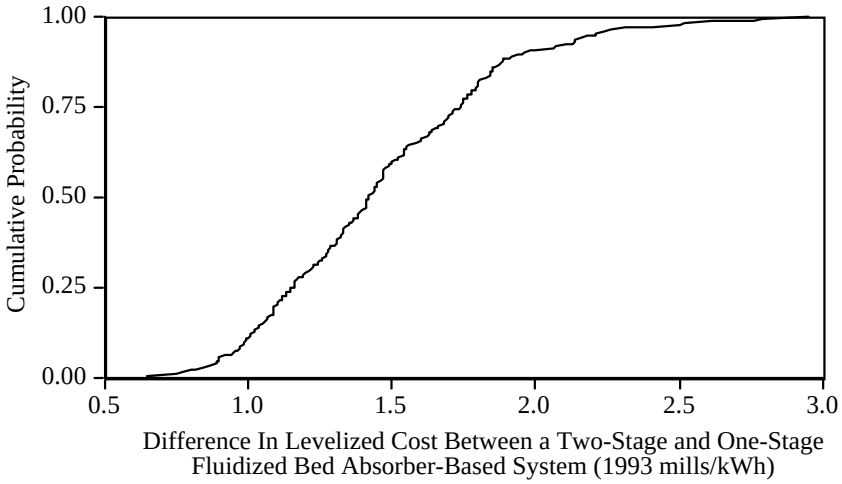

Figure 7-36 Uncertainty in the Cost Savings for a Two-Stage Absorber System Versus a One-Stage Absorber System.

7.7. Discussion and Future Work

A detailed performance and cost model of the copper oxide process has been developed. This model was applied in a series of key sensitivity and probabilistic analyses to identify key factors which affect process uncertainties and which merit further investigation. However, to determine the priority of further work on this technology requires additional comparative evaluations of the copper oxide process with respect to competing options such as flue gas desulfurization and selective catalytic reduction, and other combined SO_x/NO_x processes such as the NOXSO process. Such analyses are planned for future work. In addition, other variants of the copper oxide process, such as the moving bed process, may offer cost savings compared to the fluidized bed process. These, too, will be investigated in future work.

The results here provide a road map for further refinement of the model and the uncertainty estimates. Other applications of the probabilistic evaluation method not discussed here include: (1) evaluation of the reductions in uncertainty that may be obtained from further process research; (2) evaluation of alternative judgments regarding model parameter uncertainties by different experts as they affect model results; (3) evaluation of the importance of correlation structures in model parameter uncertainties; (4) comparative analysis of competing technologies under uncertainty; and (5) the use of decision analysis techniques to interpret modeling results. These types of applications are discussed elsewhere (e.g., Frey, 1991).

Significant uncertainties inevitably surround advanced environmental control technologies in the early stages of development. Thus, engineering performance and cost models developed to evaluate process viability must be capable of adequately analyzing and displaying the consequences of these uncertainties. Toward this end, the probabilistic modeling capability described here allows the effect of uncertainties in multiple performance and cost parameters to be evaluated explicitly. The results give a measure of overall uncertainty in key model outputs, such as cost, and serve to identify the key process variables that contribute most to overall uncertainty.

As shown in the case studies of the copper oxide process, probabilistic analysis provides explicit insights into the range and likelihood of outcomes for key measures

of plant performance and cost. In many cases, there is a probability of obtaining extreme outcomes, such as low performance or high cost, that would result in technology failure. The characterization of uncertainties in performance and cost results from the simultaneous interaction of uncertainties in many input parameters. These types of insights cannot be obtained from deterministic analysis.

Case studies for the fluidized bed copper oxide process illustrated potential applications of an integrated environmental control system framework for process design and comparative analyses. Interactions among various components of the environmental control system, which are frequently overlooked in many process studies, were found to significantly influence overall system costs. This is true, for example, in the case of air preheater modifications to capture the energy released to the flue gas in the absorber for use in heating the boiler combustion air. Probabilistic comparisons between advanced and conventional technologies can also provide quantitative assessments of the potential benefits and risks of new technology in various market situations. The potential payoff from process research and development also may be evaluated using the methods described here.

Of course, as with any other modeling approach, probabilistic methods rely on data and judgments that must be provided by the user. To be sure, different judgments or assumptions can alter the results. But forcing process developers and evaluators to consider uncertainties explicitly (rather than ignore them) in probabilistic engineering models can help improve research planning and management by allowing the implications of alternative judgments to be tested. Indeed, experience to date suggests that the process of thinking about key parameter uncertainties, as inputs to a model, often is the most valuable component of this approach that fosters improved understanding of the systems being modeled.

7.8. Nomenclature

A = Fluidized bed area, ft^2

F_s = Sorbent feed rate at absorber inlet, fresh sorbent basis, lb/min

G_{FG} = Volumetric flue gas flow rate at absorber inlet, ft^3/min

I_b = Bed inventory, lb

k_s = Reaction rate constant, 1/(min•atm)

m_s = Sorbent mass flow rate, lb/hr

M_i = Molar flow rate of species i, lbmole/hr

$M_{i,j,k}$ = Molar flow rate of species i at process area j's inlet or outlet k (e.g., $M_{SO_2,a,i}$ = molar flow of SO_2 at the absorber inlet), lbmole/hr

MW_{Cu} = Molecular weight of copper, 63.54 lb/lbmole

MW_{CuO} = Molecular weight of copper oxide, 79.54 lb/lbmole

MW_{CuSO3} = Molecular weight of copper sulfite, 143.54 lb/lbmole

MW_{CuSO4} = Molecular weight of copper sulfate, 159.54 lb/lbmole

P = Absorber inlet pressure, atm

r_{abs} = Internal radius of absorber, feet

r_{ves} = Radius of steel absorber vessel, feet

R	=	Absorber Inlet Available Cu to inlet SO_2 molar ratio, lbmole CuO/lbmole SO_2
t_{hr}	=	Thickness of hot refractory, feet
t_{ir}	=	Thickness of inner or base refractory, feet
$t_{r,a}$	=	Absorber solids residence time, min
T	=	Absorber bed temperature, K
V_s	=	Superficial flue gas velocity at absorber inlet, ft/sec
W_{Cu}	=	Weight fraction Cu as CuO in fresh sorbent, lb Cu/lb sorbent
x	=	molar fraction of copper as copper sulfate at the regenerator inlet
x_1	=	molar fraction of copper oxide converted to copper sulfite just inside regenerator
y_i	=	SO_2 inlet flue gas concentration, lbmoles SO_2/lbmole flue gas
y_o	=	SO_2 outlet flue gas concentration, lbmoles SO_2/lbmole flue gas
Z	=	Fluidized bed height, ft

7.8.1. Greek Letter Symbols

α	=	Kinetic parameter (dimensionless)
η_r	=	Overall sorbent regeneration efficiency, fraction
η_{r1}	=	Regeneration efficiency for copper sulfite, fraction
η_{r2}	=	Regeneration efficiency for copper sulfate, fraction
η_{r3}	=	Regeneration efficiency for copper oxide, fraction
η_s	=	SO_2 removal efficiency, fraction
ρ_s	=	Sorbent density (expanded bed), lb/ft^3

7.8.2. Subscripts

A	=	Absorber
Cu	=	Copper
CuO	=	Copper Oxide
$CuSO_3$	=	Copper Sulfite
$CuSO_4$	=	Copper Sulfate
fresh	=	Sorbent on a fresh basis
i	=	Inlet
o	=	Outlet
R	=	Regenerator
s	=	Sorbent
SO_2	=	Sulfur dioxide

SO_3 = Sulfur trioxide

SO_x = All sulfur oxide species

7.9. References

A. E. Roberts and Associates, Inc. (1994). Conceptual Design and Economic Evaluation of the Fluidized Bed Copper Oxide Process. Prepared for UOP, Inc. and the U.S. Department of Energy. March.

Barin, I., and O. Knacke (1973). *Thermochemical Properties of Inorganic Substances*. Springer-Verlag, New York.

Barin, I., O. Knacke, and O. Kubaschewski (1977). *Thermochemical Properties of Inorganic Substances: Supplement*. Springer-Verlag, New York.

Chase., M.W., et al. (1985). "JANAF Thermochemical Tables, Third Edition, Part 11, Cr-Zr," *Journal of Physical and Chemical Reference Data,* Vol. 14, Supplement No. 1.

Demski, R. J., S.J. Gasior, E. R. Bauer, Jr., J. T. Yeh, J.P. Strakey, and J.I. Joubert (1982). "Simultaneous Removal of SO_2 and NO_x From Flue Gas Employing a Fluidized-Bed Copper Oxide Process," 1982 Summer Session of AIChE, August 29 to September 1.

Drummond, C. J., J. T. Yeh, J.I. Joubert, and J. A. Ratafia-Brown (1985). The Design of a Dry, Regenerative Fluidized Bed Copper Oxide Process for the Removal of Sulfur Dioxide and Nitrogen Oxides from Coal-Fired Boilers. Presented at the 78th Annual Meeting of the Air Pollution Control Association, June 16-21.

Frey, H. C. (1987). Performance and Economic Model of the Fluidized Bed Copper Oxide Process. Master's Thesis. Department of Mechanical Engineering, Carnegie-Mellon University. Pittsburgh, PA. May.

Frey, H. C., E.S. Rubin, and J.S. Salmento (1989), "Evaluation of the Fluidized Bed Copper Oxide Process Using A Probabilistic Engineering Model," *Proceedings of the Sixth Annual International Pittsburgh Coal Conference*, Pittsburgh, Pennsylvania, p. 356-365.

Frey, H. C., and E.S. Rubin (1991), "Probabilistic Evaluation of Advanced SO_2/NO_X Control Technology," *Journal of the Air and Waste Management Association*, 41(12):1585-1593 (December).

Frey, H. C., and E.S. Rubin (1992), "An Evaluation Method for Advanced Acid Rain Compliance Technology," *Journal of Energy Engineering*, 118(1):38-55 (April).

Frey, H. C., and E.S. Rubin (1992a), "Evaluation of Advanced Coal Gasification Combined-Cycle Systems Under Uncertainty," *Industrial and Engineering Chemistry Research*, 31(5):1299-1307.

Frey, H. C., E.S. Rubin, and U.M. Diwekar (1994), "Modeling Uncertainties in Advanced Technologies: Application to a Coal Gasification System with Hot Gas Cleanup," *Energy* 19(4):449-463.

Harriott, P. (1992a). Personal Communication to D. Henzel, June 3.

Harriott, P. (1992b). Personal Communication to D. Henzel, August 4.

Harriott, P. (1992c). Personal Communication to C. Frey, August 14.

Harriott, P., and J.M. Markussen (1992), "Kinetics of Sorbent Regeneration in the Copper Oxide Process for Flue Gas Cleanup," *Industrial and Engineering Chemistry Research*, 31(1):373-379.

Merrow, E.W., K.E. Phillips, and C.W. Myers (1981). Understanding Cost Growth and Performance Shortfalls in Pioneer Process Plants. Prepared by Rand Corporation for U.S. Department of Energy.

Plantz, A. R., C. J. Drummond, S. W. Hedges, and F.N. Gromicko (1986). Performance of the Fluidized Bed Copper Oxide Process in an Integrated Test Facility. Presented at the 79th Annual Meeting of the Air Pollution Control Association, Minneapolis, Minnesota. June 22-27.

Rubin, E.S., J.S. Salmento, J.G. Barrett, C.N. Bloyd, and H. C. Frey (1986). Modeling and Assessment of Advanced Processes for Integrated Environmental Control of Coal-Fired Power Plants. Prepared by the Center for Energy and Environmental Studies, Carnegie-Mellon University, for the U.S. Department of Energy. July.

Rubin, E.S., J.S. Salmento, and H. C. Frey (1988). Cost-Effective Emission Controls for Coal-Fired Power Plants. *Chemical Engineering Communications*, 74. pp. 155-167. December

Rubin, E.S., J.S. Salmento, and H. C. Frey (1989), "Evaluating Combined SO_2/NO_2 Processes," *Proceedings: Fourth Symposium on Integrated Environmental Control*, Electric Power Research Institute, Palo Alto, California, EPRI Report No. GS-6519, September, p. 6-1 to 6-15.

Rubin, E.S., J.S. Salmento, H. C. Frey, A. Abu-Baker, and M. Berkenpas (1991), *Modeling of Integrated Environmental Control Systems for Coal-Fired Power Plants*, Final Report (draft), submitted by Carnegie-Mellon University to the U.S. Department of Energy, Pittsburgh, Pennsylvania, DOE Contract No. DE-AC22-87PC79864, April, 214p.

Rubin, E.S., H. C. Frey, and M. B. Berkenpas (1992), "Development of the Integrated Environmental Control Model," *Proceedings, Eighth Annual Coal Preparation, Utilization, and Environmental Control Contractor's Conference*, U.S. Department of Energy, Pittsburgh, Pennsylvania, July 27-30, pp. 619-626.

SMC (1983a). Technical and Economic Evaluation of the Fluidized Bed Copper Oxide Flue Gas Treatment Process and Integrated Sulfur-Producing Plants. Prepared by Science Management Corporation for the U.S. Department of Energy, Pittsburgh Energy Technology Center, Pittsburgh, PA. June.

SMC (1983b). Technical and Economic Evaluation of Design Optimization Issues Associated With the Fluidized Bed Copper Oxide Flue Gas Treatment Process. Prepared by Science Management Corporation for the U.S. Department of Energy, Pittsburgh, PA. November.

SMC (1983c). Economic Evaluation of the Fluidized Bed Copper Oxide Flue Gas Treatment Process and Integrated Sulfuric Acid Plant. Prepared by Science Management Corporation for the U.S. Department of Energy, Pittsburgh, PA. April.

SMC (1984). Modeling of the Regenerator Reactor for the Fluidized Bed Copper Oxide Flue Gas Treatment Process. Prepared by Science Management Corporation for the U.S. Department of Energy, Pittsburgh, PA. May.

Williamson, R.R., J. A. Morici, and T.L LaCosse (1987). Sorbent Life Cycle Testing, Fluidized Bed Copper Oxide Process. Prepared by UOP, Inc., for the U.S. Department of Energy, Pittsburgh, PA.

Yeh, J. T., C. J. Drummond, and J.I. Joubert (1987), "Process Simulation of the Fluidized-Bed Copper Oxide Process Sulfation Reaction," *Environmental Progress*, 6(2):44-50.

Yeh, J. T., R. J. Demski, J.P. Strakey, and J.I. Joubert (1984). "PETC Fluidized-Bed Copper Oxide Process for Combined SO_2/NO_x Removal from Flue Gas," AIChE 1984 Winter National Meeting, Atlanta, March 11-14.

7.10. Appendix A. Technical Background on the CuO Process

This section provides a brief overview of the fluidized bed copper oxide process to familiarize you with the system we are modeling and to help ensure that we all have a common framework for discussing uncertainties in the process. More detail about the process and the models we employ can be found in the following papers and reports, which you may already have:

6. Frey, H. C., "Performance Model of the Fluidized Bed Copper Oxide Process for SO_2/NO_x Control," Paper 93-WA-79.01 presented at the 86th Annual Meeting of the Air & Waste Management Association, Denver, CO, June 13-18, 1993.
7. Frey, H. C., and E.S. Rubin, "An Evaluation Method for Advanced Acid Rain Compliance Technology," *Journal of Energy Engineering*, 118(1):38-55 (April 1992).
8. Frey, H. C., and E.S. Rubin, "Probabilistic Evaluation of Advanced SO_2/NO_x Control Technology," *Journal of the Air and Waste Management Association*, 41(12):1585-1593 (December 1991).
9. Rubin, E.S., M. B. Berkenpas, and H. C. Frey, "Development of the Integrated Environmental Control Model," *Proceedings, Ninth Annual Coal Preparation, Utilization, and Environmental Control Contractor's Conference*, U.S. Department of Energy, Pittsburgh, Pennsylvania, July 19-22, 1993, pp. 447-454.
10. Rubin, E.S., J.S. Salmento, H. C. Frey, A. Abu-Baker, and M. Berkenpas, *Modeling of Integrated Environmental Control Systems for Coal-Fired Power Plants*, Final Report, Prepared by Carnegie-Mellon University for the U.S. Department of Energy, Pittsburgh, Pennsylvania, DOE Contract No. DE-AC22-87PC79864, April 1991, 214p.
11. Rubin, E.S., J.S. Salmento, J.G. Barrett, C.N. Bloyd, and H. C. Frey, *Modeling and Assessment of Advanced Processes for Integrated Environmental Control of Coal-Fired Power Plants*, prepared by Carnegie-Mellon University for the U.S. Department of Energy, Pittsburgh, Pennsylvania, NTIS DE86014713, July 1986.

Of these, the first paper cited here is the most relevant. It contains documentation of the newest version of the copper oxide performance model, and several illustrative deterministic case studies. It is assumed here that you are already thoroughly familiar with the fluidized bed copper oxide. Furthermore, it is also assumed that you have access to the first paper referenced above and can review it to familiarize yourself with the performance model.

A process schematic is included on the following page. Some key design assumptions are given in the next section.

7.11. Appendix B. Questions About Performance Uncertainties in the Copper Oxide Process

Here, you are asked to provide technically-informed judgments about probability distributions for parameters of a performance model for the fluidized bed copper oxide process. You are asked to consider the possibilities of potentially poor performance as well as the probability of obtaining favorable performance, based on current information about the system. The preceding sections provide an overview of uncertainty analysis and sources of technical information about the process and the models we employ.

We are interested in your technically-based judgments about uncertainties in key performance parameters related primarily to absorption, regeneration, sorbent transport and attrition, and process design. We intend to model the uncertainty in performance and cost associated with a fifth-of-a-kind, or mature, system. Thus, we are asking you to make predictions about systems that have not yet been built or operated. We are asking you to express the range of possible outcomes for these systems using probability distributions, as discussed in Part 1.

Several questions follow. These are the types of questions which we will discuss on Friday. If you would like, you may respond to the questions on these pages, or use additional paper as needed. Alternatively, you could provide your responses more informally during our meeting on Friday. See the Introduction for examples of how you might estimate uncertainty in each parameter.

7.11.1. Design Assumptions

A number of key design assumptions for the fluidized bed copper oxide process are shown in Table 7-13.

In previous work reported by Frey at the last AWMA meeting, three integration strategies are considered for the copper oxide process and a sulfuric acid plant. Case 1 represents a base case in which no measures are taken to correct for Claus plant tailgas emissions. In Case 2, the SO_2 removal efficiency in the absorber is increased to compensate for the tailgas emissions. In Case 3, the tailgas emissions are recycled to the flue gas just upstream of the absorber, and the absorber sulfur removal efficiency is increased slightly to achieve an overall 90 percent removal efficiency. Cases 2 and 3 yield the same overall removal efficiency of 90 percent, while Case 1 achieves only 85.5 percent removal efficiency. The design assumptions for SO_2 removal efficiencies in Table 7-13 are based on Case 3.

Table 7-13 ***Key Copper Oxide Process Design Assumptions***

Parameter	Value
Absorber Process Area	
Required SO_2 Removal Efficiency, %	90.0
Absorber SO_2 Removal Efficiency, %	90.5
Sulfur Plant Recovery Efficiency, %	95.0
Claus Tailgas Recycle to Flue Gas	Yes
Overall SO_2 Removal Efficiency, %	90.0
NO_x Removal Efficiency, %	90.0
Flue Gas Inlet Temp., ^oF	705
Number of Absorbers	2
NH_3/NO_x Molar Ratio	1.00
Superficial Flue Gas Velocity (ft/s)	4.5
Expanded Bed Height (inches)	48
Expanded Sorbent Density, lb/ft^3	26.6
Fluidized Bed Pressure Drop (in. H_2O)	27.7
Regenerator Process Area	
CuO Regeneration Efficiency, %	80
$CuSO_4$ Regeneration Efficiency, %	80
$CuSO_3$ Regeneration Efficiency, %	80
Conversion of CuO to $CuSO_3$, frac.	1
Regenerator Inlet Temperature, °F	900
Regenerator Methane/$CuSO_4$ Ratio	1.15
Methane Inlet Temperature, °F.	77
System Parameters	
Sorbent Copper Loading (wt-%)	7
Bed Attrition (%/hr of bed inventory)	0.020
Circulation Attrition (% of circulation)	0.047
Key Coal Properties	
Sulfur Content, wt-%	3.12

7.11.1.1. Question #1: Comments on Default Assumptions

Do the default assumptions seem reasonable? If not, adjust accordingly and explain the basis for the changes. Are there additional assumptions that should be specified for these systems? If so, please add these assumptions and explain why they are needed. Use your updated set of assumptions as the basis for answering the following questions.

7.11.1.2. Question #2. Uncertain Parameter Identification

The following is a list of the specific parameters for which uncertainty distributions are desired.

Absorber-Related Uncertainties

- Sulfation Rate Constant Model Error

- Cu/S Model Error
- Fluidized Bed Sorbent Density
- Fluidized Bed Flue Gas Pressure Drop
- Dependency on fluidized bed height (over a range of 36 to 72 inches)
- Ammonia Stoichiometry and Ammonia Slip

Regeneration-Related Uncertainties

- Formation of $CuSO_3$ in the regenerator
- Regeneration Efficiencies for Different Copper Species
  12. • Copper Oxide
  13. • Copper Sulfite
  14. • Copper Sulfate
- Regenerator Residence Time Model Error
- Regenerator Rate Constant for $CuSO_4$
- Regenerator Reaction Rate for $CuSO_4$

Other Uncertainties

- Sorbent Attrition Rate
  15. • dependency on sorbent copper loading (over a range of 5 to 10 wt-% Cu as CuO)
  16. • dependency on fluidized bed height (over a range of 36 to 72 inches)
- Sorbent Unit Cost

Are you comfortable making estimates of uncertainty for these parameters?

Are there other parameters which you believe also should be treated probabilistically (whether or not you feel comfortable making the judgment yourself) that are not included in the above list? If so, please specify what these parameters are and supply your judgments about them if you are comfortable doing so (see the following questions for examples of the types of judgments we are looking for). If not, who can we ask to estimate uncertainties for these additional parameters?

Absorber-Related Uncertainties

Uncertainty in Sulfation Rate Constant Model

The expression used in the model to calculate the rate constant is:

$$k_s = 1{,}573 \exp(-14.23\, W_{Cu}) \exp\left(-\frac{2{,}417.6}{T}\right)$$

where k_S is the reaction rate constant (1/(min*atm)), W_{Cu} is the sorbent copper loading (wt-fraction Cu as CuO), and T is the absorber bed temperature (K). Clearly, this model provides an *estimate* of the actual rate constant under different conditions of sorbent copper loading and temperature. How accurate and precise is the model? Accuracy refers to random error in predicting the rate constant, whereas precision refers to any biases (e.g., a systematic tendency to under-predict or over-predict). How likely is it that the rate constant could be higher than the estimated value? How

much higher could the rate constant be (as a percentage of the estimated value)? Could it by lower? By how much?

Uncertainty in the Estimated Cu/S Molar Ratio

The uncertainty in this parameter can be estimated by comparing model results with experimental results. This is done in the following figure:

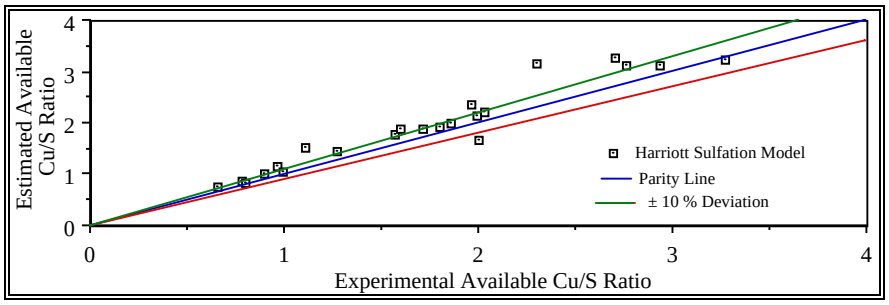

Comparison of Experimental and Model Results for Available Cu/S Ratio

The limitation of this approach is that the experimental data may not be representative of the operating conditions for a full-scale commercial plant, either due to different design assumptions or to scale-up effects. In your opinion, do these data provide a reasonable indication of the uncertainty for predicting Cu/S ratios for a commercial size unit (which may be larger than the 40 inch by 48 inch test unit from, which the data were taken, by a factor of 300 in terms of sorbent bed inventory)? What is your estimate of uncertainty in the predicted value of the Cu/S ratio, especially for ratios in the range of 1.5 to 2.0?

Fluidized Bed Sorbent Density

Analysis of data from the 40 by 48 inch tests conducted at FETC in the mid-1980s indicates that there is variability in the expanded sorbent density across the tests. While the average sorbent density was approximately 26 lb/ft^3, it varied by about ± 17%. This variation was not explainable by differences in superficial gas velocity, although there appears to be a weak dependence on bed height (density increases with bed height). Even accounting for differences in bed height, the variation is ± 12 %. What is the source of this variation? Is it likely to average out over time for a given absorber?

Fluidized Bed Pressure Drop

The flue gas pressure drop across the absorber has implications for induced draft fan electrical requirements. A simple linear model of pressure drop versus bed height has been employed based on FETC test results:

Pressure Drop (inches of H_2O) = 10.2 + 0.365 H (inches of bed height)

Does this model provide a reasonable approximation over a range of bed heights in excess of those from the FETC test results (e.g., for bed heights of 48 to 72 inches)?

Ammonia Stoichiometry and Ammonia Slip

The ammonia-to-nitrogen oxides stoichiometric ratio required for a given NO_x removal efficiency can be estimated empirically using regression models developed based on FETC test data. The scatter in these data appear to be on the order of approximately ±5% or ±10%. The data indicate that ammonia removal efficiency increases with bed height for a given NH_3/NO_x molar ratio. While the performance and cost of the copper oxide process are not particularly sensitive to differences in ammonia injection rates, the issue of ammonia slip is not well understood for this system. One study by UOP in 1987 reported that ammonia slip appeared to be less

than 50 ppmv. However, such levels could be excessive. For 90 percent NO_x removal, what is your best estimate as to best case, worst case, and most likely ammonia slip levels?

Regenerator-Related Uncertainties

Formation of $CuSO_3$ in the Regenerator

Some studies have suggested that potentially many other copper species besides Cu, CuO, and $CuSO_4$ may play an important role, particularly with regard to regeneration. For example, $CuSO_3$ may be formed by the reaction of SO_2 in the exiting off-gas with CuO in the incoming sorbent. The question here is: how much (if any) $CuSO_3$ is formed in this manner?

Regeneration Efficiencies

A key input to the regenerator kinetic model used to estimate required sorbent residence time is the regeneration efficiency of $CuSO_4$. This parameter is assumed to have a value of 80 percent in the default design basis.

What is the relationship between the regeneration efficiency of $CuSO_3$ and that of $CuSO_4$? For example, Harriott and Markussen (IECR, 31:1, p.378) indicate that the regeneration efficiency of $CuSO_3$ could be substantially less than that of $CuSO_4$.

What is the relationship between the regeneration of CuO and $CuSO_4$? What are reasonable assumptions to make? What ranges of values can be used? For example, is the regeneration efficiency for CuO the same as for $CuSO_4$?

Regenerator Residence Time Model

How accurate and precise are predictions made by the regenerator residence time model described in Frey's paper (the model itself was developed by Harriott based on experimental work done by Harriott and Markussen). Assuming that all inputs to the model were known with certainty, how much scatter could we expect to see between model predictions and actual process performance? What are some sources of discrepancies (e.g., channeling of flow with the regenerator bed, masking by contaminants, unaccounted for chemical reactions, etc.)? How much longer could the residence time be, as a percentage of the model estimate? How much lower?

Regenerator Rate Constant

How accurate and precise are the predictions of the rate constant for the regeneration of copper sulfate? These predictions are given by the following model:

$$k_{s,r} = \begin{cases} 4.2\times10^{7} \times F_w \times \exp\left(\dfrac{-21{,}700}{T}\right) & \text{if } T \le 1{,}355^\circ\text{R} \\ 11.2\times10^{5} \times F_w \times \exp\left(\dfrac{-16{,}800}{T}\right) & \text{if } T > 1{,}355^\circ\text{R} \end{cases}$$

where the factor F_W is a correction based on the sorbent copper loading:

$$F_w = 2.04\exp(-14.23\,W_{Cu})$$

For example, as a percentage of the value estimated by the model, how much higher might the actual rate constant be? How much lower might it be?

Regenerator Reaction Rate

The copper sulfate regeneration reaction rate is estimated using the following expression, based on a memo by Harriott. The reaction rate is estimated for each of a

number of increments within the regenerator (the nomenclature used here is defined in the recent paper by Frey):

$$r_k = \frac{k_{s,R,k}\ P_{CH4,k}\ (\eta_{r2,eq,k} = k\Delta\eta_{r2})}{1 + K_1\ P_{CH4,k} + K_2\ P_{SO2,k} + K_3\ P_{CO2,k}} \qquad (7\text{-}34)$$

where:

$$\eta_{r2,eq,k} = 1 - 0.9\ P_{CH4,k} \qquad (7\text{-}35)$$

The partial pressures for each gas are estimated throughout various increments in the regenerator. The average reaction rates are calculated for each increment based on the inlet and outlet partial pressures. The parameters of the reaction rate equation, K_1, K_2, and K_3, are estimated by Harriott to be 5, 16, and 6, respectively.

Date reported by Harriott and Markussen (IECR, 31(1):373-379) in Table 7-13 provide some quantitative indication of uncertainty in the reaction rate. However, it is not clear that these data translate directly to a commercial scale absorber, which may have flow distribution problems and in which other gases not included in the tests (e.g., water vapor) may be present. How likely is it that the reaction rate will be higher? Lower? By how much?

Other Uncertainties

Sorbent Attrition Rate

Sorbent attrition rate can be characterized in a number of ways. One approach used in the current study is to separately consider attrition occurring from sorbent particle motion in the fluidized bed absorber from that associated with sorbent transport. The new design basis for the copper oxide process employs a dense phase transport system. What are your estimates of worst case, best case, and most likely sorbent attrition rates for the absorber bed and the sorbent transport system, assuming a base case 7 wt-% Cu (as CuO) sorbent?

How will attrition rates change for different sorbent copper loadings? Consider a sorbent with 5 wt-% Cu versus one with 10 wt-% CuO.

Sorbent Unit Cost

A common assumption in economic evaluations of the copper oxide process is that sorbent will cost $5.00/lb for a 7 wt-% Cu formulation. This assumption has been used for a number of years now. Is it still reasonable? How likely is the cost to be higher than this? To be lower? How low could it be? How high could it be?

How would the sorbent cost be different for a 5 wt-% formulation versus that of a 10 wt-% formulation?

8. NOXSO Process

8.1. Introduction

The NOXSO process is an advanced technology that removes both SO_2 and NO_x simultaneously using a sorbent prepared by spraying sodium carbonate on the surface of γ-alumina spheres. It is designed to achieve SO_2 removal efficiencies above 90% and NO_x removal at levels above 80%. The main features of this process are:

- Simultaneous SO_2 and NO_X removal in a single absorber vessel
- Regenerative use of sorbent, thereby avoiding the production of liquid or solid waste
- Production of a saleable byproduct in the form of sulfur or sulfuric acid

The NOXSO process was developed in the early 1980s and successfully demonstrated at the small-scale (0.17 MW) in 1983-85 at TVA's Shawnee Steam Plant facility (Haslbeck & Neal, 1985; Yates, 1983). This was followed by Process Development Unit (PDU) tests on a slightly larger scale (0.75 MW) in cooperation with USDOE FETC in the mid-eighties. A Life-Cycle Test Unit (LCTU) was built (0.06 MW) in 1988 to examine the NOXSO process in an integrated continuous mode operation (Yeh, Drummond, Haslbeck, & Neal, 1987; Yeh, Ma, Pennline, Haslbeck, & Gromicko, 1990). Finally a Proof-of-Concept (POC) unit was built in the early 1990s at a 5 MW scale as the last test before full-scale demonstration (Black, Woods, Friedrich, & Leonard, 1993; Ma, 1994-95; Ma, Haslbeck, et. al., 1993). Based on these tests, conceptual designs of commercial scale units are now being developed.

There are several similarities between the NOXSO process and the fluidized bed copper oxide process another integrated emission control technology supported by USDOE FETC and modeled in the IECM. The key *differences* between these processes are twofold:

1. NOXSO uses a sorbent that consists of sodium carbonate sprayed on the surface of γ-alumina spheres while the CuO process uses copper oxide as a sorbent. The latter requires operation at high temperatures upstream of the air preheater, where the NOXSO catalyst operates at lower temperatures downstream of the preheater.
2. NOXSO recycles the NO_x removed from the flue gas back to the furnace along with combustion air. By injecting it into the fuel-rich high temperature combustion zone it is decomposed to N_2 and O_2. The

CuO process, on the other hand, requires the use of ammonia as an additional reagent to reduce NO_x to N_2.

8.2. NOXSO Performance Model

This section provides a description of the NOXSO process and refines the existing performance models in the literature and in the IECM computer model. Special attention is given to the fact that no installations currently exist at a commercial size of 200 MW or greater. This lack of information at a large scale introduces additional uncertainty and requires that models parametrized using data from pilot plants of about 5 MW be extrapolated. The process model presented in this chapter uses principles of thermodynamics and mass transfer for unit operations of the NOXSO process. These models are then parametrized using data from pilot scale studies and subsequently used for conceptual design of planned commercial size plants.

The accuracy of model predictions depends in large part on how completely all the relevant processes have been modeled. Past experience in industry has shown that mass transfer units, especially for solid-gas and liquid-gas exchange, are difficult to scale up. This can lead to uncertainty in predicting the performance of commercial-scale installations. In this chapter, process performance models developed by NOXSO Corporation, which have been parametrized against Proof-of-Concept (POC) data have been used. These process models were then integrated into the IECM framework to provide an overall system model for the NOXSO process in which uncertainties can be modeled explicitly.

8.2.1. Organization of Chapter

The discussion of performance models is organized as follows: The first subsection provides a description of the unit operations used in the NOXSO process. The second provides some theoretical background for modeling fluidized beds. The third subsection provides mass balance models for all NOXSO process areas along with emission control design equations for the adsorber and regenerator. The final subsection provides a numerical example illustrating the use of these models for conceptual design of a commercial scale NOXSO plant.

8.2.2. Process Description

A schematic of the NOXSO process is shown in Figure 8-1. It consists of four main units: the adsorber, sorbent heater, regenerator, and the sorbent cooler. SO_2 and NO_x are adsorbed from the flue gas onto the surface of the sorbent at 320°F in a single-stage fluidized bed adsorber. The SO_2 reacts with the sodium bicarbonate on the sorbent surface to form sodium sulfates. The sorbent is then transported into the three-stage fluidized bed sorbent heater using a dense-phase conveyer, where it is heated to 1150°F to desorb NO_x. The desorbed NO_x is recycled to the furnace where about 65% is reduced to N_2. Following NO_x desorption, the sorbent is transported via a J-valve to a regenerator where natural gas and steam are used to reduce the sulfate on the sorbent to SO_2 and H_2S which are also desorbed. These offgases are sent to a Claus plant or a sulfuric acid plant to recover the sulfur. Finally, sorbent is transported to a three-stage fluidized bed cooler (via a second J-valve) where it is cooled to 320°F and transported back to the adsorber via a third J-valve.

Provided in the following sections is a brief description of each unit operation along with its associated process chemistry. Discussion regarding the modeling of the mass transfer operations for each unit can be found in "NOXSO Process Performance Model" on page 218.

8.2.2.1. Adsorber

The adsorber consists of a single-stage fluidized bed containing the Na_2CO_3 covered γ-alumina beads of 1/16 inch diameter. The operating temperature of the bed is 320°F at which temperature Na_2CO_3 is reduced to Na_2O. If necessary, the flue gas is first cooled to 320°F by spraying water into the flue gas ducts. It then passes through the adsorber at a superficial velocity at least as large as the minimum fluidization velocity. The SO_2 and NO_x in the flue gas are adsorbed onto the surface of the alumina beads via solid-gas mass transfer.

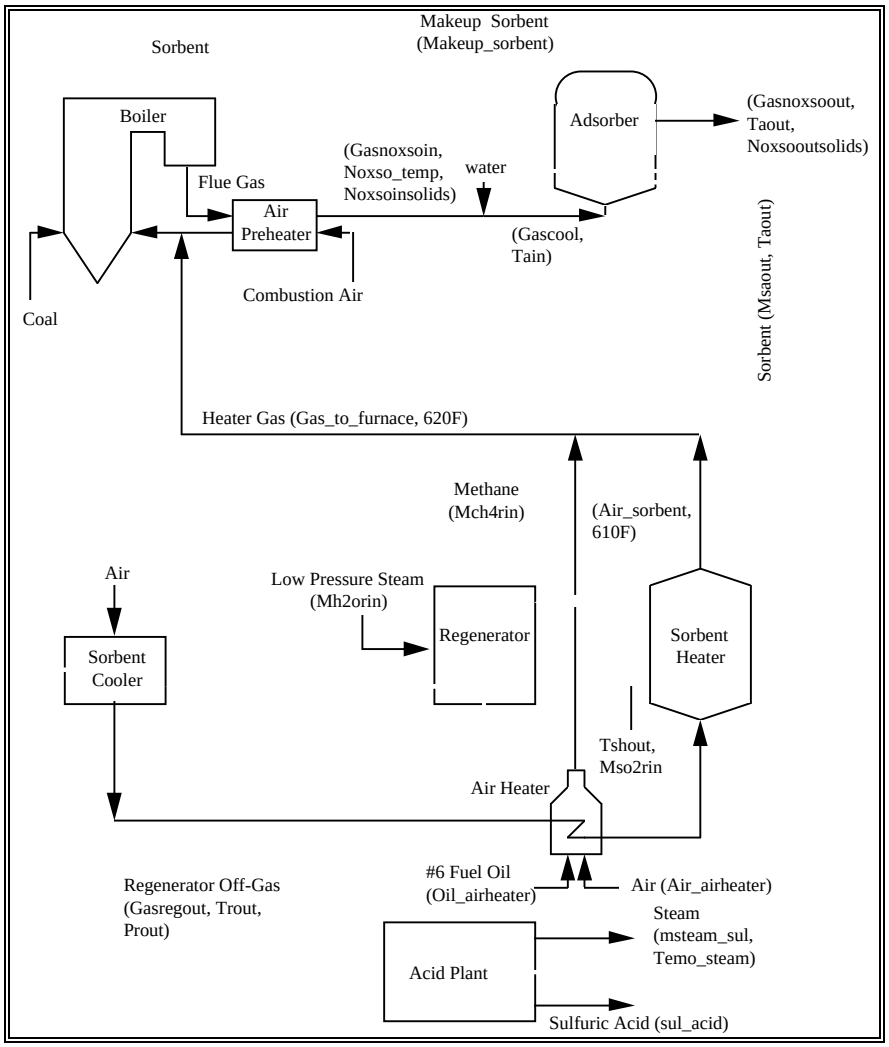

Figure 8-1 A Schematic of the NOXSO Process Flowsheet

Based on laboratory experiments and the results obtained from the POC tests the proposed mechanism for the SO_2/NO_x adsorption is as follows:

$$Na_2O + SO_2 \Leftrightarrow Na_2SO_3 \qquad (8\text{-}1)$$

$$Na_2SO_3 + 1/2\,O_2 \Leftrightarrow NaSO_4 \qquad (8\text{-}2)$$

$$Na_2O + SO_2 + NO + O_2 \Leftrightarrow Na_2SO_4 + NO_2 \qquad (8\text{-}3)$$

$$Na_2O + 3\,NO_2 \Leftrightarrow 2\,NaNO_3 + NO \qquad (8\text{-}4)$$

The overall reaction summarizing Equations (8-1) and (8-2) is given by:

$$Na_2O + SO_2 + 1/2\,O_2 \Leftrightarrow NaSO_4 \qquad (8\text{-}5)$$

The overall reaction summarizing Equations (8-3) and (8-4) is given by:

$$4\,Na_2O + 3\,SO_2 + 2\,NO + 3\,O_2 \Leftrightarrow 3\,Na_2SO_4 + 2\,NaNO_3 \qquad (8\text{-}6)$$

Examining Equations (8-5) and (8-6), we see that 2 moles of SO_2 are adsorbed for every mole of NO. The rate of reactions for both SO_2 and NO_x adsorption have been established as first-order based on experimental data. Therefore, the reaction rate is:

$$\frac{dC_i}{dt} = -k_i[C_i]S$$

where k_i is the reaction rate constant, $[C_i]$ is the concentration of SO_2 or NO_x, and S is the available surface area of the sorbent. The available surface area depends on the gas-solid mixing and flow conditions in the fluidized bed. Modeling the flow in a fluidized bed is quite complex and often difficult, therefore, the available surface area is usually experimentally determined.

8.2.2.2. Sorbent Heater

The saturated sorbent from the bottom bed of the adsorber is transported to the top of the sorbent heater using a dense phase conveyor system. The sorbent heater is a three-stage fluidized bed reactor. A natural gas fired air heater supplies hot air to heat the sorbent to 1150°F. During the heating process all of the NO_x (65%-75% NO_2, balance NO) and some of the SO_2 desorbs from the sorbent. In commercial applications the heater off-gas, which is rich in NO_x, is returned to the furnace. The introduction of NO_x recycle into the furnace results in: (a) inhibited NO_x production due to higher NO_x concentrations, and (b) reduction of NO_x to N_2. As noted earlier, about 65% of the recycled NO_x is reduced to N_2.

NO_x desorbtion in the sorbent heater produces both NO and NO_2, where the latter is about 65-75% of the total NO_x. The type of gas used (i.e., the constituents of hot air plus combustion byproducts) to heat the sorbent does not affect the ratio of NO to NO_2 (in NO_x) significantly. A small fraction of SO_2 is also desorbed. Based on experimental findings the following reaction mechanisms have been proposed to explain the desorbtion process:

$$2\,NaNO_3 \rightarrow Na_2O + 2\,NO_2 + 1/2\,O_2 \qquad (8\text{-}7)$$

$$2\,NaNO_3 \rightarrow Na_2O + NO_2 + NO + O_2 \qquad (8\text{-}8)$$

$$Na_2SO_3 \Leftrightarrow Na_2O + SO_2 \qquad (8\text{-}9)$$

Fluidized bed reactors have excellent heat transfer properties, and it has been experimentally observed that all of the adsorbed NO_x is desorbed in the sorbent heater. In this work, the sorbent heater is modeled purely as a heat and mass transfer device resulting in 100% NO_x removal and 0-5% SO_2 removal.

8.2.2.3. Regenerator

The regenerator is of a moving bed type, i.e., the sorbent continuously moves from the top to the bottom of the regenerator bed. The hot sorbent from the bottom of the

sorbent heater is transported to the top of the regenerator via J-valves. Natural gas is used to treat the hot sorbent and reduce the sulfate to SO_2, H_2S, and sulfide. In the lower part of the regenerator bed steam is used to hydrolyze any residual sulfide to H_2S. The off-gas streams from the natural gas treater and steam treater are mixed and fed either to a Claus plant, which converts gases to elemental sulfur, or to a sulfuric acid plant.

The reaction mechanisms for regeneration of the sorbent based on POC results are as follows:

$$1/4\,CH_4 + Na_2SO_4 \rightarrow 1/4\,CO_2 + SO_2 + 1/2\,H_2O + Na_2O \quad (8\text{-}10)$$

$$SO_2 + Na_2O \rightarrow Na_2SO_3 \quad (8\text{-}11)$$

$$3/4\,CH_4 + Na_2SO_3 \rightarrow 3/4\,CO_2 + H_2S + 1/2\,H_2O + Na_2O \quad (8\text{-}12)$$

$$Na_2S + H_2O \Leftrightarrow H_2S + Na_2O \quad (8\text{-}13)$$

$$CO_2 + Na_2S \rightarrow COS + Na_2O \quad (8\text{-}14)$$

$$1/2\,CO_2 + Na_2S \rightarrow 1/2\,CS_2 + Na_2O \quad (8\text{-}15)$$

Equations (8-10), (8-11), and (8-12) represent the regeneration in the upper part of the moving bed, and can be summarized as follows:

$$CH_4 + Na_2SO_4 \rightarrow CO_2 + H_2S + H_2O + Na_2O \quad (8\text{-}16)$$

The residual sulfide is hydrolized in the lower part of the moving bed:

$$3\,Na_2S + H_2O + 1.5\,CO_2 \rightarrow 3\,Na_2O + H_2S + COS + 1/2\,CS_2 \quad (8\text{-}17)$$

The reaction rates are governed by the available surface area and the reaction rate constants can be determined experimentally.

8.2.2.4. Sorbent Cooler

The sorbent from the regenerator flows into a three-stage fluidized bed sorbent cooler via a second J-valve. The sorbent is cooled to 320°F using ambient air supplied by a fan. The heat is recovered by using the air for combustion in the air heater. The cooled and regenerated sorbent is recycled back to the adsorber via a third J-valve. The cooling of the regenerated sorbent does not involve any chemical reactions and is modelled purely as a heat transfer operation.

8.2.3. Fluidized Bed Reactors

Fluidizing a bed of solid particles with gas provides a means of bringing the two into intimate contact and thus enhancing mass and heat transfer. The heat transfer properties of fluidized beds are excellent and even when accommodating strongly exothermic or endothermic reactions, the beds remain isothermal due to good solids mixing. Additionally, because of their liquid-like properties, fluidized beds can be mechanically transferred by pumping from one container to another. In many industrial processes the gas mixing in a fluidized bed often is not good due to gas bubbles, which can severely reduce the contact between gas and solids. There can also be problems with particle attrition and break-up caused by the vigorous agitation of particles and their impingement on vessel walls. Often, however, the advantages outweigh the disadvantages and the use of fluidization in industrial processes is fairly common.

In designing a fluidized bed reactor two main factors are considered: (1) the formation of bubbles in the fluidized bed, which is determined by the minimum fluidization velocity U_{mf}, and (2) reactive mass transfer in the fluidized bed. In the following paragraphs models for the calculation of U_{mf} and for reactive mass transfer for fluidized bed reactors are described (Davidson & Harrison, 1971; Kunii & Levenspiel, 1969; Yates, 1983.

8.2.3.1. Minimum Fluidization Velocity

Fluidization of a bed with solid particles occurs when the superficial gas velocity in a vessel is large enough so that the drag force on the particles equals the gravitational pull of the particle. At this velocity, called the minimum fluidization velocity, U_{mf}, the bed takes on the appearance of a fluid with a flat surface responding in the same way as a fluid to stirring or pouring. If the superficial gas velocity increases above U_{mf}, bubbles form in the bed and rise to the surface where they burst through in the same way as gas bubbles in a boiling liquid. At these velocities the bed is essentially divided into two phases — the dense or emulsion phase where the gas percolates through as in a packed bed, and the lean or bubble phase where much of the gas is not in contact with the solids. If the superficial velocity is increased further the gas bubbles increase in size and might become as large as the diameter of the container itself. The bed is then said to be "slugging" and is characterized by considerable heaving of the surface.

The expressions available for estimating U_{mf} in terms of the physical properties of the solid particles and the fluidizing gas are based on the principle of taking a gas velocity-pressure drop relationship and extending it to the point where particles become fluidized and the gas velocity is U_{mf}. The Ergun equation (Yates, 1983) provides an expression for pressure drop through a vertical bed of particles (for size > 150 μm) of height H_{mf} :

$$\frac{\Delta p}{H_{mf}} = \frac{150\,(1-\varepsilon)^2}{\varepsilon^3} \times \frac{\mu \times V}{(\psi\, d_p)^2} + \frac{1.75\,(1-\varepsilon)}{\varepsilon^3} \times \frac{\rho_g\, V^2}{\psi\, d_p} \qquad (8\text{-}18)$$

where

Δp	=	pressure drop through the bed
H_{mf}	=	bed height
ε	=	voidage fraction of bed
μ	=	fluid viscosity
V	=	gas velocity
ψ	=	sphericity factor
d_p	=	particle diameter
ρ_g	=	density of gas
ρ_s	=	density of solid

At the point of minimum fluidization the force exerted by the upward flowing fluid is equal to the gravitational force of the particles, i.e.,

$$\frac{\Delta p}{H_{mf}} = (1-\varepsilon_{mf})\,(\rho_s - \rho_g)\,g \qquad (8\text{-}19)$$

The minimum fluidization velocity can then be estimated by substituting Equation (8-19) for the pressure drop in Equation (8-18):

$$(1-\varepsilon_{mf})(\rho_s-\rho_g)g=\frac{150(1-\varepsilon_{mf})^2}{\varepsilon_{mf}^3}\times\frac{\mu\times V}{(\psi d_p)^2}+\frac{1.75(1-\varepsilon_{mf})}{\varepsilon_{mf}^3}\times\frac{\rho_g V^2}{\psi d_p} \qquad (8\text{-}20)$$

Usually the voidage fraction at fluidization velocity is unknown. Wen and Yu (Yates, 1983) found that for a range of particle types and sizes the following empirical relationships were valid:

$$\frac{1-\varepsilon}{\psi^2\varepsilon_{mf}^3}\approx 11 \quad \frac{\varepsilon}{\psi\varepsilon_{mf}^3}\approx 14$$

Using the Ergun equation with the above empirical relations, a generalized correlation for the estimation of minimum fluidization velocity can be written as:

$$Re_{mf}=[(33.7)^2+0.0408Ga]^{1/2} \qquad (8\text{-}21)$$

where

$$Re_{mf}\equiv\frac{V_{mf}\, d_p\, \rho_g}{\mu}$$

$$Ga\equiv\frac{d_p\, \rho_g\, (\rho_s-\rho_g)\, g}{\mu^2}$$

8.2.3.2. Fluidized Bed Reactor Modeling

Modeling a fluidized bed reactor is critical for evaluating design parameters such as sorbent residence time and sorbent flow rate. The performance of the fluidized bed reactor is determined by a combination of chemical factors and hydrodynamic factors. The chemical factors are determined by the reaction kinetics and the stoichiometry of the reaction. The hydrodynamic factors are determined by the gas distribution, bubble size and residence time, and the interphase exchange rate. In order to quantify the way in which these factors affect the reactor performance we present a model based on the theory of two-phase flow in fluidized beds which makes explicit the contribution of these factors.

Most reactor models assume that if the superficial velocity is greater than U_{mf} then the gas entering the bed divides into two streams, one flowing through the emulsion phase and the other flowing as bubbles. Gas flowing in the emulsion phase is in intimate contact with the solid particles so the reaction can proceed efficiently. Bubbles, however, are essentially empty of particles and gas within them can only react at the walls of the bubble. However, there is an exchange of gas between the emulsion and bubble phase, the bubbles thereby acting as a secondary source of fresh reactant as they rise through the bed. A general one-dimensional two-phase flow model is shown in Figure 8-2.

For an irreversible, first-order gas-solid reaction with no accompanying volume change, a mass balance for the emulsion phase (Equation (8-22)) and bubble phase (Equation (8-23)) is written as follows:

$$V_e\frac{dy_{Ae}}{dz}+K_{be}(y_{Ae}-y_{Ab})+k_e\, y_{Ae}\, S=0 \qquad (8\text{-}22)$$

$$V_b\frac{dy_{Ab}}{dz}+K_{be}(y_{Ab}-y_{Ae})=0 \qquad (8\text{-}23)$$

Where

V	=	velocity
Y_A	=	concentration of species A
K_b	=	interphase mass transfer rate per unit volume of bubble gas
k	=	reaction rate constant
S	=	surface area of solid available for reaction

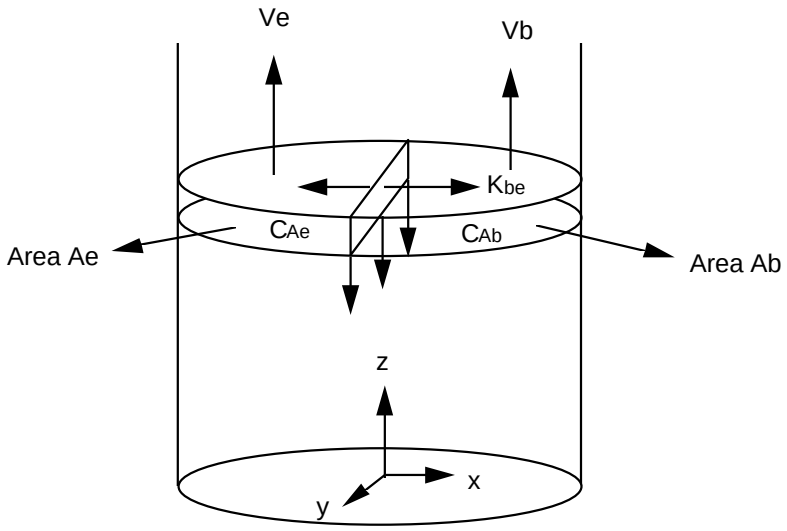

Figure 8-2 The General One-Dimensional Two-Phase Flow

The subscript 'e' is used for emulsion phase and subscript 'b' is used for bubble phase. These equations have been simplified using the following assumptions: (i) the reactor operates in steady state, (ii) the gas is in plug flow in both phases and hence there is no back flow, and (iii) no chemical reaction occurs in the bubble phase.

These model formulations provide an alternative form to the models described below. An advantage is that this formulation explicitly recognizes the two separate phases, especially the bubble phase which may limit performance in future process scale-up. Further development of Equations (8-22) and (8-23), however, remains a subject for future research.

8.2.4. NOXSO Process Performance Model

The four main process areas for the NOXSO process were described in "Process Description" on page 212. Across these areas, the adsorber, sorbent heater, and sorbent cooler use a fluidized bed for improved gas-solid contact. The sorbent heater and sorbent cooler utilize a fluidized bed mainly for efficient heat transfer between gas and solid sorbent particles. As discussed in that earlier section, the fluidized bed provides excellent heat transfer properties and provides isothermal conditions. The adsorber, on the other hand, is used primarily for reactive mass transfer, involving pollutant removal. The modeling of the adsorber performance will be discussed in some detail. The regenerator is a moving bed reactor which is used for regenerating sulfur. The reactive mass transfer model for this unit also is treated in some detail.

The performance models that are developed in this section are based on principles of thermodynamics and mass/energy transfer for unit operations of the NOXSO process. Data from various pilot studies has been used to parameterize these models.

8.2.4.1. Fluid Bed Adsorber Model

A mathematical model based on first principles has been developed by NOXSO Corporation for the design of future commercial installations (Ma and Haslbeck, 1993). The reaction rate constants for SO_2 and NO_x sorption were derived using data from the process development unit (PDU), life cycle-test unit (LCTU), and proof of concept (POC) tests. The rate constants have been lumped to treat the hydrodynamics of the gas-solid contact and the reaction kinetics in one variable. The main purpose of this model is to provide design equations for calculating key design parameters such as sorbent inventory and sorbent residence time for a desired level of SO_2 and NO_x removal. We have rewritten the equations developed by NOXSO Corporation to provide explicit relations for the design variables. Since the equations are quite detailed, and it is easy to get lost in the nomenclature, we first provide an overview of the equations.

Equations (8-24) to (8-28) express the pollutant removal efficiency in terms of the operating parameters of the fluidized bed (W, Fs) and physical constants (K_i, ρ, etc). The main objective here is to progressively rewrite the equations in terms of variables and functions which are readily measured and can be provided as inputs to the model. Equation (8-29) and (8-30) provide a set of equations for removal efficiencies, operating parameters and physical constants. Equations (8-31) to (8-34) provide a set of relations for the physical constants determined from experimental data. Finally, Equations (8-35) and (8-36) provide the design equations for the operating parameters of the fluidized bed absorber.

The fluid bed mass balance in the vertical direction is derived using the following assumptions: (i) there is no bubbling in the fluidized bed, (ii) the gas is in plug flow, (iii) the solids are in mixed flow, and (iv) SO_2 and NO_x absorption are first-order reactions with respect to their concentrations. Therefore the mass balance is written as follows:

$$- V C_0 (y_{oi} - y_{fi}) = \rho \lambda_i n K_i P \bar{y}_i (1 - \bar{X}) H \qquad (8\text{-}24)$$

Notice that unlike Equation (8-22), the mass balance has been written for the total bed by using a mean value for the concentration of gas species 'i'.

Defining the removal fraction as:

$$\phi_i = \left(1 - \frac{y_{fi}}{y_{oi}} \right)$$

Equation (8-24) can be rewritten as follows:

$$\phi_i = \frac{W}{F_g} \lambda_i n K_i P \frac{\bar{y}_i}{y_{oi}} (1 - \bar{X}) \qquad (8\text{-}25)$$

When sorption takes place in the adsorber, both SO_2 and NO_x compete for active sites on the sorbent. A mass balance on the sorbent material in a mixed flow reactor results in:

$$F_s (\bar{X} - X_0) = W P (K_1 \bar{y}_1 + K_2 \bar{y}_2) (1 - \bar{X}) \qquad (8\text{-}26)$$

Combining Equations (8-25) and (8-26), the removal efficiency for the i^{th} gas species can be rewritten as:

$$\phi_i = \frac{W\,E_i}{F_g} K_i\, P\, \frac{\bar{y}_i}{y_{oi}} \frac{1}{1 + \frac{W}{F_s} P\,(K_1\,\bar{y}_1 + K_2\,\bar{y}_2)} \qquad (8\text{-}27)$$

where

$$E_i = \lambda_i\, n\,(1 - X_0)$$

Since the alumina substrate also adsorbs SO_2 and NO_x from the flue gas, the stochiometric ratio of reactant gas to active sorbent must include contributions from both sodium and alumina. In order to avoid having to make this distinction, an empirical relationship has been developed to calculate the stoichiometry as a ratio of adsorber temperature:

$$\begin{aligned} &For\ SO_2 : \frac{1}{\lambda_1} = 0.3761 + 0.0052\,T_a \\ &For\ NO_x : \frac{1}{\lambda_2} = -4.789 + 0.075\,T_a \end{aligned} \qquad (8\text{-}28)$$

where T_a is in degrees Celcius.

Since the gas flow in the fluidized bed is assumed to be plug flow and the reaction is first-order, $\bar{y}_i$ can be taken as the logarithmic mean expressed in terms of the removal efficiency as follows:

$$\bar{y}_i = \frac{-y_{oi}\,\phi_i}{\ln(1 - \phi_i)}$$

Substituting for $\bar{y}_i$ in Equation (8-27), the removal efficiencies can be written as follows:

For SO_2:

$$\ln(1-\phi_1) - \frac{W}{F_s} P \frac{A}{A_0} \left(K_1\, y_{01} + K_2\, y_{02} \frac{\phi_2}{\ln(1-\phi_2)} \frac{\ln(1-\phi_1)}{\phi_1} \right) \phi_1 + \frac{W\,E_1}{F_g} P\,K_1 \frac{A}{A_o} = 0 \qquad (8\text{-}29)$$

For NO_x:

$$\ln(1-\phi_2) - \frac{W}{F_s} P \frac{A}{A_0} \left(K_2\, y_{02} + K_1\, y_{01} \frac{\phi_1}{\ln(1-\phi_1)} \frac{\ln(1-\phi_2)}{\phi_2} \right) \phi_2 + \frac{W\,E_2}{F_g} P\,K_2 \frac{A}{A_o} = 0 \qquad (8\text{-}30)$$

Note that since removal is a sorption reaction, the rate constant is proportional to sorbent surface area which has been introduced into the equations (refer to "Adsorber" on page 213). Equations (8-29) and (8-30) can be solved simultaneously for the removal efficiencies in terms of the following exogenously specified variables :

1. The key operating parameters of the fluidized bed, i.e., sorbent residence time (W/F_s) and sorbent inventory (W),

2. Key inlet conditions including the mole fractions of SO_2 and NO_x (y_{oi}) entering the adsorber, and the flue gas flow rate (F_g),
3. Key physical constants including the lumped kinetic constants (K_i), the available surface area (A/A_o), and the available unused sorbent capacity (E_i).

The physical constants have been determined by NOXSO Corporation using experimental data from the PDU, LCTU, and POC tests. In the following paragraphs we describe the parametrizations used for solving the above equations.

The sorbent's SO_2 and NO_x capacities are calculated as follows:

$$\text{For } SO_2: E_1 = \left(\lambda_1 n + \frac{0.8 - S_r}{3200}\right)\frac{A}{A_0} \qquad (8\text{-}31)$$

$$\text{For } NO_x: E_2 = \left(\lambda_2 n + \frac{0.8 - S_r}{3200}\right)\frac{\lambda_2}{\lambda_1} \qquad (8\text{-}32)$$

where

$$n = \frac{n_{Na}}{2300} - \frac{n_{SiO_2}}{6000}$$

Typically the sorbent contains 3.5-5% sodium and 6-7% silicon by weight.

The factor 0.8 in Equations (8-31) and (8-32) is the average sulfur content (% wt) of the regenerated sorbent in the PDU tests used as a reference for the above parameterization. The temperature dependent rate constants were derived by NOXSO Corporation by using PDU data along with Equations (8-29) and (8-30) to solve for K_i at different temperatures. A least squares fit was used to obtain the following relations:

$$\text{For } SO_2: K_1 = 52.15 \exp\left(\frac{-1840.2}{T_a + 273}\right) \qquad (8\text{-}33)$$

$$\text{For } NO_x: K_2 = 14.75 \exp\left(\frac{-912.14}{T_a + 273}\right) \qquad (8\text{-}34)$$

The available surface area A/A_O has a value of 0.6 based on PDU test data collected after sorbent surface area had stabilized.

For designing the adsorber, we need to estimate the operating parameters of the fluidized bed for given removal efficiencies for SO_2 and NO_x. The key parameters are the sorbent circulation rate, sorbent inventory, sorbent residence time and fluidized bed height. Equations (8-29) and (8-30) can be solved for sorbent inventory and sorbent circulation rate. Note that sorbent residence time also can be calculated from these two variables. The result is:

$$\frac{W}{F_s} = \frac{a_1 b_3 + a_3 b_1}{a_2 b_3 + a_3 b_2}$$
$$W = \frac{b_1(a_2 b_3 + a_3 b_2) - b_2(a_1 b_3 + a_3 b_1)}{b_3(a_2 b_3 + a_3 b_2)} \qquad (8\text{-}35)$$

where

$$a_1 = \ln(1 - \phi_1)$$

$$b_1 = (\ln(1 - \phi_2);$$

$$a_2 = P\frac{A}{A_0}\left(K_1\, y_{01} + K_2\, y_{02}\, \frac{\phi_2}{\ln(1-\phi_2)}\, \frac{\ln(1-\phi_1)}{\phi_1}\right);$$

$$b_2 = P\frac{A}{A_0}\left(K_2\, y_{02} + K_1\, y_{01}\, \frac{\phi_1}{\ln(1-\phi_1)}\, \frac{\ln(1-\phi_2)}{\phi_2}\right);$$

$$a_3 = \frac{E_1}{F_g} P\, K_1\, \frac{A}{A_0}$$

$$b_3 = \frac{E_2}{F_g} P\, K_2\, \frac{A}{A_0}$$

The height of the fluidized bed is calculated as follows:

$$H = \frac{W}{\rho\ A_a} \qquad (8\text{-}36)$$

The total sorbent inventory is calculated by adding the sorbent in the regenerator and the solids heater and cooler as follows:

$$S_{inv} = W + F_s\ \left(t_{CH_4} + t_{H_2O}\right) + 2\ A_{SH/SC}\ H_{SH/SC}\ \rho$$

where $A_{SH/SC}$ is the cross-sectional area of the sorbent heater/cooler and $H_{SH/SC}$ is the height of the sorbent. It has been assumed that the cross-sectional area for solids heater and the solids cooler is the same. The total pressure drop in the fluidized bed is easily calculated by considering the total weight of sorbent that is fluidized by the flue gas, i.e.

$$\Delta p = \frac{W}{A_a}$$

Sorbent attrition is caused by physical and thermal stresses that the sorbent experiences as it is transported through the processing loop. These stresses can fracture the sorbent beads and erode the surface of the beads. Sorbent makeup is then required to maintain a constant sorbent inventory. The attrition rate has been measured experimentally at the pilot plant and is equivalent to 0.026% of the inventory per hour. The makeup sorbent is calculated as follows:

$$m_{makeup} = AR_{sorbent} \times S_{inv}$$

where $AR_{sorbent}$ is the sorbent attrition rate.

Figure 8-3 and Figure 8-4 graph the sensitivity of the two design variables (W and W/F_s) to different SO_2 and NO_x removal efficiencies. These sensitivities are plotted for a medium sulfur (2.6%S) Appalachian coal. The sorbent residence time (W/F_s) increases with the required SO_2 and NO_x removal (Figure 8-3). Similarly, the sorbent inventory (W) also increases with SO_2 and NO_x removal (Figure 8-4).

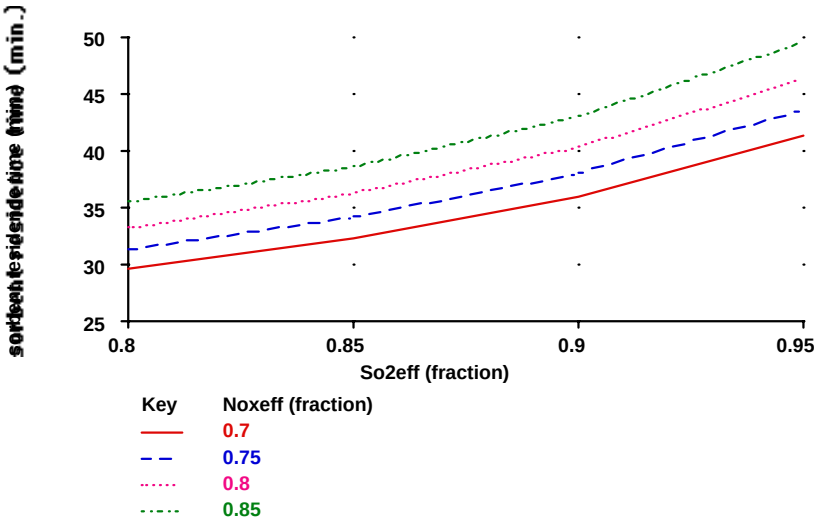

Figure 8-3 Sorbent Residence Time in Adsorber (Medium Sulfur Appalachian Coal)

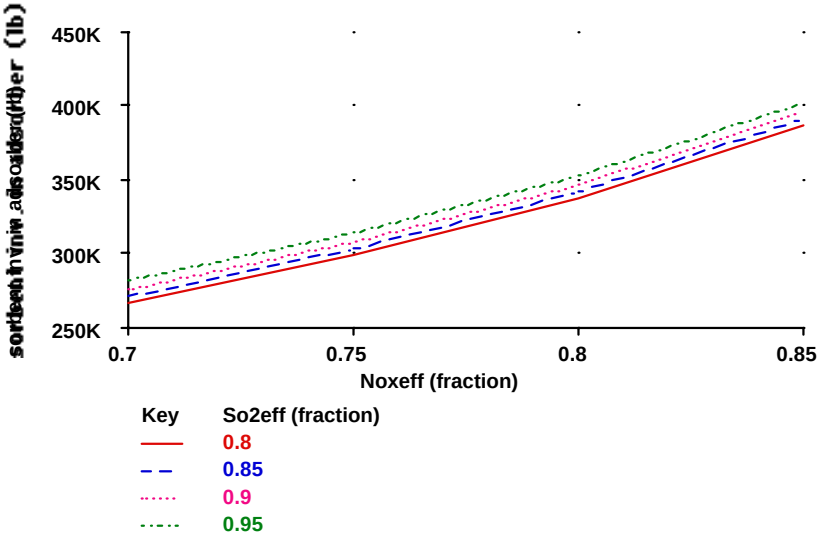

Figure 8-4 Sorbent Inventory in Adsorber (Medium Sulfur Appalachian Coal)

A promising alternative to the single-stage fluidized bed design described above is a design featuring two fluidized beds in series. A schematic of the two-stage fluidized bed absorber is shown in Figure 8-5. In the two-stage design, regenerated sorbent enters a first stage fluidized bed, where the sorbent reacts with flue gas which has already passed through a second stage sorbent bed. The partially sulfated sorbent from the first bed then goes to a second bed, where it contacts inlet flue gas. Each of the two beds can have different bed heights and removal efficiencies. The overall removal efficiency is given by:

$$\phi_i = \phi_i^2 + \left(1 - \phi_i^2\right) \phi_i^1 \qquad i = SO_2, NO_x$$

where the subscripts 1,2 refer to the stage-1 and stage-2 fluidized beds. For each of the two beds, the general models given in Equation (8-35) and Equation (8-36) apply. However, the input conditions for each bed is different. Since the output flue gas from the first stage enters the second stage, the SO_2 and NO_x concentrations are

lower. Conversely, the regenerated sorbent enters the first stage and adsorbs SO_2 and NO_x before it enters the second stage. This is shown schematically in Figure 8-5.

The calculation procedure for a 2-stage bed requires the specification of the overall SO_2 (or NO_x removal efficiency) and a second stage removal efficiency. The removal efficiency for the 1st-stage is calculated as follows:

$$\phi_i^1 = \frac{\phi_i - \phi_i^2}{1 - \phi_i^2}$$

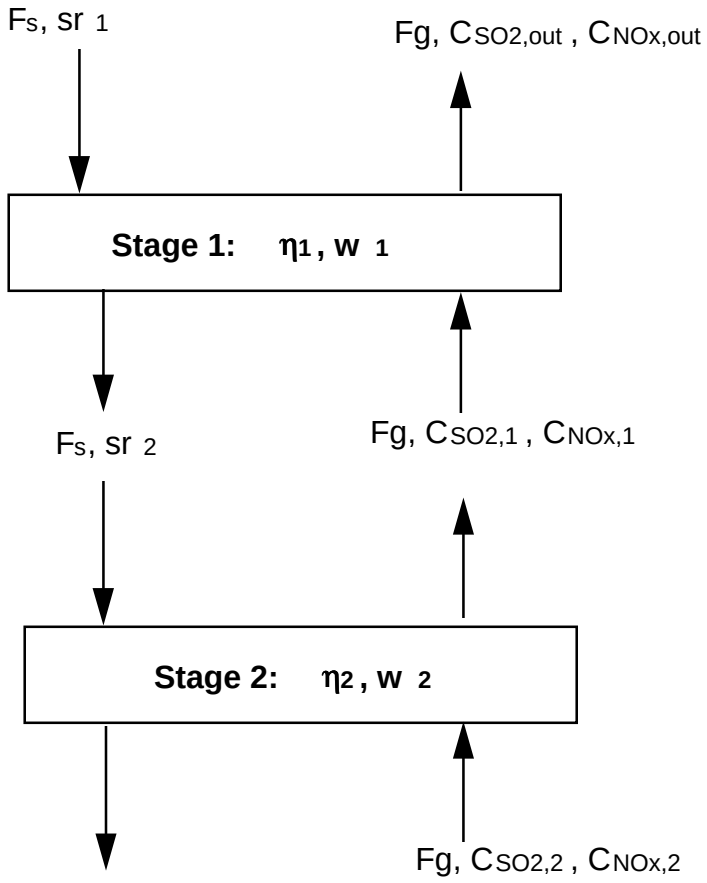

Figure 8-5 A Two-Stage Adsorber

The corresponding fluidized bed height (or sorbent inventory) and the sorbent circulation rate for stage-1 and stage-2 is calculated using Equations (8-35) and (8-36) as before. The larger sorbent circulation is used for costing purposes. It is assumed that SO_2 and NO_x removal are distributed between the two stages in a similar fashion.

8.2.4.2. Regenerator Model

The regenerator consists of two sections as shown in Figure 8-6. The sorbent moves down in a moving bed, while the regenerating gases move upward. The flow is assumed to be approximately plug flow. Natural gas enters the bottom of the upper section of the regenerator and reduces the sulfate on the sorbent to SO_2, H_2S, and sulfide. SO_2 and H_2S evolve as gases and sulfide remains on the sorbent surface.

Steam is introduced in the lower section of the regenerator and hydrolyzes the sulfide to H_2S.

The models presented here determine the main operating parameters of the regenerator which are the sorbent residence times for natural gas reduction and steam reduction. The total residence time in the regenerator is used to size the regenerator and to estimate the

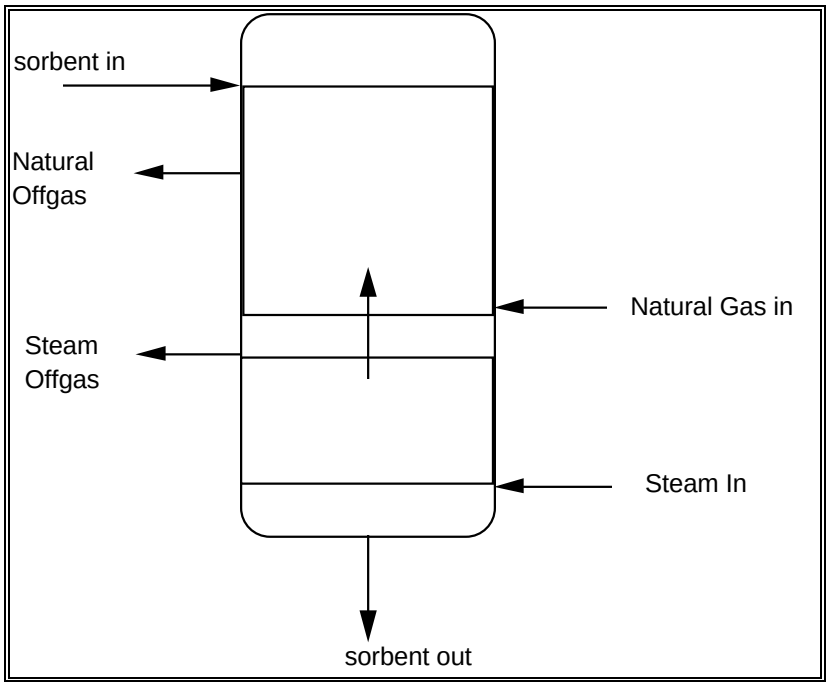

Figure 8-6 Schematic of the NOXSO Regenerator

sorbent inventory required for the regenerator. Moreover, the total height of the regenerator is calculated based on the respective residence times for natural gas and stream reduction. Equation (8-37) provides a mass balance for sulfur which has been used as a basis for interpreting experimental data. Equation (8-38) provides the rate constants for the two reduction reactions given by Equations (8-16) and (8-17). Finally, Equation (8-38) provides the design equations for sorbent residence times.

The sulfur molar balance provides the rate of sulfur regeneration as a function of sorbent flow rate and sorbent inventory as follows:

$$F_s\, S_a\, dX_r = r_s\, dW \Rightarrow X_r = \frac{W}{F_s\, S_a} r_s \qquad (8\text{-}37)$$

where

$$X = 1 - S/S_a$$

The sulfur regeneration rate has been studied extensively in the POC plant. The experimental results indicate that regeneration consists of two main reactions and both are first-order with respect to sorbent sulfur content. The first set of reactions, corresponding to Equation (8-16), uses natural gas to reduce the sulfate. The second reaction corresponds to Equation (8-17) and uses steam to hydrolyze sulfide on the sorbent surface. Data from the POC plant was plotted as X_r vs. $W/(F_s\, S_a)$ based on Equation (8-32). This plot consists of two straight lines with different slopes. The

lines correspond to the reaction rates of Equations (8-16) and (8-17), respectively. The reaction rate of Equation (8-16) is eight times higher than that of Equation (8-17). The reaction rates have been parametrized using experimental data from the POC tests, and are given as follows (Ma and Haslbeck, 1993):

$$r_{s_1} = k_1 \exp\left(-\frac{E_1}{RT}\right) S_a$$
$$r_{s_2} = k_2 (1 - 0.6) S_a \qquad (8\text{-}38)$$

Where,

$$\frac{E}{R} = 34554.0$$
$$\ln(k_1) = 38.97$$
$$k_2 = 0.85$$
$$S_a = 0.01$$

Another result of these experimental studies is that 60% of the sulfur on the spent sorbent is regenerated by natural gas, while the steam treatment regenerates 20-30% of the remaining sulfides on the sorbent. The shift in sulfur regeneration from reaction 1 to reaction 2 at $X_{shift} = 0.6$ is independent of the inlet sorbent temperature. However, the amount of sulfur that is regenerated by the steam treater (X_{final}) depends on the inlet sorbent temperature. Typically, varying the inlet temperature from 1100-1250°F increases the sulfur regeneration from 20% to 30%. Assuming a linear relationship, this is written as:

$$X_{final} = (0.001T - 0.35 - X_{shift}) \qquad (8\text{-}39)$$

The heat of regeneration for both reactions also has been estimated from experimental data:

$$\Delta H_1 = 917.2 \text{ Btu/lb sulfur}$$

$$\Delta H_2 = 2032 \text{ Btu/lb sulfur}$$

The design equations for sorbent residence times are now straightforward:

$$t_{CH_4} = \frac{X_{shift} S_a}{r_{s_1}}$$
$$t_{H_2O} = \frac{(X_{final} - X_{shift}) S_a}{r_{s_2}} \qquad (8\text{-}40)$$

Figure 8-7 plots the sensitivities of the total regenerator residence time (t_{CH4}+t_{H20}) as a function of the SO_2 and NO_x removal efficiencies. The regenerator residence time increases with increasing SO_2 removal. However, with increasing NO_x removal, the total SO_2 removed decreases and this decreases the residence time required in the regenerator. The regenerator temperature is assumed to be 1150°F. Figure 8-8 examine the sensitivity of the total regenerator residence time to the regenerator temperature and the fraction of sulfur on the sorbent removed by methane reduction reactions, for 90% SO_2 removal and 80% NO_x removal. A 2.6% sulfur Appalachian coal is assumed. The residence time decreases with increasing temperature of the sorbent since the rate of the reduction reactions increases with temperature.

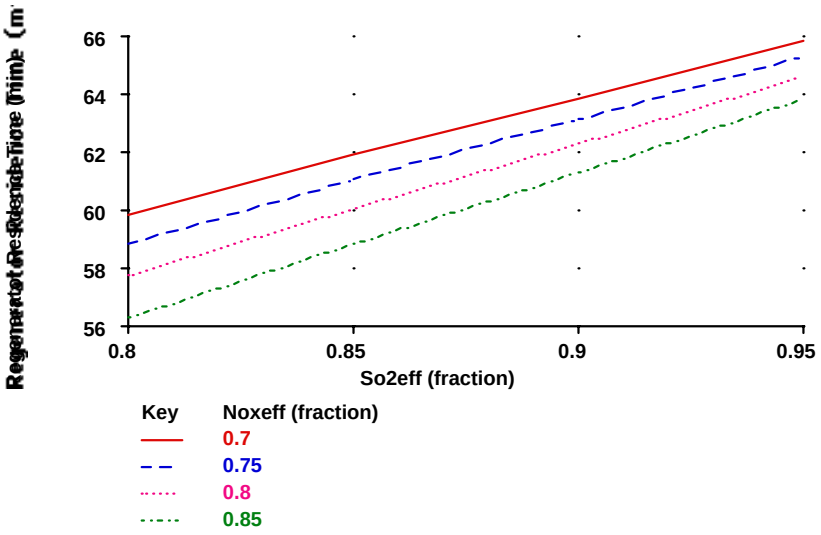

Figure 8-7 Sorbent Residence Time for Methane Reduction in Regenerator

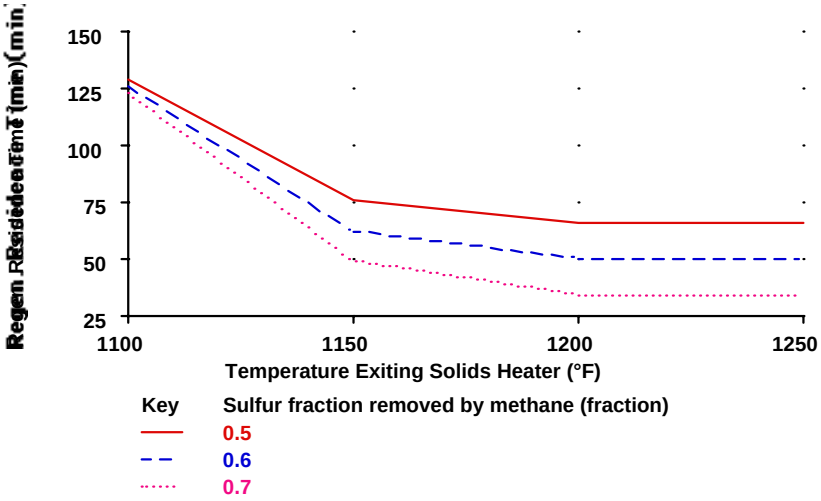

Figure 8-8 Regenerator Residence Time vs. Temperature and Sulfur Removal

8.2.4.3. Sorbent Heater and Cooler

Models of the sorbent heater and cooler are limited to simple mass and energy balances. The heat exchange between the sorbent and the hot air is treated as a simple energy balance. Similarly, the cooling of the sorbent is also treated as a simple energy balance as follows:

$$F_g C_p (T - T_0) = \pm F_s c_{ps} (T_s - T_{s0}) \qquad (8\text{-}41)$$

where the subscript "0" refers to initial condition, and

F_g = gas flow rate (kmole/sec)

c_p = gas specific heat kcal/mole (°C)

F_s = sorbent flow rate (kg/sec)

c_{p_S} = sorbent heat capacity (kcal/kg°C)

T_s = sorbent temperature (°C)

The $\pm$ signs are chosen depending on whether sorbent is being cooled or heated. These heat exchange models are used to calculate the energy requirement for sorbent heating and the related calculation of natural gas consumption.

The mass balance equations are used to evaluate the amount of NO_x and SO_2 that are recycled to the boiler as part of the combustor gas. The NO_x from the sorbent is completely desorbed in the sorbent heater and about 5-10% of the SO_2 is desorbed. Since this extra amount of SO_2 and NO_x is recycled back to the flue gas, the absorber needs to actually remove a large fraction of these species in order to achieve the same levels of emissions as if there were no recycle. Mass balance equations are used to calculate the actual removal efficiencies for a desired level of emissions. A schematic of the recycle loop is shown in Figure 8-9.

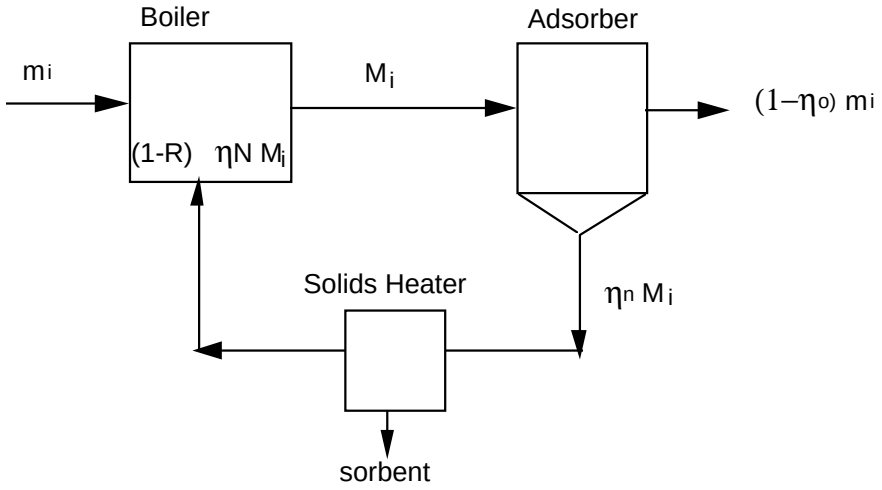

Figure 8-9 Schematic of the Recycle Loop

The initial mass flow rate for each species (SO_2, NO_x) is denoted by m_i and the mass flow rate with recycle is denoted by M_i. The desired emission level of $(1-\eta_O)\ m_i$ is specified with respect to m_i and let us assume that the required removal efficiency is η_O. Since the emission levels should not change with recycle, the actual removal efficiency η_N required to achieve this is given by

$$M_i\,(1-\eta_N) = m_i\,(1-\eta_O) \qquad (8\text{-}42)$$

Moreover, from mass balance the recycle mass flow for species i (M_i) is related to original mass flow rate m_i as shown below:

$$M_i = m_i + (1-R_i)\ \eta_N\ M_i \qquad (8\text{-}43)$$

Solving these equations for η_N we get

$$\eta_N = \frac{\eta_O}{1-(1-\eta_O)\ (1-R_i)} \qquad (8\text{-}44)$$

where R_i is the recycle fraction for each species (94% for SO_2 and 65% for NO_x).

8.2.4.4. A Numerical Example

Provided here is a conceptual design of a commercial NOXSO plant of size 300 MW achieving 90% SO_2 removal and 80% NO_x removal. The coal used is a medium sulfur Appalachian coal (2.6% sulfur, and 1.12% nitrogen). The design specifications are:

Parameter	Value
Plant Size	300 MW, 842 Kacfm (at 320°F)
Temp. of flue gas entering adsorber	320°F
SO_2 removal requirement	90%
NO_x removal requirement	80%
Inlet SO_2 conc. (η_{SO2})	1516 ppm (calculated by IECM)
Inlet NO_x conc. (η_{NOx})	400 ppm (calculated by IECM)
Sorbent	Na_2CO_3 on γ-alumina spheres

Actual Removal Efficiencies

Since some NO_x and SO_2 are recycled back to the boiler, we need to calculate the actual absorber removal efficiencies required to achieve the desired design. This can be calculated by a simple mass balance of SO_2 and NO_x around the power plant once the recycle fractions are known. Based on the current NOXSO design, these fractions are 94% for SO_2 and 65% for NO_x. Thus,

$$\phi_{N,1} = \frac{\eta_{SO_2}}{1-\left(1-\eta_{SO_2}\right)\left(1-R_{SO_2}\right)} = \frac{0.9}{1-(1-0.9)\times(1-0.06)} = 0.905$$

$$\phi_{N,2} = \frac{\eta_{NO_x}}{1-\left(1-\eta_{NO_x}\right)\left(1-R_{NO_x}\right)} = \frac{0.8}{1-(1-0.8)\times(1-0.35)} = 0.86$$

Adsorber

Physical parameters required for the calculations are first estimated. Substituting the adsorber temperature of 275°F in Equation (8-28) we estimate the stochiometric ratios as follows:

$\lambda_1 = 0.93$

$\lambda_2 = 0.19$

Similarly, the temperature-dependent rate constants obtained from Equations (8-33) and (8-34) are:

$K_1 = 0.5734\,(\text{atm sec})^{-1}$

$K_2 = 1.577\,(\text{atm sec})^{-1}$

The sorbent capacities are calculated using Equations (8-31) and (8-32). Based on pilot plant data, the weight fraction of sodium in the sorbent is taken to be 3.8%, silicon content is about 5.2%, the sulfur content of regenerated sorbent is 0.25%, and the available surface area fraction is 0.6. Thus,

$$For\ \mathrm{SO_2}: \mathrm{E_1} = \left(\lambda_1 n + \frac{0.8 - S_r}{3200}\right)\frac{A}{A_0}$$

$$= \left(0.93 \times 1.65 \times 10^{-3} + \frac{0.8 - 0.25}{3200}\right) \times 0.6 = 1.02 \times 10^{-3}$$

$$For\ \mathrm{NO_x}: \mathrm{E_2} = \left(\lambda_2 n + \frac{0.8 - S_r}{3200}\right)\frac{\lambda_2}{\lambda_1}$$

$$= \left(0.19 \times 1.65 \times 10^{-3} + \frac{0.8 - 0.25}{3200}\right) \times \frac{0.93}{0.19} = 0.3 \times 10^{-3}$$

Now the key operating parameters, sorbent residence time and sorbent inventory, can be calculated using Equation (8-35). The calculation of the intermediate variables is not shown.

$$\frac{W}{F_s} = -\frac{a_1 b_3 + a_3 b_1}{a_2 b_3 + a_3 b_2}$$

$$= -\frac{-2.36 \times 11.5 \times 10^{-6} - 12.4 \times 10^{-6} \times 1.97}{0.95 \times 10^{-3} \times 11.5 \times 10^{-6} + 12.4 \times 10^{-6} \times 0.84 \times 10^{-3}}$$

$$= 2416\,\mathrm{sec.}$$

$$W = \frac{b_1 - b_2 \times W / F_s}{b_3} = -\frac{-1.97 - 0.84 \times 10^{-3} \times 2416}{11.5 \times 10^{-6}}$$

$$= 347{,}780\,\mathrm{lbs\ of\ sorbent\ required}$$

Therefore, the sorbent flow rate F_s is 347,780 / (2416/3600) = 518,210 lbs/hr.

Regenerator

Once again the reaction rates are evaluated using Equation (8-38).

$$r_{s_1} = k_1 \exp\left(-\frac{E_1}{RT}\right) S_a = \exp(38.97 - 34554/895)0.0136 = 0.0188$$

$$r_{s_2} = k_2 (1 - 0.6)\,\mathrm{S_a} = 0.85 \times 0.4 \times 0.0136 = 0.0046$$

The shift in the reducing reaction from methane to water is at X_{shift}=0.6 and X_{final}=0.8. Therefore the residence time of the sorbent is calculated as follows using Equation (8-40):

$$t_{CH_4} = \frac{X_{shift} S_a}{r_{s_1}} = \frac{0.6 \times 0.0136}{0.0185} \times 60 = 26.5\,\mathrm{min}$$

$$t_{H_2O} = \frac{(X_{final} - X_{shift})\,\mathrm{S_a}}{r_{s_2}} = \frac{0.2 \times 0.0136}{0.0045} \times 60 = 36.3\,\mathrm{min}$$

The total residence time in the regenerator is used to determine the sorbent inventory. This is used to estimate the cost of startup inventory.

$$Inventory = (F_S / 60) \times (t_{CH_4} + t_{H_2O})$$

$$= \frac{518{,}210}{60}(26.5 + 36.3)$$

$$= 536{,}600 \text{ lbs}$$

8.3. NOXSO Cost Models

8.3.1. Overview of Cost Modeling Methods

Because the NOXSO process is a new technology still under development, cost information is still extremely limited. Recent published reports (Leonard et al 1994, Haslbeck et al 1993, Cichanowicz et al 1991) have provided estimates of the total capital requirement, but with little supportive detail. Prior to the present study, a 1986 EPRI study remains the only published cost estimate of the NOXSO process with process area detail. That study was the basis for the NOXSO cost model originally developed for the IECM (CMU, 1986). Thus, unlike other IECM components, for which detailed engineering cost studies have been completed more recently, little recent information for NOXSO process costs is available in the open literature.

For this reason, two approaches to cost modeling are presented in this chapter. The first method is based on the earlier economic evaluation of the NOXSO process performed for EPRI. This 1986 cost analysis is useful since it is the only study based on detailed equipment costing which is available in the open literature. Moreover, recent NOXSO reports continue to report capital cost estimates which are virtually identical to the cost estimate provided in the 1986 EPRI study.

A new (1995) cost model also has been developed for the NOXSO process, and implemented in the IECM. The new model is based on a detailed cost model of the fluidized bed copper oxide process recently developed for the IECM (Frey and Rubin, 1994). The rationale for this approach is twofold:

1. The NOXSO process and the fluidized bed copper oxide process are structurally similar. Both processes use a regenerable sorbent which is cycled through a fluidized bed adsorber, sorbent heater, a combustor for the sorbent heater, a regenerator, sorbent cooler and a dense phase conveyor system for transporting the sorbent. As a result of this structural similarity, both processes use largely the same set of equipment. A key difference is that NOXSO, unlike the CuO process, does not require ammonia injection for NO_x removal. However, it does require recycle of NO_x to the furnace.
2. The difference in capital cost between these processes arises primarily from differences in the sizing of equipment since the operating conditions for the two processes are different. In particular, the NOXSO adsorber is operated at 320°F while the CuO process operates at 700°F. However, since the equipment cost models developed for the CuO process are sensitive to differences in operating parameters, these same models can be used to estimate costs for the NOXSO process conditions. Allowances also can be made for other cost items that distinguish these two processes.

The remainder of this section is organized as follows: the first subsection presents the new capital cost models for the NOXSO process, together with a comparison with results from the earlier EPRI study. The next subsection provides models of fixed and variable operating and maintenance (O&M) costs. The third combines the capital costs with annual O&M costs to calculate a levelized revenue requirement or cost of electricity. The fourth provides a numerical example of costing the NOXSO process, and compares current results with earlier EPRI studies. The final subsection outlines a list of issues that need to be addressed to further improve the current models.

8.3.2. Capital Cost Model

In this section we provide a detailed description of two capital cost models developed for the NOXSO process. First, the cost model originally developed for the IECM based on the 1986 EPRI report is reviewed. We refer to this as the 1986 model. Then, a new cost model is developed based on the recent modeling of the fluidized bed copper oxide (CuO) process. We refer to this as the 1995 model. Then, results from the two models are compared to illustrate the difference in the cost estimates generated by each model.

8.3.2.1. 1986 Capital Cost Model

This model is based on a case study by EPRI (1986), and is similar to the original IECM cost model for NOXSO, except that a number of plant components have been updated. Capital costs were estimated for a base plant of 1000 MW with 4% sulfur coal. The main operating parameters for this base case design, which are used for scaling capital cost estimates, are provided in Table 8-1.

Table 8-1 ***Base Case Design Parameters (1000 MW plant)***

Parameters	Values
Flue gas flow rate, acfm	3.6×10^6
Sorbent flow rate, lb/hr	1.36×10^6
Makeup sorbent flow rate, lb/hr	880
Surface area of adsorber, ft^2	2542
Methane consumption, lb/hr	7200

The EPRI report lists plant components by section with itemized delivered equipment costs. The cost of components for each process area has been summed to obtain the process facilities capital cost, as shown in Table 8-2. Two major changes were made to the EPRI assumptions regarding the process facilities cost:

1. The EPRI report assumed the use of synthesis gas produced on site for regeneration. This has been replaced with the use of methane which is treated as one of the consumables. In order to account for this we eliminated the capital cost for a Texaco gasifier that was used in the original design as part of the regenerator (process area 40).
2. The original design used oil in the solids combustor. This, too, has been replaced with the use of methane. We assumed that the capital costs for storing and pumping methane would be similar to that of oil. However, the capital cost equations are now scaled by the amount of methane used rather than oil.

Table 8-2 ***Process Facilities Cost Based on 1986 EPRI Report***

Area	Description	Equipment Cost (10^6 1986$)
10	Reagent Feed System	2.6
20	SO_2 Removal System	5.3
30	Flue Gas Handling System	20.6
40	Sorbent Regenerator System	15.13
70	General Support Equipment	0.29
80	Air Preheater Modification	-
90	Sulfur Byproduct Recovery	-
100	Initial Sorbent Inventory	-

The cost model for each process area was parameterized on one or more of the main operating parameters enumerated in Table 8-1. Coefficients were estimated by adding all component costs associated with each parameter and normalizing them to the base case. As a conservative estimate, an exponential scaling factor of 0.7 was used in the 1986 model to estimate costs for designs different from the EPRI base case. Thus, the canonical form used for all process area cost models is as follows:

$$C_i = \sum_i a_i \, x_i^{0.7}$$

where x_i is the operating parameter used for scaling and a_i is the cost coefficient for each parameter.

Reagent Feed System

The reagent feed system consists of equipment for the preparation and transportation of the makeup sorbent to the adsorber. The pumps and storage tanks required for methane are also included in this process area. The capital cost for the reagent feed system is based on the makeup sorbent flow rate and methane consumption as shown below:

$$C_{10} = 14350\, m_{ms}^{0.7} + 1.925\, m_{CH4}^{0.7}$$

SO2 Removal System

The SO_2 removal system includes the absorber vessels and the sorbent pneumatic conveying system. The capital cost is scaled based on the cross sectional area of the adsorber vessels and is provided as:

$$C_{20} = 2188(N_{towers} + N_{spares})A_{absorber}$$

Flue Gas Handling System

The flue gas handling system includes equipment for transporting flue gas such as I.D. fans, ductwork and inlet/outlet manifolds. The cost models are scaled based on flue gas flow rate as follows:

$$C_{30} = 530\, G_{FG}^{0.7}$$

Sorbent Regeneration System

The regeneration system includes the regenerator vessels, and regenerated sorbent handling equipment. The capital costs are based on sorbent flow rate and are given as follows:

$$C_{40} = 770\, m_{sorbent}^{0.7}$$

General Support Equipment

This process area accounts for all the miscellaneous equipment required for process areas 10, 20, 30, and 40. The cost model is defined as a fraction of the other process facilities cost as shown:

$$C_{70} = 0.007(C_{10} + C_{20} + C_{30} + C_{40})$$

Air Preheater Modifications

Capital cost for air preheater, modifications to allow off-gas from the solids heater to preheat incoming combustion air is based on the change in the heat transfer in the air preheater. The IECM air preheater model is used for this purpose. The capital cost is scaled based on the UA product (Btu/K, a product of the heat transfer coefficient and the heat transfer area) of the heat exchanger. The capital cost is given as a function of the change in UA as follows:

$$C_{80} = 2.6\times10^{-3}\left(UA_{air}^{0.6} - UA_{orig}^{0.6}\right)$$

Sulfur Byproduct Recovery

A performance and cost model of a sulfur byproduct recovery process (Claus plant) has been developed for the IECM and is documented in an earlier report to DOE (Rubin, et al., 1991). That model has been employed here.

Sorbent Inventory

The initial sorbent requirement is governed by the amount of sorbent hold up in the fluidized bed adsorber, the regenerator, and the solids heater. It is assumed that the sorbent hold up in the transport system is small. The cost for initial sorbent is given as follows:

$$C_{100} = (\rho_s\, Z_A\, A_A + m_s\, t_R + 2\,\rho_S\, Z_{SH}\, A_{SH})S_{cost}$$

Total Process Facilities Cost

The total process facilities cost is the total of all process area costs and is given by:

$$PFC = C_{10} + C_{20} + C_{30} + C_{40} + C_{70} + C_{80} + C_{90} + C_{100}$$

Figure 8-10 graphs the sensitivity of the process facility cost to power plant size and coal type. Only medium to high sulfur coals are considered since the NOXSO process has not been tested for low sulfur coals. The Chemical Engineering plant cost index has been used to convert 1986 dollars to 1993 costs. The graph illustrates the economy of scale as plant size increases for a particular coal. Capital costs also are sensitive to coal properties. Higher sulfur content increases cost (e.g., 4%S Illinois coal vs. 2.6% Appalachian coal). However, other coal properties such as

heating value that affect the flue gas volumetric flow also are important. Thus, although the North Dakota lignite has a lower sulfur content than the Appalachian coal, its heating value also is substantially lower; this generates a larger gas volume per MW of power produced, resulting in larger equipment sizes and higher cost. All of these interactions are captured in the IECM.

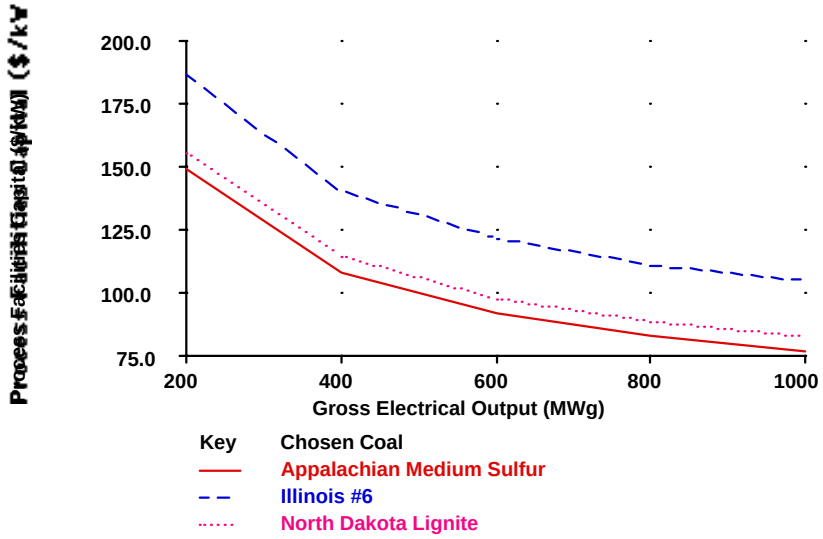

Figure 8-10 Total Process Facilities Cost (1993$) Based on the 1986 Model

8.3.2.2. 1995 Capital Cost Model

The capital cost model presented in this section is based on a new cost model recently developed for the fluidized bed CuO process (CMU 1994). Appropriate changes have been made to tailor the models to the NOXSO process. Compared to the 1986 model, the new cost model is more highly disaggregated by process area.

Fluidized Bed Adsorbers

The process capital cost of the fluidized bed absorbers includes the absorber vessel, structural supports, dampers, isolation valves, refractory lining for the inside of the absorber, ductwork, instrumentation and control, and installation costs.

The absorber vessels are refractory-lined carbon steel of minimum one-half inch thickness. Each absorber vessel may be approximated as a cylinder. The internal diameter of the absorber vessel is determined based on the superficial gas velocity requirement. The materials cost of the absorber is proportional to the surface area of the absorber vessel. The absorber vessel internal radius is given by:

$$r_A = \sqrt{\frac{G_{FG}}{60\,\pi\, V_s\, N_{towers}}} \qquad (8\text{-}45)$$

The diameter of the absorber vessel must be larger than this internal radius to accommodate the thickness of refractory lining. The design basis developed by A. E. Roberts and Associates (AERA) for the copper oxide absorber includes a two-inch thick base or inner refractory covering the internal surface of the absorber vessel. This two-inch base or inner refractory lining also is assumed to be sufficient for the NOXSO process. The CuO process has an additional "hot base" refractory layer which is approximately six inches thick. However, since the adsorber temperature for the NOXSO process is only 320°F (as compared to 700°F for the CuO process), the

"hot base" is assumed to be unnecessary for the NOXSO vessel. Thus, the vessel internal diameter is:

$$r_{V,A} = r_A + t_{ir} \qquad (8\text{-}46)$$

The surface area of the absorber vessel is approximated by the following equation for the surface area of a cylinder:

$$SA_A = 2\pi \left(r_{V,A}\right)^2 + 2\pi\, r_{V,A}\, h_A \qquad (8\text{-}47)$$

The design height of the copper oxide absorber vessel is approximately 70 feet. The total height of the absorber assembly is larger when flue gas outlet ductwork is taken into consideration. The straight wall portion of the absorber vessel that is covered with refractory lining is approximately 35 feet.

The direct cost for the steel absorber vessel is estimated based on the ratio of surface areas referenced to a base case design. The copper oxide design is predicated on a flue gas volumetric flow rate of approximately 500,000 scfm at 705°F and a superficial gas velocity of 4.5 ft/sec. For this case, the approximate surface area of the absorber vessel is 24,875 ft^2. The base cost estimate is $1,434,000 (in 1993 dollars) for a single absorber vessel of this size. Therefore, the direct cost model for the cost of the NOXSO steel absorber vessel is given by:

$$C_{A,V} = 1434\, N_{total} \left(\frac{SA_A}{24{,}875}\right) \frac{PCI}{1993\, PCI}$$

where the smaller surface area for the NOXSO process is calculated from Equations (8-45) to (8-47). Typically, there will be two 50% capacity absorber vessels with no spares.

The cost of refractory is given by the refractory surface area, required to cover the sides of the absorber vessel, and a unit cost for refractory per square foot:

$$C_{A,R} = 2\pi\, r_A\, h_{A,S}\, N_{towers}\, R_{cost}$$

In 1993 dollars, the unit cost of the total of 8 inches of refractory required for the absorber was approximately $55/$ft^2$.

Each absorber requires structural supports. In the copper oxide design, these are estimated at $100,000 per vessel. The structural support is assumed here to have some economy of scale with respect to size. A six-tenths scaling rule traditionally used in the process technology and chemical engineering literature is assumed:

$$C_{A,S} = 100\, N_{total} \left(\frac{SA_A}{24{,}875}\right)^{0.6} \frac{PCI}{1993\, PCI}$$

The surface area of the absorber vessel is used as a surrogate variable for the size of the absorber system and, hence, the proportional size of the structural supports.

The Costs for flue gas ductwork, flue gas isolation valves, and dampers are assumed to be proportional to the flue gas volumetric flow rate. Moreover, economies of scale are assumed. In the absence of more detailed information, the following direct cost model was adapted based on the copper oxide study:

$$C_{A,d} = 300\, N_{total} \left(\frac{G_{FG}}{1.1\times 10^6\, N_{towers}}\right)^{0.6} \frac{PCI}{1993\, PCI}$$

In this model, the cost of ductwork, isolation valves, and dampers is estimated for a single absorber vessel, and is multiplied by the total number of absorber vessels. The total direct cost for the absorber process area is then given by:

$$C_A = (1 + f_{ic,a})\,(C_{A,V} + C_{A,R} + C_{A,S} + C_{A,d})$$

where $f_{ic,a}$ is an installation cost factor for the absorber process area. A default value of 0.45 is suggested for the CuO process and adopted as well for the NOXSO process.

In addition to these direct costs, there is a cost associated with using a new induced draft fan to overcome the pressure drop of the flue gas in the adsorber. The fan efficiency is typically 85 percent. The cost of the ID fan differential is:

$$C_{ID} = 180\, N_{A,t} \left(\frac{EC_{ID}}{4600} \right)^{0.6} \frac{PCI}{1993\, PCI}$$

Regenerator

The regenerator cost model assumes a carbon steel cylindrical vessel sized to accommodate sorbent storage for a specified sorbent residence time. The base case copper oxide design has a regenerator with a sorbent hold-up volume of 8,800 ft^3. The regenerator design features a 28 foot straight wall height. Here, it is assumed that the straight wall height is held fixed, and the radius is adjusted to accommodate various residence times. Usually, columns that are higher than 28-30 feet require buildings with high roofs which increase construction costs. The required regenerator radius for the NOXSO process is therefore given by:

$$r_R = \sqrt{\frac{m_{s,R}\; t_R}{60\, \rho_s\; N_{towers}\; \pi\; h_{R,S}}}$$

The total height of the regenerator is the straight wall height plus inlet and outlet clearances for gas flows. These clearances add approximately 17 feet to the straight wall height. The inside of the regenerator vessel walls are covered with two layers of refractory totaling 8 inches in thickness. Therefore, the steel vessel diameter is:

$$r_{V,R} = r_R + t_{ir}$$

The surface area of the regenerator vessel is approximated by the surface area of a cylinder:

$$SA_R = 2\pi \left(r_{V,R}\right)^2 + 2\pi\, r_{V,R}\; h_R$$

For the copper oxide process, the regenerator has an equivalent overall height of 78 feet and a radius of 10 feet, yielding a surface area of 5530 ft^2. The direct cost of the NOXSO regenerator vessel is then estimated as:

$$C_{R,d} = 475\, N_{total} \left(\frac{SA_R}{5530\, N_{R,t}} \right)^{0.6} \frac{PCI}{1993\, PCI}$$

The additional direct cost of refractory is given by:

$$C_{R,R} = 2\pi\, r_R\; h_{R,S}\; N_{R,t}\; R_{cost}$$

Each regenerator requires structural supports. In the base case design, this cost is estimated at $42,500 per vessel. The structural support is assumed here to have some economy of scale with respect to size. A six-tenths scaling rule again is assumed:

$$C_{R,s} = 42.5\, N_{total} \left(\frac{SA_R}{5530\, N_{R,t}} \right)^{0.6} \frac{PCI}{1993\, PCI}$$

The surface area of the absorber vessel is used as a surrogate variable for the size of the regenerator system and, hence, the proportional size of the structural supports.

The costs for ductwork, isolation valves, and dampers are assumed to be proportional to the regenerator off-gas volume flow rate. Moreover, economies of scale are assumed. In the base case analysis, approximately 626 lbmole/hour of off-gas is evolved from each of the two copper oxide regenerator vessels. At 900°F, the volumetric flow rate is 21,900 ft^3/min. Thus, in the absence of more detailed information, the following direct cost model was developed:

$$C_{R,d} = 350\, N_{total} \left(\frac{G_{FG}}{626\, N_{R,t}} \right)^{0.6} \frac{PCI}{1993\, PCI}$$

In this model, the cost of ductwork, isolation valves, and dampers is estimated for a single absorber vessel, then multiplied by the total number of absorber vessels.

A methane feed system, a booster compressor and motor are required for the inlet methane to overcome the pressure drop through the regenerator. The booster compressor cost is assumed to be proportional to the methane flow rate. Again scaling costs from the copper oxide model gives:

$$C_{R,CH4} = 350\, N_{total} \left(\frac{M_{R,CH4}}{187\, N_{R,t}} \right)^{0.6} \frac{PCI}{1993\, PCI}$$

The total direct cost for the absorber process area is given by:

$$C_R = (1 + f_{ic,R})\,(C_{R,V} + C_{R,R} + C_{R,S} + C_{R,d} + C_{R,CH4})$$

where $f_{ic,R}$ is an installation cost factor for the absorber process area. A default value of 0.45 again is suggested.

Solids Heater

The solids heater is assumed to be a carbon steel cylindrical vessel. For the copper oxide process, AERA has designed a solids heater with an internal radius of 10 feet and a height of 50 feet. The side walls of the heater are lined with refractory material. The internal diameter of the solids heater is proportional to the mass flow of sorbent entering the vessel. The vessel contains two sorbent beds in which hot combustion gases from a methane combustor contact the sorbent in counter-current flow. Thus, for fixed bed heights in each stage, the solids heater internal radius varies with the sorbent mass flow rate as follows:

$$\sqrt{\frac{m_{s,SH}\, t_{SH}}{400{,}000 N_{SH,t}}}$$

The inside of the solids heater vessel walls are covered with two layers of refractory totaling 8 inches in thickness. Therefore, the steel vessel diameter is:

$$r_{V,SH} = r_{SH} + t_{ir}$$

The surface area of the solids heater vessel is approximated by the surface area of a cylinder. Thus, for a single vessel, the surface area is:

$$SA_{SH} = 2\pi \left(r_{V,SH}\right)^2 + 2\pi\, r_{V,SH}\, h_{SH}$$

In the base case, the solids heater has an equivalent overall height of 50 feet and an internal radius of 10 feet. Scaling results for the copper oxide process, the direct cost of the NOXSO regenerator vessel is:

$$C_{SH,V} = 360\, N_{total} \left(\frac{SA_{SH}}{4060\, N_{SH,t}} \right)^{0.6} \frac{PCI}{1993\, PCI}$$

The additional direct cost of refractory is given by:

$$C_{SH,V} = 2\pi\, r_{SH}\, h_{SH,S}\, N_{SH,t}\, R_{cost}$$

Each solids heater requires structural supports. In the copper oxide design, these are estimated at $72,500 per vessel. The structural support is assumed here to have some economy of scale with respect to size. A six-tenths scaling rule gives:

$$C_{SH,s} = 72.5\, N_{SH,t} \left(\frac{SA_{SH}}{4060\, N_{SH,t}} \right)^{0.6} \frac{PCI}{1993\, PCI}$$

The surface area of the solids heater vessel is used as a surrogate variable for the size of the NOXSO solids heater system and, hence, the proportional size of the structural supports.

The costs for ductwork, isolation valves, dampers, booster fans and motors are assumed to be proportional to the solids heater exit gas volumetric flow rate. Again, economies of scale are assumed. In the copper oxide process, approximately 6,500 lbmole/hour of gas exits the solids heater at 830°F. Thus, the following direct cost model was developed:

$$C_{SH,d} = 608\, N_{total} \left(\frac{G_{SH,off}}{6467\, N_{SH,t}} \right)^{0.6} \frac{PCI}{1993\, PCI}$$

In this model, the cost of ductwork, isolation valves, dampers, booster fans, and booster fan motors is estimated for a single solids heater vessel, and multiplied by the total number of absorber vessels.

The total direct cost for the solids heater is:

$$C_{SH} = (1 + f_{ic,SH})\,(C_{SH,V} + C_{R,r} + C_{SH,S} + C_{SH,d})$$

where $f_{ic,R}$ is an installation cost factor for the absorber process area. A default value of 0.45 is suggested.

Sorbent Transport System

A dense phase pneumatic transport system is employed to transport sorbent from the regenerator outlet to the absorber inlet. The transport system includes valves, compressors, piping, filters, and surge bins. The dense phase transport system was

sized for a sorbent circulation rate of 1,000,000 lb/hr. The total cost for this system for the copper oxide process is $6,580,000. The cost of the NOXSO transport system is assumed to be proportional to the sorbent circulation rate. Thus, the equipment cost for the dense phase transport system is:

$$C_{ST,e} = 6580 \left(\frac{m_{sorbent}}{1{,}000{,}000} \right)^{0.6} \frac{PCI}{1993\,PCI}$$

In addition, a sorbent storage silo is required. The cost of these silos is proportional to the sorbent circulation rate and the sorbent attrition rate, which determine the sorbent make-up rate. The nominal sorbent makeup rate is 500 lb/hr in the base case design. Therefore, the cost of the storage silos with air locks is:

$$C_{ST,s} = 330 \left(\frac{m_{makeup}}{500} \right)^{0.6} \frac{PCI}{1993\,PCI}$$

The total direct cost for the sorbent transport system is:

$$C_{ST} = (1 + f_{ic,ST})\,(C_{ST,e} + C_{ST,s})$$

where $f_{ic,ST}$ is an installation cost factor for the solids transport process area. A default value of 0.45 is suggested.

Solids Heater Combustor

The cost of the combustor for the solids heater is assumed to be proportional to the methane requirement: Scaling results for the copper oxide combustor gives:

$$C_{SH,s} = 330\ (1 + f_{ic,SH,c}) \left(\frac{m_{CH4,SH}}{225} \right)^{0.6} \frac{PCI}{1993\,PCI}$$

where $f_{ic,SH,c}$ is an installation cost factor for the solids heater combustor process area. A default value of 0.45 is suggested.

Byproduct Recovery

A performance and cost model (C_{By}) of a byproduct sulfur recovery plant has been developed previously (Rubin et al., 1991). This model has been adapted for the NOXSO process.

Air Preheater Modifications

The NOXSO process produces off-gas from the solids heater at temperatures of about 610°F. This can be used to preheat the combustion air going into the boiler. The cost of air preheater modifications (C_{APH}) to allow this was shown previously.

Initial Sorbent Inventory

The initial sorbent requirement is governed primarily by the amount of sorbent hold up in the fluidized bed absorber, the regenerator, and the solids heater. It is assumed that the quantity of sorbent hold up in the transport system is small by comparison. The cost for initial sorbent fill is therefore:

$$C_{S,I} = \left(\rho_s\ Z_A\ A_A + m_s\ t_R + 2\,\rho_S\ Z_{SH}\ A_{SH} \right) S_{cost}$$

Total Process Facilities Cost

The total process facilities cost is the sum of the plant section direct costs. The cost of initial catalyst charge is also included in the direct costs because it is a large and integral part of the NOXSO system. Therefore, the total direct cost is given by:

$$PFC = C_A + C_{ID} + C_R + C_{SH} + C_{ST} + C_{SH,s} + C_{By} + C_{APH} + C_{S,I}$$

Figure 8-11 graphs the sensitivity of process facilities cost for different coals as a function of plant size. As in Figure 8-10 shown earlier, this graph illustrates the economy of scale achieved in capital costs with increasing size, as well as sensitivity to fuel properties.

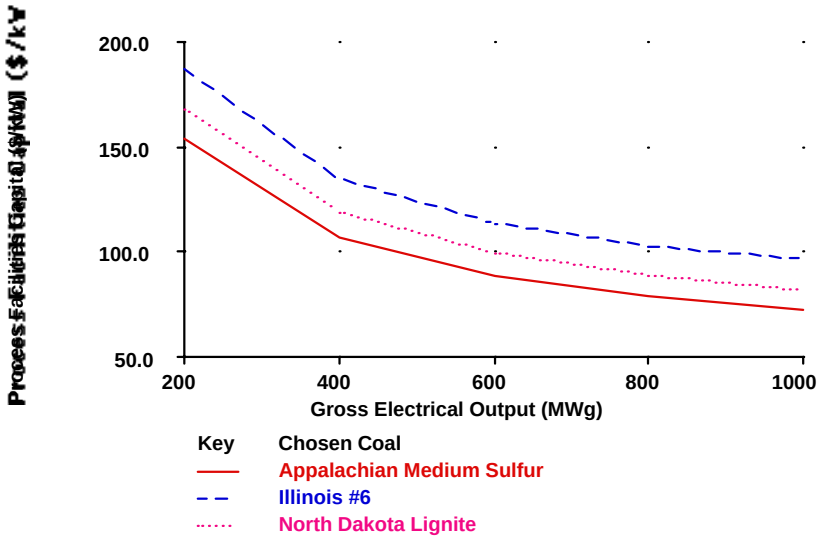

Figure 8-11 Total Process Facilities Cost (1993$) for the 1995 Model

8.3.2.3. Total Capital Requirement

All IECM cost models employ a standard set of "indirect" cost factors based on the EPRI costing methodology. These are model parameters that can be set by the user. Most of these factors are expressed as fractions of the total process facilities cost (PFC).The default values of all indirect cost factors associated with the NOXSO process have been adopted from the CuO study since both technologies are at similar stages of development. We enumerate the various indirect cost factors in Table 8-3 with the default values used.

Table 8-3 ***Indirect Cost Factors***

Indirect Cost Factor	Default Value	Formula
General Facilities Cost	10%	$C_{GFC} = f_{GFC}$ (PFC)
Engineering & Home Office Fees	15%	$C_{EHO} = f_{EHO}$ (PFC)
Project Contingency	20%	$C_{ProjC} = f_{ProjC}$ (PFC)
Process Contingency	20%	$C_{ProcC} = f_{ProcC}$ (PFC)
Total Plant Cost		TPC=PFC+C_{GFC}+C_{EHO} +C_{ProjC}+C_{ProcC}
Royalties	2%	$C_{Royal} = f_{Royal}$ (TPC)
Preproduction Costs	2%	$C_{PP}=f_{PP}$ (TPI)
Inventory Capital	0.5%	$C_{IC} = f_{IC}$ (TPC)

The total plant cost (TPC) is the overnight construction cost. An allowance for funds used during construction (AFUDC) is calculated based on the TPC as a function of the time to construct the NOXSO system. A 36 month construction period for a new plant is assumed. Methods for computing the AFUDC are documented elsewhere (e.g., EPRI, 1993) and are not repeated here. The total plant investment (TPI) represents the sum of the total plant cost and the AFDC.

The final measure of capital cost is the total capital requirement (TCR). The TCR includes the total plant investment plus costs for royalties, startup costs, and initial inventories of feedstocks. Preproduction costs typically include one month of both fixed operating costs (FOC) and variable operating costs (VOC) plus two percent of total plant investment. Inventory capital is estimated as 0.5 percent of total process capital excluding catalyst. For the NOXSO process, the costs for initial catalysts and chemicals is zero. The NOXSO initial sorbent requirement is included in the process capital costs. Thus, the total capital requirement for the NOXSO system is:

$$TCR = \frac{VOC + FOC}{12} + (1 + f_{PP} + f_R)(TPI) + f_{IC}(TPC)$$

8.3.2.4. Comparison of Capital Cost Models

This section presents a numerical example which compares the new model cost estimates for the NOXSO process to the earlier 1986 model estimate based on the EPRI study. The comparison demonstrates the behavior of the NOXSO cost models and highlight parts of the models that need to be further refined. We compare costs for a design with the performance characteristics shown in Table 8-4. The various performance parameters in Table 8-4 have been calculated using the NOXSO performance model which has been implemented in IECM.

Since the process area descriptions are different in the two models we present the cost estimates separately in Table 8-5 and Table 8-6. Both models have been adjusted to report costs in 1993 dollars. Only the process facility costs are shown since this is the only source of differences between the two models.

It is interesting to note that the total process facilities cost estimates from the two models are within 5 percent of each other, when put on a common basis, with the 1995 model estimates being slightly higher. Thus, although the new model has been developed from a different basis it provides cost estimates similar to those reported earlier in the literature. For different plant sizes, the new model yields slightly greater economies of scale than the earlier 1986 model.

Table 8-4 ***NOXSO Process Design Assumptions for a 500 MW Plant***

Parameter	Value
Required SO_2 Removal Efficiency, %	90
Actual SO_2 Removal Efficiency, %	90.5
Required NOx Removal Efficiency, %	80
Actual NOx Removal Efficiency, %	86
Flue Gas Inlet Temp. at Adsorber, °F	300
Absorber Sorbent Inventory, lbs	579,000
Regenerator Sorbent Inventory, lbs	894,000
Solids Heater Sorbent Inventory, lbs	931,000
Sorbent Circulation Rate, lb/hr	432,000
Makeup Sorbent, lb/hr	624
Train Size per Adsorber, acfm	425,000
Number of Absorbers (spares)	1(0)
Sorbent Absorber Residence Time, min	40
Superficial Flue Gas Velocity, ft/s	2.8
Expanded Bed Height, inches	32
Fluidized Bed Pressure Drop, in. H_2O	27
Solids Heater Outlet Temp., °F	1150
Methane Consumption, lb/hr	1952
Steam Consumption, lb/hr	2192
Sorbent Regenerator Residence Time, min	62
Sulfur Content of Spent Sorbent, wt %	2.7
Sulfur Content of Regenerated Sorbent, wt %	0.25

Table 8-5 ***NOXSO Process Capital Costs Using 1995 Model***

Process Area* and Equipment	(1993 M$)
Adsorber (Area 10)	6.57
Adsorber Vessel	2.95
Refractory lining	0.90
Structural support	0.20
Ductwork	0.48
ID Fan Differential (Area 20)	0.39
Regenerator (Area 40)	4.71
Regenerator Vessel	1.16
Refractory lining	0.61
Structural support	0.10
Ductwork	0.43
Boosterfan	0.96
Solids Heater (Area 50)	7.45
Adsorber Vessel	0.78
Refractory lining	0.37
Structural support	0.15
Ductwork	3.83
Sorbent Transport System (Area 60)	9.18
Dense Phase Transport	6.0
Sorbent storage	0.3
Solids Heater Combustor (Area 70)	7.15
Sulfur Byproduct Recovery (Area 90)	8.40
Initial Sorbent Inventory (Area 100)	2.73
Adsorber inventory	0.87
Regenerator inventory	1.3
Solids heater inventory	0.52
Total Process Facilities Cost (M $)	46.57
*An installation cost factor of 0.45 is assumed for each process area. Thus, the total installed cost is 1.45 times the total equipment cost shown for each process area.	

Table 8-6 ***NOXSO Process Capital Costs Using 1986 Model***

Process Areas	(1993 M$)
Reagent Feed System (10)	1.62
SO_2 Removal System (20)	1.57
Flue Gas Handling System (30)	11.16
Sorbent Regenerator System (40)	18.4
General Support Equipment (70)	0.23
Sulfur Byproduct Recovery (90)	8.40
Initial Sorbent Recovery (100)	2.73
TOTAL	44.11

8.3.3. Annual O&M Cost model

The annual operating and maintenance (O&M) costs for the NOXSO process consist of fixed operating and maintenance cost and variable operating costs. Cost models for these two components are summarized below.

8.3.3.1. Fixed Operating Costs

Fixed operating costs include operating labor, maintenance labor and materials, and overhead costs associated with administrative and support labor. The operating labor cost is based on an estimate of the number of personnel hours required to operate the NOXSO process multiplied by an average labor rate. It is common to assume that four shifts per day are required for plant operation, allowing two hours overlap for transition between shifts. Furthermore, an allowance for personnel on sick leave or vacation can be incorporated into the "shift factor." A shift factor of 4.75 is assumed as a default in this study, based on Bechtel (1988). For the NOXSO process we do not have any independent estimates for the labor, material and overhead costs. Therefore we have assumed the same set of default values as used for the CuO process.

The number of operators required per shift is assumed to be five. The total operating labor cost is estimated by summing the number of plant operators per shift for all process areas, applying the shift factor, and applying the average labor rate as follows:

$$OC_L = ALR \frac{2{,}080\ \text{hrs}}{\text{yr}} SF(1 + 2N_{A,O})$$

The cost for maintenance material and labor for new technologies is typically estimated as a percentage of the installed capital cost for each process section. The total maintenance cost for the plant is given by:

$$OC_M = f_M (TPC)$$

where a typical value of the maintenance cost multiplier, f_M, is 0.045 for a solids handling system. The total maintenance operating cost may be disaggregated into material and labor components using fractions suggested by EPRI:

$$OC_{MM} = 0.60\,\text{OC}_\text{M}$$

$$OC_{ML} = 0.40\,\text{OC}_\text{M}$$

The administrative and support labor cost is assumed to be 30 percent of the operating and maintenance labor cost:

$$OC_{AS} = 0.30(OC_L + OC_{ML})$$

The total fixed operating and maintenance costs is:

$$\mathrm{FOC_{Total}} = \mathrm{FOC_L} + \mathrm{FOC_M} + \mathrm{FOC_{As}}$$

The total fixed O&M costs for different coals and plant size is graphed in Figure 8-12. This graph shows a nearly linear increase in the total fixed O&M cost with gross power plant size. As the plant becomes larger, the labor and maintenance costs exhibit a slight economy of scale. Since some of the fixed O&M costs are estimated as fractions of plant capital cost, total fixed cost also exhibits a sensitivity to fuel type, reflecting the cost differences seen earlier in Figure 8-11.

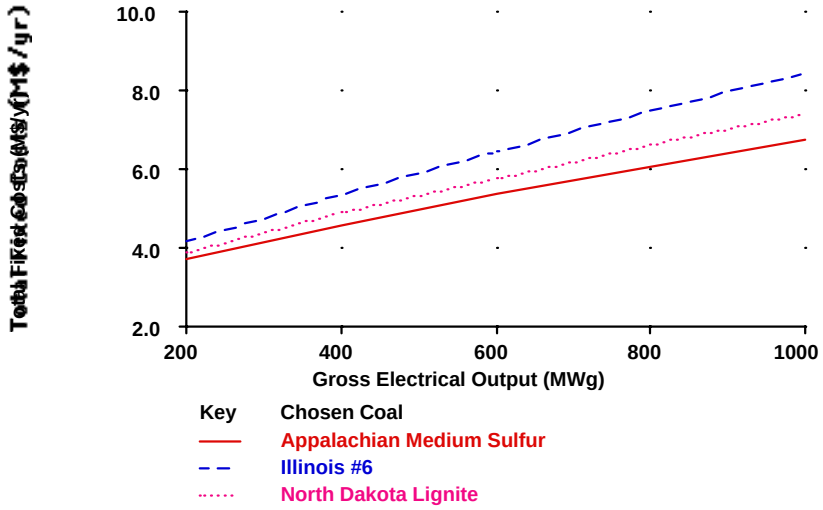

Figure 8-12 Fixed O&M Costs for Different Plant Configurations (1993$)

8.3.3.2. Variable Operating Costs

Variable operating costs include all consumable materials required for operation of the process. These include the costs of sorbent for makeup of attrition losses, the cost of methane and steam required for regeneration and solids heating. In addition, the electricity and steam consumption of the NOXSO process results in an energy penalty.

The annual costs for sorbent makeup, methane and steam consumption are given by:

$$\mathrm{VOC_{sorbent}} = 8760\,\mathrm{cf}\;\mathrm{m_{makeup}}\;\mathrm{R_{sorbent}}$$

$$\mathrm{VOC_{CH4}} = 8760\,\mathrm{cf}\;\left(\mathrm{m_{CH4,SH}} + \mathrm{m_{CH4,R}} + \mathrm{m_{CH4,By}}\right)\mathrm{R_{CH4}}$$

$$\mathrm{VOC_{steam}} = 8760\,\mathrm{cf}\;\left(\mathrm{m_{steam,R}}\right)\mathrm{R_{steam}}$$

Note that methane is required for solids heating, as a reducing gas for the regeneration reactions, and also as a reducing gas for off-gas pretreatment in the Claus plant.

The energy required to overcome the absorber flue gas pressure drop is:

$$EC_{ID} = \frac{G_{FG}\ \Delta P_A\ N_{A,O}}{8512\,\eta_{fan}}$$

Additional energy requirements for sorbent transport and for overcoming the pressure drop in the solids heater are calculated as follows:

$$EC_{sorbent} = \frac{1795\,(kW)}{1.36\times10^{6}\ (lb/hr)}\,m_{sorbent}$$

$$EC_{AH} = \frac{G_{Offgas}\ \Delta P_{AH}}{8512\,\eta_{fan}}$$

where the pressure drop ΔP_{AH} in the solids heater is typically about 4 inches of H_2O, and the fan efficiency is in the range of 50-85%, combining the three equations above yields the overall electrical energy operating cost:

$$VOC_{Elec} = 8760\,cf\,(EC_{sorbent} + EC_{AH} + EC_{ID})R_{Elec}$$

Note that in the IECM the internal cost of electricity either can be specified by the user or calculated by the model based on generating costs for a new power plant.

Finally, the variable operating costs also include a byproduct credit for the sale of elemental sulfur produced by the Claus plant. The amount of this credit is given by:

$$VOC_{By} = 8760\,cf\,\eta_{By}\left(\frac{32\,M_{SO2,\,R}}{2000}\right)R_S$$

Summarizing the above terms, the total variable operating cost is:

$$VOC_{Total} = VOC_{sorbent} + VOC_{CH4} + VOC_{steam} + VOC_{Elec} - VOC_{By}$$

The total variable cost for different coals and plant sizes is graphed in Figure 8-13. As with fixed O&M cost, the total variable cost also increases in a nearly linearly fashion with plant size, reflecting larger input and output flows of plant materials and energy requirements. In this case, however, there is a slight upward curvature, indicating slightly higher variable costs with increasing plant size. This is primarily due to nonlinearities that result in higher sorbent requirements and attrition losses with larger vessel sizes. Overall, however, this is not a significant factor affecting economics of scale.

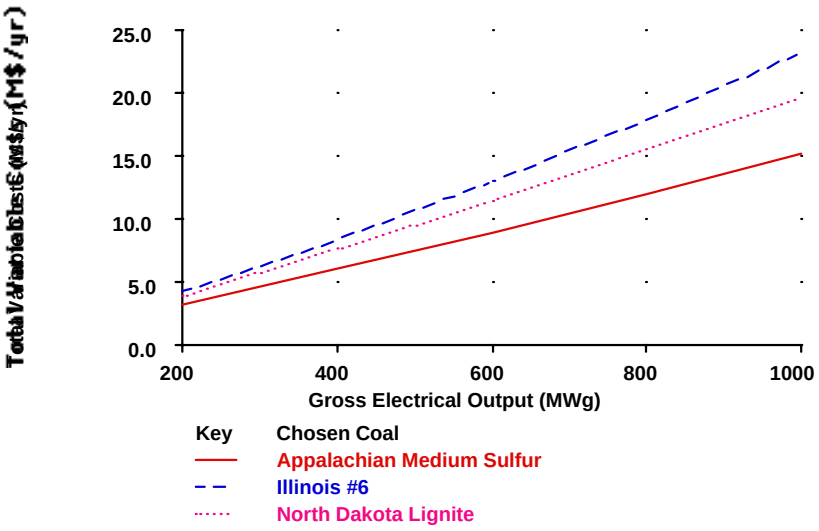

Figure 8-13 Variable O&M Costs for Different Plant Configurations (1993$)

8.3.4. Total Levelized Cost Model

Typically, the capital and O&M costs are combined to determine a total annualized or levelized cost based on various financial parameters and the book life of the technology. A detailed discussion of levelized cost calculations can be found in EPRI TAG V3 (1989). The levelized cost is calculated as follows:

$$C_{NOXSO,Lev}(\$/MWh) = \frac{(fcf)(TCR) + (FOC + VOC)vclf}{8760(cf)(MW)} \qquad (8\text{-}48)$$

The IECM already contains a routine for calculating the levelized cost given the various input factors for a specific technology.

8.4. References

Black, J. B., Woods, M., Friedrich, J. J. and C. A. Leonard (1993). "The NOXSO Clean Coal Technology Project: Commercial Plant Design." *In Proceedings of The Thirteenth EPRI/EPA/DOE SO2 Control Symposium*, Boston, MA.

Cichanowicz, J.E., C. E. Dene, W. DePriest and R. P. Gaikwad (1991). "Engineering Evaluation of Combined SO_2/NO_x Controls for Utility Application," In *Proceedings of the 1991 SO_2 Control Symposium*, EPRI/EPA, Miami, FL.

Davidson, J. F. and D. Harrison (Ed.) (1971). *Fluidization*. London, UK: Academic Press.

DePriest, W., R. P. Gaikwad and J. Jarvis (1986). "Technical and Feasibility Assessment of Combined SO_2/NO_x Processes," EPRI Report, TR-102820, V1, EPRI, Palo Alto, CA.

Frey, H. C. and E.S. Rubin (1994). "Performance and Cost Models for the Fluidized Bed Copper Oxide Process", Report No. DE-AC22-92PC91346-8, U.S. Department of Energy, Pittsburgh, PA.

Haslbeck, J. L. and L.G. Neal (1985). “The NOXSO Process Development: An Update.” *In Ninth EPA/EPRI Symposium on Flue Gas Desulfurization,* Cincinnati, OH.

Haslbeck, J.L., M.C. Woods, W.T. Ma, S.M. Harkins and J.B. Black (1993). "NOXSO SO_2/NO_x Flue Gas Treatment: Proof-of-Concept Test", *In Proceedings of 1993 SO_2 Control Symposium*, EPRI/DOE, Boston, MA.

Kunii, D. and O. Levenspiel (1969). *Fluidization Engineering*. New York: Wiley.

Leonard, C.A., J.L. Haslbeck, J.J. Friedrich and M.C. Woods (1994). "NOXSO Economics," Technical Report prepared by NOXSO Corp., Unpublished Manuscript.

Ma, W. T., J.L. Haslbeck, et al. (1993). “Proof-of-Concept Testing of the Advanced NOXSO Flue Gas Cleanup Process,” Report of Contract No. DE-AC22-89PC88889, U.S. Department of Energy, Pittsburgh, PA.

Rubin, E.S., J.S. Salmento, H. C. Frey, A. Abu-Baker and M. Berkenpas (1991). “Modeling of Integrated Environmental Control Systems for Coal-Fired Power Plants,” Report DE-AC22-87PC79864, U.S. Department of Energy, Pittsburgh, PA.

Yates, J. G. (1983). *Fundamentals of Fluidized-Bed Chemical Processes*. Boston, MA: Butterworths.

Yeh, J. T., Drummond, C. J., Haslbeck, J. L. and L.G. Neal (1987). “The NOXSO Process: Simultaneous Removal of SO_2 and NO_x from Flue Gas.” *In Proceedings of Spring National Meeting of the AIChE,* Houston, TX.

Yeh, J. T., Ma, W. T., Pennline, H. W., Haslbeck, J. L. and F.N. Gromicko (1990). Integrated Testing of the NOXSO Process: Simultaneous Removal of SO_2 and NO_x from Flue Gas. *In Proceedings of AIChE Spring National Meeting*, Orlando, FL.

9. Appendix

9.1. Introduction to "Integrated Environmental Control Modeling of Coal-Fired Power Systems"

This appendix contains the text, figures and tables from a technical paper delivered at the Air & Waste Management Association meeting held in the summer of 1996. The paper was published in their journal the following year.† The paper is provided as an example of the power, applicability, and ease of the IECM. For a complete copy of the actual paper, please refer to the journal directly.

9.2. Abstract

The capability to estimate the performance and costs of advanced environmental control systems for coal-fired power plants is critical to a variety of planning and analysis requirements faced by utilities, regulators, researchers and analysts in the public and private sectors. This paper describes a computer model developed for the U.S. Department of Energy (USDOE) to provide an up-to-date capability for analyzing a variety of pre-combustion, combustion, and post-combustion options in an integrated framework. A unique feature of the model allows performance and costs of integrated environmental control concepts to be modeled probabilistically as a means of characterizing uncertainties and risks. Examples are presented of model applications comparing conventional and advanced emission control designs. The magnitude of technology risks associated with advanced technologies now under development are seen to vary markedly across applications. In general, however, integrated environmental control concepts show significant potential for more cost-effective methods of emissions control.

9.3. Introduction

Over the past two decades, new environmental control requirements have substantially altered the design of fossil fuel power plants, especially for coal-fired plants, which supply nearly 60 percent of U.S. electricity demand. The development of environmental regulations has been a largely piecemeal approach, focused on one environmental medium at a time (air, water, solids), with a changing set of standards

† Rubin, E.S.; Kalagnanam, J.R.; Frey, H.C.; Berkenpas, M.B. "Integrated Environmental Control Modeling of Coal-Fired Power Systems," *Journal of the Air & Waste Management Association*. **1997**, 11:47, 1180-1188.

and requirements for individual pollutants. In turn, new technologies have been added to address each new problem or requirement that arises. The result of this piecemeal approach has been high cost and often unsatisfactory performance of environmental control technology.

More recently, the concept of integrated environmental control has emerged as an important new paradigm for the design of electric power systems. This concept has a number of dimensions. One involves the integration of pollution control functions currently carried out in separate devices or unit operations, for example the replacement of separate processes for SO_2 and NO_x control by a single system for combined removal of both pollutants. Integration also includes the consideration of methods to control air pollutants, water pollutants and solid wastes simultaneously, as opposed to separate solutions for each environmental medium. Finally, the concept of integrated control includes an examination of environmental control options at different stages of the fuel cycle, for example, control methods that can be applied before, during and after the combustion process, as opposed to a focus on one area alone.

This paper describes a computerized modeling framework developed for the U.S. Department of Energy (USDOE) to provide the capability to analyze the performance and cost of integrated emission control concepts for coal-fired electric power plants. This capability is critical to a variety of planning, analysis, and design requirements faced by utility companies, regulators, researchers and analysts. A unique capability of the model is that it allows performance and costs to be characterized probabilistically, using Monte Carlo methods to quantify performance and cost uncertainties and risks. The Integrated Environmental Control Model (IECM) is intended to support a variety of applications related to technology assessment, process design, and research management. Examples of questions that can be addressed with the model include the following:

- What uncertainties most affect the overall performance and costs of a particular technology?
- What are the key design trade-offs for a particular process?
- What are the potential payoffs and risks of advanced processes vis-a-vis conventional technology?
- Which technologies appear most promising for further process development?
- What conditions or markets favor the selection of one system design (or technology) over another?
- How can technical and/or economic uncertainties be reduced most effectively through further research and development?

9.4. Implications

Estimating the performance and cost of advanced technologies still under development is one of the most difficult tasks facing decision makers, policy analysts and research managers in the public and private sectors. The modeling framework described in this paper offers an approach to help minimize technological risks by explicitly considering uncertainties in the development of performance and cost estimates for integrated environmental control options applicable to modern coal-based power generation systems.

9.5. Modeling Framework

The IECM allows systematic analysis of emission control options for coal-fired power plants employing a variety of pre-combustion, combustion and post-combustion control methods. The model was developed to provide preliminary performance and cost estimates for new baseload power plants as well as existing plants considering technology retrofits. Of particular interest are a number of advanced environmental control technologies being developed with support from USDOE. For comparative purposes, however, a set of "baseline" technologies representing current commercial systems also is part of the IECM framework.

Table 9-1 lists the technologies currently included in the model. For each technology, a process performance model accounts for all energy and mass flows, including air pollutants, reagent requirements, and solid wastes associated with that process. The performance models also determine key process design parameters, such as the specific collection area (SCA) of an electrostatic precipitator, or the reagent stoichiometry of a flue gas desulfurization (FGD) system. Coupled to each performance model, an economic model estimates the capital cost, annual operating and maintenance (O&M) costs, and total levelized cost of each technology based on plant and performance model parameters, including all emission constraints. The technology models developed for the IECM in the mid-to-late 1980s recently have been updated and enhanced to reflect current design criteria and associated performance and costs. The status of major IECM components is briefly reviewed below. Additional details are provided elsewhere.[1,2]

Table 9-1 Emission cnontrol technology options for the IECM

Plant Area	Baseline Processes	Advanced Processes
Physical Coal Cleaning	• Level 2 Plant • Level 3 Plant • Level 4 Plant • Froth Flotatation	• Selective Heavy Liquid Cyclones • Coal-Pyrite Flotation • Magnetic Separation
Combustion Controls	• Low NO_x Burners	• Reburning (gas)[a] • Slagging Combustor[a]
Post-Combustion Controls	• Selective Catalytic Reduction (Hot- & Cold-Side) • Wet Limestone FGD • Wet Limestone with Additives • Wet Lime FGD • Lime Spray Dryer • Electrostatic Precipitator (Cold-Side) • Reverse Gas Fabric Filter • Pulse Jet Fabric Filter	• NOXSO • Copper Oxide • Electron Beam • Advanced SO_2/NO_x Removal[a]
Waste Disposal & Byproduce Recovery	• Landfill • Ponding	• Sulfur Recovery • Sulfuric Acid Recovery • Gypsum

[a] Planned for future model versions.

9.5.1. Coal Cleaning Processes

The IECM includes models of both conventional and advanced coal cleaning processes. The conventional processes include four plant designs of increasing complexity, which provide increasing capability for sulfur as well as ash removal.[3] Each of these plant designs (referred to as cleaning levels 2, 3, 4 and 5) can be optimized to achieve a target sulfur or ash reduction while maximizing overall yield (thus minimizing costs). Data requirements for these models includes coal-specific washability data plus cleaning circuit design parameters such as top size and bottom size for different coal fractions.

Models of several advanced physical coal cleaning processes also have been developed based on limited data for several U.S. coals.[1,2] While these processes are capable of achieving higher levels of sulfur and ash reduction than conventional processes, their costs also are higher. Several of these processes have been developed to provide "super-clean" coal for use in coal-liquid mixture fuels, which compete with other premium fuels such as oil or gas.

9.5.2. Base Power Plant

Performance and cost models of a base power plant are needed to accurately characterize the cost of integrated emission control systems, particularly when coal cleaning is employed. The IECM base plant performance model includes detailed mass and energy balances, fuel combustion equations, and thermodynamic relationships to calculate flue gas flow rates, plant efficiency, and net power generation. The environmental performance of the furnace also is determined from mass and energy balances where possible, or from empirical relationships where necessary, as in the case of NO_x emissions. A detailed model of the air preheater also has been developed[2] to properly account for energy credits for advanced environmental control processes.

Revised cost models for the base power plant have been developed based on recent data from the Electric Power Research Institute (EPRI) for furnace designs appropriate for different coal ranks (bituminous, subbituminous and lignites).[4] The new cost algorithms estimate capital costs and annual O&M costs as a function of key plant design and operating parameters.[5] A feature of all the IECM cost models is that each technology is disaggregated into a number of different process areas, typically four to eight areas per technology, depending on its complexity. The direct cost of each process area is calculated based on appropriate flowsheet parameters such as a mass or volume flow rate, species concentration, temperature, pressure, etc.. Additional indirect costs are estimated based on the total process facilities costs, following standard EPRI accounting methods.[4] In this way, the IECM captures important linkages between process design, performance and cost.

9.5.3. NO_x Controls

The IECM includes both in-furnace and post-combustion NO_x control options. Currently, the in-furnace combustion controls include low NO_x burners for a new power plant meeting or exceeding U.S. federal New Source Performance Standards. Additional combustion options suitable for NO_x retrofits currently are being developed.

Post-combustion control methods include both "hot-side" and "cold-side" selective catalytic reduction (SCR) systems. New SCR performance and cost models incorporate recent data and experience from SCR units worldwide. The revised models contain a larger number of system design parameters, a more detailed characterization of catalyst activity, and additional details related to capital cost and

O&M cost parameters.[6] While SCR systems on coal-fired plants are only now emerging commercially in the United States, their widespread use in Europe and Japan[7] represents the benchmark design for comparisons with advanced emissions control systems being developed by DOE.

9.5.4. Particulate Emission Controls

The IECM includes performance and cost models for cold-side electrostatic precipitators (ESP) and fabric filters. Performance and cost models for both technologies recently have been updated to reflect current applications.[8,9] The revised ESP performance model calculates total flyash removal as a function of ash composition and flue gas properties, while fabric filter performance is related primarily to the air-to-cloth ratio. The latter models also have been expanded to include both reverse gas and pulse jet fabric filter designs. Recent design studies for EPRI[10,11] have been used to update the economic models for all particulate collectors.

9.5.5. Flue Gas Desulfurization Systems

Substantial improvements in FGD system design, accompanied by reductions in cost, have been seen over the past decade, and recent enhancements to the IECM modules now reflect these changes.[12] New FGD performance and cost models have been developed for the IECM for four common types of FGD systems: (1) wet limestone with forced oxidation; (2) wet limestone with dibasic acid additive; (3) magnesium-enhanced wet lime system; and (4) a lime spray dryer system. The new cost models reflect the results of recent studies,[13] while the new performance models represent the capabilities of modern commercial systems.[14]

9.5.6. Combined SO_2-NO_x Removal Processes

A key element of USDOE's Clean Coal Technology program focuses on advanced processes for combined SO_2 and NO_x removal to achieve high environmental performance goals at lower cost than the conventional combination of SCR plus FGD. Models of three SO_2/NO_x control systems have been developed for the IECM: the fluidized-bed copper oxide process, the electron beam process and the NOXSO process. The copper oxide and NOXSO processes are of continuing interest to USDOE, and earlier versions of the performance and cost models for these two processes have been refined and updated based on recent proof-of-concept testing.[15,16]

9.5.7. Waste Disposal and By-Product Recovery Systems

The IECM treats solid waste disposal as a variable cost item associated with a particular control technology, consistent with the costing method used by EPRI and others. Thus, boiler bottom ash disposal is included in the base plant model, fly ash disposal costs are incorporated in the ESP or fabric filter models, and FGD wastes or by-product credits are treated in the FGD cost models.

Advanced processes employing combined SO_2/NO_x removal produce by-product sulfur or sulfuric acid rather than a solid waste. Because the sulfur or sulfuric acid plant is a significant part of the overall plant cost, separate engineering models have been developed for these two components.[2] These models are sensitive to input gas composition and other parameters affecting overall process economics.

9.6. Probabilistic Capability

A unique feature of the IECM is its ability to characterize input parameters and output results probabilistically, in contrast to conventional deterministic (point estimate) models. This method of analysis offers a number of important advantages over the traditional approach of examining uncertainties only through sensitivity analysis. Probabilistic analysis allows the interactive effects of variations in many different parameters to be considered simultaneously, in contrast to sensitivity analysis where only one or two parameters at a time are varied, with all other parameters held constant. In addition, probabilistic analysis provides quantitative insights about the *likelihood* of various outcomes, and the probability that one result may be more significant than another. This type of information on technical and economic risks often is of greater value than simple bounding or "worst case" analyses obtained from sensitivity studies, which contain no information on the likelihood of worst case occurrences.

The ability to perform probabilistic analysis comes from the use of a software system which uses a non-procedural modeling environment designed to facilitate model building and probabilistic analysis.[17] In addition to a number of standard probability distributions (e.g., normal, lognormal, uniform, chance), the IECM can accommodate any arbitrarily specified distribution for input parameters. Given a specified set of input uncertainties, the resulting uncertainties induced in model outputs are calculated using median Latin Hypercube sampling, an efficient variant of Monte Carlo simulation. Results typically are displayed in the form of a cumulative probability distribution showing the likelihood of reaching or exceeding various levels of a particular parameter of interest (e.g., efficiency, emissions or cost).

9.7. Model Applications

The IECM recently has been modified to allow estimation of retrofit costs as well as new plant costs. A series of user-specified retrofit factors may be applied at the process area level for a particular system to estimate the higher costs of retrofit facilities. To use the model, a graphical interface has been developed which provides an extremely user-friendly mode of operation.[18]

Here we present results illustrating the capabilities of the IECM to evaluate and compare conventional and advanced emissions control systems. The base case plant shown in Figure 9-1 achieves 90% SO_2 removal employing a wet limestone FGD system with forced oxidation, and 90% NO_x removal using low-NO_x burners plus a hot-side SCR system. A cold-side ESP is used for flyash collection to meet the federal New Source Performance Standard of 0.03 lbs/10^6 Btu. The base plant produces solid wastes (gypsum and ash) that are disposed of in a landfill.

The advanced process modeled in this illustration is the fluidized bed copper oxide process, being developed with support from USDOE. This plant is designed to achieve the same emission levels as the base plant. A brief overview of the copper oxide process provides background for the comparative analysis that follows.

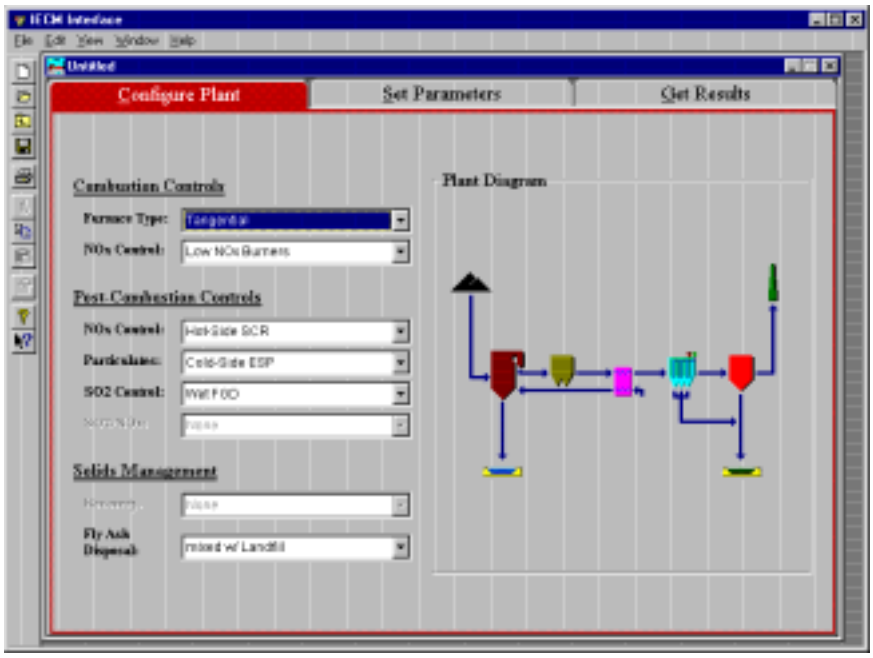

Figure 9-1 User interface screen showing the base case plant configuration

9.7.1. Copper Oxide Process Overview

The fluidized-bed copper oxide process is designed to achieve at least 90 percent removal of both SO_2 and NO_x from power plant flue gases in a single reactor vessel. The process is regenerative, producing a marketable sulfur or sulfuric acid byproduct in lieu of a solid waste containing spent sorbent. A simple schematic of a power plant with the copper oxide process is shown in Figure 9-2.

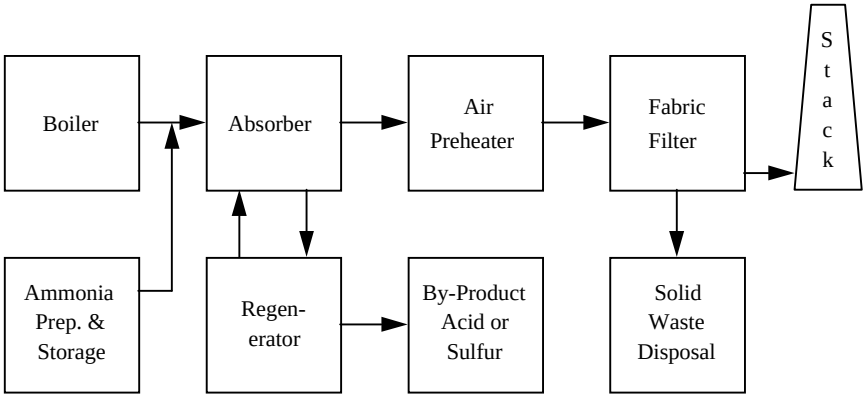

Figure 9-2 Coal-fired power plant design with a copper oxide emission control system

In a commercial-scale process, a bed of copper-impregnated sorbent, consisting of small diameter alumina spheres, is fluidized by the power plant flue gas. Removal of SO_2 and SO_3 in the flue gas occurs by reaction with copper oxide in the sorbent, while NO_x is removed by reaction with ammonia injected into the flue gas upstream of the absorber. The reaction is catalyzed by copper sulfate and promoted by mixing within the fluidized bed. The absorber reactions are exothermic, and this incremental thermal energy can be recovered in the power plant air preheater, resulting in an

energy credit. The sulfated sorbent is transported from the fluidized bed absorber to a solids heater and then to a regenerator. Regeneration of the sorbent occurs by reaction with methane, converting the copper sulfate and unreacted copper oxide to elemental copper. An off-gas containing sulfur dioxide is further processed to recover elemental sulfur in a modified Claus plant. The regenerated sorbent is then transported back to the absorber.

The copper oxide process performance model includes the fluidized bed absorber, sorbent heater, regenerator, solids transport system, and ammonia injection system. The IECM also characterizes the performance of an integrated sulfur recovery plant and the power plant air preheater. In previous studies, the performance and cost of the fluidized bed copper oxide process were analyzed extensively, and compared to a conventional plant meeting the same emission standards with FGD and SCR.[19] Previous studies also examined the potential of targeted research and development to lower costs and improve process competitiveness.[20] Earlier studies, however, were based on models of conventional FGD and SCR systems reflecting experience and designs of the early 1980s, and on limited bench-scale data for the copper oxide process performance. The earlier copper oxide data now have been supplemented by more recent data from a life cycle test unit (LCTU), additional bench-scale data on regeneration, and a detailed conceptual design of a commercial-scale plant.[15]

In this paper we employ the newly revised performance and cost models of both the "conventional" emission control systems and the fluidized bed copper oxide process. Integrated systems employing physical coal cleaning in addition to post-combustion controls also are considered. Table 9-2 shows the properties of two coals used for the analysis: a high-sulfur Illinois coal (4.4% S) and a medium-sulfur Pittsburgh seam coal (2.2% S). A gross power plant size of 522 MW with an annual capacity factor of 65 percent is assumed. In-plant energy requirements are calculated by the model, and both plants meet the same emission standards. Assumptions regarding the uncertainties in model parameters are shown in Table 9-3 for the base plant environmental control system, and in Table 9-4 for the advanced emission control system using copper oxide. Many of these uncertainties pertain to the process performance models, which determine key physical properties (such as reagent requirements and vessel size) that affect the cost of meeting a given emission limit. Other uncertainties apply directly to parameters of the component cost models. Table 9-5 shows additional uncertainties common to both designs, including base power plant operating parameters, and financial parameters that determine the fixed charge factor used to amortize capital costs. All costs are reported in constant 1993 dollars and normalized on net plant output.

Table 9-2 Coal properties for case studies

Property	Illinois #6 Coal	Pittsburgh #8 Coal
Heating Value, Btu/lb	10,190	13,400
Sulfur, wt%	4.36	2.15
Carbon, wt%	57.0	74.8
Hydrogen, wt%	3.7	4.6
Oxygen, wt%	7.2	5.3
Nitrogen, wt%	1.1	1.4
Moisture, wt%	12.3	2.7
Ash, wt%	14.34	9.05
Coal Cost (at mine), $/ton	26.10	33.40
Transport Cost, $/ton	7.90	7.90
Delivered Cost, $/ton	34.00	41.30

Table 9-3 Uncertainties for baseline system environmental control design

Model Parameter	Deterministic (Nominal) Value[a]	Prob Dist[b]	Values (or σ as % of mean)[c]
Selective Catalytic Reduction			
Minimum Activity	0.5	U	(1x - 1.5x)
Relative Activity	0.90	N	(2.9%)
Activity at Reference Time	0.85	N	(3%)
Total Pressure Drop	9 in H2O g	N	(5%)
Ammonia Slip	5 ppmv	T	(1x, 1.001x, 2x)
Energy Requirement	(calc)% MWg	N	(5%)
Process Facility Capital	(calc) M$	N	(10%)
General Facilities Capital	10% PFC	N	(10%)
Eng. & Home Office Fees	10% PFC	T	(0.7x, 1x, 1.5x)
Project Contingency Cost	10% PFC	N	(20%)
Process Contingency Cost	(calc)% PFC	N	(30%)
Misc. Capital Costs	2% TPI	N	(10%)
Inventory Capital	0.5% TPC	N	(10%)
Ammonia Cost	150 $/ton	U	(1x - 1.5x)
Catalyst Cost	300 $/ton	T	(0.67x, 1x, 1.33x)
Total Maintenance Cost	2% TPC	N	(10%)
Admin. & Support Cost	(calc)% PFC	N	(10%)
Cold-Side Electrostatic Precipitator			
Specific Collection Area	(calc) acfm/ft2	N	(5%)
Energy Requirement	(calc)% MWg	N	(10%)
Process Facility Capital	(calc) M$	N	(10%)
General Facility Capital	1% PFC	N	(10%)
Eng. & Home Office Fees	5% PFC	N	(10%)
Project Contingency Cost	20% PFC	N	(10%)
Process Contingency Cost	(calc)% PFC	N	(10%)
Disposal Cost	10.24$/ton	T	(0.8x, 1x, 1.2x)
Total O&M Costs	(calc) M$/yr	N	(10%)
Wet FGD System			
No. Operating Trains	2 @50% ea.		
No. Spare Trains	0		
Molar Stoichiometry	1.03 mol Ca/S	T	(1.02, 1.03, 1.05)
Energy Requirement	(calc) % MWg	N	(calc)

Reagent Feed System	(calc) M$	N	(calc)
SO2 Removal System	(calc) M$	N	(calc)
Flue Gas System	(calc) M$	N	(calc)
Solids Handling System	(calc) M$	N	(calc)
General Support Area	(calc) M$	N	(calc)
Miscellaneous Equipment	(calc) M$	N	(calc)
Process Facility Capital	(calc) M$	N	(10%)
General Facilities Capital	10% PFC	L	(1.3 %)
Eng. & Home Office Fees	10% PFC	½ N	(17%)
Project Contingency Cost	15% PFC	U	(0.67x - 1.33x)
Process Contingency Cost	2% PFC	½ N	(50%)
Limestone Cost	15 $/ton	U	(0.7x - 1.3x)
Disposal Cost	8.15 $/ton	T	(0.61x, 1x, 1.84x)
Total O&M Costs	(calc) M$/yr	N	(10%)

[a] Values labeled “Calc” are calculated within the model.

[b] L = Lognormal, N = Normal, U = Uniform.

[c] x Denotes the determinstic value.

Table 9-4 Uncertainties for advanced system environmental control design

Model Parameter	Deterministic (Nominal) Value[a]	Prob Dist[b]	Values (or σ as % of mean)[c]
Copper Oxide Process			
No. Operating Trains	2 @50% ea.		
No. Spare Trains	0		
Regenerator Residence Time	(calc) min	N	(10%)
Ratio of Avail. Cu to SO_x	(calc) mol CuO/SO_x	N	(5%)
Ammonia Stoichiometry	(calc) mol NH_3/NO_x	N	(6.25%)
Sorbent Attrition			
Circ. System	0.047 wt% Circ.	T	(0.43x, 1x, 1x)
Fluidized Bed	0.02 wt% Bed Inv.	T	(0.5x, 0.55x, 1x)
Sorbent Fluid. Bed Density	26.6 lb/cu ft	T	(0.92x, 1x, 1.08x)
Installation Cost Factor	45%	N	(10%)
Process Facility Capital	(calc) M$	N	(10%)
General Facilities Capital	10% PFC	N	(10%)
Eng. & Home Office Fees	15% PFC	N	(10%)
Project Contingency Cost	20% PFC	N	(20%)
Process Contingency Cost	(calc) % PFC	N	(30%)
Misc. Capital Costs	2% TPI	N	(10%)
Inventory Capital	0.5% TPC	N	(10%)
Sorbent Cost	5.00 %/lb	T	(0.5x, 1x, 1x)
Natural Gas Cost	3.50 $/mscf	%T	(0.7x, 1x, 1.3x)
Ammonia Cost	150 $/ton	U	(1x – 1.5x)
Sulfur Credit	(calc) $/ton	T	(0.5x, 1x, 1x)
Sulfuric Acid	53 $/ton	-½ N	(10%)
Maintenance Cost	4.5% TPC	N	(10%)
Total O&M Cost	(calc) M$/yr	N	(10%)
Fabric Filter			
Gross Air to Cloth Ratio	2.0 acfm/sq ft	N	(5%)
Bag Life	4 yrs	N	(30%)
Process Facility Capital	(calc) M$	N	(10%)
General Facility Capital	1% PFC	N	(10%)
Eng. & Home Office Fees	5% PFC	N	(10%)
Project Contingency Cost	20% PFC	N	(10%)
Process Contingency Cost	(calc) % PFC	N	(10%)
Fabric Filter Bag Cost	80 $/bag	N	(5%)
Disposal Cost	10.24 $/ton	T	(0.8x, 1x, 1.2x)
Total O&M Cost	(calc) M$/yr	N	(10%)

[a] Values labeled “Calc” are calculated within the model.

[b] L = Lognormal, N = Normal, U = Uniform.

[c] x Denotes the determinstic value.

Table 9-5 Uncertainties for base power plant system.

Model Parameter	Deterministic (Nominal) Value	Prob Dist	Values (or σ as % of mean)
Power Plant			
Gross Cycle Heat Rate	9500 Btu/kWh	-½ N	(1.8%)
Capacity Factor	65%	N	(7%)
Excess Air to Boiler	20%	N	(2.5%)
Leakage Across Air Preheater	19%	N	(2.5%)
Financial Parameters			
Real Return on Debt	4.6%	N	(10%)
Real Return on Common Stock	8.7%	N	(10%)
Real Return on Preferred Stock	5.2%	N	(10%)
Real Escalation Rate	0%	½ N	(0.06%)

9.7.2. Case Study Results

Figure 9-3 shows the total capital cost of emission control systems for SO_2, NO_x and particulates for the two power plant designs, based on 100 iterations of the model. For the case of the Pittsburgh coal, the copper oxide system cost is generally lower, but shows greater uncertainty than the base plant with SCR/FGD. For the higher sulfur Illinois coal, however, the base plant costs are generally lower than the copper oxide plant. Figure 9-4 Total levelized cost of conventional and advanced emission controls

shows a similar comparison for the total levelized cost of emissions control. For the two coals modeled, these costs range from about 8 to 15 mills/kWh for the base plant, and 7 to 17 mills/kWh for the advanced plant. In both cases, the high end of the range corresponds to the high sulfur coal plants, whose average cost is 2.5 to 3.8 mills/kWh higher than for the medium sulfur plants. Both the mean and variance of the costs for each plant configuration increase with increasing sulfur content. Table 9-6 summarizes the mean values of cost results for the two plants, along with the 90 percent confidence interval from the stochastic simulations. Note that the IECM software provides additional measures of overall cost, including $/ton removed for a given pollutant using conventional technology. However, the latter measure is not meaningful for integrated systems that remove more than one pollutant since costs cannot be allocated unambiguously. Hence, the levelized cost in mills/kWh is preferred for this analysis.

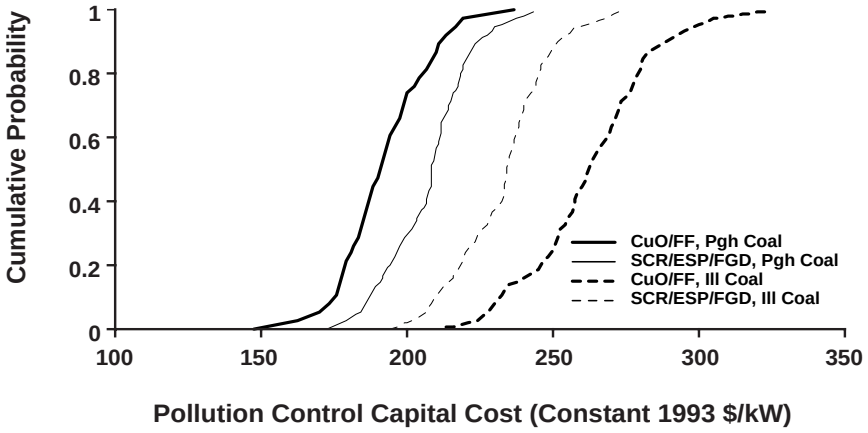

Figure 9-3 Total capital cost of conventional and advanced emission controls

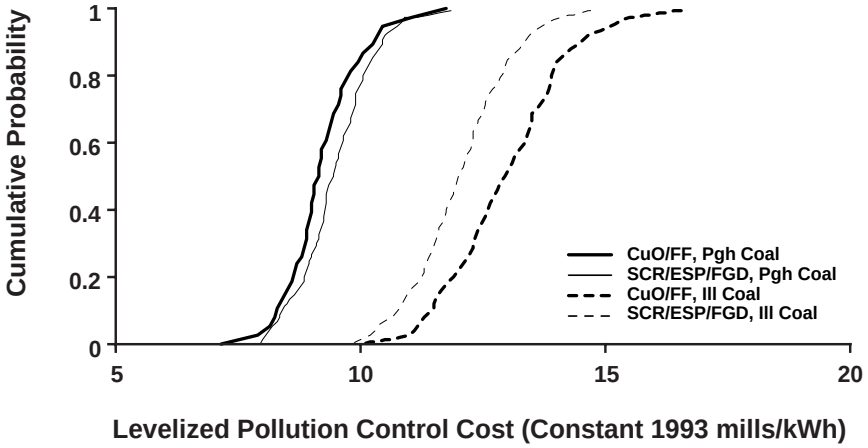

Figure 9-4 Total levelized cost of conventional and advanced emission controls

Table 9-6 Summary of case study cost results (mean values and 90% CI of emission control costs constant $1993)[a]

Case	Illinois #6 Coal		Pittsburgh #8 Coal	
	$/kW	mills/kWh	$/kW	mills/kWh
Base Plant (SCR/ESP/FGD)	233 (207-258)	12.0 (10.3-13.7)	207 (184-230)	9.5 (8.2-10.8)
Advanced Plant (CuO/FF)	262 (227-298)	13.0 (11.1-15.1)	192 (169-217)	9.2 (8.1-10.5)
Advanced Plant w/Pulse-Jet FF	237 (201-270)	12.3 (10.5-14.3)	167 (143-191)	8.6 (7.5-10.0)

[a] Range in parenthesis is the 90% confidence interval (CI).

Because of the considerable overlap in cost for the two systems, a more insightful comparison comes from examining the *difference* in costs between the base plant and advanced plant designs. A probabilistic representation of cost differences can be obtained by a numerical procedure that insures that parameters common to the two systems (such as the fixed charge factor, reagent costs, labor costs, etc.) have identical values when those parameters are sampled in the stochastic simulation.

The results of such an analysis are displayed in Figure 9-5, which shows the levelized cost *savings* of the copper oxide system over the base plant design for the two coals. A negative value on this graph thus indicates that the advanced plant design is actually *more* costly than the base plant design. Indeed, for the high sulfur Illinois coal, the likelihood of the copper oxide system producing a net cost savings is only about 20 percent. For the medium sulfur Pittsburgh coal, however, there is a much higher probability — around 70 percent — that the advanced system design will be less costly than the conventional plant with SCR and FGD. Thus, the copper oxide system is most attractive for medium and lower sulfur coal applications. This is largely because of the strong link between sorbent flow rate and the size of process equipment: process sorbent requirements increase rapidly with increasing coal sulfur content, adding considerably to both capital and operating costs.

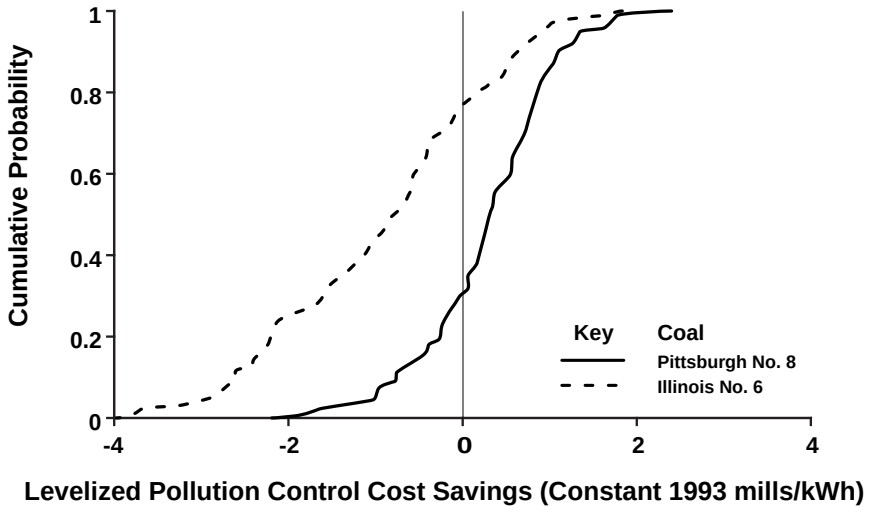

Figure 9-5 Savings of copper oxide system over base plant with SCR/ESP/FGD

Other variations of these plant configurations also were modeled to determine their cost implications. One integrated plant design explored the use of physical coal cleaning to reduce the sulfur and ash content of coal prior combustion, thus reducing the capital and operating costs of environmental control equipment at the power plant. Previous studies[19] had shown that reducing the coal sulfur content by approximately 30 percent using a modern (Level 4) cleaning plant could lower the expected cost of the base plant design for the high-sulfur Illinois coal. However, with the updated cost and performance models described in this paper, the small cost advantage found in the previous study was no longer realized. This is primarily because the lower cost of modern FGD systems yielded much smaller post-combustion control equipment cost savings, which were insufficient to offset the cost of coal cleaning. Cost results for integrated system designs employing pre-combustion cleanup of coal, however, tend to be highly site-specific, so that the results of these particular case studies cannot be generalized to other situations.

Additional studies were performed to explore other process integration issues and cost advantages that may not be apparent when environmental control technologies are examined individually. One such advantage for the conventional power plant design is the gas conditioning effect from the use of an SCR system upstream of an electrostatic precipitator. The SCR performance model converts some of the sulfur dioxide in the flue gas stream to SO_3 which, in turn, affects the performance of the cold-side ESP, reducing the plate collector area needed to achieve a given flyash removal efficiency. The presence of an SCR system thus reduces the capital cost of the ESP, in this case by approximately $5/kW. At the same time, excessive ammonia

slip in an SCR system can affect the salability of collected flyash for byproduct applications. In the present case studies all flyash is assumed to be disposed in a landfill, and ammonia slip is kept to a nominal design level of 5 ppmv. However, the effect of alternative ammonia slip levels on overall plant economics, including byproduct credits for flyash, is readily modeled in the IECM.

For the copper oxide system, a key integration issue involves tradeoffs regarding the air preheater and downstream particulate collector. In order to fully recover the energy released in exothermic chemical reactions associated with sulfur removal, a larger (more expensive) air preheater is required. If the preheater is not re-sized, the higher flue gas temperature generated by the copper oxide system increases the capital cost of downstream particulate equipment, whose cost depends on the actual volumetric gas flow rate. Thus, an integrated analysis is required to determine the least-cost solution for a particular application.

Another integration issue for the advanced plant design is the choice of particulate collector downstream of the SO_2/NO_x removal system. In the examples above, a conventional reverse gas fabric filter was assumed. In this application, a fabric filter is preferable to an ESP because of the low sulfur content of the flue gas. However, advanced fabric filter technology employing a pulse jet system instead of current reverse gas cleaning offers the potential to reduce the capital cost of the advanced plant design by at least $25/kW, according to the results of additional analysis. On a levelized cost basis, this improves the likelihood of the copper oxide plant design being less costly than the conventional system. For example, for the plant burning Pittsburgh seam coal the probability of a cost savings increases to approximately 90 percent with a pulse jet fabric filter, as compared to 70 percent with the conventional reverse gas system (Figure 9-6). The absolute value of expected cost savings also increases as the cumulative probability distributions in Figure 9-5 shift toward the right.

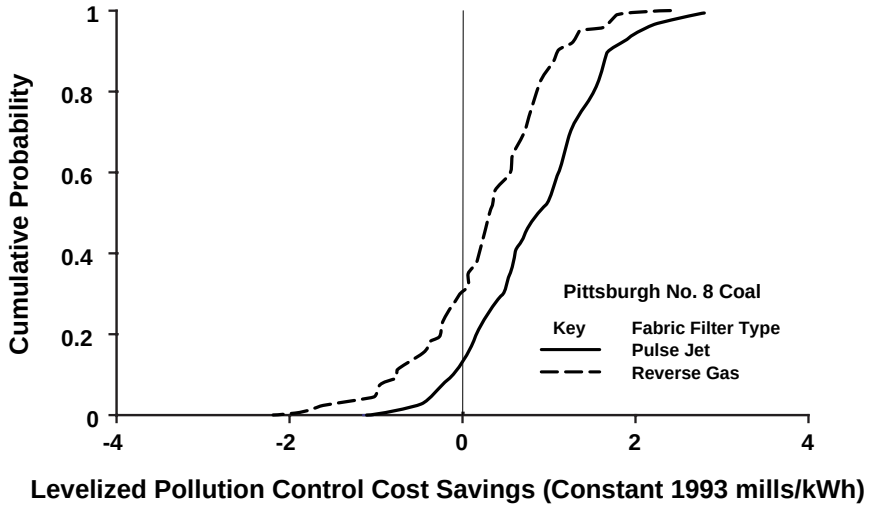

Figure 9-6 Effect of fabric filter choice on cost savings for copper oxide system

9.8. Discussion

The results presented here can be a starting point for further analyses to explore the primary sources of uncertainty, and the potential for R&D to improve performance and lower costs by reducing the uncertainties that matter most. Other recent papers[12,20] illustrate how results from the IECM can be used in conjunction with

statistical and decision analysis methods to explore such issues. For example, partial rank correlation coefficients (PRCC) can be used to identify the key process variables and uncertainties that most affect system cost. Research efforts can then concentrate on those areas that offer the greatest potential payoff for process improvements. Decision analysis methods can be used to quantify the expected benefits of a targeted program of process development.

Improvements in conventional technologies such as FGD and SCR also put downward pressure on the level of allowable emissions. For example, SO_2 removal efficiencies of 95% to 98% or more are now available with commercial guarantees, as compared to no more than 90% less than a decade ago. Regulatory requirements reflecting the most effective available technology thus can be expected to grow more stringent over time, imposing new requirements for advanced technology.

In the case of the copper oxide process, for instance, the performance limits of the fluidized bed design modeled in this paper may be inadequate to economically achieve combined SO_2/NO_x removal efficiencies of 95% or more, as may be required at some locations over the next decade. Thus, the USDOE is currently pursuing a new design involving a moving bed reactor to achieve higher efficiencies. Future enhancements to the IECM will incorporate the results of this on-going research to reflect updated assessments of process performance and cost in a stochastic framework. Readers interested in acquiring the IECM should contact the authors, or P. Rawls at DOE's Pittsburgh Energy Technology Center.

9.9. Conclusion

This paper has described an integrated modeling framework for evaluating the cost and performance of conventional and advanced power plant emission control systems. The IECM framework also facilitates comparisons between alternative systems, particularly advanced technologies that may offer improved performance and/or cost characteristics. In such cases, the probabilistic capability of the models described here can be especially helpful in quantifying the risks as well as potential payoffs of advanced technologies, investment strategies, and R&D priorities.

9.10. Acknowledgments

The model described in this paper were developed under Contract No. DE-AC22-92PC91346 from the U.S. Department of Energy, Pittsburgh Energy Technology Center (DOE/PETC). The authors alone are responsible for all results, conclusions and discussions presented in this paper.

9.11. References

1. Rubin, E.S., J.S. Salmento, J.G. Barrett, H.C. Frey and C.N. Bloyd, *Modeling and Assessment of Advanced Processes for Integrated Environmental Control of Coal-Fired Power Plants*, DE-FG22-83PC60271, U.S. Department of Energy, Pittsburgh Energy Technology Center, Pittsburgh, PA; also NTIS Report No. 86014713, Springfield, VA, 396p, July, 1986.
2. Rubin, E.S., J.S. Salmento, H.C. Frey, A. Abu-Baker, and M. Berkenpas, *Modeling of Integrated Environmental Control Systems for Coal-Fired Power Plants*, DE-AC22-87PC79864, U.S. Department of Energy, Pittsburgh Energy Technology Center, Pittsburgh, PA; also NTIS Report No. 92016847, Springfield, VA, 214p, April, 1991.
3. Skea, J.F. and E.S. Rubin, "Optimization Model of Coal Benefication Plants for SO_2 Emissions Control," *Journal of the Air Pollution Control Association*, Vol. 38, No. 10, p.

1281-1288, October, 1988.
4. *Technical Assessment Guide, Electric Supply — 1993*, EPRI TR-102276, Electric Power Research Institute, Palo Alto, CA, 1993. Also, private communication with Dr. C. McGowin, EPRI, 1995.
5. Kalagnanam, J.R., and E.S. Rubin, *Cost Models for Pulverized Coal Base Plants*, DE-AC22-92PC91346-10, U.S. Department of Energy, Pittsburgh Energy Technology Center, Pittsburgh, PA; also NTIS Report No. 95015602, Springfield, VA, April, 1995.
6. Frey, H.C., "Engineering-Economic Evaluation of SCR NO_x Control Systems for Coal-Fired Power Plants", *Proceedings of the American Power Conference*, Vol. 57, Illinois Institute of Technology, Chicago, Illinois. April 1995.
7. Lowe, P.A., W. Ellison, and M. Perlsweig, "Understanding the German and Japanese Coal-Fired SCR Experience," *Proceedings of 1991 Symposium on Stationary Combustion Nitrogen Oxide Control*, Electric Power Research Institute, Palo Alto, CA, March 1991.
8. Kalagnanam, J.R. and E.S. Rubin, *Performance and Cost Models for Electrostatic Precipitators*, DE-AC22-92PC91346-7, U.S. Department of Energy, Pittsburgh Energy Technology Center, Pittsburgh, PA; also NTIS Report No. 95001968, Springfield, VA, July, 1994.
9. Kalagnanam, J.R. and E.S. Rubin, *Performance and Cost Models for Fabric Filters*, DE-AC22-92PC91346-6, U.S. Department of Energy, Pittsburgh Energy Technology Center, Pittsburgh, PA; also NTIS Report No. 94014551, Springfield, VA, April, 1994.
10. Gaikwad, R.P. and D.G. Sloat, *Economic Evaluation of Particulate Control Technologies*, Report No. EPRI TR-100748, Electric Power Research Institute, Palo Alto, CA, 1992.
11. Sloat, D.G., R.P. Gaikwad and R.L. Chang, "The Potential of Pulse-Jet Baghouses for Utility Boilers. Part 3: Comparative Economics of Pulse-Jet Baghouse, Precipitators and Reverse-Gas Baghouses," *J. Air & Waste Management Assoc., 43*, 120, 1993.
12. Rubin, E. S., J.R. Kalagnanam and M.B. Berkenpas, "New Models for FGD Performance, Cost and Hazardous Air Pollutant Removal," *Proceedings of 1995 SO_2 Control Symposium*, Electric Power Research Institute, Palo Alto, CA, March, 1995.
13. Keeth, R.J., D.L. Baker, P.E. Tracy, G.E. Ogden and P.A. Ireland, *Economic Evaluation of Flue Gas Desulfurization Systems*, GS-7193, RP1610-6, Electric Power Research Institute, Palo Alto, CA 1991.
14. Kalagnanam, J.R. and E.S. Rubin, *Performance and Cost Models for Flue Gas Desulfurization Processes*, DE-AC22-92PC91346-11, U.S. Department of Energy, Pittsburgh Energy Technology Center, Pittsburgh, PA; also NTIS Report No. 9600352, Springfield, VA, June, 1995.
15. Frey, H.C., "Performance Model of the Fluidized Bed Copper Oxide Process for SO_2/NO_x Control," Paper No. 93-WA-79.01, *Proceedings of the 86th Annual Meeting*, Air and Waste Management Association, Pittsburgh, PA, June 1993.
16. Kalagnanam, J.R. and E.S. Rubin, *Performance and Cost Models for the NOXSO Process*, DE-AC22-92PC91346-12, U.S. Department of Energy, Pittsburgh Energy Technology Center, Pittsburgh, PA; also NTIS Report No. 96009831, Springfield, VA, December, 1995.
17. Lumina Decision Systems, *Analytica User Guide: Release 1.0*, Lumina Decision Systems, Los Altos, CA, 1996.
18. Berkenpas, M.B. and E.S. Rubin, *IECM User's Manual*, Prepared for U.S. Department of Energy, Pittsburgh Energy Technology Center, by Center for Energy and Environmental Studies, Carnegie Mellon University, Pittsburgh, PA, 1996.
19. Frey, H.C. and E.S. Rubin, "Probabilistic Evaluation of Advanced SO_2/NO_x Control Technology," *Journal of Air & Waste Management Association*, Vol. 41, No. 12, p. 1585-1593, December, 1991.
20. Frey, H.C. and E.S. Rubin, "Evaluation Method for Advanced Acid Rain Compliance Technology," *Journal of Energy Engineering*, Vol. 118, No. 1, p. 38-55, April, 1992.

10. Glossary of Terms

11. Index

Error! No index entries found.